Chemical, electrical, hormonal and nutrient signaling in the mammalian central nervous system

Jack Pryor BSc (Hons)

A thesis written in partial fulfillment of the criteria set for the degree of Doctor of Philosophy

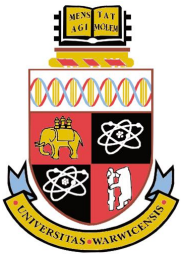

Warwick Medical School 2017

Funded by Neurosolutions Ltd., The Leverhulme Trust and The Association of Rhodes Scholars in Australia

Table of Contents

List of Figures

List of Tables

Acknowledgements

Thank you to Neurosolutions Ltd., The Association of Rhodes Scholars in Australia and The Leverhulme Trust for financial support and resources provided over the course of my PhD. I would like to express my gratitude to Dr. Marco van den Top, Dr. Andrew Whyment and Dr. Ross Jeggo for the supervision and guidance provided in the initial stages of my doctoral training program. My warmest thanks go to the Department of Physiology at Monash University, but especially to Professor Iain Clarke and Professor Michael Cowley for their patience, company and council. To Professor David Spanswick, thank you for accepting me as a student, irrespective of my personal circumstances. I could not have asked for a more knowledgeable and principled scientist as a mentor. Earnest thanks go to Dr. Stephanie Simonds, who over the last three years has proved to be the most loyal and generous friend I could ask for. The extent of her benevolence is rivaled only by her love of beige food. Most of all, thanks to Mum, Dad, Alice, Joe and PC Papadeemus for their humor, generosity and love, this thesis is dedicated to them.

To Chloe: Mentioning you here feels like an effective way of putting a curse on our relationship. I'll probably get your name tattooed on my forehead instead.

To mum: Guacamole is not pronounced like 'whack-a-mole'.

To Sybil: It was either the desire to impress you or genetic determinism that lead me to study biology. Either way, you're to blame for this book.

Declaration

I hereby declare that this thesis has been composed solely by myself and that it has not been accepted in any previous application for a degree. All work has been done by myself and all sources used have been specifically acknowledged by means of a reference.

Publications

SE Simonds, JT Pryor, IS Farooqui, E Rauvinson, F Greenway, R Dileone, AM Allen, J Bassi, JK Elmquist, MG Myers, J Licinio, RD Brown, PJ Enririo, S O'Rahilly, S Sternson, DC Spanswick, KL Grove, MA Cowley (2014) Leptin Mediates the Increase in Blood Pressure Associated with Obesity. Cell, 159, 1404-1416

Abstracts

JT Pryor, SE Simonds, MA Cowley, DC Spanswick (2016) Functional, energy status-dependent plasticity of glucose-sensing in NPY/AgRP neurons. Keystone Symposia, Obesity and Adipose Tissue Biology

JT Pryor, IS Parhar, DC Spanswick, IJ Clarke (2014) Electrophysiological and pharmacological profile of GnIH neurons in the rat *in vitro.* International Congress of Neuroendocrinology

Summary

1. The visualized whole-cell patch-clamp technique was used to record from renilla-green fluorescent protein tagged neuropeptide-Y (NPY-GFP) neurons of the murine arcuate nucleus of the hypothalamus (ARH). Here, passive and active membrane properties were quantified and the effects of energy status and ambient glucose concentration were investigated. Key findings here are that NPY neurons of the ARH have a significantly shorter action potential duration in the fasted state, with brain slices incubated in artificial cerebrospinal fluid (aCSF) containing 1 mM glucose, compared to neurons of fed animals, incubated in 1 mM glucose-containing aCSF.

Also observed was a redistribution in the profile of active conductances expressed by NPY neurons, when comparing 'fed' and 'fasted' populations. A T-type calcium conductance was associated with more positive energy states, whereas a hyperpolarization-activated non-selective cation conductance (I_T) was associated with negative energy states, in these neurons. Herein this thesis uses the term 'positive energy state' to describe neurons recorded *in vitro*, the environmental condition of which replicating a fed, sated, high blood and central glucose concentration state *in vivo*. Furthermore this thesis will use the term "negative energy state' to describe neurons recorded *in vitro*, the environmental condition of which replicating a fasted, hungry, low blood and central glucose concentration state *in vivo*.

2. The visualized whole-cell patch-clamp technique was used to record from NPY-eGFP neurons of the murine ARH. NPY neuron sensitivity to glucose and ghrelin was quantified, both in neurons of brain slices taken from animals fed *ad libitum* prior to culling, and in neurons of brain slices taken from mice subjected to an 18-

hour fast prior to culling. A major finding of this study was that an increased proportion of NPY-eGFP neurons are glucose responsive (GR) following an 18-hour fast. Glucose inhibited (GI) and glucose excited (GE) NPY eGFP neurons are recruited by fasting.

Another major finding in this study was that fasting increases the excitatory effects of ghrelin on NPY eGFP neurons. NPY neuron depolarization induced by both glucose and ghrelin is via K_{ATP} channels, therefore the effect of one factor upon the channel can impact the ability of other K_{ATP} modulators to effect neuronal excitability.

3. The visualized whole-cell patch-clamp technique was used to record from murine proopiomelanocortin enhanced-green fluorescent protein (POMC-eGFP) neurons of the ARH. The contribution of T-cell protein tyrosine phosphatase (TCPTP) and phosphoinositide-3 kinase (PI3K) to ARH POMC neuron insulin signal transduction was investigated. Here we found insulin to exert differential effects on POMC neurons, with some excited, some inhibited, whilst some neurons were insensitive to bath application insulin.

A major finding of this study was that the insulin-induced excitation of POMC neurons in the presence of a TCPTP inhibitor was significantly larger in magnitude than the excitation observed in the presence of a PI3K inhibitor. This result indicates that TCPTP exerts an inhibitory tone upon insulin-induced PI3K-dependent POMC neuron excitation.

Also observed were considerable differences in the proportion of insulin-induced excitations and insulin-induced inhibitions, when comparing experimental groups. Groups included a population of control POMC neurons, a population of POMC neurons incubated in a TCPTP inhibitor, and a population of POMC neurons

incubated in a PI3K inhibitor. Under control conditions around half of POMC neurons were inhibited by insulin, approximately 10% were excited and the remaining 40% did not respond to insulin. Inhibition of neuronal TCPTP decreased the proportion of insulin-inhibited, and increased the proportion of insulin-excited POMC neurons, compared to control. Neuronal inhibition of PI3K resulted in an insulin response distribution, similar to that observed in the TCPTP inhibitor group, with an increased proportion of insulin-induced excitations, and a reduced proportion of insulin-induced inhibitions, relative to control. This result is somewhat paradoxical, as ostensibly both inhibition and disinhibition of PI3K signaling in POMC neurons, drives an increased excitatory response to insulin.

4. The visualized whole-cell patch-clamp technique was used to record from murine yellow fluorescent protein-tagged leptin receptor-expressing (LepR) neurons of the murine dorsomedial hypothalamus (DMH). The electrophysiological effects of leptin on LepR neurons of the mouse DMH were investigated. Leptin depolarized 38.2% of DMH LepR neurons, hyperpolarized 14.7% of DMH LepR neurons, whilst the remaining 47.1% did not respond. Leptin-induced membrane excitation was via the activation of a non-selective cation conductance. Leptin-induced membrane hyperpolarization was via the activation of a potassium conductance. Leptin-induced excitation measured in whole-cell patch clamp experiments *in vitro* was associated with obesity-related increases in blood pressure and heart rate measured *in vivo* by Dr. Stephanie Simonds. This work formed part of her PhD research and is now published (see above).

5. The visualized whole-cell patch-clamp technique was used to characterize the electrophysiological and pharmacological properties of rat DMH gonadotropin inhibitory hormone (GnIH) neurons. Major findings of these experiments include

the identification of glutamatergic and GABAergic synaptic inputs to GnIH neurons. Additionally I identify a number of voltage-sensitive active conductances expressed in rat GnIH neurons. There include a time- and voltage-dependent inward rectification (I_H) and a transient outwardly rectifying potassium conductance (I_{TR}). GnIH neurons were depolarized by noradrenaline, via activation of a non-selective cation conductance. 5-HT induced a complex profile of responses in GnIH neurons. 15.8% were inhibited by 5-HT, 42.1% were excited by 5-HT, whilst the remaining 42.1% responded to 5-HT with a biphasic, inhibitory-excitatory membrane potential response. Thyrotropin releasing hormone (TRH) depolarized GnIH neurons via a non-selective cation conductance, whilst ghrelin depolarized GnIH neurons through the inhibition of a potassium conductance.

6. The visualized whole-cell patch-clamp technique was used to investigate the electrophysiological properties of electrotonically-coupled interneurons located in layers 1 and 2 of the murine prefrontal cortex (PFC). The properties of electrical synapses between fast spiking (FS) and non-fast spiking (NFS) interneurons were investigated. Major findings of these studies were that layer 2 FS interneurons are depolarized by 5-HT, via the activation of a non-selective cation conductance, consistent with 5-HT_3 receptor activation. Furthermore, the gap junction blocker carbenoxolone decoupled synchronized epileptiform activity, whilst the anticonvulsant benzoylamino-benzopyran compounds Tonabersat and Carabersat significantly inhibited gap junctional intercellular communication (GJIC).

Abbreviations

4-AP	4-aminopyridimine
5-HT	5-hydroxytryptamine
ABC	ATP binding cassette
aCSF	Artificial cerebrospinal fluid
ACTH	Adrenocorticotropic hormone
ADP	Adenosine diphosphate
AgRP	Agouti-related peptide
AHP	Afterhyperpolarisation potential
AMP	Adenosine monophosphate
AMPK	AMP-activated protein kinase
α-MSH	α-melanocyte stimulating hormone
ANS	Autonomic nervous system
AP	Action potential
APV	D-(-)-2-Amino-5-phosphonopentanoic acid
AR	Adrenoceptor
ARH	Arcuate nucleus of the hypothalamus
ATP	Adenosine triphosphate
AMPA	Alpha-Amino-3-Hydroxy-5-Methyl-4-Isoxazole Propionic Acid
AVPV	Anteroventral periventricular nucleus
BAT	Brown adipose tissue
BBB	Blood-brain barrier
BMI	Body mass index
BnST	Bed nucleus of the stria terminalis
BP	Blood Pressure

cAMP	Cyclic adenosine monophosphate
cADP	Cyclic adenosine diphosphate
CART	Cocaine and amphetamine-regulated transcript
CBX	Carbenoxolone
CC	Coupling coefficient
CCK	Cholecystokinin
ChAT	Choline acetyltransferase
CNS	Central nervous system
CR	Calretinin
CRH	Corticotropin-releasing hormone
Cx	Connexin
Δ	Delta
DAG	Diacyl glycerol
db	Leptin receptor gene
DMH	Dorsomedial hypothalamic nucleus
DMV	Dorsal motor nucleus of the vagus
DOPA	Dihydroxyphenylalanine
DRN	Dorsal raphe nucleus
EEG	Electroencephalography
eEPSP	Electrical excitatory post-synaptic potential
eIPSP	Electrical inhibitory post-synaptic potential
EPSP	Excitatory post-synaptic potential
FOXO1	Forkhead box protein O1
FS	Fast spiking interneuron
GABA	γ-Aminobutyric acid

GAD	Glutamate decarboxylase
GE	Glucose excited
GI	Glucose inhibited
GIRK	G-protein coupled inwardly rectifying potassium channel
GJIC	Gap junctional intercellular communication
GK	Glucokinase
GLUT	Glucose transporter
GLP-1	Glucagon-like peptide-1
GnIH	Gonadotropin inhibitory hormone
GnRH	Gonadotropin releasing hormone
GPCR	G-protein coupled receptor
GR	Glucose-responsive
HPA	Hypothalamic-pituitary-adrenal axis
HPG	Hypothalamic-pituitary-gonadal axis
HPT	Hypothalamic-pituitary-thyroid axis
HR	Heart rate
ICV	Intracerebroventricular
IFSECN	The International Federation of Societies for Electroencephalographers
IP_3	Inositol triphosphate
IP	Intraperitoneal
IPSP	Inhibitory post-synaptic potential
IR	Insulin receptor
IRS	Insulin receptor substrate
IV	Intravenous
JAK	Janus kinase

JC	Junctional conductance
K_{ATP}	ATP-sensitive potassium channel
Kir	Inwardly rectifying potassium channel
K_M	Michaelis constant
KNDy	Kisspeptin/neurokinin B/Dynorphin
L	Cortical layer
LC	Locus coeruleus
LH	Lateral hypothalamus
LS	Late spiking interneuron
MAPK	Mitogen-activated protein kinase
MCR	Melanocortin receptor
ME	Median eminence
MES	Maximal electroshock test
MEST	Maximal electroshock seizure threshold test
MPOA	Medial preoptic area
MSN	Medium spiny neuron
mV	Millivolt
MΩ	Megaohm
NA	Noradrenaline
NFS	Non fast spiking interneuron
NBQX	2,3-Dioxo-6-nitro-1,2,3,4-tetrahydrobenzo [*f*]quinoxaline-7-sulfonamide
NDS	Normal donkey serum
NGS	Normal goat serum
NMDA	N-Methyl-D-aspartic acid
NO	Nitric oxide

NPY	Neuropeptide-Y
nS	Nanosiemen
NTS	Nucleus tractus solitarius
ob	Leptin gene
ObR	Leptin receptor
pA	Picoamp
Panx1	Pannexin1
PBS	Phosphate buffered saline
PFA	Paraformaldehyde
PFC	Prefrontal cortex
PI3K	phosphoinositide-3 kinase
PIP_2	Phosphorylate phosphatidylinositide (4,5)-bisphosphate
PIP_3	Phosphorylate phosphatidylinositide (3,4,5)-bisphosphate
PKA	cAMP-dependent protein kinase
PKB	Protein kinase B
PKC	Protein kinase C
PLC	Phospholipase-C
PNS	Parasympathetic nervous system
POA	Preoptic area
POMC	Pro-opiomelanocortin
PTP1B	Protein tyrosine phosphatase 1B
PTZ	Pentylenetetrazole
PV	Parvalbumin
PVH	Paraventricular nucleus of the hypothalamus
PVT	Paraventricular thalamic nucleus

PVZ	Hypothalamic periventricular zone
RCT	Randomized control trial
RIA	Radioimmunoassay
RP	Related peptide
RyR	Ryanodine receptor
SCN	Suprachiasmatic nucleus
SN	Substantia nigra
SNA	Sympathetic nerve activity
SNS	Sympathetic nervous system
SOCS3	Suppressor of cytokine signaling 3
SOM	Somatostatin
SON	Supraoptic nucleus
SPZ	Subparaventricular zone
SSRI	Selective serotonin reuptake inhibitor
STAT3	Signal transducer and activator of transcription 3
SUR	Sulphonylurea receptor
T	Testosterone
T2DM	Type 2 diabetes mellitus
TCPTP	T-cell protein tyrosine phosphatase
TH	Thyroid hormone
TMN	Tuberomamillary nucleus
TRH	Thyrotropin-releasing hormone
TRPC	Transient receptor potential cation channel
TSH	Thyroid stimulating hormone
TTX	Tetrodotoxin

UCP-1	Uncoupling protein-1
VMH	Ventromedial hypothalamic nucleus
VIP	Vasoactive intestinal polypeptide
VTA	Ventral tegmental area
WAT	White adipose tissue
WHO	World Health Organization

Chapter 1: General Introduction

1.1 Energy homeostasis

Energy homeostasis is the regulation of caloric intake and energy expenditure in order to maintain a consistent internal environment. A key regulator of energy homeostasis is the autonomic nervous system (ANS), which modulates the innervation of the internal organs through both its subdivisions; the sympathetic nervous system (SNS) and parasympathetic nervous system (PNS). Both of these arms of the ANS are comprised of pre-ganglionic neurons in the spinal cord, and post ganglionic neurons in the periphery. The pre-ganglionic neurons have afferent connections within the hypothalamus, and along with brainstem nuclei the hypothalamus is one of the key control centers for energy homeostasis, integrating both central and peripheral signals, formulating functional outputs in the form of electrical codes, neurotransmitter and neuropeptide release to drive appropriate target innervation.

1.2 Obesity

Obesity and its associated co-morbidities are immense health and socioeconomic burdens, especially in western societies where high calorie foods are increasingly available and sedentary lifestyles are more commonplace. The most common method of quantifying obesity is the body mass index (BMI) calculated as: Body weight (Kg)/ height $(m)^2$ (Gray and Fujioka, 1991). The world health organization (WHO) defines a value > 25 as overweight, and >30 as obese. In 2005 23.2% of the global adult population was overweight (24.0% men, 22.4% women) (Kelly et al.,

2008). Finkelstein *et al* project obesity rates in the USA to reach 42% by 2030 (Finkelstein et al., 2012). Excess body fat is associated with a number of secondary diseases including type-II diabetes, cardiovascular disease and cancer and as such obesity is an avoidable drain on healthcare resources (Dixon, 2010). Of the USA, estimates from 2008 put the healthcare costs of obese individuals at 41.5% higher than healthy weight individuals, and the total obesity-associated healthcare costs are estimated to be $86 billion USD (Finkelstein et al., 2009). Prevention and intervention strategies aimed at curtailing the current obesity epidemic will result in health and economic benefits.

1.3 The hypothalamus

The hypothalamus is located in the ventral diencephalon, and surrounds the third ventricle. The hypothalamus is located immediately dorsal to the pituitary gland, and exerts direct control over gonadotropin, thyrotropin and corticotropin release through the production and secretion of releasing hormones. It functions as a site of neuronal and hormonal integration. Neurons within it respond to afferent central and peripheral hormonal stimuli in order to generate functional outputs. The hypothalamus exerts a regulatory effect over diverse physiological processes such as, reproduction, blood pressure, temperature regulation, osmoregulation, circadian rhythms, sleep, stress, food intake, and energy expenditure.

The role of the hypothalamus in the regulation of energy homeostasis was initially suggested by (Erdheim, 1904), previous to which dysfunction of the pituitary gland had been assumed to be the etiology of diseases such as obesity (Fröhlich, 1901). Hypothalamic control of energy balance was first formally documented in 1940 with studies by Hetherington and Ranson, showing bilateral

electrolytic lesions in rat the hypothalamus, caused extensive damage to the dorsomedial hypothalamus (DMH), ventromedial hypothalamus (VMH), arcuate nucleus (ARH), the fornix, 'and that portion of the lateral hypothalamic area ventral to it'. The resulting rats were obese, some of which being twice as heavy as controls. Conversely rats given lesions in the lateral hypothalamus (LH) reduced their food intake (Hetherington, 1940). Further work by Anand and Brobeck found that bilateral lesions of the LH resulted in the complete cessation of food intake, causing death by starvation (Anand and Brobeck, 1951). This work indicated that the hypothalamus contained function-specific neuroanatomical loci, controlling specific physiological processes, including a feeding center in the LH and a satiety center in the VMH. Subsequent work has supplanted the view of the hypothalamus as housing function specific "centers", with the concept that it contains discreet neuronal populations, expressing characteristic profiles of receptors, neuropeptides and transmitters.

1.4 The arcuate nucleus of the hypothalamus

The arcuate nucleus of the hypothalamus (ARH) surrounds the ventral end of the third ventricle and is immediately dorsal to the median eminence. The median eminence itself is a circumventricular organ, with a relatively passive blood brain barrier, allowing for proteins as large as horseradish peroxidase to enter the hypophyseal blood (Broadwell and Brightman, 1976) and circulatory factors including the 16 kDa hormone leptin to pass from the blood, into the arcuate nucleus (Banks et al., 1996).

Damage to the ARH caused by gold thioglucose administration is associated with hyperphagia and weight gain in addition to the reduction of both

Neuropeptide-Y (NPY) and pro-opiomelanocortin (POMC) mRNA (Debons et al., 1982, Bergen et al., 1998). 90% of arcuate NPY neurons co-express agouti-related peptide (AgRP) (Broberger et al., 1998), and as such these neurons are termed NPY/AgRP, whilst POMC is co-expressed in neurons with cocaine and amphetamine-regulated transcript (CART) (Elias et al., 1998), these neurons being referred to in the literature as POMC/CART. NPY/AgRP and POMC/CART neurons of the ARH have been extensively studied and are known to be sensitive to glucose and a number of peripheral hormones including leptin, insulin and ghrelin (Spanswick et al., 1997, van den Top et al., 2004, Cowley et al., 2001, Spanswick et al., 2000). In addition to the action of circulatory factors, central inputs also modulate arcuate neuron electrical activity. Arcuate neurons have reciprocal connections with second order neurons in other hypothalamic nuclei including the paraventricular nucleus (PVN), dorsomedial hypothalamic nucleus (DMH), ventromedial hypothalamic nucleus (VMH), lateral hypothalamus (LH) and medial preoptic area (MPO) (Williams et al., 2001, Bouret et al., 2004). These second order neurons then project to extrahypothalamic nuclei such as the nucleus tractus solitarius (NTS) and the dorsal motor nucleus of the vagus (DMV) (Smith and Ferguson, 2008), these pathways providing conduits through which the ARH exerts its influence upon energy homeostasis. The location of hypothalamic nuclei in relation to one another is outlined in Figure 1.1, below:

1.5 NPY/AgRP Neurons

NPY/AgRP neuronal activity promotes feeding and reduces energy expenditure. Optogenetic and pharmacogenetic activation of NPY/AgRP neurons is sufficient to elevate food intake (Aponte et al., 2011, Atasoy et al., 2012, Krashes et al., 2011),

whilst pharmacogenetic inhibition causes a reduction of food intake (Krashes et al., 2011). Ablation of NPY/AgRP neurons in the adult mouse causes a cessation of food intake, ultimately resulting in death by starvation (Luquet et al., 2005). Fasting has been reported to increase NPY/AgRP neuron electrical activity (Takahashi and Cone, 2005), in addition to elevating both NPY and AgRP mRNA expression in the ARH (Hahn et al., 1998).

Multiple peripheral hormones, indicative of energy status, affect the electrical activity of NPY/AgRP neurons. These include membrane hyperpolarization by the adipokine leptin, and membrane depolarization by the gut-derived orexigen ghrelin (van den Top et al., 2004). Insulin is also known to act upon NPY/AgRP neurons (Konner et al., 2007) and has been shown to inhibit neurons of the ARH via the activation of ATP-sensitive potassium (K_{ATP}) channels (Spanswick et al., 2000).

In addition to NPY and AgRP, γ-aminobutyric acid (GABA) is also synthesized within and released by arcuate NPY/AgRP neurons (Horvath et al., 1997). Both NPY and AgRP, when administered through intracerebroventricular (ICV) injection *in vivo* act as orexigens, stimulating food intake (Rossi et al., 1998, Billington et al., 1991). The GABA agonists muscimol and baclofen also stimulate food intake when injected ICV (Olgiati et al., 1980, Ebenezer, 1990).

NPY/AgRP neurons have been shown to receive excitatory glutamatergic innervation from the DMH and to a greater extent from Thyrotropin-releasing hormone (TRH) and pituitary adenylate cyclase-activating polypeptide (PACAP)-expressing neurons of the paraventricular hypothalamus (PVH). Chemogenic stimulation of this synapse *in vivo* results in NPY/AgRP neuron activation and the stimulation of food intake (Krashes et al., 2014).

NPY/AgRP neurons have diverse projection targets including the anterior portion of the bed nucleus of the stria terminalis (aBNST), PVH, paraventricular thalamus (PVT), lateral hypothalamus (LH), central nucleus of the amygdala (CEA), parabrachial nucleus (PBN), POMC neurons and possibly other NPY/AgRP neurons within the ARH itself (Betley et al., 2013). NPY/AgRP target sites affecting food intake to the greatest degree are the BNST, PVH and LH (Betley et al., 2013).

In addition to food intake regulation NPY/AgRP neurons also exert a degree of control over glucose homeostasis. Konner *et al.* demonstrated that insulin signaling within NPY/AgRP neurons is required for the suppression of hepatic glucose production (Konner et al., 2007). NPY/AgRP neurons are also important in the regulation of energy expenditure. In low energy contexts the ARH NPY/AgRP neurons reduce sympathetic outflow and brown adipose tissue (BAT) thermogenesis via the inhibition of dopaminergic PVH neurons (Shi et al., 2013). Together these data indicate a complex population of function-specific NPY/AgRP neurons in the ARH.

1.6 POMC/CART Neurons

POMC/CART neuron activity helps maintain normal energy homeostasis by promoting a decrease in food intake and an increase in energy expenditure (Schwartz et al., 2000). Chronic chemogenic activation of arcuate POMC/CART neurons elevates food intake whilst their ablation results in hyperphagia and obesity (Zhan et al., 2013). POMC neuron activity is elevated in positive energy states, with threefold increases in POMC mRNA expression observed in response to involuntary overfeeding in rats (Hagan et al., 1999). POMC/CART neuron electrical activity is affected by a number of peripheral hormones, including

membrane depolarization by leptin (Cowley et al., 2001) and hyperpolarization by insulin (Williams et al., 2010).

POMC is the precursor of a number of peptides produced within POMC/CART neurons, with post-translational modification yielding a number of functional peptides including the α-, β- and γ_2- melanocyte stimulating hormones (MSHs), corticotrophin (ACTH), corticotrophin-like intermediate peptide (CLIP) and β-endorphin. Also produced are intermediate peptides, resulting from peptide cleavages, the function of which remains unclear (Millington, 2007). Intracerebroventricular (ICV) administration of α-MSH β-MSH and γ_2-MSH can reduce food intake, however α-MSH is the only POMC derivative capable of reducing weight gain (Tung et al., 2006) indicating that it is likely to be the primary anorectic agent produced in these neurons. Chronic ICV CART injection also reduces food intake and bodyweight (Dornonville de la Cour et al., 2001) in rats (Nakhate et al., 2011). Subpopulations of POMC/CART neurons can be distinguished in terms of differential GABA and glutamate expression (Wittmann et al., 2013, Dicken et al., 2012, Hentges et al., 2009). This heterogeneity may be indicative of functional divergences.

POMC/CART neurons receive local GABAergic afferents from arcuate NPY/AgRP neurons and non-NPY/AgRP neurons (Cowley et al., 2001, Vong et al., 2011) as well as glutamatergic innervation from neurons of the medial VMH (Sternson et al., 2005). POMC/CART neuron afferents project to nuclei within the hypothalamus including the ARH, DMH, VMH, LVN, LH, PVN, supraoptic nucleus (SON) and extrahypothalamic areas including the brainstem, nucleus accumbens and amygdala (Bagnol et al., 1999). POMC/CART projections to the PVN are those with the most potent ability to suppress feeding (Bouret et al., 2004).

1.7 The melanocortin system

NPY/AgRP and POMC/CART neurons of the ARH, and the second order neuronal population to which they both project forms the arcuate melanocortin system, which is the key regulator of energy homeostasis within the hypothalamus (Cone, 2005). Five melanocortin receptors (MCRs) exist (MC1R to MC5R), with only MC3R and MC4Rs expressed in the brain (Kishi et al., 2003) (Haskell-Luevano et al., 1999). Melanocortins, released by POMC/CART neuron terminals are the endogenous agonists of MC3 and MC4Rs whilst AgRP released by NPY/AgRP neurons is the endogenous antagonist of these receptors (Cone, 2005). Functionality of the melanocortin receptors is highlighted by the obesity associated with MC3R and MC4R knockout mice (Huszar et al., 1997, Butler et al., 2000). The integration of both POMC/CART and NPY/AgRP neuron signals at the MCR-expressing second order neuron is the site of signal integration, with MCR antagonism promoting feeding, and agonism promoting satiety. Current dogma suggests that in positive energy states, increased POMC/CART neuron activity and decreased NPY/AgRP neuron activity will result in an increased α-MSH and decreased AgRP release at second order neuron melanocortin receptors, promoting receptor agonism, reduced food intake and elevated energy expenditure. Conversely in negative energy states, decreased POMC/CART neuron activity and increased NPY/AgRP neuron activity will result in decreased α-MSH and increased AgRP at second order neuron melanocortin receptors, promoting receptor antagonism, this inducing an increase in food intake and a reduction of energy expenditure.

NPY/AgRP and POMC/CART neurons are functionally antagonistic. Both glucose and hormonal energy status secretagogues affect the electrical activity of

NPY/AgRP and POMC/CART neurons. Orexigenic peptides such as ghrelin excite NPY/AgRP neurons directly. NPY/AgRP neuron activation increases GABA release onto POMC/CART neurons, GABA acting to inhibit POMC neurons (Cowley et al., 2001). Anorexigenic peptides such as leptin and insulin inhibit NPY/AgRP neurons via activation of K_{ATP} channel and excite subpopulations of POMC/CART neurons (Belgardt et al., 2009). The K_{ATP} channel is also the signal transduction endpoint of glucose sensing in POMC/CART neurons, making it a critical regulator of hypothalamic energy homeostasis (van den Top et al., 2007, Parton et al., 2007).

1.8 K_{ATP} channels

K_{ATP} channels are hetero-octamers of four inwardly rectifying potassium channel subunits (Kir6.1, Kir6.2) and four sulphonylurea receptor (SUR1, SUR2) subunits (Miki et al., 1999). K_{ATP} channels are expressed in the heart, brain, skeletal muscle and pancreatic β-cells where they couple the metabolic state of the cell, to the electrical excitability of the cell (Ashcroft, 1988). Coexpression of Kir6.2 and SUR1 in COS-1 cells generates inwardly rectifying potassium channels with single channel conductances of 76 pS at 140 mM K^+ either side of the membrane. These channels are inhibited by ATP in a concentration-dependent manner and exhibited an IC_{50} of 10 μM. The sulphonylureas tolbutamide and glibenclamide inhibit K_{ATP} channels whilst diazoxide stimulates channel activity (Inagaki et al., 1995, Miki et al., 1999).

K_{ATP} channels are vital to glucose homeostasis and hormone signaling in the hypothalamus (Miki et al., 2001, Spanswick et al., 1997, Spanswick et al., 2000) and are expressed on both NPY/AgRP and POMC/CART neurons (Ibrahim et al., 2003, van den Top et al., 2007). In neurons, an increased intracellular ATP/ADP ratio

results in channel closure, resulting in membrane depolarization, conversely a reduction in the ATP/ADP ratio results in channel opening and membrane hyperpolarization (van den Top et al., 2007). In glucose-excited hypothalamic neurons, elevated extracellular glucose concentrations, glucose uptake and metabolism to ATP leads to K_{ATP} channel inhibition and neuron depolarization (Ashford et al., 1990a). K_{ATP} channels are also the signal transduction endpoint of many peripheral hormones that act upon hypothalamic neurons including insulin and leptin (van den Top et al., 2004, Spanswick et al., 1997, Spanswick et al., 2000).

1.9 Ghrelin

Ghrelin is a 28 amino acid orexigenic peptide and is the endogenous ligand of the growth hormone secretagogue receptor (GHSR). Ghrelin is produced within and secreted from A-cells in oxyntic glands of the stomach (Dornonville de la Cour et al., 2001, Sakata et al., 2002). Circulatory ghrelin concentrations rise pre-prandially and fall post-prandially (Cummings et al., 2001, Tschop et al., 2001a). Chronic peripheral administration of ghrelin can induce obesity in mice and rats (Tschop et al., 2000) and in humans, plasma ghrelin concentration is negatively correlated with adiposity (Tschop et al., 2001b). The GHSR1a is the target and signal transducer for ghrelin and is expressed in the anterior pituitary, pancreatic islets, adrenal gland, thyroid, myocardium, hippocampus, substantia nigra pars compacta (SNc), ventral tegmental area (VTA), raphe nuclei, in growth hormone releasing hormone (GHRH) neurons and NPY/AgRP neurons of the ARH (Zigman et al., 2006, Willesen et al., 1999).

The orexigenic effects of ghrelin have been attributed to its actions at arcuate NPY/AgRP neurons as knockout of both NPY and AgRP in mice prevents

ghrelin from inducing feeding (Chen et al., 2004). Van den Top *et al* demonstrated that ghrelin depolarizes NPY/AgRP pacemaker neurons of the ARH, with rhythmic firing resulting from the activation of low-threshold T-type calcium, and outwardly rectifying potassium conductances, with this increase in orexigenic neuron output attributed to ghrelin-induced hyperphagia (van den Top et al., 2004).

1.10 Insulin

Insulin was isolated in 1921 (Bliss, 1982), and in 1955 it became the first protein to have its primary amino acid structure sequenced, winning Fred Sanger his first Nobel prize (Sanger, 1988). It is produced within pancreatic β-cells from which it is secreted in response to elevated blood glucose (Rorsman and Braun, 2013). Insulin functions to lower plasma glucose concentration by increasing glucose uptake to peripheral muscle and fat and reducing hepatic glucose production (Woods et al., 2006). The mechanism of secretion is K_{ATP} channel-dependent, with glucose uptake via GLUT1 and GLUT3 in humans and GLUT2 in rodents, followed by metabolism to ATP, inhibition of K_{ATP} channels, membrane depolarization and insulin exocytosis (Rorsman and Braun, 2013).

The insulin receptor (IR) is expressed throughout the CNS, including the olfactory bulb, cerebellum, dentate gyrus, hippocampus, choroid plexus and ARH (Marks et al., 1990). Centrally acting insulin has been shown to reduce food intake and hepatic glucose production via arcuate POMC/CART and NPY/AgRP neurons respectively (Benoit et al., 2002, Konner et al., 2007). Electrophysiological evidence has demonstrated that insulin activates K_{ATP} channels in the lean rat ARH (Spanswick et al., 2000), and that it hyperpolarizes both POMC/CART neurons

(Williams et al., 2010) and NPY/AgRP neurons (Konner et al., 2007) via phosphoinositide-3 kinase (PI3K) and K_{ATP} channels (Plum et al., 2006b).

1.11 Leptin

Leptin, the 16kDa product of the ob gene (Zhang et al., 1994), is produced in adipocytes and plasma leptin levels are proportional to body adiposity (Considine et al., 1996). Leptin regulates energy homeostasis through actions at leptin receptor (LepR)-expressing neurons throughout the hypothalamus including arcuate NPY/AgRP, POMC/CART neurons, and LepR-expressing neurons in the DMH (Cowley et al., 2001, Enriori et al., 2011, Spanswick et al., 1997). In the ARH leptin has been shown to hyperpolarize a population of neurons via K_{ATP} channel activation, these neurons are now understood to be NPY/AgRP neurons (Spanswick et al., 1997). It has also been demonstrated that leptin depolarizes POMC neurons (Cowley et al., 2001) leading to elevated αMSH and increased MC4R-dependent activation of neurons in the PVH, resulting in elevated energy expenditure and reduced food intake (Cone, 2005).

One major reason for the development of obesity is that, despite increased circulatory leptin with increased fat mass, ARH neurons develop leptin resistance and no longer recognize exogenous leptin (Enriori et al., 2007). Despite the development of leptin resistance in the ARH in obesity, resistance is not observed in other hypothalamic nuclei including the DMH, here leptin has been shown to regulate sympathetic outflow, BAT thermogenesis and blood pressure via LepR neuron depolarization (Simonds et al., 2014, Enriori et al., 2011).

1.12 Leptin Signaling

The long-form leptin receptor (ObRb) is a member of the cytokine family of receptors, structurally associated with Janus-activated kinase 2 (JAK2). Leptin receptor activation initiates receptor structural conformation change allowing autophosphorylation of JAK2 following BOX1 binding. JAK2 then phosphorylates the leptin receptor at tyrosine (Y) residues 985, 1077 and 1138. Y1138 phosphorylation activates signal transducer and activator of transcription 3 (STAT3). Phosphorylated STAT3 then translocates to the nucleus where it dimerizes and modifies gene expression (Increased POMC and reduced AgRP).

Nuclear pSTAT3 activates suppressor of cytokine signaling 3 (SOCS3) that effects negative feedback on leptin signaling, inhibiting Y985 phosphorylation by JAK2. Y985 phosphorylation initiates SHP2 phosphorylation and stimulation of MAPK signaling. SHP2 disinhibits leptin signaling via competing with SOCS3 for JAK2 binding, preventing dephosphorylation. Activated JAK2 also phosphorylates insulin receptor substrate 2 (IRS2), stimulating the phosphatidylinositide 3-kinase (PI3K) signaling cascade. Here, phosphatidylinositide (4,5)-bisphosphate (PIP_2) is phosphorylated on position 3 of its inositol ring, forming phosphatidylinositide (3,4,5)-bisphosphate (PIP_3). PIP_3 signaling includes AMPK inhibition and K_{ATP} channel activation (Zhang et al., 2015). An overview of leptin receptor signal transduction is outlined in figure 1.2.

Although the functional significance of leptin-induced MAPK signaling remains unclear, SHP2 is required for the activation of ERK, which is protective against hyperphagia and hyperglycemia (Krajewska et al., 2008). STAT3 is required for normal energy homeostasis and hypothalamic signaling is drives decreased food intake and increased energy expenditure. Disruption of STAT3

signaling in POMC neurons results in hyperphagic, obese mice (Xu et al., 2007, Saadat et al., 2012). Conversely activation of STAT3 in AgRP neurons confers resistance to obesity via increased energy expenditure (Mesaros et al., 2008).

Leptin simulation of the PI3K pathway can be effected through two mechanisms, 1: IRS stimulation of PI3K, assisted by P85 and p110 (Xu et al., 2005). 2: Inhibition of phosphatase tensin homologue (PTEN) by leptin, resulting in PI3K disinhibition. Although leptin and insulin can activate PI3K concomitantly, insulin is unable to inhibit PTEN. Differences in the physiological response to central leptin and insulin signaling may be attributable to this divergence in signaling. PI3K signaling in hypothalamic neurons mediates changes in electrical activity. In NPY/AgRP neurons of the ARH, increased intracellular PIP_3 activates K_{ATP} channels, inducing membrane hyperpolarization, and this signaling is required for the anorectic effects of leptin *in vivo* (Niswender and Schwartz, 2003). In arcuate POMC neurons, PI3K-activated PLC activates transient receptor potential cation channels (TRPC), resulting in membrane depolarization (Qiu et al., 2010).

1.13 Insulin signaling

Insulin receptors are also expressed on both NPY/AgRP and POMC/CART neurons. Binding of insulin to the insulin receptor (IR) initiates Y1162 and Y1163 phosphorylation, IRS2 phosphorylation and PI3K activation. The conversion of PIP_2 to PIP_3 then stimulates protein kinase B (PKB) to phosphorylate forkhead box protein (FOXO1), increasing POMC and decreasing AgRP expression. Insulin-induced elevated cytoplasmic PIP_3 also activates K_{ATP} channels, hyperpolarizing the neuron (Zhang et al., 2015). POMC neurons of the ARH are depolarized by

insulin via TRPC channels (Qiu et al., 2014). An overview of Insulin and Leptin receptor signaling is outlined in figure 1.2, below:

1.14 Protein tyrosine phosphatases; hypothalamic leptin signaling

The protein tyrosine phosphatases T cell protein tyrosine phosphatase (TCPTP) and protein tyrosine phosphatase 1B (PTP1B) have been implicated in attenuating central leptin and insulin signaling (proposed sites of action are shown in figure 1.2).

Increased expression levels of TCPTP and PTP1B in both NPY/AgRP and POMC/CART neurons of obese mice has been suggested responsible for the central leptin and insulin resistance associated with clinical obesity (Loh et al., 2011). PTP1B attenuates leptin signaling by dephosphorylating tyrosine residues 1007 and 1008 in the JAK2 activation loop. Knockout of PTP1B in neurons and glia results in mice resistant to diet-induced obesity, with decreased food intake, elevated energy expenditure and increased leptin sensitivity (Bence et al., 2006).

TCPTP impairs the ability of leptin to regulate gene expression via the dephosphorylation of nuclear STAT3. Brain-specific TCPTP knock out promotes STAT3 signaling and increased expression of POMC expression and reduced expression of AgRP (Loh et al., 2011). SOCS3 is an additional negative regulator of hypothalamic leptin signaling, activated by nuclear pSTAT3. SOCS3 dephosphorylates and in doing so, inhibits the ability of JAK2 to activate signal transduction (Bjorbaek et al., 1999). SOCS3 knockout mice are resistant to obesity (Kievit et al., 2006)

1.15 Protein tyrosine phosphatases; hypothalamic insulin signaling

Both PTP1B and TCPTP attenuate insulin signaling via dephosphorylation of 1162 and 1163 tyrosine residues of the IR. Hypothalamic PTP1B knockdown increases insulin signaling and produced DIO resistant rats (Picardi et al., 2008) (Dodd et al., 2015).

1.16 Glucose

The provision of glucose is a prerequisite for mammalian life and is the primary fuel source of the brain. Glucose is used to synthesize the ATP required for neuronal maintenance and the production of brain-derived transmitters and metabolites (Mergenthaler et al., 2013). All glucose utilized by the CNS is absorbed from the circulation, as such central glucose concentration is the product of peripheral glucose concentration and is around 20% of that found in the blood (Simpson et al., 2007). Glucose transport across the BBB is mediated primarily by GLUT1, which is also responsible for uptake from extracellular fluid to astrocytes, oligodendrocytes and microglia whilst GLUT3 is primarily responsible for neuronal uptake (Simpson et al., 2007).

All neurons rely upon glucose to function, however specialized neuronal populations regulate glucose homeostasis by facilitating changes in food intake, energy expenditure and hepatic gluconeogenesis (Lam, 2010). Whilst some of these neurons respond to circulatory hormones indicative of somatic energy status, others are intrinsic glucose sensors, altering their electrical activity in direct response to changes in ambient glucose concentration (Spanswick et al., 1997, Routh, 2010). Glucose sensing regions of the hypothalamus are the LH, VMH and the ARH. Both the ARH and VMH are in close apposition to the BBB, leaving

them exposed to constant fluctuations in peripheral glucose concentrations. Glucose-sensing neurons can be divided into glucose inhibited (GI) and glucose excited (GE). GI neurons decrease their electrical activity in response to elevated extracellular glucose whilst GE neurons increase their electrical activity in response to increased central glucose concentration. Multiple mechanisms of neuronal GI have been proposed and include Na^+/K^+ ATPase pump, K^+, and Cl^- channels (Oomura et al., 1974, Fioramonti et al., 2007, Burdakov and Gonzalez, 2009, Jordan et al., 2010, Canabal et al., 2007). The mechanism of GE in both the VMH ad ARH has been determined to occur via glucose-induced ATP-dependent K_{ATP} channel inhibition (Spanswick et al., 1997, Ashford et al., 1990a, Ashford et al., 1990b). This mechanism is analogous to β-cell glucose sensing whereby cellular glucose uptake is mediated by a GLUT, followed by glycolysis, elevated ATP/ADP ratio, K_{ATP} channel inhibition and membrane depolarization (Schuit et al., 2001).

Both NPY/AgRP and POMC/CART neurons express functional K_{ATP} channels (Parton et al., 2007, van den Top et al., 2007) and both cell types contain glucose-sensing subpopulations (Claret et al., 2007). Previous studies have determined NPY/AgRP neurons to be GI (Muroya et al., 1999), whilst POMC/CART neurons have been found to be GE (Ibrahim et al., 2003). It has been demonstrated that functional K_{ATP} channels on POMC neurons is required for normal glucose tolerance (Parton et al., 2007), whilst K_{ATP} channels on NPY/AgRP neuron membranes are required for hepatic glucose production (Konner et al., 2007).

All cells of the CNS require glucose for survival. Astroglia outnumber neurons in the CNS and some evidence suggests that glia-neuron connectivity is a mechanism of central glucose sensing. Glia modulate synaptic properties and neuronal activity through the removal of neuronal transmitters from the

extracellular space and through the release of gliotransmitters (Belanger et al., 2011, Belanger and Magistretti, 2009). Gliotransmitters include glutamate D-serine, ATP and adenosine (Volterra and Meldolesi, 2005, Belanger et al., 2011). For some time, glia have been implicated in central glucose metabolism. Magistretti *et al* suggest that glucose is taken-up by glia, within which it is metabolized to lactate. Lactate is then released into the extracellular space and transported into neurons, which then use it as a substrate for oxidative metabolism (Magistretti et al., 1999). More recent work suggests that glucose sensing in arcuate NPY/AgRP is via glial release of adenosine. Yang *et al* conclude that the release of adenosine from hypothalamic astrocytes activates A_1 adenosine receptors on NPY/AgRP neurons, inhibiting them (Yang et al., 2015). Some evidence exists, linking adenosine receptors to K_{ATP} channels (Heurteaux et al., 1995, Kleppisch and Nelson, 1995, Tang et al., 1999). Hypothalamic adenosine receptor-K_{ATP} channel signal transduction may well be a critical mechanism of central glucose sensing.

1.17 Adenosine

Adenosine is a ribonucleoside important in multifarious biochemical processes in all life. It is most recognizable as one of the four building blocks of nucleic acids and as a coenzyme, when in its phosphorylated state; adenosine triphosphate (ATP) (Watson and Crick, 1953, Knowles, 1980). In addition to its role in cellular metabolism, adenosine has been shown to act as a neuromodulatory agent in the CNS. Here adenosine has a regulatory role in physiological processes such as arousal, memory and learning, cognition and sleep and has been implicated in a

number of pathophysiological processes including Parkinson's disease, stroke, epilepsy, pain, schizophrenia and depression (Sebastiao and Ribeiro, 2009).

Adenosine is produced as a product of adenosine monophosphate (AMP) hydrolysis by ecto-5'-nucleotidases, this occurring both within CNS cells and in the extracellular space (Latini and Pedata, 2001). Adenosine does not function as a classical neurotransmitter in that its release mechanism is not via synaptic vesicles but is instead via nucleoside transporters (Gu et al., 1995). Four G-protein coupled adenosine receptors exist within the CNS; A_1, A_{2A}, A_{2B} and A_3 (Fredholm et al., 1994). Adenosine receptors would appear to be somewhat ubiquitous throughout the CNS, with A_1 and A_{2A} receptors being present in all neurons and glia (Sebastiao and Ribeiro, 2009). Generally, A_1 and A_3 receptor activation elicits inhibitory effects whilst A_{2A} and A_{2B} mediate excitatory actions on CNS cells (Klinger et al., 2002).

1.17.1 The A_1 adenosine receptor

A_1 receptors are exclusively coupled to G_i and G_o proteins (Klinger et al., 2002). Here, G-proteins inhibit adenylate cyclase and reduce intracellular cAMP production from ATP and in turn reduce the activity of cAMP-dependent protein kinase (PKA) (Dunwiddie and Masino, 2001). A_1 receptor signaling is inhibitory and is neuroprotective in hypoxic and excitotoxic conditions (Latini and Pedata, 2001). A_1 activation can elicit membrane hyperpolarization independent of cAMP, via G protein-gated inwardly rectifying K^+ channels (GIRKs) (Bunemann and Pott, 1995), and can also induce neuronal membrane inhibition via the reduction of N-type calcium channels (Mynlieff and Beam, 1994). Inhibition of AgRP neurons via

astrocytic adenosine release and A_1 receptor activation has been demonstrated to inhibit food intake in mice (Yang et al., 2015).

1.17.2 The A_{2A} adenosine receptor

A_{2A} receptors are G_s-protein coupled (Klinger et al., 2002), ligand binding activating the cAMP-dependent pathway through increasing adenylate cyclase activity and stimulating PKA activity (Dunwiddie and Masino, 2001). In arterial myocytes adenosine-induced membrane hyperpolarization has been suggested to be via an A_2-PKA-K_{ATP} channel-dependent mechanism (Kleppisch and Nelson, 1995).

1.17.3 The A_{2B} adenosine receptor

A_{2B} receptors couple to both G_s and G_q proteins and have a low affinity for adenosine relative to other adenosine receptors (>10 μM vs. 0.1-1 μM) (Klinger et al., 2002). G_s signaling activates the cAMP-dependent pathway, whilst G_q signaling activates phospholipase-C (PLC) to hydrolyze PIP_2 to diacylglycerol (DAG) and inositol triphosphate (IP_3), with DAG then activating protein kinase C (PKC) (Dunwiddie and Masino, 2001).

1.17.4 The A_3 adenosine receptor

A_3 receptors are coupled to G_i and G_o proteins (Klinger et al., 2002) and bind adenosine with similar affinity to the A_1 receptor. Signal transduction inhibits adenylate cyclase and reduces intracellular cAMP production, reducing the activity of PKA (Dunwiddie and Masino, 2001). This inhibitory adenosine receptor differs

from A_1 in that it undergoes rapid, agonist-dependent desensitization (Palmer et al., 1996).

1.18 The dorsomedial nucleus of the hypothalamus

The dorsomedial nucleus of the hypothalamus (DMH) is located lateral to the dorsal-end of the third ventricle, immediately posterior to the PVH (Paxinos, 2008). The DMH has been implicated in a variety of physiological processes including food intake, reproduction, stress, circadian rhythms, energy expenditure and blood pressure regulation (Simonds et al., 2014, Bernardis, 1972, Coolen et al., 1996, Gallo, 1981, Inglefield et al., 1994, Keim and Shekhar, 1996, Bellinger et al., 1976, Enriori et al., 2011). The DMH receives afferent inputs from the suprachiasmatic nucleus (SCN), the hypothalamic periventricular zone (PVZ), ARH, VMH and PVH and sends intrahypothalamic projections to the PVH, preoptic area (POA), ARH and LH (Gautron et al., 2010), whilst extrahypothalamic efferents include the Raphe pallidus nucleus (RPa) and the rostral ventrolateral medulla (RVLM), the former connection being important in BAT thermoregulation (Zhang et al., 2011) and the latter more closely controlling blood pressure (Horiuchi et al., 2006). The molecular and pharmacological profiles of DMH neurons remain relatively uncharacterized, when compared to other hypothalamic nuclei. However, it is known that some DMH neurons express leptin receptors (Enriori et al., 2011). Another peptide expressed in DMH neurons is gonadotrophin inhibitory hormone (GnIH) (Soga et al., 2014).

1.19 Gonadotropin inhibitory hormone

In 2000, Tsutsui *et al.,* discovered a novel neuropeptide in the quail hypothalamus, capable of inhibiting luteinizing hormone (LH) and follicle stimulating hormone (FSH) release from the anterior pituitary (Tsutsui et al., 2000). Previous to this, gonadotropin-releasing hormone (GnRH) was thought to be the only hypothalamic peptide involved in the regulation of gonadotropin release. In mammals, two GnIH variants are translated; GnIH-RP-1 and GnIH-RP-3 (Tsutsui et al., 2010). In the rat, GnIH is produced within neurons of the DMH and tuberomamillary nucleus (TMN) (Johnson et al., 2007). Extrahypothalamic GnIH neuron projections have been demonstrated throughout the amygdala, bed nucleus of the stria terminalis (BnST), septal nuclei and the paraventricular thalamic nucleus (PVT) (Johnson et al., 2007) whilst GnIH projections within the hypothalamus include the medial preoptic area (MPOA) and other neurons within the DMH (Johnson et al., 2007). In the rat 75% of GnIH projections in the MPOA have been shown to co-localize with GnRH cell bodies (Johnson et al., 2007) whilst in sheep and primates GnIH immunoreactive terminals have been observed in the neurosecretory zone of the median eminence (Clarke et al., 2008, Ubuka et al., 2009a, Ubuka et al., 2009b). The lack of interspecies consistency of GnIH neuron projection sites suggests a degree of variation in the specific regulatory mechanisms of gonadotropin secretion.

GnIH is the endogenous agonist of the GPR147 receptor, the receptor being located in both the gonads and CNS (Ubuka et al., 2013). In the ovine brain, GPR147 is expressed in the suprachiasmatic nucleus, supraoptic nucleus periventricular nucleus and the pars tuberalis of the anterior pituitary (Clarke, 2011). In the Siberian hamster over 85% of GnRH-expressing neurons in the POA

express GPR147 (Ubuka et al., 2012) and in the mouse application of GnIH-3 has been found to inhibit a subset of GnRH neurons (Ducret et al., 2009). Wu *et al.* indicate the mechanism of inhibition to be via potassium conductance activation (Wu et al., 2009).

Reproductive competence is affected by various factors including stress and energy status (ECWG, 2006). Changes in nutrient availability are coupled with fluctuations in the central concentration of energy status secretagogues, such as ghrelin and thyrotropin releasing hormone (TRH). Although there is a lack of literature regarding the effects of TRH on reproductive function, ghrelin is known to inhibit GnRH and LH pulse frequency *in vivo* (Fernandez-Fernandez et al., 2004). Serotonin and noradrenaline are central transducers of environmental stress signals. Some evidence suggests that the central noradrenergic and serotonergic systems negatively regulate the hypothalamic-pituitary-gonadal axis via actions at GnIH neurons (Tobari et al., 2014, Geraghty et al., 2015, Soga et al., 2010).

1.20 5-Hydroxytryptamine

5-Hydroxytryptamine (5-HT) was first isolated and characterized in 1948 by Rapport and Page (Rapport et al., 1948). Its role as a neurotransmitter was initially proposed in 1957 by Brodie and Shore (Brodie and Shore, 1957), whilst Dahlstrom and Fuxe were the first to map the distribution of 5-HT expression in the CNS (Dahlstrom and Fuxe, 1964). 5-HT, a monoamine is synthesized from tryptophan. The amino acid is hydroxylated by tryptophan hydroxylase to form 5-hydroxytryptophan (5-HTP), and then decarboxylated by tryptophan decarboxylase to form 5-HT (Clark et al., 1954).

Within the CNS, 5-HT is produced within neurons of the raphe nuclei in the brainstem, some of which send descending projections, to the medulla and spinal cord whilst ascending projections extend to areas of the forebrain including the hypothalamus (Dahlstrom and Fuxe, 1964). 5-HT has been implicated in the regulation of hypothalamic processes including food intake, body weight and reproductive function (Blundell, 1984, Soga et al., 2015, Soga et al., 2010).

There are 14 subtypes of 5-HT receptors, divided into 7 classes (5-HT_1 through 5-HT_7), all of which are metabotropic with the exception of the ionotropic 5-HT_3-receptor (Derkach et al., 1989, Puig and Gulledge, 2011). Metabotropic 5-HT receptors are G-protein-coupled, 7-transmembrane domain receptor class receptors. With the exception of 5-HT_3 receptors, all 5-HT receptors mediate their electrophysiological effects on neurons through potassium channel modulation. 5-HT 1A, 1D, 1F, 2A, 2B, 3A, 5A, 5B, 6 and 7 receptors (but not 2C, 3B or 4) are expressed in all GnIH neurons (Soga et al., 2010) and the selective serotonin reuptake inhibitor (SSRI) citalopram can cause sexual dysfunction (de Jong et al., 2005) (Soga et al., 2010). Citalopram treatment is also associated with reduced GnRH and elevated GnIH mRNA expression (Soga et al., 2010, Prasad et al., 2015).

1.20.1 The 5-HT_1 receptors

The 5-HT_1 receptor class contains five isoforms; 5-HT_{1A}, 5-HT_{1B}, 5-HT_{1D}, 5-HT_{1E} and 5-HT_{1F}. All subtypes couple to $G_{i/o}$-proteins to inhibit adenylyl cyclase and decrease intracellular adenosine-mono-phosphate (cAMP) (Barnes, 2011). 5-HT_{1A} is expressed throughout the CNS including the limbic system, raphé nuclei and hypothalamus, located on soma, dendrites and axon hillocks. It functions as an auto-receptor on all serotonergic neurons. 5-HT_{1B} is found throughout the

mammalian CNS including the hippocampus, striatum, cerebellum and basal ganglia. It is expressed on both serotonergic and non-serotonergic neuron axon terminals. 5-HT_{1D} expression levels are highest in the raphé nuclei whilst expression is also found in the amygdala and caudate-putamen. 5-HT_{1E} functions remain unclear however it is expressed in the cortex caudate-putamen and amygdala (Bruinvels et al., 1994). 5-HT_{1F} receptors are expressed at relatively low levels within the CNS, but are found in areas including the raphé nuclei, hippocampus, striatum, thalamus, trigeminal ganglion and vestibular nucleus (Barnes, 2011).

1.20.2 The 5-HT_2 receptors

There are three isoforms of 5-HT_2 receptors, 5-HT_{2A}, 5-HT_{2B} and 5-HT_{2C}, all of which excite neurons through coupling to $G_{q/11}$-proteins, increasing intracellular IP_3 and diacylglycerol (DAG). 5-HT_{2A} receptors are expressed in the hippocampus, hypothalamus, amygdala, substantia nigra and cerebral cortex. 5-HT_{2A} agonists are psychotomimetic and as such this receptor is the target for antipsychotic medications (Barnes, 2011). The physiological significance of 5-HT_{2B} receptors remains unclear however expression is found in the cerebellum, amygdala and raphé nuclei. 5-HT_{2C} receptors are expressed in the choroid plexus, substantia nigra and globus pallidus. 5-HT_{2C} receptors are expressed on POMC neurons of the ARH and are a target for appetite suppressive drugs (Doslikova et al., 2013).

1.20.3 The 5-HT_3 receptor

This 5-HT receptor is an exception in that it is a ligand gated non-selective cation channel, not a GPCR, mediating fast, excitatory neurotransmission. Highest levels

within the CNS are found in brainstem nuclei, including the dorsal motor nucleus of the vagus nerve, area postrema and NTS (Pratt et al., 1990). Expression is also found within the hippocampus, amygdala and caudate putamen (Barnes, 2011).

1.20.4 The 5-HT$_4$ receptor

5-HT$_4$ receptors are G_s-protein coupled and activation excites neurons via increasing intracellular cAMP levels and potassium channel inhibition. CNS expression levels are highest in the substantia nigra, globus pallidus, caudate putamen, nucleus accumbens, hypothalamus, hippocampus and cortex (Varnas et al., 2003) and would appear to be predominantly postsynaptic.

1.20.5 The 5-HT$_5$ receptors

Both 5-HT$_{5A}$ and 5-HT$_{5B}$ receptors are $G_{i/o}$-protein coupled, and inhibit neurons through decreasing intracellular cAMP and activating a potassium conductance (Hurley et al., 1998). 5-HT$_{5A}$ receptor expression is found in the hypothalamus, raphe nuclei, locus coeruleus, and amygdala and to a lesser extent in the cerebral cortex, hippocampus substantia nigra, ventral tegmental area (VTA) and cerebellum (Pasqualetti et al., 1998). 5-HT$_{5B}$ receptor expression is found in the hippocampus, dorsal raphé, habenula, entorhinal cortex, piriform cortex and olfactory bulb (Matthes et al., 1993).

1.20.6 The 5-HT$_6$ receptors

5-HT$_6$ receptors are G_s-protein coupled and excite neurons via activating adenylyl cyclase, increasing intracellular cAMP levels and inhibiting a potassium

conductance. Expression is found in the striatum, nucleus accumbens, hippocampus and neocortex (Lieben et al., 2005). Receptor agonism has been found to improve memory and cognition (Ramirez, 2013).

1.20.7 The 5-HT_7 receptor

5-HT_7 receptors are Gs-protein coupled and excite neurons via increasing intracellular cAMP levels and inhibiting a potassium conductance. Receptor expression in found within the thalamus, hypothalamus, hippocampus and amygdala (Bonaventure et al., 2011). Some evidence suggests that 5-HT_7 receptor antagonism may be an effective antidepressant strategy (Hedlund, 2009).

1.21 Noradrenaline

Central noradrenaline (NA) is produced within neurons of the locus coeruleus, dorsal vagal complex and ventrolateral medulla (Dahlstrom and Fuxe, 1964, Sawchenko and Swanson, 1981). NA, a catecholamine, is synthesized from tyrosine. Tyrosine is hydroxylated to dihydroxyphenylalanine (DOPA), decarboxylated to dopamine (DA) by aromatic L-amino acid decarboxylase. DA-β-hydroxylase then converts DA to NA (Fernstrom and Fernstrom, 2007). In dopaminergic neurons DA-β-hydroxylase is not expressed, and DA is not hydroxylated to NA. NA functions in the CNS to regulate sensory, memory and motor and mood processes (Berridge and Waterhouse, 2003). Noradrenergic neurons of the locus coeruleus project throughout the CNS, with a notable absence of terminals in the striatum and globus pallidus (Berridge and Waterhouse, 2003).

Multiple hypothalamic nuclei including the PVN and supraoptic nucleus (SON) receive noradrenergic afferents (Sawchenko and Swanson, 1981), and NA-

sensitive neurons have been detected in other hypothalamic nuclei including orexin-neurons of the LH (Yamanaka et al., 2006) and NPY/AgRP neurons of the ARH (Kang et al., 2000). Elevated extracellular NA has also been implicated in the DMH-dependent panic response (Shekhar et al., 2002). Injection of NA to the PVH stimulates food intake, and elevates plasma coritcosterone and vasopressin (Leibowitz et al., 1988). Both α-adrenoceptors (α-ARs) and β-adrenoceptors (β-ARs) are GCPRs and bind both NA and adrenaline (Cotecchia et al., 1998). The α-AR group contains α_{1a}, α_{1b}, α_{1d}, α_{2a}, α_{2b} and α_{2c} whilst the β-ARs include β_1, β_2 and β_3 (Cotecchia et al., 1998). α_1-AR activation generally mediates neuronal excitation whilst α_2-AR and β-AR activation results in membrane hyperpolarization (Hein, 2006). Of the α-ARs, α_1-ARs are $G_{q/11}$ coupled and receptor activation results in PLC activation, elevations in intracellular IP3 and calcium mobilization (Koshimizu et al., 2007). α_2-ARs are $G_{i/o}$ coupled and receptor activation results in adenylate cyclase inhibition, reductions in intracellular cAMP, inhibition of voltage-gated Ca^{2+} channels and activation of G-protein coupled inwardly rectifying potassium channels (GIRKs) (Hein, 2006).

1.22 Thyrotropin-releasing hormone

Thyrotropin-releasing hormone (TRH) is a key regulator of plasma thyroid hormone (TH) concentration (Lechan and Fekete, 2006). Neurons originating in the PVH and LH release TRH at the median eminence, stimulating thyrotropin secreting hormone (TSH) from the pituitary, which in turn stimulates the thyroid gland to produce the thyroid hormones T_3 and T_4. Thyroid hormones then provide negative feedback to hypothalamic TRH neurons, completing the self-regulatory

loop (Ghamari-Langroudi et al., 2010). T_3 and T_4 are key regulators of tissue development, membrane transport and cellular metabolism (Davis et al., 2016).

TRH neurons, in addition to hormonal regulation by T_3 and T_4, are innervated by arcuate NPY and POMC neurons (Toni et al., 1990, Fekete et al., 2000), brainstem noradrenergic neurons (Tapia-Arancibia et al., 1985, Shioda et al., 1986) and neurons of the DMH (Ghamari-Langroudi et al., 2010). The hypothalamic-pituitary-thyroid (HPT) axis is regulated by energy status and TRH gene expression is positively regulated by leptin (Ghamari-Langroudi et al., 2010). Reduced plasma leptin, resulting from reduced food intake, results in reduced TRH expression and reduced somatic energy expenditure. Leptin increases TRH neuron activity both directly at leptin receptors on TRH neurons, and via MC4R agonism due to increased POMC neuron activity (Ghamari-Langroudi et al., 2010).

1.23 Gap-junctions and electrotonic coupling

Gap-junctions are transmembrane proteins, providing direct intercytoplasmic links between adjacent cells in animals, allowing for the electrical and metabolic coupling of extensive cellular networks (Harris, 2001, Orellana et al., 2009, Saez et al., 2005). Two distinct protein families are responsible for gap-junction formation; pannexins and connexins. Pannexins are found in all eumotazoa with the exception of echinoderms. Orthologous proteins in non-chordates are termed innexins. Connexins are found exclusively in chordates (Abascal and Zardoya, 2013).

To date, 20 connexin (Cx) genes have been identified in mice, and 21 in humans, 19 of which are considered to be orthologous (Sohl and Willecke, 2004). Connexin isoforms are differentially expressed both temporally and spatially in

mammalian tissues, gap-junctions would seem to be somewhat ubiquitous, with the few naive cell populations including circulatory cells (Dbouk et al., 2009).

All connexin proteins share a conserved topology, with four transmembrane domains, termed M1, M2, M3 and M4. The N and C termini are both located on the cytoplasmic face of the membrane with the N terminus upstream of M1, and the C-terminus downstream of M4. Two extracellular loops, E1 and E2, connect M1 to M2 and M3 to M4 respectively, whilst an intracellular loop domain connects M2 to M3 (Harris, 2001, Meier and Dermietzel, 2006). Connexin-based gap-junction channels consist of two 'docked' hemichannels or connexons, one contributed by each cell membrane. Each hemichannel is a hexamer of connexin subunits, which oligomerize in the endoplasmic reticulum. The hemichannel is then processed through the golgi apparatus (Segretain and Falk, 2004), trafficked to and inserted in the plasma membrane. These channels then dock to other hemichannels in opposing plasma membranes via their extracellular E1 and E2 moieties. This results in the formation of an intercellular gap junction channel (IGJC) (Harris, 2001). However hemichannels may remain undocked within the plasma membrane where they may act as functional ion channels (Saez et al., 2005). Connexin subunit and hemichannel topology are outlined in Figure 1.3.

Hemichannels exist in both homomeric and heteromeric combinations, homomeric describing a hemichannel composed of six identical connexin isoforms, whilst heteromeric describes a hemichannel formed of a combination of two or more isoforms (Dbouk et al., 2009, Harris, 2001). Furthering the degree of structural heterogeneity amongst connexins is the existence of both homotypic and heterotypic gap junction formation, with homotypic describing a junction

formed of two symmetrical hemichannels and heterotypic referring to a structurally asymmetrical junction. Some hemichannels are only capable of forming homotypic gap junctions (e.g. Cx36) whilst other isoforms are capable of docking with multiple others. As each connexin has unique biophysical properties, heterotypic channels confer specific biophysical properties to the junction such as channel rectification and the existence of sub-conductance states (Harris, 2001).

1.24 Connexins in the Central Nervous System

11 connexins are expressed in the rodent CNS (Belousov and Fontes, 2013), six of which are expressed in neurons (Sohl et al., 2005). The differential expression of connexins is outlined in table 1.1, below:

Isoform	Cell type
26	Neuron, astrocyte
29	Oligodendrocyte
30	Astrocyte
32	Neuron, oligodendrocyte
36	Neuron, oligodendrocyte, microglia
37	Neuron
40	Neuron (developing), astrocyte
43	Neuron, astrocyte, microglia (activated)
45	Neuron, astrocyte
46	Astrocyte
47	Neuron, astrocyte, oligodendrocyte

Table 1.1: Differential tissue expression of connexin isoforms

Adapted from (Nakase and Naus, 2004).

Differential knock out of CNS connexin isoforms yields a variety of phenotypes in mouse models, outlined in table 1.2, below:

Knockout mouse	Phenotype
Cx26	Embryonic lethal
$Cx26^{fl/fl}$ Otog-cre	Hearing impairment
Cx30	Sever hearing impairment
Cx32	PNS demyelination, CNS hyperexcitability, Increased ischemic injury
Cx36	Visual deficit Desynchronization of cortical and hippocampal gamma oscillations Desynchronization of neocortical interneuron activity
Cx43	Neonatal lethal Embryonic neural crest migration deficit Embryonic neocortical neuron migration deficit
(Cx43+/-)	Increased ischemic injury
$Cx43^{fl/fl}$ GFAP-cre	Increased spreading depression in hippocampus Increased ischemic injury
Cx45	Embryonic lethal
Cx47	Vacuolation in nerve fibers
Cx47/32 (Double KO)	Severe CNS demyelination

Table 1.2: Phenotype of specific connexin knockout mouse models

Adapted from (Nakase and Naus, 2004).

Connexin 36 (Cx36) would appear to be the predominant isoform responsible for neuron-to-neuron electrotonic coupling (Belousov and Fontes, 2013). Cx36 mRNA expression is found throughout the adult rodent CNS with higher levels expressed during prenatal and neonatal development (Belluardo et al., 2000). Regions with high Cx36 mRNA expression include the inferior olive, cerebellum, striatum, hippocampus, thalamus and cerebral cortex (Belluardo et al., 2000). In many CNS regions Cx36 displays highly regulated spatio-temporal specificity, with the incidence of electrotonic coupling and mRNA expression in spinal motor neurons found to be at its highest during late embryonic development, and falling within the first few postnatal days (Belousov and Fontes, 2013). In the cortex and hypothalamus CX36 expression increases during the first two postnatal weeks and subsequently decreases therein (Belousov and Fontes, 2013). Such observations of transient connexin expression and its correlation with neuronal differentiation implicate connexins as having a role in neural development, allowing for the intercellular exchange of signaling molecules, driving differentiation (Rozental et al., 2000). However, in many CNS regions neuronal connexin expression persists into adulthood, and functional electrical synapses can be found in the inferior olive, retina, spinal cord, hippocampus and cerebral cortex (Rash et al., 2000).

GJICs permit current flow between neurons. Any depolarization or hyperpolarization of cell(s) within a coupled network, generates a transjunctional voltage, and drives current through electrical synapses (Spray et al., 1985). Cx36 based channels are relatively voltage-insensitive (Srinivas et al., 1999), as such electrical synapses are bidirectional, reliably conducting both excitatory and inhibitory postsynaptic currents without delay. Electrical Inhibitory postsynaptic

potentials (eIPSPs) can result from the electrotonic dissemination of hyperpolarizing chemical PSPs or can result from the transmission of a presynaptic afterhyperpolarisation potential (AHP) across the junction. Conversely excitatory PSPs (eEPSPs) can result from the electrotonic spread of depolarizing chemical PSPs, or action potentials. In the latter case, if the transjunctional conductance is of sufficient magnitude, synchronous suprathreshold activity can be generated in multiple neurons within the network (Logan et al., 1996). Such activity patterning is known to regulate neurotransmitter release, with burst firing capable of initiating more transmitter release than high frequency repetitive firing (Poulain and Wakerley, 1982, Murase et al., 1993).

Gap junctions act as low pass filters, filtering the amplitude of fast events such as action potentials to a greater extent than slower events such as AHPs. As a result, the filtered remnants of presynaptic action potentials appear as truncated, biphasic membrane oscillations or 'spikelets' in the postsynaptic neuron (Nolan et al., 1999). Factors that also contribute to the postsynaptic oscillation waveform are the electrophysiological characteristics of the coupled cells (e.g. conductances contributing to the action potential waveform), the topographical organization of the gap junction(s) and the number of individual channels contributing to the junction(s). As such the characteristics and function of electrotonic coupling may vary substantially both within and between coupled networks.

1.25 Cx36-Based Electrical Synapses

The connexin isoforms that constitute any given channel confer single channel conductance, ionic selectivity and voltage gating characteristics (Bukauskas, 2012). Therefore the existence of both heterotypic and heteromeric channels

provides a huge array of channel characteristics. Cx36 only forms homotypic channels (Harris, 2001). Other connexin isoforms known to only form homotypic channels include Cx31 and Cx23 (Harris, 2001, Schalper et al., 2012). In these cases, the inability to form heterotypic channels is ascribed to atypical Cysteine residue patterning in the extracellular loop domains, which is highly conserved amongst most connexins. However this conserved Cysteine pattern is indeed found in the Cx36 amino acid sequence (Condorelli et al., 1998) and as such, either another mechanism exists to confer Cx36 its selectivity profile, or heterotypic channels do exist, but are yet to be identified. Homotypic Cx36 channels, have a unitary conductance of ~15 nS (Harris, 2001), they do not rectify current and any ostensible rectification is usually due to differences in neuronal capacitance on either side of the junction. Cx36 channels in both neurons and pancreatic β cells have been demonstrated to be cation-selective (Bukauskas, 2012) suggesting a specialized role in electrical synaptic communication, as opposed to metabolic communication, via negatively charged signaling molecules such as cAMP, IP_3, ATP, ADP, AMP and phosphocreatine (Bukauskas, 2012). Cx36 hemichannels aggregate into plaques within plasma membranes (Lauf et al., 2002) allowing for connexons on opposing neurons to dock via the interdigitation of extracellular moieties (Foote et al., 1998). The number of channels per plaque can range from fewer than a dozen to thousands (Segretain and Falk, 2004). Cx36 can form gap-junctions between dendrites, somata and axons of apposing neurons (Traub et al., 2003). Electrotonic coupling between interneurons would appear to be predominantly dendro-dendritic whist some principal cells are coupled via axo-axonal gap junctions (Bukalo et al., 2013).

The endogenous mechanisms of Cx36 channel gating are poorly understood, however studies have found Cx36 mediated electrical synaptic transmission to be modulated by glucose, pH, intracellular calcium, connexin phosphorylation state, dopaminergic and glutamatergic synaptic transmission, redox state and nitric oxide (NO). (Srinivas et al., 1999, Gonzalez-Nieto et al., 2008, Del Corsso et al., 2012, Orellana et al., 2009, Orellana et al., 2013, Saez et al., 2005, Pizarro-Delgado et al., 2014).

1.26 Project aims

1. Electrophysiological characterization of arcuate NPY neurons

- Determine the effects of fasting and extracellular glucose concentration on the passive membrane properties of arcuate NPY neurons.
- Determine the effects of fasting and glucose concentration on the active membrane properties of arcuate NPY neurons.

2. Energy status-dependent plasticity of arcuate NPY neurons

- Determine the effects of energy-status (fed versus fasted) and ambient physiologically relevant glucose levels on the electrophysiological properties of arcuate NPY neurons.
- Investigate glucose sensitivity of NPY neurons in fed and fasted conditions.
- Investigate the ionic mechanisms underlying glucose-induced changes in NPY neuron excitability.

3. To investigate the effects of ghrelin on arcuate NPY neurons under fed and fasted conditions and the relationship between ghrelin signaling and glucose levels.

- Investigate the effect of ghrelin upon NPY/AgRP neurons in fed and fasted conditions and in the presence of physiologically relevant ambient glucose levels.
- Investigate the mechanism of ghrelin excitation in NPY/AgRP neurons

4. Protein tyrosine phosphatases and insulin signaling in arcuate POMC neurons

- Characterize the effects of insulin on wild type arcuate POMC neurons.
- Characterize the effects of TCPTP knockout in arcuate POMC neurons on insulin-induced changes in neuronal excitability.
- Characterize the effects of a TCPTP inhibitor on insulin-induced responses in wild-type arcuate POMC neurons.

5. Electrophysiological characteristics of leptin receptor expressing neurons of the dorsomedial hypothalamus

- Characterize the electrophysiological properties of LepR-expressing neurons in the mouse DMH.
- Characterize the electrophysiological effects and mechanism of action of leptin on LepR-expressing neurons in the DMH.

6. An electrophysiological and pharmacological characterization of GnIH neurons in the rat

- Characterize the electrophysiological properties of rat GnIH neurons.
- Characterize the electrophysiology and pharmacology of afferent inputs to GnIH neurons.
- Determine GnIH neuron sensitivity to neurotransmitters and peptides, known to modulate energy homeostasis and gonadotroph secretion.

7. Electrotonic coupling and electrical synaptic transmission in cortical interneurons

- Investigate the electrophysiological properties and function of electrotonic coupling between cortical interneurons.
- Investigate the sensitivity of these coupled neurons to 5-HT
- Investigate the effects of putative gap-junction blockers on epileptiform activity

Figure 1.1: Anatomy of murine hypothalamic nuclei

A cartoon, highlighting the anatomical location of the murine hypothalamic arcuate nucleus (ARH) in two dimensions, adapted from (Choi et al., 2013, Breton, 2013, Paxinos, 2008).

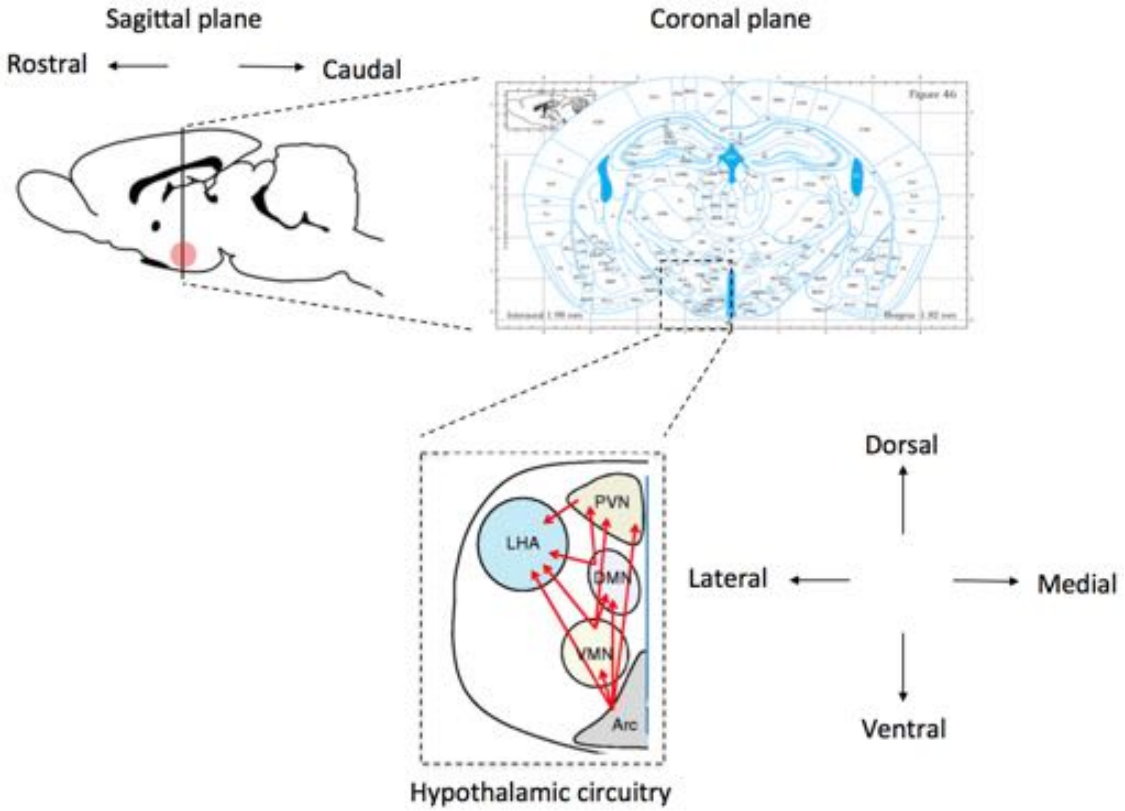
Sagittal plane
Coronal plane
Rostral
Caudal
PVN
LHA
DMN
VMN
Arc
Dorsal
Lateral
Medial
Ventral
Hypothalamic circuitry

Figure 1.2: Leptin and insulin receptor signal transduction

Cartoon schematic, demonstrating insulin and leptin receptor signal transduction. Recruited second messenger pathways of the insulin receptor include PI3K, whilst leptin receptor signaling recruits JAK-STAT signaling. Short-term effector mechanisms include ATP-sensitive potassium channels and transient receptor potential channels, whilst AKT/Foxo1 and STAT-dependent gene transcription mediates long-term effects of leptin and insulin, respectively.

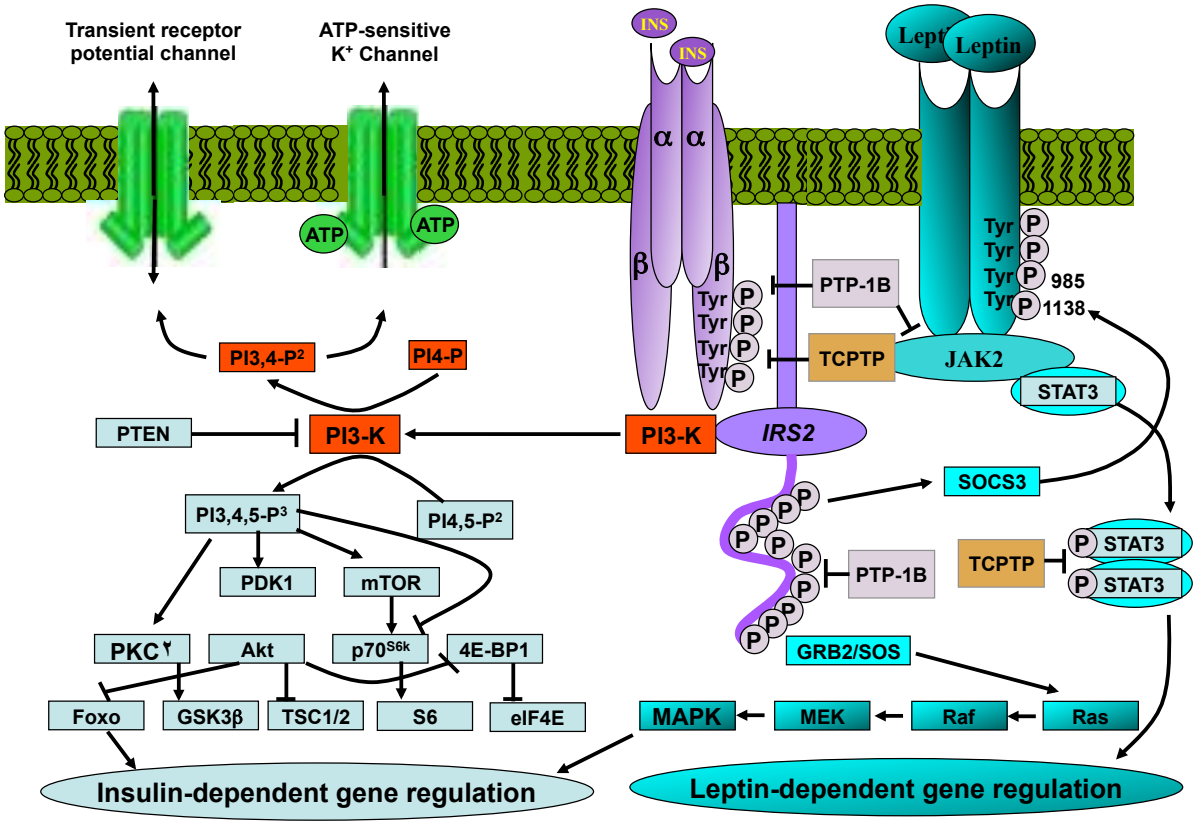
Transient receptor potential channel
ATP-sensitive K+ Channel
INS
INS
Lept
Leptin
α α
β β
ATP
ATP
Tyr P
Tyr P
Tyr P
Tyr P
985
1138
PTP-1B
TCPTP
JAK2
STAT3
PI3,4-P2
PI4-P
PTEN
PI3-K
PI3-K
IRS2
SOCS3
PI3,4,5-P3
PI4,5-P2
PDK1
mTOR
PTP-1B
TCPTP
STAT3
STAT3
PKCζ
Akt
p70S6k
4E-BP1
GRB2/SOS
Foxo
GSK3β
TSC1/2
S6
eIF4E
MAPK
MEK
Raf
Ras
Insulin-dependent gene regulation
Leptin-dependent gene regulation

Figure 1.3: Connexin and connexon topology

Cartoon highlighting two dimensional connexin structure (left panel), and three dimensional gap-junction channel (right panel) topology, in relation to the phospholipid membrane, adapted from (Meier and Dermietzel, 2006).

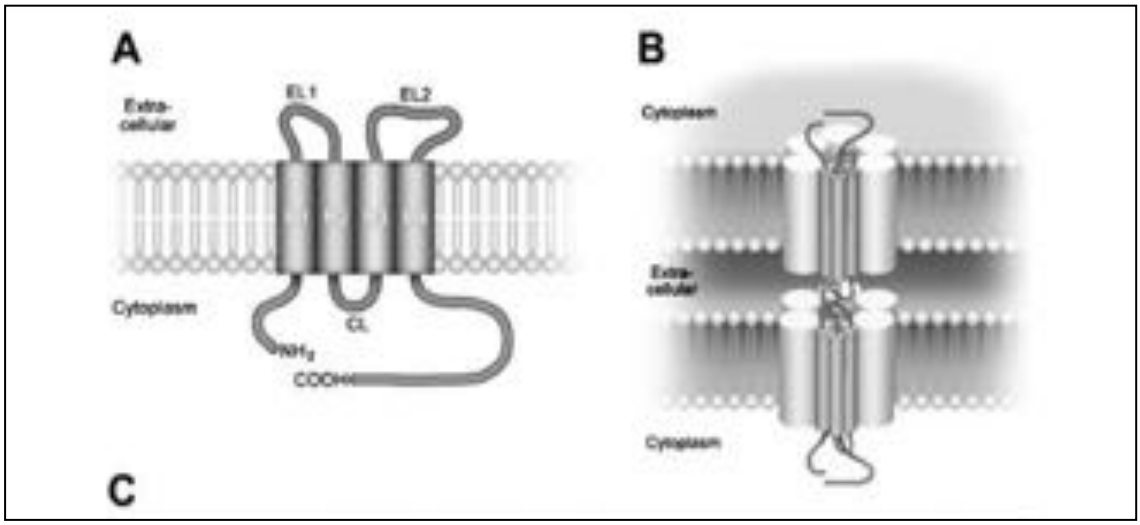
A
Extra-
cellular
EL1
EL2
Cytoplasm
CL
NH_2
COOH
B
Cytoplasm
Extra-
cellular
Cytoplasm
C

Chapter 2: Experimental Procedures

All animal procedures described here were conducted with approval of Monash Animal Research Platform (MARP) ethics committee (2008/31, 2010/51, 2011/174, 2015/104) and in accordance with the Australian National Health and Medical Research Council (NHMRC) code of practice. Mice and rats were housed in the Animal Research Laboratory, Building 77, Monash University, Clayton, Victoria 3800 and The Large Animal Facility, Building 13F, Monash University, Clayton, Victoria, 3800. Both female and male animals were employed over the course of this study. Unless otherwise stated, animals were always housed in groups of 3-5 per cage, in a temperature-controlled room, on a 12-hour light/dark cycle, with food and water administered *ad libitum*. Table 2.1 gives details of rodents used in this study, below:

Rodent	Age	Source
GnIH-EGFP Wistar Rat	> 6 weeks	Bred internally (Monash). Previously described by (Soga et al., 2014).
POMC Z/EG TCPTP $^{lox/lox}$ mouse	> 6 weeks	Bred internally (Monash). Previously described by (Dodd et al., 2015).
LepR YFP Mouse	> 6 weeks	Bred internally (Monash). Previously described by (Simonds et al., 2014).
NPY renilla GFP Mouse	> 6 weeks	Bred internally (Monash). Previously described by (Cowley et al., 2003)
POMC eGFP Mouse	> 6 weeks	Bred internally (Monash). Previously described by (Cowley et al., 2001)
Wild type C57BL/6 Mouse	> 6 weeks	Bred internally (Monash). Originally obtained from The Jackson Laboratory, USA.

Table 2.1: Details of rodents used in this study

2.1 Generation and validation of animal models

GnIH-EGFP Wistar Rat; > 6 weeks old; Bred internally (Monash), previously described by (Soga et al., 2014). To generate the GnIH-EGFP Wistar Rat, GnIH-EGFP transgene was produced using pEGFP-1 plasmid (Clontech Laboratories, Inc.) and the predicted GnIH promoter region (1.7 kb of the 5' upstream sequence). The rat GnIH gene was amplified using PCR, the product of which was cloned into pGEM-T Easy Vector plasmid (Promega) and transformed into Escherichia coli. To construct the GnIH-EGFP plasmid, the pGEM-T vector was digested with *Hind*III and *Bam*HI and ligated into the pEGFP plasmid. The resulting GnIH promoter–EGFP plasmid was then digested with *Zsp*2I (Vivantis Technologies) and the resulting 3.5 kb DNA fragment was purified using agarose gel electrophoresis. This DNA fragment was then microinjected into the pronuclei of fertilized oocytes (PhoenixBio, Co, Ltd.). A caveat of this model is that as it is unknown what other else may be coded in the 1.7 kb fragment 5' to the GnIH gene. Indeed in this rat model EGFP-positive, GnIH negative neurons are found in the ventromedial hypothalamus (VMH) whilst GnIH positive, EGFP negative fibers are found in the median eminence of this model. This should be considered whilst interpreting results of experiments conducted on this animal model.

POMC Z/EG TCPTP $^{lox/lox}$ mouse; > 6 weeks old; Bred internally (Monash), previously described by (Dodd et al., 2015). To generate the POMC Z/EG TCPTP $^{lox/lox}$ mouse, the TCPTP-floxed mouse *Ptpn2*$^{fl/fl}$ were mated with Z/EG (C57BL/6) reporter mouse (Jackson Laboratories). In these animals, 92% of arcuate POMC neurons expressed GFP, and no non-POMC neurons expressed GFP.

LepR YFP Mouse; > 6 weeks old; Bred internally (Monash), previously described by (Simonds et al., 2014). *LepRb-internal ribosome entry site (IRES)-*

Cre recombinase mice generated using homologous recombination to introduce an *IRES-nuclear localization sequence (NLS)-Cre* cassette into the region immediately 3 prime to the LepRb stop codon. Cre recombinase is only expressed in cells that produce the LepRb. *LepRb-IRES-Cre* mice were then crossed with mice with the *EYFP* gene inserted into the *ROSA26* locus. EYFP gene transcriptional stop codon was flanked with *lox-P* sites. Upon successful recombination, the transcriptional termination sequence is excised allowing EYFP expression in LepRb-expressing cells. In the absence of a recombination event, premature transcription termination results in no EYFP expression.

NPY renilla GFP Mouse; > 6 weeks old; Bred internally (Monash), previously described by (Cowley et al., 2003). To generate the NPY renilla GFP Mouse, the FRT-Kan-FRT cassette from the pIGCN21 plasmid was amplified using PCR and inserted into the Mlul site of phrGFP-1 (Stratagene) producing in the phrGFP-FRT-Kan-FRT plasmid which contained 114 kb 5' and 29 kb 3' of the murine *NPY* gene. This plasmid was transformed into EL250 bacteria and amplified using PCR. Amplified DNA was purified and microinjected into the pronuclei of fertilized FVB mice (Jackson Laboratories).

POMC eGFP Mouse; > 6 weeks old; Bred internally (Monash), previously described by (Cowley et al., 2001). To generate the POMC eGFP Mouse, the *EGFP* cassette was inserted into the 5' untranslated region of exon 2 of the mouse *Pomc* gene fragment with 13 kb 5' and 2 kb 3' flanking sequences. The transgene was then microinjected into the pronuclei of C57BL/6J mice (Jackson Laboratories). Double EGFP-POMC immunohistochemistry demonstrated >99% localization in the ARH but no colocalization of EGFP with tyrosine hydroxylase or NPY.

Wild type C57BL/6 Mouse; > 6 weeks old; Bred internally (Monash); originally obtained from The Jackson Laboratory, USA.

2.2 Mice

All mice included in experiments were from lineages that had been backcrossed onto a C57B1/6J background. Said C57B1/6J mice were obtained from Monash animal services (MAS), Monash University, Clayton, Victoria, Australia.

2.2.1 Generation of POMC Z/EG TCPTP $^{lox/lox}$ mice

This study used mice, produced as previously described by (Dodd et al., 2015). *Pomc*-Cre transgenic mice were crossed with *Ptpn2*$^{fl/fl}$ mice to selectively delete TCPTP from POMC neurons (Loh et al., 2011). These mice were then crossed onto a *Z/EG* reporter line, causing GFP expression in neurons only within which a Cre-dependent recombination event had occurred.

2.2.2 POMC-eGFP, POMC Z/EG TCPTP $^{lox/lox}$ and NPY-GFP mouse brain slices

Hypothalamic slice preparations containing the arcuate nucleus (ARH) were obtained from mice over 6 weeks of age. Brain slice preparations were 250 µm thick, and cut in the coronal plane. Mice were split into one of “fed” and “fasted” experimental groups. Here “fed” animals were administered food *ad libitum,* whilst “fasted” animals were subjected to an 18-hour fast prior to culling.

2.2.3 LepR-YFP mouse brain slices

Hypothalamic slice preparations containing the dorsomedial hypothalamus (DMH) were obtained from LepR-YFP transgenic mice over 6 weeks of age. Brain slice preparations were 250 μm thick, and cut in the coronal plane.

2.2.4 Wild type C57BL/6 mouse brain slices

Cortical slice preparations were obtained from C57BL/6 mice. Brain slice preparations were 250 μm thick, and cut in the coronal plane.

2.2.5 GnIH-EGFP Wistar rat brain slices

Hypothalamic slice preparations containing the dorsomedial hypothalamus (DMH) were obtained from transgenic GnIH-GFP Wistar rats over 6 weeks of age. Brain slice preparations were 250 μm thick, and cut in the coronal plane.

2.3 Fasting protocol

Mice to be included in 'fasted' experimental groups were always collectively housed to minimize stress. Food was removed from the cage hopper and cage floor 18 hours prior to culling. The fast period was always kept constant with respect to the light/dark cycle. Fasting always began three hours prior to the dark period. Water was always available to animals *ad libitum*. Animals fasted but not culled were not subjected to another fast for at least one week to ensure recovery.

2.4 Physiology

2.4.1 Diet

At 4-6 weeks of age mice were weaned and placed on solid food diets. Mice were given a chow diet (Specialty Feeds, meat-free rat and mouse diet, Western Australia, Australia) containing 3.1 kcal/g, 4.8% fat. In some experiments mice were given a high fat diet (Specialty Feeds, meat-free rat and mouse diet, Western Australia, Australia) containing 4.75 kcal/6 and 42% fat.

2.4.2 Food Intake

Food intake was quantified in multiple studies outlined here. Food intake was always measured post-surgery in order to monitor the health and recovery progress of mice. Food intake measurements were always taken at the same time each day, immediately prior to the onset of the dark period. Mice whose food intake was monitored were always individually housed. To check intake, food from the cage hopper was transferred to the scale, with care taken to look for scraps of food within the cage itself. All food intake measurements were taken on a UME 600 ± 0.1g Z series scale.

2.4.3 Body Weight

Body weight was taken as a measurement throughout multiple studies, and was always taken alongside food intake measurements. Body weight was always measured at the same time each day, immediately prior to the onset of the dark period. Mice subjected to these experiments were always individually housed and all measurements were taken on a UME 600 ± 0.1g Z series scale.

2.5 Electrophysiology

2.5.1 Slice Preparation

Rats and mice were euthanized using terminal inhalation anesthesia (Isoflurane, Baxter Healthcare, NSW, Australia) followed by decapitation. Following decapitation, the brain was swiftly removed from the cranial cavity and transferred into freshly prepared, ice-cold (<4°C), carbogen (95% O_2, 5% CO_2) gassed artificial cerebrospinal fluid (aCSF). pH and osmolarity of aCSF was regularly checked and maintained at 7.4 and between 310-315 $mOsm.kg^{-1}$, respectively. For experiments requiring the use of aCSF containing <10 mM glucose, osmolarity was compensated with the addition of D-mannitol at levels equimolar to the glucose levels removed.

Dura, arachnoid and pia matter were removed from the surface of the brain using fine forceps (Fine Science Tools). The cerebellum was removed using a razorblade to provide a flat edge for the remaining brain to be adhered to a tissue plate of a vibratome (Leica VTS 1000S, Leica Microsystems Nussloch, Germany) using cyanoacrylate glue. Coronal slices (200-300 μm) containing the dorsomedial hypothalamus (DMH), arcuate nucleus (ARH), and/or cortex were cut using the vibratome. The vibratome cutting chamber was filled with ice-cold aCSF, and was regularly replaced to keep temperature as constant as possible during slicing. The arcuate nucleus was identified as: the area immediately dorsal to the median eminence and immediately lateral to the third ventricle. The dorsomedial hypothalamus was identified as the area immediately lateral to the dorsal end of the third ventricle, and immediately posterior to the paraventricular nucleus, both in accordance with coordinates determined from a brain atlas (Paxinos, 2008). Once brain slices were cut, they were immediately transferred from the cutting

bath to a 200 ml beaker containing aCSF warmed to 34°C in a water bath where they were incubated for 20 minutes. After incubation the beaker was removed from the water bath and placed on the lab bench to acclimatize to room temperature for at least an hour before the slices were used for recording. Prior to recording slices were transferred to a recording chamber for electrophysiological experiments. The slices were secured to the cover slip-bottomed recording chamber with a custom-made nylon grid, weighted with a platinum arc to prevent any movement of the tissue during recording. The recording chamber was constantly perfused with room temperature, carbogen-bubbled aCSF, and the flow rate of aCSF was maintained between 2-10 ml/min.

2.5.2 Recording Procedure

Brain slices and individual cells were visualized using a Zeiss Axioskop 2 microscope (Carl Zeiss Ltd., Welwyn Garden City, UK) equipped with a Zeiss Axiocam MRc camera (Carl Zeiss Ltd., Welwyn Garden City, UK) connected to a computer running Axiovision 4.1 imaging software (Carl Zeiss Vision). The microscope was fitted with two immersion lenses (20X and 63X) and a 2.5X booster lens mounted in the microscopes rotational magazine allowing for slice visualization at 20X, 50X and 63X and 157.5X. The microscope was also fitted with a fiber optic fluorescent light source (Carl Zeiss Vision) and filter sets 37 and 46 allowing for the visualization neurons expressing eGFP and YFP, respectively.

Whole-cell current-clamp and voltage-clamp recordings were performed using recording electrodes pulled from borosilicate, filamented, thin-walled glass capillaries (GC150TF-10) using a horizontal electrode puller (P1000 or P-97,

Sutter Instrument Co, Novato, CA, USA) and had resistances of 4-9 MΩ when back-filled with intracellular pipette solution.

Electrophysiological recordings were made with an Axon 700B amplifier (Axon Instruments, Foster City, CA, USA) connected to a personal computer running multiclamp, pClamp 9 (Axon Instruments) and Axiovision 4.1 (Carl Zeiss Vision) software. Experimental data was monitored online using Clampex 9 (Axon instruments) and Multiclamp (Axon instruments) software. Data was filtered at 1-5 KHz (for voltage-clamp experiments), digitized at 2-100 KHz (Digidata 1322A, Axon instruments) and was saved directly to the PC hard drive for analysis using Clampfit 9 (Axon instruments) software.

Resting membrane potential and firing rate was established from traces in Clampfit software (Axon Instruments) and value offsets due to liquid junction potentials were not accounted for. Input resistance was calculated from Ohm's Law (R=V/I) using an experimental protocol in which square-wave current steps (-5 to -100 pA, 500 ms to 1000 ms) were injected and the amplitude of the evoked membrane voltage deflections subsequently measured.

All electrophysiological recordings were made at room temperature as it was deemed unrealistic to perform long-term recordings at physiological temperature. It must be noted that this is a caveat of research described here, not least because the hypothalamus contains populations of temperature-sensitive neurons.

In experiments demanding recordings of fluorescent neurons, cell phenotype was confirmed after whole-cell access was attained. This was achieved under fluorescent illumination, observing that the flurophore had been partially drawn-up into the recording electrode. In these experiments, any neuron in which

this was not observed was deemed to not contain the flurophore and was discarded.

Electrotonic coupling between pairs of cortical interneurons was confirmed when the injection of negative current into only one of two simultaneously recorded neurons, evoked a voltage change in both neurons. Neuronal input resistance and coupling coefficients were determined from membrane potential responses to injection of a range of depolarizing and hyperpolarizing current pulses into either neuron. Coupling coefficients were determined as the ratio of the postsynaptic to presynaptic membrane potential change elicited in response to current injection. The junctional conductance (gj) was estimated from the experimentally determined input resistance and coupling coefficients using a model system whereby each neuron was represented by a single compartment connected via a resistor constituting the electrical synapse. Thus gj between two cells was estimated from:

$$gj_{1\text{-}2} = R_1 k_{1\text{-}2} / ((R_1 R_2) - R_1 k_{1\text{-}2})^2)$$

In which R_1 and R_2 represent the input resistances of the pre-and postsynaptic neurons respectively and $k_{1\text{-}2}$ represents the coupling coefficient between these neurons (See (Nolan et al., 1999).

2.6 Solutions

2.6.1 aCSF

The composition of aCSF used in this study is shown in table 2.2, below:

	1 mM Glucose aCSF (mM)	**2 mM Glucose aCSF (mM)**	**3 mM Glucose aCSF (mM)**	**5 mM Glucose aCSF (mM)**	**10 mM Glucose aCSF (mM)**
NaCL	127	127	127	127	127
KCL	1.9	1.9	1.9	1.9	1.9
KH_2PO_4	1.2	1.2	1.2	1.2	1.2
$NaHCO_3$	26	26	26	26	26
D-Glucose	1	2	3	5	10
D-Mannitol	9	8	7	5	0
Ascorbic Acid	0.34	0.34	0.34	0.34	0.34
$CaCl_2$	2.4	2.4	2.4	2.4	2.4
$MgCl_2$	1.3	1.3	1.3	1.3	1.3

Table 2.2: aCSF composition

2.6.2 Pipette solution

Intracellular pipette solution was made daily from stock solutions kept at 4°C except adenosine triphosphate (ATP) which was stored at -20°C. The compositions of pipette solutions used in this study are shown in table 2.3, below:

	2mM ATP pipette solution (mM)	**4mM ATP pipette solution (mM)**
K-gluconate	140	140
HEPES	10	10
KCL	10	10
EGTA	1	1
Na_2ATP	2	4
Biocytin	5	5

Table 2.3: Pipette solution composition

The pH was adjusted to 7.4 with KOH and osmolarity adjusted to within 10 $mOsm.kg^{-1}$ below that of the aCSF (typically 290 -310) with sucrose.

2.6.3 Solutions used in thesis chapters

aCSF glucose concentration and pipette solution ATP concentration was tailored to the requirements of the experiment on the day. During tissue preparation, brain slices were maintained in aCSF of identical glucose concentration to that used in experimental control conditions. aCSF flow rate was kept between 2 – 5 ml/min and system volume was around 15 ml meaning that upon drug/ glucose application, the intended concentration of drug/glucose was present in the recording chamber after a maximum of 7.5 minutes. aCSF glucose and pipette solution ATP concentration used in experiments presented in this thesis are shown in table 2.4, below:

Thesis Chapter	aCSF Glucose (mM)	aCSF Mannitol (mM)	Pipette Solution ATP (mM)
Chapter 3	1 or 5	9 or 5	2
Chapter 4	1 or 5	9 or 5	2
Chapter 5	3	7	2
Chapter 6	2	8	2
Chapter 7	5	5	2
Chapter 8	10	0	4

Table 2.4: Composition of aCSF and pipette solution

2.7 Reversal Potentials

Reversal potentials were calculated from current-voltage relationship plots. These plots were generated from programmed Clampex protocols for both control and

test conditions. Here, negative, square-wave current pulses were injected at decreasing magnitude and equal integer with the most negative current pulse being sufficient to hyperpolarize the neurons membrane potential beyond -90 mV. Reversal potentials were determined from the intersection or extrapolated intersection of current-voltage scatter plots.

Ionic reversal potentials were determined using the Nernst Equation:

$$E_{ion} = \frac{RT}{zF} \ln \frac{[ion]_o}{[ion]_i}$$

Where E_{ion} is the equilibrium potential for the ion in question, R is the gas constant (8.315 J K^{-1} mol^{-1}), T is absolute temperature (273.16 + T [25°C]), Z is the valency of the ion in question, F is Faraday's constant (96,485 C mol^{-1}), $[Ion]_o$ is the extracellular concentration of the ion in question and $[ion]_I$ is the intracellular concentration of the ion in question. Reversal potentials of ions critical to the maintenance of membrane voltage are given in table 2.5, below:

Ion	Extracellular Concentration (mM)	Intracellular Concentration (mM)	Reversal Potential (mV)
Na^+	153	6	81.6
Cl^-	136.3	10	-65.8
Ca^{2+}	2.4	0.001	196
K^+	3.1	150	-97.7

Table 2.5: Ionic reversal potentials

2.8 Drugs

Drugs were applied to brain slices during recording through the use of 60 ml syringes connected to the aCSF bath perfusion setup via three-way taps. Drugs were prepared as a stock solution at a concentration >1000 times that of the concentration used for experimentation, and were stored at <-20°C. Stock solutions were made using either distilled water or DMSO as a solvent. Final bath concentrations of DMSO never exceeded 0.1%. Drug stocks were defrosted and added to 60 ml syringes ready for bath application at the desired concentration at the last convenient moment to minimize drug oxidation or degradation. Drugs used in these experiments are listed below in table 2.6, below:

Drug	**Concentration**	**Solvent**
Tetrodotoxin citrate (TTX)	1µM	Distilled water
Bicuculine methiodide	20 µM	Distilled water
6-nitro-7sulphamoybenzo(*f*)-quinoxaline-2,3-dione (NBQX)	10 µM	Distilled water
Ghrelin	3 nM, 10 nM, 30 nM, 100 nM	Distilled water
Leptin	100 nM	Distilled water
Insulin	100 nM	HCl
Thyrotropin releasing hormone (TRH)	400 nM	Distilled water
Carbenoxolone (CBX)	30 µM, 100 µM	Distilled water
4-amino pyrimidine (4-AP)	1 mM	DMSO
5-hydroxytryptamine (5-HT)	50 µM	Distilled water
Noradrenaline (NA)	40 µM	Distilled water

Compound 8 (TCPTP inhibitor)	20 nM	Distilled water
Tonabersat	10 µM	Distilled water
Carabersat	10 µM	Distilled water
(2*R*)-amino-5-phosphonopentanoate (APV)	20 µM	Distilled water
Nickel Chloride (NiCl2)	1 mM	Distilled water
Cesium Chloride (CsCl)	500 µM	Distilled water
Barium Chloride ($BaCl_2$)	100 µM	Distilled water
PSB 603 (A_{2B} antagonist)	100 nM	DMSO
MRS 1523 (A_3 antagonist)	300 nM	DMSO
Istradefylline (A_{2A} antagonist)	50 nM	DMSO
DPCPX (A_1 antagonist)	1 µM	DMSO
LY294002 (PI3K inhibitor)	10 µM	DMSO
SB224289 (5-HT 1B antagonist)	10 µM	DMSO
(S)-WAY 100135 (5-HT 1A antagonist)	100 nM	DMSO
SB-269970 hydrochloride (5-HT 7 antagonist)	100 nM	Distilled Water
β-estradiol	400 nM	DMSO
Coritcosterone	400 nM	DMSO

Table 2.6: Drugs used in experiments

2.9 Statistical Analysis

Statistical analysis was performed using Excel (Microsoft) and Graphpad (Graphpad Software Inc. San Diego, USA) and all values are expressed as a mean ± SEM. Numbers of observations are stated as *n* values. Statistical significance was

determined using a two-tailed student's t-test, paired or unpaired, 1-way ANOVA, 2-way ANOVA or Chi-square test, as appropriate.

Chapter 3: Electrophysiological characterization of NPY/AgRP neurons

3.1 Introduction

Active and passive membrane properties are critical biophysical parameters that can define the computational power of neurons, directly modulating the gain of neuronal inputs and outputs. Passive membrane properties include the capacitance and resistance of the neuron membrane whilst active membrane properties include biophysical characteristics modulated by voltage, ligands and or second messengers. Passive membrane properties can be indicative of the size of the neuron, its level of compartmentalization and degree of connectivity with neighboring neurons in the case of electrotonically coupled networks. Suprathreshold active conductances include all of those, sodium, potassium and calcium conductances that can contribute to action potential firing (Meech, 1978). Also associated with suprathreshold active conductances are those that contribute to afterpotentials (afterhyperpolarisation (AHP) and in some cases afterdepolarization (ADP)). The AHP is a critical determinant of action potential firing frequency and can comprise of multiple conductances including potassium and calcium-activated potassium conductances (Wu et al., 2004). ADP's following action potentials rather than regulating firing frequency tend to promote extended periods of increased action potential firing. Other conductances critical to regulating neuronal excitability are subthreshold active conductances i.e. those conductances that are generally activated by subthreshold changes in membrane potential and contribute driving or regulating suprathreshold activity. Examples of

subthreshold active conductances include: T-type calcium (I_T) and hyperpolarization-activated cyclic nucleotide gated non-selective cation channels (I_H), both of which promote regenerative rhythmic patterns of activity in many neurons (van den Top et al., 2004, McCormick and Pape, 1990); instantaneous, anomalous inwardly rectifying potassium conductances (Kir; I_{AN}), activated at negative membrane potentials and thought important in maintaining neuronal membrane potential within a functionally operative window; transient outward rectification (I_{TOR}) observed as a delayed return to rest following membrane hyperpolarization or as a delay in reaching threshold from negative resting potentials (Whyment et al., 2011). Voltage-sensing channels confer specific biophysical properties to the neuron within which they are expressed. The endpoints of many endogenous and exogenous ligands are ion channels. Increases or decreases in single channel conductance or channel voltage-gating properties can affect neuron excitability and output. Furthermore these conductances change with development, in disease states and in responses to environmental perturbations and are critical determinants of both physiological and pathophysiological output from neural networks to drive appropriate changes in behavior (Dworakowska and Dolowy, 2000, Ashcroft, 2006).

Previous studies have characterized the morphological and electrophysiological properties of hypothalamic neuron populations (Fioramonti et al., 2004, Burdakov and Ashcroft, 2002, Armstrong, 1995, Tasker and Dudek, 1991, Stern, 2001, Pennartz et al., 1998, Gonzalez et al., 2012). Three electrophysiologically distinct neuronal populations residing in the arcuate nucleus of the hypothalamus (ARH) have been defined, in terms of their membrane response to the offset of negative square-phase current injection: 1; rebound

depolarization, 2; no rebound depolarization, and 3; transient outward rectification (Burdakov and Ashcroft, 2002).

To date, a thorough characterization of the active and passive membrane properties of functionally defined neurons of known chemical phenotype has not been undertaken. Neuropeptide Y (NPY) neurons of the ARH are the key central neural population responsible for driving food intake and hunger. NPY neurons are required for the maintenance of food intake and glucose homeostasis (Luquet et al., 2005, Konner et al., 2007). NPY neurons elevate their electrical activity in negative energy states (Takahashi and Cone, 2005). Pharmacological and optogenetic excitation of NPY neurons elicits elevations in food intake, whilst neuronal inhibition results in food intake reductions (Aponte et al., 2011, Atasoy et al., 2012, Krashes et al., 2011). NPY neurons are sensitive to glucose and a number of peripheral hormones including leptin, insulin and ghrelin (Belgardt et al., 2009, van den Top et al., 2004, Vong et al., 2011, Konner et al., 2007, Claret et al., 2007).

Despite the obvious critical role of NPY neurons in the central control of energy balance and food intake, there have been no electrophysiological studies to date showing how these neurons process and adapt to changes in energy or hunger status and formulate electrically coded commands to drive appropriate behavioral changes. Changes in active and passive membrane properties may be indicative of functionality *in vivo* and is of value to our understanding of hypothalamic neuron function and their regulation of somatic energy homeostasis.

Aims of this study are to characterize the active and passive membrane properties of NPY/AgRP neurons in fed and fasted conditions, and investigate the effects of extracellular glucose concentration on these parameters.

3.2 Results

Whole-cell recordings were obtained from 40 NPY eGFP neurons located in the arcuate nucleus of hypothalamic brain slices bathed in aCSF containing 1 mM glucose, taken from animals subjected to an 18-hour fast prior to culling. Whole-cell recordings were also obtained from 40 NPY eGFP neurons of brain slices bathed in aCSF containing 1 mM glucose, taken from animals fed *ad libitum*. Finally, whole-cell recordings were obtained from 40 NPY eGFP neurons of brain slices bathed in aCSF containing 5 mM glucose, taken from animals fed *ad libitum*.

To investigate subthreshold and suprathreshold voltage-sensitive conductances expressed by NPY eGFP neurons, the membrane current-voltage relationship of neurons was investigated. Here hyperpolarizing and depolarizing square-phase current steps of equal increment were injected (<±100 pA, 200 ms duration), with negative current sufficient to drive membrane voltage to around -100 mV and positive current sufficient to induce action potential firing.

3.2.1 Effects of Energy status and D-glucose levels on EPSC frequency

Of the Fasted 1 mM glucose population, voltage clamp recordings were obtained from 16 NPY eGFP neurons. Neurons were held at a potential of -90mV to maximize EPSC current amplitude. Of neurons recorded in 1mM D-glucose from slices prepared from fasted animals, mean EPSC frequency was 0.86 ± 0.13 Hz. Of the Fed 1 mM glucose population, voltage clamp recordings were obtained from 16 NPY eGFP neurons. Of neurons recorded, mean EPSC frequency was 0.55 ± 0.06 Hz. Of the Fed 5 mM glucose population, voltage clamp recordings were obtained from 13 NPY eGFP neurons. Of neurons recorded, mean EPSC frequency was 1.01 ± 0.13 Hz. Neurons of the Fed 1 mM glucose group had a significantly lower EPSC

frequency than the neurons of the Fed 5 mM glucose groups (p=>0.05; one-way ANOVA & post-hoc Bonferroni test) (figure 3.1). The GABA receptor antagonist bicuculine was not bath applied during these experiments.

3.2.2 Passive membrane properties

NPY neurons recorded in brain slices from fasted mice, incubated in 1 mM glucose aCSF, had a mean resting membrane potential of -39.44 ± 0.82 mV and mean neuronal input resistance of 1484 ± 166 MΩ. Of these neurons 35 of 40 (87.5%) were spontaneously active with mean spontaneous firing rate of 1.52 ± 0.22 Hz. The mean threshold for action potential firing was -24.28 ± 2.35 mV and the mean action potential amplitude amounted to 42.6 ± 3.7mV. Here, mean action potential duration at ½ amplitude was 2.6 ± 0.1 ms, whilst mean action potential duration at threshold was 6.6 ± 0.5 ms, this gave a threshold to ½ duration ratio of 2.4 ± 0.1. NPY eGFP neurons recorded from fasted animals in 1mM glucose had mean membrane time constant of 59.5 ± 7.4 ms. Mean AHP amplitude was measured at 17.0. ± 0.8 mV and AHP ½ decay was 313 ± 48 ms (n=40).

Recordings obtained from brain slices from mice fed *ad libitum*, incubated in 1 mM glucose aCSF, revealed NPY eGFP neurons had mean resting membrane potential of -39.05 ± 0.49 mV and input resistance of 1975 ± 292 MΩ. Of these neurons 38 of 40 (95%) were spontaneously active with mean spontaneous firing rate was 1.41 ± 0.14 Hz. In this population, mean threshold for action potential firing was -26.4 ± 1.5 mV and mean action potential amplitude was 44.2 ± 2.6 mV. The mean action potential duration at ½ amplitude was 3.5 ± 0.2 ms, whilst mean action potential duration at threshold was 9.3 ± 0.5 ms, giving a threshold to ½ duration ratio of 2.64 ± 0.08. Of these NPY eGFP neurons the mean membrane time

constant was 73.2 ± 5.7 ms. Mean AHP amplitude was measured at 16. ± 0.7 mV and AHP ½ decay was 461± 48 ms (n=40).

In brain slices from mice fed *ad libitum*, incubated in 5 mM glucose aCSF, NPY eGFP neurons had a mean resting membrane potential of -39.3 ± 0.9 mV and input resistance of 1686 ± 131MW. Of these neurons 33 of 40 (82.5%) were spontaneously active with mean spontaneous firing rate of 1.8 ± 0.3 Hz. The mean threshold for action potential firing was -26.22 ± 0.44 mV and mean action potential amplitude amounted to 42.9 ± 1.2 mV. The mean action potential duration at ½ amplitude was 3.1 ± 0.2 ms, whilst mean action potential duration at threshold was 8.0 ± 0.6 ms, this gave a threshold to ½ amplitude duration ratio of 2.6 ± 0.1. Of these NPY eGFP neurons mean membrane time constant was 70.4 ± 9.2 ms. Mean AHP amplitude was measured at 18.00 ± 0.84 mV and AHP ½ decay was 442± 73 ms (n=40). When comparing Fasted 1mM glucose and Fed 1 mM glucose populations, statistical significance was obtained when comparing action potential duration, both at ½ amplitude, and at action potential duration at threshold (p=0.0005 and 0.0001, respectively; 2-way ANOVA, post-hoc Bonferroni test).

3.2.3 Pharmacological properties of action potentials in NPY neurons

Action potentials were sensitive to 1 μM TTX (n=6), whilst oscillations in membrane potential persisted, most likely mediated via calcium-dependent mechanisms (figure 3.7B).

3.2.4 Subthreshold active membrane properties

IV relations were investigated in all neurons to identify subthreshold active conductances expressed in NPY neurons under the various fed, fasted and extracellular glucose conditions. Of recordings obtained from NPY neurons in brain slices from fasted mice, incubated in 1 mM glucose aCSF, membrane response to hyperpolarizing and depolarizing current injection revealed that 30% of these neurons did not express any obvious subthreshold active, voltage-dependent conductances under these conditions. In a further 30% of NPY eGFP neurons I_H was the only conductance expressed. I_H was identified as a depolarizing sag in the membrane response to large amplitude hyperpolarizing current pulse injection and as a rebound excitation at the offset of these responses to current injection (see figure 3.2C). Ih was also confirmed by its sensitivity to extracellular cesium chloride (500 μM; n=4). A further 22.5% of neurons in this population were characterized by expression of I_T only. I_T was characterized by a rebound depolarization at the offset of membrane responses to hyperpolarizing current injection (see figure 3.2D). To ensure the presence of I_T as opposed to I_H, I_T was also characterized as a peak depolarizing "hump" in response to depolarizing current pulses from relatively negative holding potentials (>-60mV). I_T can be distinguished from I_H by the fact that I_H is hyperpolarizing, not depolarizing activated whereas T-type is de-inactivated by hyperpolarization but only activated by depolarization. I_T expression in NPY neurons was further confirmed by its sensitivity to extracellular Nickel chloride (1mM; n=4). 15% of this population of NPY neurons expressed I_H and I_T, whereas 2.5% of neurons expressed I_H, I_T and I_{AN}. Ian was identified as an instantaneous inward rectification observed as a fall in

neuronal input resistance at negative membrane potentials (>-80mV) (see figure 3.2Bi and Bii).

IV relations from NPY neurons recorded in brain slices from mice fed *ad libitum*, incubated in 1 mM glucose aCSF, revealed that 40% of NPY eGFP neurons do not express any subthreshold voltage-dependent conductances under these conditions. Furthermore experiments revealed 12.5% of neurons to express I_H only, 30% of neurons expressed I_T only, 5% of NPY eGFP neurons expressed I_H and I_T whilst 12.5% of neurons expressed I_T and I_{AN} (figure 3.5).

IV relations in NPY neurons recorded in brain slices from mice fed *ad libitum*, incubated in 5 mM glucose aCSF, revealed that 35% of NPY eGFP neurons do not express any voltage-dependent conductances under these conditions. 52.5% of neurons expressed I_T only, 7.5% of neurons expressed I_H only, 2.5% expressed I_H and I_T, and a further 2.5 % expressed I_T and I_{AN} (figure 3.5).

3.3 Discussion

Here, for the first time passive and active membrane properties of NPY eGFP neurons in *in vitro* conditions, replicating positive and negative energy states are reported. The ARH is well recognized as containing glucose-sensitive neurons (Spanswick et al., 1997, Ibrahim et al., 2003) and NPY neurons have been reported exclusively glucose inhibited (Burdakov and Gonzalez, 2009, Muroya et al., 1999). Here I show glucose and feeding status-dependent changes in passive and active NPY neuron membrane properties.

3.3.1 Energy status-sensitive EPSC frequency

NPY neurons of the Fed 1 mM glucose group had a significantly lower spontaneous EPSC frequency than NPY neurons from the Fed 5 mM populations. The relatively elevated EPSC frequency in 1 mM glucose, compared to 5 mM glucose, is in agreement with previous research and fits with our current understanding of arcuate NPY neurons; elevated excitation under negative energy states drives increases in food intake and suppresses energy expenditure (Kong et al., 2016, Krashes et al., 2014). The absence of significance when comparing the Fasted 1 mM and fed 5 mM glucose groups seems somewhat paradoxical, but may indicate that changes in afferent excitatory innervation of NPY neurons is an acute rather than chronic effector of behavioral and physiological changes. Further work is required to investigate the nuances of energy status sensing neurotransmission at arcuate NPY neurons. It must be acknowledged that, as neuronal membrane potential was held more negative than the reversal potential for chloride under our recording conditions, EPSCs ostensibly observed may indeed be reversed IPSCs. As such the implications of this data is limited.

3.3.2 Passive membrane properties

Neurons of the Fasted 1 mM glucose population had significantly shorter action potential duration at ½ amplitude ($p=0.0007$) and action potential duration at threshold ($p=0.0002$), compared to neurons of the Fed 1 mM population.

No statistical significance was observed when comparing the passive membrane properties of Fasted 1 mM glucose and Fed 5 mM glucose experimental groups. However neurons of the Fasted 1 mM glucose group did display a trend for shorter

action potential duration at threshold (p=0.069; 2-way ANOVA, post-hoc Bonferroni test) relative to Fed 5 mM neurons.

No statistical significance was observed when comparing the passive membrane properties of Fed 1 mM glucose and Fed 5 mM glucose experimental populations.

Here I show that negative energy state is associated with faster action potential and AHP kinetics. Our current understanding is that *In vivo* NPY neuron activity is elevated in negative energy states, and faster rise and decay times increases the neurons competence for high frequency discharge (Krashes et al., 2014, Cone, 2005). Further work would be of use, using larger samples of neurons, to determine if other passive membrane parameters are subtly yet significantly altered in differing energy states.

3.3.4 Active membrane properties

Here I show energy-status-dependent plasticity of expression of active conductances differentially expressed in NPY neurons depending on glucose levels and energy status (fed versus fasted). Of note is a negative correlation between energy abundance and I_H conductance expression, with 7.5% of NPY eGFP neurons expressing this conductance in the Fed 5 mM glucose population, 12.5 % of neurons in the Fed 1 mM glucose population expressed I_H, whereas 30% of NPY neurons expressed I_H in the Fasted 1 mM glucose group.

Also of note is a positive correlation between energy abundance and I_T conductance expression, with 52.5% of neurons expressing this conductance in the Fed 5 mM glucose group, 30% of NPY neurons expressed I_T in the Fed 1 mM

population, whereas only 22.5% of neurons expressed I_T in the Fasted 1 mM glucose population.

In this study, there was a notable absence of any clear instantaneous inward rectification, upon membrane hyperpolarization. Arcuate NPY neurons express potassium inward rectifier 6.2 (Kir6.2) and it may therefore seem surprising that I_{AN} expression was observed so seldom. However the Kir6.2 isoform confers weak rectification properties unto the neuron in question, and therefore the ostensible absence of this conductance does not indicate the absence of functional Kir channels in the NPY neuron membrane (Kurata et al., 2004, van den Top et al., 2007).

A degree of plasticity was also observed in the Coexpression of I_H and I_T, with 2.5% of neurons expressing both in the Fed mM glucose group, 5% co-expressing I_H and I_T in the Fed 1 mM group and 15% of neurons expressing both I_H and I_T in the Fasted 1 mM population.

Both I_H and I_T conductances can generate pacemaker-like activity, which has previously been observed in orexigen-sensing arcuate neurons, and also in my experiments (van den Top et al., 2004). Data presented here would suggest that I_H and not I_T is more associated with states of negative energy balance. NPY neurons are known to elevate electrical activity during energy deficit *in vivo*, as such one can postulate that elevated I_H expression under such conditions, contributes to NPY neuron firing frequency and firing pattern. Furthermore, NPY neurons co-expressing AgRP can differentially regulate release of AgRP versus NPY and GABA depending on the physiological status of the organism. These changes in intrinsic membrane conductances may therefore be fundamental to encoding and

formulating output that drives differential release of these peptides and/or amino acid transmitters appropriate to physiological energy status.

The proportion of neurons expressing no active conductances was relatively consistent across experimental groups with 35% in Fed 5 mM conditions, 40% in Fed 1 mM conditions and 30% in Fasted 1 mM conditions. This may suggest that these neurons contribute a subpopulation of non-energy-sensing population of NPY neurons in the ARH. Further work should use anterograde or retrograde tracing to investigate how differences in electrophysiological properties pertain to target innervation and physiological output functions.

Previous publications have highlighted the heterogeneity of arcuate NPY neurons, in terms of their molecular expression profile, afferent inputs, efferent connections and physiological function (Krashes et al., 2014, Betley et al., 2013, Konner et al., 2007, Shi et al., 2013). However a thorough investigation of the electrophysiological heterogeneity of arcuate NPY neurons has been lacking, as has research into the manner in which electrophysiological characteristics are affected by feeding status. Research presented here represents the first description of feeding state-dependent changes in arcuate NPY neuron characteristics and contributes significantly to our current understanding of NPY neuron function *in vivo*. It is clear that in order to better understand these neurons, we must attain a better appreciation of their complexity as a network of cells and as individual information processing units. Work presented here is a positive step in that direction.

Figure 3.1: The frequency of excitatory post-synaptic currents (EPSCs) is modulated by extracellular glucose concentration and feeding state

A: Voltage clamp recording taken from an NPY eGFP neuron held at -90 mV, from a mouse fed *ad libitum* prior to culling with brain slices incubated in aCSF containing 1 mM glucose.

B: Voltage clamp recording taken from an NPY eGFP neuron held at -90 mV, from a mouse subjected to an 18-hour fast prior to culling with brain slices incubated in aCSF containing 1 mM glucose.

C: Voltage clamp recording taken from an NPY eGFP neuron held at -90 mV, from a mouse fed *ad libitum* prior to culling with brain slices incubated in aCSF containing 5 mM glucose.

D: Current clamp recording taken from a NPY eGFP neuron, of a mouse subjected to an 18-hour fast prior to culling with brain slices incubated in aCSF containing 1 mM glucose. Here excitatory postsynaptic potentials (EPSPs) are sufficient to evoke action potential firing.

Figure 3.1

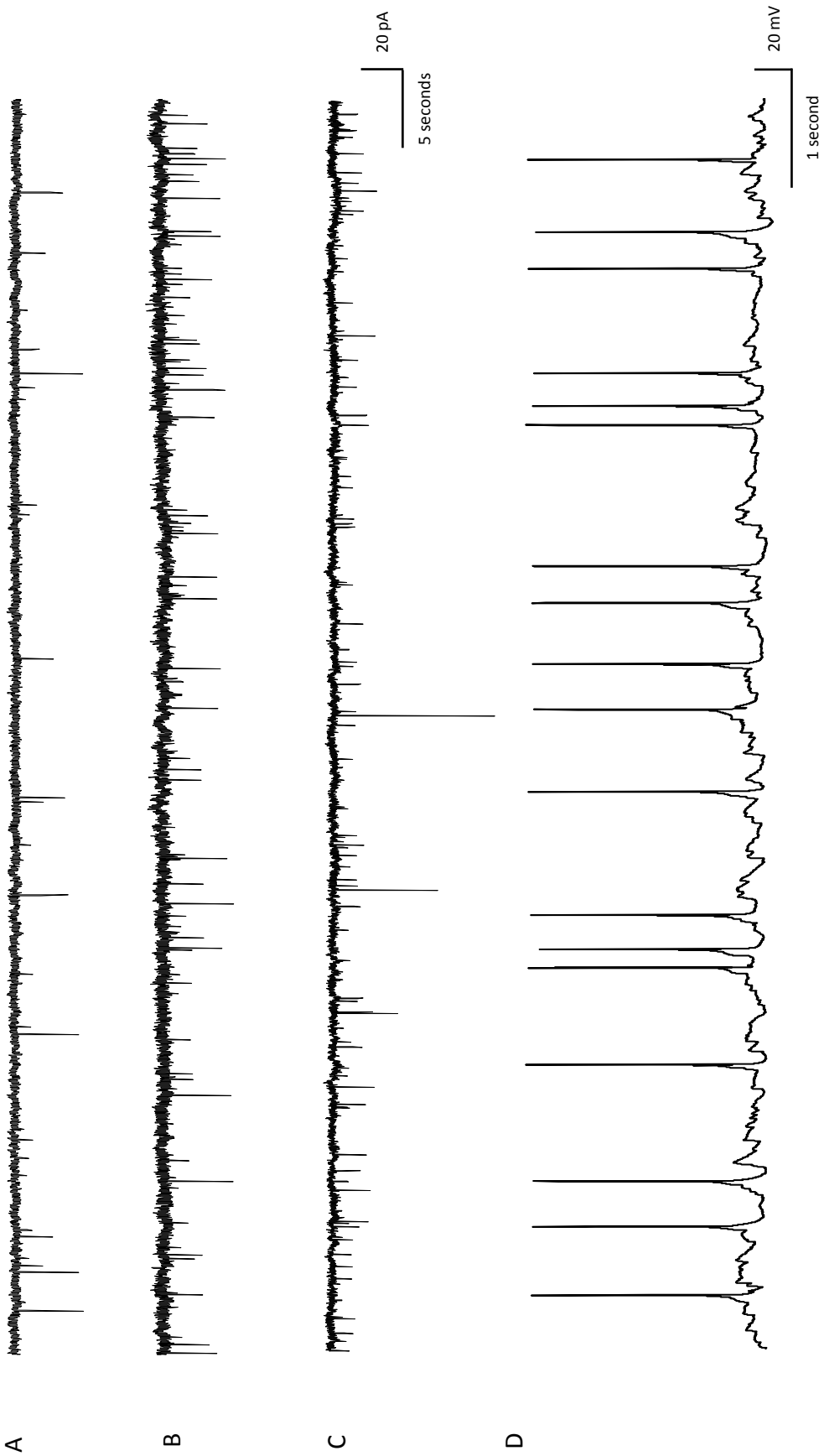

Figure 3.2: Active and passive neuronal membrane properties

A: Current clamp recording showing action potential and afterhyperpolarisation potential. Annotations highlight parameters quantified.

Bi: Superimposed samples of a continuous current clamp recording highlighting an anomalous inwardly rectifying potassium conductance (I_{AN}), observed as a reduction in neuron input resistance at more hyperpolarized membrane potentials

Bii: Graph highlighting the current-voltage relationship of a neuron exhibiting anomalous inward rectification.

C: Current clamp recording showing a membrane response to hyperpolarizing current injection (inset) highlighting a hyperpolarization-activated cation conductance (I_H), observed as a time- and voltage-dependent reduction in neuron input resistance, upon membrane hyperpolarization and a rebound depolarization at the offset of the response to current injection.

D: Current clamp recording highlighting a T-type calcium conductance (I_T), observed as an overshoot in membrane potential, at the offset of membrane hyperpolarization.

Figure 3.2

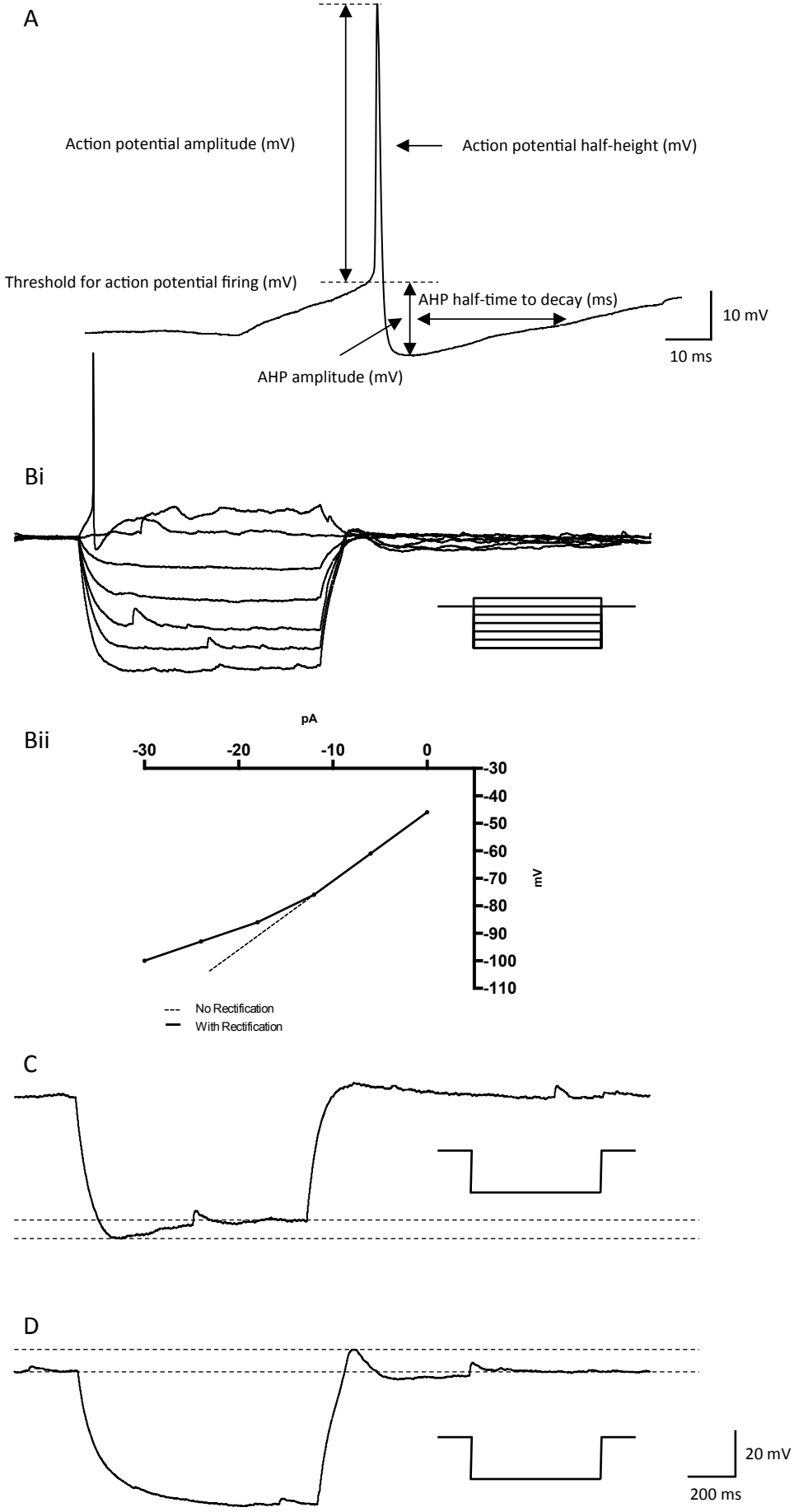
A
Action potential amplitude (mV)
Action potential half-height (mV)
Threshold for action potential firing (mV)
AHP half-time to decay (ms)
AHP amplitude (mV)
10 mV
10 ms
Bi
Bii
pA
-30
-20
-10
0
-30
-40
-50
-60
-70
-80
-90
-100
-110
mV
No Rectification
With Rectification
C
D
20 mV
200 ms

Figure 3.3: Passive membrane properties

A: Table summarizing the passive membrane properties of NPY neurons obtained from brain slices incubated in either 1 mM or 5 mM glucose, of mice either fed *ad libitum* or fasted for 18 hours prior to culling.

Figure 3.3

A

	Fasted 1 mM Glucose (n=40)	Fed 1 mM Glucose (n=40)	Fed 5 mM Glucose (n=40)	2-Way ANOVA Significance	Bonferroni Post-Hoc Analysis p Value *
Spontaneous activity (%)	87.5	95	82.5	NS (Chi-square; 0.215)	N/A
Membrane potential (mV)	-39.44 ± 0.83	-39.05 ± 0.49	-39.27 ± 0.94	NS (0.9358)	>0.9999 >0.9999 >0.9999
Spontaneous Firing rate (Hz)	1.52 ± 0.22	1.41 ± 0.14	1.84 ± 0.35	NS (0.4468)	>0.9999 >0.9999 0.6667
Input resistance (MΩ)	1484 ± 166	1975 ± 292	1686 ± 131	NS (0.2682)	0.3245 >0.9999 0.9972
Membrane time-constant (ms)	59.45 ± 7.44	73.18 ± 5.70	70.45 ± 9.23	NS (0.3571)	0.525 0.8445 >0.9999
Threshold for action potential (AP) firing (mV)	-24.28 ± 2.35	-26.39 ± 1.50	-26.22 ± 0.44	NS (0.6111)	>0.9999 >0.9999 >0.9999
AP amplitude (mV)	42.59 ± 3.75	44.18 ± 2.57	42.87 ± 1.19	NS (0.9088)	>0.9999 >0.9999 >0.9999
AP half-height duration (ms)	2.64 ± 0.15	3.53 ± 0.19	3.07 ± 0.18	**S (0.0007)**	**0.0005** 0.1715 0.1295
AP threshold duration (ms)	6.62 ± 0.54	9.33 ± 0.54	8.05 ± 0.58	**S (0.0002)**	**0.0001** 0.0692 0.1261
AP ratio; threshold: half-height	2.45 ± 0.10	2.64 ± 0.08	2.60 ± 0.09	NS (0.1186)	0.1744 0.2919 >0.9999
Afterhyperpolarisation potential (AHP) amplitude (mV)	16.99 ± 0.79	16.04 ± 0.66	18.00 ± 0.84	NS (0.1664)	>0.9999 0.9858 0.1772
AHP half-decay time (ms)	313 ± 48	461 ± 48	442 ± 73.34	NS (0.1183)	0.1756 0.2873 >0.9999

*

Top:	Fasted 1 mM	vs.	Fed 1 mM
Middle:	Fasted 1 mM	vs.	Fed 5 mM
Bottom:	Fed 1 mM	vs.	Fed 5 mM

Figure 3.4: NPY neurons express multiple subthreshold active conductances

Samples of continuous whole-cell recordings are shown of membrane responses to current injection.

A: Superimposed current clamp recording of an NPY eGFP neuron with membrane potential held at -60 mV, in control conditions.

B: Superimposed current clamp recordings from an NPY eGFP neuron with membrane potential held at -60 mV, in the presence of 1 μM TTX.

C: Superimposed current clamp recordings from an NPY eGFP neuron with membrane potential held at -60 mV, in the presence of 1 μM TTX and the inward rectifier blocker, barium chloride 100 μM.

D: Superimposed current clamp recordings from of an NPY eGFP neuron with membrane potential held at -60 mV, in the presence of 1 μM TTX, 100 μM barium chloride and the Ih inhibitor cesium chloride 500 μM. Note the loss of the hyperpolarizing sag in response to larger amplitude current injections.

E: Superimposed current clamp recordings from an NPY eGFP neuron with membrane potential held at -50 mV, in the presence of 1 μM TTX, 100 μM barium chloride and 500 μM cesium chloride. Note the small rebound excitation at the offset of the response to hyperpolarizing current injection that persists under these recording conditions.

F: Superimposed current clamp recordings from an NPY eGFP neuron with membrane potential held at -50 mV, in the presence of 1 μM TTX, 100 μM barium chloride, 500 μM cesium chloride and the low threshold T-type calcium channel blocker, nickel (1 mM nickel chloride).

Figure 3.4

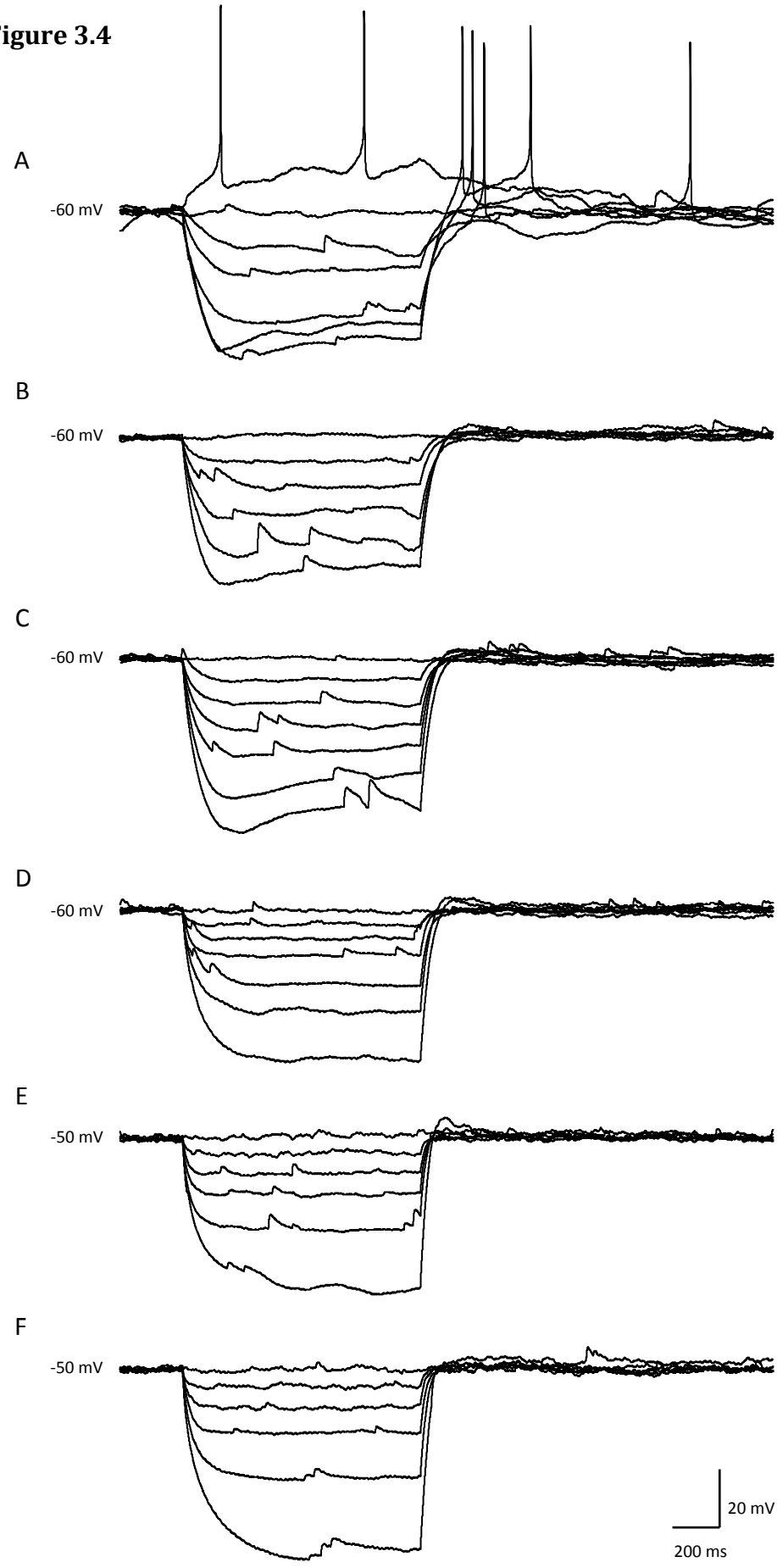

Figure 3.5: Energy Status-dependent plasticity of subthreshold active conductance expression

A: Bar chart summarizing the active conductance expression profile of arcuate NPY eGFP neurons in fed and fasted conditions and in the presence of fasted (1mM) or fed (5mM) levels of D-glucose.

B: Table summarizing the differences in active conductance expression profile of arcuate NPY eGFP neurons in fed and fasted conditions and in the presence of fasted (1mM) or fed (5mM) levels of D-glucose. *p*-values as calculated from Chi-square testing.

Figure 3.5

A

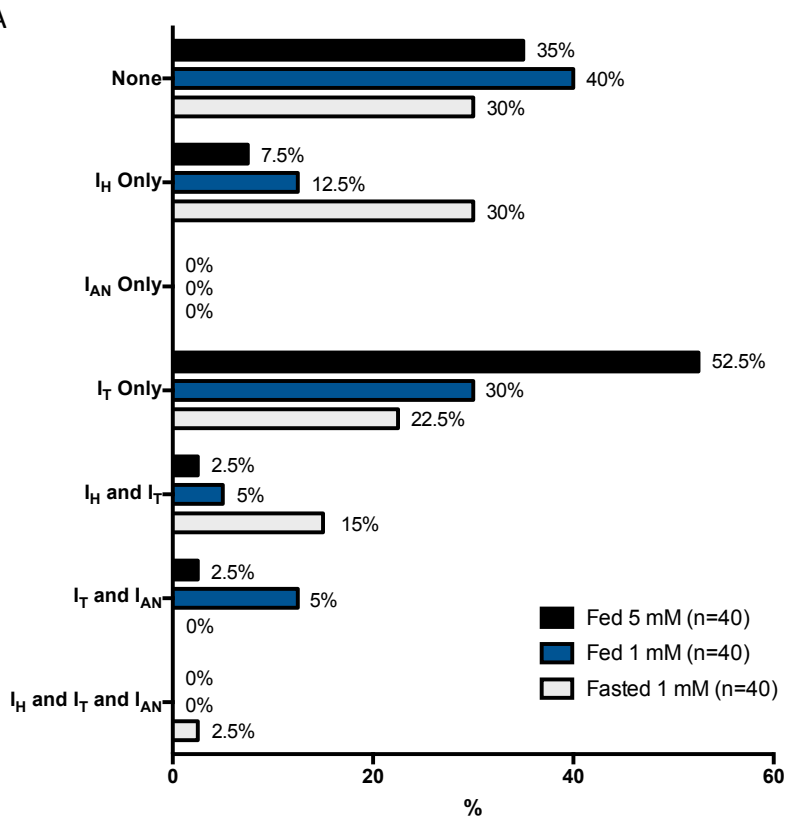

B

Fasted 1 mM vs. Fed 1 mM	***p* = 0.0364**
Fasted 1 mM vs. Fed 5 mM	***p* = 0.0071**
Fed 1 mM vs. Fed 5 mM	*p* = 0.1927

Figure 3.6: Differential expression of subthreshold active conductances in NPY eGFP neuron subpopulations

Samples of continuous whole-cell recordings are shown of membrane responses to current injection.

A: An NPY eGFP neuron ostensibly lacking the expression of any subthreshold active conductances.

B: An NPY eGFP neuron only expressing the I_H conductance.

C: An NPY eGFP neuron only expressing the I_T conductance.

D: An NPY eGFP neuron expressing I_T and I_{AN} conductances.

Figure 3.6

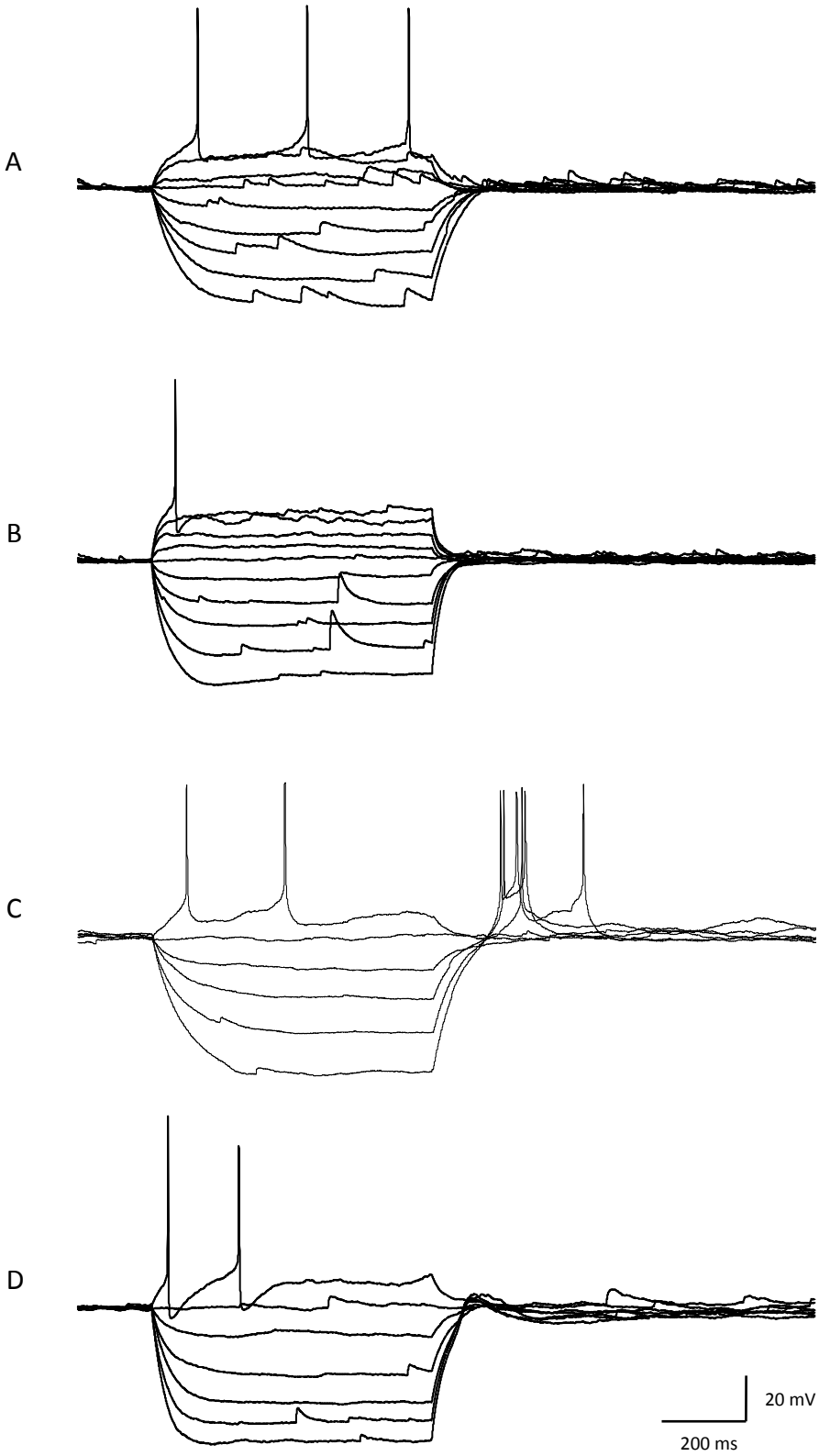

Figure 3.7: Voltage-dependence of oscillatory membrane activity

Ai: An NPY eGFP neuron with membrane potential held around -38 mV, displaying tonic firing.

Aii: The same NPY eGFP neuron as shown in Ai, with membrane potential held around -45 mV, displaying tonic activity, yet at slower firing frequency as in Ai.

Aiii: The same NPY eGFP neuron as shown above, with membrane potential held around -48 mV, displaying tonic activity beginning to transition into burst firing.

Aiv: The same NPY eGFP neuron as shown above, with membrane potential held around -55 mV, with more pronounced bursting activity, with a longer interburst interval than as in Aiii.

Av: The same NPY eGFP neuron as shown above, with membrane potential held around -70 mV, with more pronounced bursting activity, with a longer interburst interval than as in Aiii and Aiv.

Avi: The same NPY eGFP neuron as shown above, with membrane potential held around -85 mV, with oscillatory activity totally abolished.

B: An NPY eGFP neuron bathed in TTX (1μM), with membrane potential held around -50 mV. Here, action potentials are abolished, but the underlying oscillations persist.

Figure 3.7

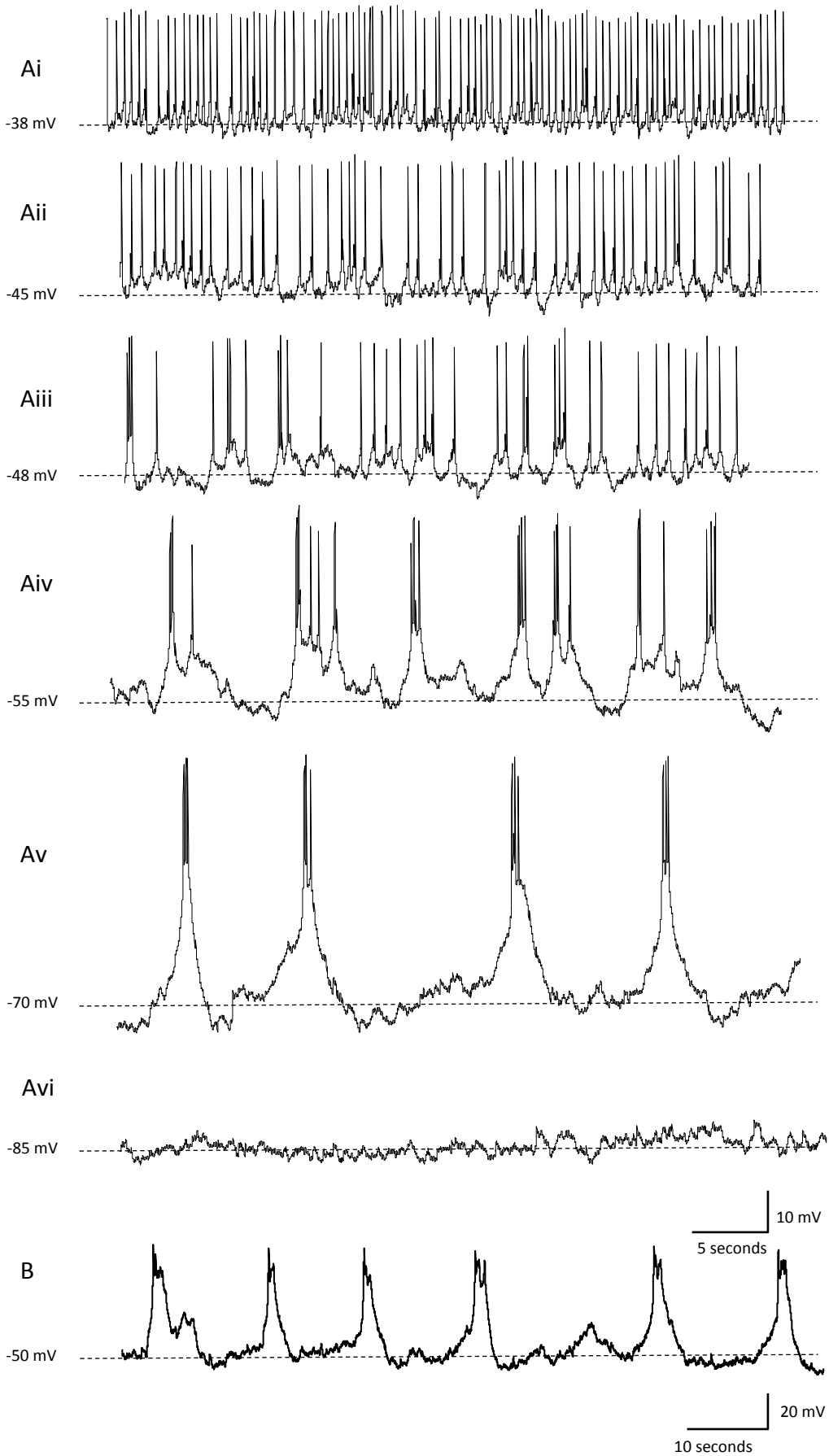
Ai
-38 mV
Aii
-45 mV
Aiii
-48 mV
Aiv
-55 mV
Av
-70 mV
Avi
-85 mV
10 mV
5 seconds
B
-50 mV
20 mV
10 seconds

Chapter 4: Functional, energy status-dependent plasticity of glucose sensing in NPY/AgRP neurons

4.1 Introduction

Metabolic substrates are required for energy generation in al life. In mammals, dietary fats, proteins and carbohydrates are catabolized for the generation of adenosine triphosphate (ATP), whilst excess calories are stored predominantly as white fat and hepatic glycogen. Glucose homeostasis is regulated by central and peripheral mechanisms, and through reciprocal hormonal-neuronal communication. Peripheral mechanisms of glucose homeostasis include hepatic, pancreatic and adrenomedullary processes whilst central mechanisms involve the hedonic and homeostatic control of food intake. Direct glucose-sensing cells exist within pancreatic islets and in central nervous system (CNS) regions close to the third and fourth ventricles, including the hypothalamus (McCrimmon, 2009, Lam, 2010). Physiological counter-regulatory mechanisms to hypoglycemia include reduced insulin secretion, increased glucagon secretion and increased adrenomedullary catecholamine release via ventromedial hypothalamic-sympathetic nervous system (VMH-SNS) recruitment, all of which act to decrease peripheral glucose uptake and increase glucose production by the liver and kidneys (Hoffman, 2007, Borg et al., 1995). Conversely, the physiological response to hyperglycemia includes increased insulin secretion, decreased glucagon release, reduced SNS tone and increased parasympathetic nervous system (PNS) recruitment, all of which decreases hepatic and renal glucose production, and increases glucose uptake to skeletal muscle and peripheral organs. These

mechanisms ensure the tight control of blood glucose concentration. Physiological plasma glucose concentration lies between 4 and 7 mM whilst cerebrospinal fluid (CSF) glucose levels are approximately 10 to 30% of peripheral levels, and have been estimated to be around 1 to 2.5 mM (McNay and Gold, 1999, Silver and Erecinska, 1994). In pathophysiological hyperglycemia, plasma glucose concentration can rise as high as 15 mM whilst central levels can reach 4.5 mM (Silver and Erecinska, 1994). Hypoglycemia can result in peripheral glucose falling as low as 2.8 mM and central glucose concentrations decreasing to 0.16 mM (Silver and Erecinska, 1994). These data indicate that central glucose concentrations may fluctuate from a tenth of a micromolar to as high as 15 millimolar. As such a more modest and physiological range of 1 mM glucose – replicating fasted conditions – and 5 mM – replicating fed conditions – are used in the experimental design outlined herein.

Hypothalamic glucose levels have been measured at around 1.4 mM, however in areas such as the arcuate nucleus (ARH), in close apposition to more permeable blood-brain-barrier (BBB) structures such as the median eminence, glucose concentrations may fluctuate to a greater degree (Banks, 2008). Furthermore, in pathophysiological conditions such as obesity and diabetes, elevated central glucose concentrations are an inevitable consequence of chronic hyperglycemia. The effects of this on neuronal function are yet to be determined. Previous reports have observed reductions in neuronal insulin signaling in the hypothalamus of obese rats (Spanswick et al., 2000).

The brain requires a constant supply of glucose from the periphery, as astrocytic glycogen stores are negligible. Central metabolism of glucose is in part limited by peripheral glucose concentration and glucose transporter kinetics. Glucose

transporters (GLUTs) are responsible for the trafficking of glucose into both peripheral and central tissues (Vannucci et al., 1997). Seven GLUT isoforms are expressed in mammalian tissues. Their differential expression is outlined in table 4.1, below:

GLUT Isoform	Tissue Expression
GLUT1 (55kDa)	Erythrocytes, BBB (K_M: 17.6 mM)
GLUT1 (45 kDa)	Glia, neurons, choroid plexus
GLUT2	Liver, kidney, pancreas, astrocytes (K_M: 42.3 mM)
GLUT3	Placenta, sperm, platelets, neurons (K_M: 10.6 mM)
GLUT4	Heart, muscle, adipocytes
GLUT5	Small intestine, macrophage, sperm, microglia
GLUT6	Pseudogene
GLUT7	Liver, kidney, astrocytes

Table 4.1: Differential tissue expression of mammalian GLUT isoforms

Table adapted from (Gould et al., 1991, Vannucci et al., 1997).

Glucose is required for the function of all cells in the CNS including neurons and astroglia, both of which use it as the main substrate to generate energy (Yang et al., 2015). Central glucose signaling can occur via neuron-only mechanisms and through the integration of both neuronal and glial signals. Astroglia outnumber neurons in the CNS and form the bulk of CNS parenchyma (Nedergaard et al., 2003). In the CNS, astroglia function to scale synaptic strength and modulate neuronal circuits through the release of gliotransmitters (Belanger and Magistretti, 2009, Volterra and Meldolesi, 2005). Gliotransmitters include glutamate, D-serine

ATP and adenosine (Belanger et al., 2011, Volterra and Meldolesi, 2005). Astroglia release transmitters via calcium-dependent exocytosis and through non-exocytotic mechanisms (Volterra and Meldolesi, 2005). Connexin 43 (Cx43) hemichannels have been shown to mediate ATP release (Stout et al., 2002, Arcuino et al., 2002). ATP and adenosine signaling from glia to neurons may present a mechanism by which hypothalamic neurons sense fluctuations in central glucose concentrations and generate functional behavioral outputs (Newman, 2003, Yang et al., 2015).

The hypothalamus is required for glucose homeostasis and contains neurons that couple extracellular glucose and metabolic secretagogue concentration to electrical excitability. Changes in electrical activity generate functional outputs that regulate physiological processes such as food intake, energy expenditure and hepatic glucose production (Hahn et al., 1998, Luquet et al., 2005, Muroya et al., 1999, Shi et al., 2013, van den Top et al., 2004, Konner et al., 2007, Parton et al., 2007, Claret et al., 2007). Hypothalamic loci containing glucose-sensitive neurons include the VMH, lateral hypothalamus (LH) and ARH (Ashford et al., 1990a, van den Top et al., 2004, Spanswick et al., 2000, Oomura et al., 1974). Glucose responsive (GR) neurons can be divided into glucose excited (GE) and glucose inhibited (GI) neurons. GR neurons of the ARH include both orexigenic neuropeptide Y/ agouti-related peptide (NPY/AgRP) and anorexigenic proopiomelanocortin/cocaine and amphetamine-regulated transcript (POMC/CART) neurons, both of which are required for normal energy homeostasis (Parton et al., 2007, Spanswick et al., 2000, Konner et al., 2007).

Optogenetic and pharmacogenetic activation of NPY/AgRP neurons elevates food intake, whilst neuronal inhibition results in decreased food intake (Aponte et al., 2011, Atasoy et al., 2012, Krashes et al., 2011). The functional

importance of arcuate NPY/AgRP neurons is underlined by work demonstrating that ablation of these neurons in adult mice is sufficient to induce starvation (Luquet et al., 2005). Fasting has been reported to increase action potential firing rate in NPY/AgRP neurons (Takahashi and Cone, 2005). NPY/AgRP neurons have historically been assumed to be GI, are excited by orexigenic peptides such as ghrelin, and are inhibited by the anorexigenic peptides insulin and leptin (van den Top et al., 2004, Spanswick et al., 1997, Spanswick et al., 2000). Although NPY/AgRP neurons have been thoroughly characterized for their role regulating food intake, they are also important in the maintenance of glucose homeostasis (Konner et al., 2007). The functional and anatomical heterogeneity of NPY/AgRP neurons is highlighted by work investigating the differential orexigenic effect of efferent target innervation *in vivo* (Betley et al., 2013).

NPY/AgRP neurons have been shown to regulate POMC/CART neuron activity via inhibitory GABAergic synapses (Cowley et al., 2001). Functionally antagonistic NPY/AgRP and POMC/CART neurons of the ARH form the melanocortin system, which regulates food intake and energy expenditure. The melanocortin system affects physiological parameters through agonism and antagonism of the melanocortin-4 receptor (MC4R) at second order neurons (with both NPY/AgRP and POMC/CART considered first order). α-melanocyte-stimulating hormone (α-MSH) released by POMC/CART neurons is the endogenous agonist of the MC4R, whilst AgRP is the endogenous antagonist of the MC4R (Atasoy et al., 2012). NPY/AgRP and POMC/CART neurons share common projection sites including paraventricular hypothalamic (PVH) neurons. Increased agonism of MC4 receptors promotes satiety and energy expenditure whilst MC4R antagonism promotes feeding and decreased energy expenditure. Central glucose

concentration affects the tone of the melanocortin system via GR NPY/AgRP and POMC/CART neurons.

The ARH contains both GE and GI neuronal populations, with NPY/AgRP assumed to be GI and POMC/CART assumed to be GE. Mechanisms of neuronal GI include Na^+/K^+ ATPase pump, K^+, and Cl^- channel activation (Oomura et al., 1974, Fioramonti et al., 2007, Burdakov and Gonzalez, 2009, Jordan et al., 2010, Canabal et al., 2007). The mechanism of GE in the ARH has been shown to be via ATP-sensitive potassium (K_{ATP}) channel inhibition and has been described as analogous to pancreatic β-cell depolarization (Ashford et al., 1990a, van den Top et al., 2007, Spanswick et al., 1997, Ashford et al., 1990b). A K_{ATP}-independent mechanism of GE has been reported, but is activated at supraphysiological concentrations, between 5 and 20 mM glucose (Fioramonti et al., 2004). K_{ATP} channels couple metabolic state to membrane potential by modulating plasma membrane potassium flux (Ashcroft, 1988). Both NPY/AgRP and POMC/CART neurons express functional K_{ATP} channels (van den Top et al., 2007, Ibrahim et al., 2003).

K_{ATP} channels are hetero-octamers, with four pore forming inwardly rectifying potassium channel (Kir6.x) subunits surrounded by four sulfonylurea receptor (SURx) subunits (Inagaki et al., 1995, Miki et al., 1999). Pancreatic β-cells express Kir6.2 and SUR1 whilst neuronal K_{ATP} channels have been reported to be composed of all possible combinations of Kir6.1, Kir6.2, SUR1 and SUR2A (Karschin et al., 1998). Kir6.x subunits confer channel rectification properties and are the site of ATP binding, which initiates channel inhibition (Ashcroft, 2005). SUR subunits belong to the ATP-binding cassette (ABC) transporter family and confer channel sensitivity to Mg^{2+} nucleotides, channel openers such as diazoxide and channel inhibitors such as the sulphonylureas tolbutamide and glibenclamide

(Ashcroft, 2005). Sulphonylureas are widely used in the treatment of type-II diabetes, and can stimulate β cell insulin secretion via K_{ATP} channel inhibition (Ashcroft and Gribble, 2000). K_{ATP} channels are required for the secretion of glucagon from pancreatic α cells, insulin from pancreatic β cells, somatostatin from D cells and glucagon-like peptide-1 (GLP-1) from L cells (Ashcroft et al., 1984, Gopel et al., 2000b, Gopel et al., 2000a, Gribble et al., 2003). In many central neurons, K_{ATP} channels open only under pathophysiological conditions and offer neuroprotection for hypoxia-induced seizure and excitotoxic cell death (Yamada et al., 2001, Hernandez-Sanchez et al., 2001).

In specialized populations of central GR neurons including those of the VMH and ARH, K_{ATP}-regulated electrical activity controls glucostatic functions such as hepatic glucose production, energy expenditure and food intake (Miki et al., 2001, Spanswick et al., 2000). The process of K_{ATP} mediated neuronal GE involves GLUT3-dependent glucose uptake followed by glycolysis and oxidative metabolism, with the rate-limiting step in β cells being glucose phosphorylation to glucose-6-phosphate by glucokinase (GK) (Sakura et al., 1998). Increased glucose metabolism results in an elevated intracellular ATP/ADP ratio, increased ATP-Kir6.x subunit binding, K_{ATP} channel inhibition and membrane depolarization (Sakura et al., 1998).

NPY/AgRP are sensitive to a number of peripheral hormones, including leptin, insulin and ghrelin (van den Top et al., 2007, van den Top et al., 2004, Spanswick et al., 2000, Spanswick et al., 1997, Cone, 2005). Insulin and leptin hyperpolarize NPY/AgRP neurons through the activation of phosphoinositide-3 kinase (PI3K) signal transduction, increasing intracellular phosphatidylinositol (3,4,5)-trisphosphate (PIP_3), and the opening of K_{ATP} channels (Plum et al., 2006b,

Spanswick et al., 1997, Spanswick et al., 2000, Harvey et al., 2000). Ghrelin is a potent orexigenic hormone, secreted from A-cells of gastric mucosa (Dornonville de la Cour et al., 2001). Plasma ghrelin concentration increases pre-prandially and falls post-prandially (Cummings et al., 2001, Tschop et al., 2001a). Chronic administration of ghrelin can induce obesity (Tschop et al., 2000). The ghrelin receptor growth hormone secretagogue receptor 1a (GHSR1a) is expressed in multiple CNS regions including the VMH and ARH (Guan et al., 1997, Bennett et al., 1997). The orexigenic actions of ghrelin are attributed to its actions at GHSR1a receptors on NPY/AgRP neurons and afferent glutamatergic neurons (Chen et al., 2004, Yang et al., 2011). Ghrelin has been shown to induce pacemaker-like activity in NPY/AgRP neurons that is dependent upon the modulation of a voltage-sensitive low-threshold t-type calcium conductance, intrinsic to NPY/AgRP neurons (van den Top et al., 2004).

The ghrelin-induced depolarization of glutamatergic neurons afferent to NPY/AgRP neurons has been shown to be via a GHSR1-G$\alpha/_{q11}$-AMPK-cADP ribose-ryanodine receptor (RyR)-Ca^{2+} release-dependent mechanism (Yang et al., 2011, Aponte et al., 2011). AMP-activated protein kinase (AMPK) is expressed in a multiple hypothalamic nuclei including the ARH, VMH, PVH and LH and is a central regulator of cellular metabolism, detecting cellular energy status (Mihaylova and Shaw, 2011, Lopez et al., 2008, Minokoshi et al., 2004). AMPK is a serine/threonine protein kinase that is activated under negative energy states due to an increased intracellular AMP/ATP ratio. AMPK signaling in both NPY/AgRP and POMC/CART neurons is required for ARH glucose sensing and normal energy homeostasis (Claret et al., 2007). AgRP-AMPK α2 subunit deletion results in a lean mouse phenotype and POMC- α2 deletion results in obesity due to reduced energy

expenditure (Claret et al., 2007). α2 deletion results in neuronal glucose resistance but does not affect leptin and insulin sensitivity (Claret et al., 2007).

Many *in vitro* electrophysiological studies into the effects of glucose and hormones on the electrical activity of hypothalamic neurons have used sub- and supra-threshold glucose concentrations in artificial cerebrospinal fluid (aCSF); the solution in which brain slices are incubated (Takahashi and Cone, 2005, Spanswick et al., 1997, Ashford et al., 1990a). Results from these studies, although useful may not be representative of *in vivo* conditions.

In this study I used the visualized whole-cell patch-clamp technique to explore the effects of fasting upon NPY/AgRP neuron electrical activity, and also to investigate the effect that fasting has upon glucose sensitivity in these neurons. A key difference of this work compared to previous studies on the same topic such as (Takahashi and Cone, 2005) is that here I describe the effects of fasting on neurons incubated in physiologically relevant glucose concentrations post-dissection, and during experimentation. I also look at the effect that fed state and ambient glucose concentration has upon the sensitivity of NPY/AgRP neurons to ghrelin *in vitro*.

4.2 Results

4.2.1 The effects of ambient extracellular glucose concentrations and feeding state on active and passive membrane properties of NPY eGFP neurons

Whole-cell patch clamp recordings were obtained from NPY eGFP neurons in hypothalamic brain slice preparations from mice fed *ad libitum* and from mice fasted for 18 hours. The effects of extracellular glucose on passive and active membrane properties were investigated.

NPY eGFP neurons of the fed population were exposed to and maintained in 5 mM glucose (n=70). Of the neurons in this population 86% were spontaneously active and the remaining 14% were silent at rest. These neurons had a mean resting membrane potential of -39.60 ± 0.84 mV, mean spontaneous action potential firing rate of 2.18 ± 0.24 Hz and neuronal input resistance of 1827 ± 132 MΩ.

NPY eGFP neurons of an *ad libitum* fed population were also exposed and maintained in fasted levels, 1 mM, extracellular glucose (n=40). Of the neurons in this population, 95% were spontaneously active and the remaining 5% were silent at rest. NPY eGFP neurons of the 'fed 1 mM glucose' population had a mean resting membrane potential of 38.68 ± 0.63 mV, mean spontaneous action potential firing rate of 1.33 ± 0.14 Hz and neuronal input resistance of 1680 ± 136 MΩ.

NPY eGFP neurons of the fasted population were exposed to and maintained in 1 mM extracellular glucose (n=240). Of the neurons in this population 79% of neurons were spontaneously active and the remaining 21% of neurons were silent at rest. NPY eGFP neurons of the 'fasted 1 mM glucose' population had a mean resting membrane potential of 41.04 ± 0.57 mV, mean spontaneous action potential firing rate of 1.61 ± 0.11 Hz and neuronal input resistance of 1538 ± 66 MΩ.

Analysis of these groups revealed statistically significant differences between these populations. The mean action potential firing rate of the 'fed 5 mM glucose' population is significantly different to that observed in both the 'fed 1 mM glucose' population and the 'fasted 1 mM glucose' population (p-values; < 0.05, 2-way ANOVA). Statistical significant differences were also observed in neuronal input resistance. Mean neuronal input resistance of the 'fed 5 mM glucose'

population being significantly higher than the 'fasted 1 mM glucose population ($p=<0.05$; 2-way ANOVA). See figures 4.1 and 4.2.

4.2.2 Fasting-induced reorganization of glucose sensing in the arcuate NPY/AgRP neuron population

NPY/AgRP neuron responsiveness to an increase in extracellular glucose from 1 mM to 5 mM was determined in neurons in hypothalamic brain slices taken of mice fed *ad libitum* and mice subjected to an 18-hour fast prior to culling. Of the NPY eGFP neurons recorded from 'fed' animals, increasing extracellular glucose concentration from 1 to 5 mM resulted in membrane depolarization in 25% of neurons, membrane hyperpolarization in 29% of neurons, and no discernable response in 46% of NPY eGFP neurons tested (n=36) (figure 4.5A). Of the NPY eGFP neurons from 'fasted' animals increasing extracellular glucose depolarized 40% of neurons, hyperpolarized 34% of neurons and in the remaining 26%, no response to glucose was observed (n=73) (figure 4.5B). Although not a statistically significant change in response distribution, Chi-square analysis indicated a trend towards a significant redistribution ($p=0.0783$; fed vs. fasted).

4.2.3 Ionic mechanism underlying glucose-induced inhibition of NPY eGFP neurons under fed and fasted conditions

Of the 'fed' glucose-induced inhibitory (GI) responses, membrane hyperpolarization from -52.73 ± 1.54 mV to -59.39 ± 1.76 mV was associated with a decrease in spontaneous action potential firing rate from 0.08 ± 0.06 Hz to 0.03 ± 0.03 Hz, and a decrease in input resistance from 1759 ± 318 MΩ to 1410 ± 342 MΩ (n=10). Of the 'fasted' GI responses, membrane hyperpolarization from –49.79 ±

1.41 mV to -55.90 ± 1.73 mV, was associated with a decrease in action potential firing rate from 0.11 ± 0.08 Hz to 0.03 ± 0.03 Hz, and a decrease in input resistance from 1559 ± 165 MΩ to 1150 ± 174 MΩ (n=25). When comparing GI responses of fed and fasted groups, no statistical significance was observed in the magnitude of responses, measured in terms of membrane potential, spontaneous action potential firing rate and input resistance (see figure 4.6E). The decreased input resistance associated with glucose-induced inhibition in both the fed and fasted states was accompanied by a reversal potential around -70 mV, indicated by the point of intersection of voltage-current relations generated in response to injection of a range of depolarizing and hyperpolarizing rectangular-wave current pulses (figure 4.3Biii). This reversal potential suggests that in these neurons, glucose-induced the activation of a chloride conductance under our recording conditions. Reversal potentials associated with inhibitory responses to glucose varied between neurons tested here, ranging from -50.00 mV to -87.00 mV with a mean of -67.45 ± 2.40 mV (n=20). The inhibitory effects of glucose on NPY eGFP neurons persisted in the presence of TTX suggesting activity-dependent synaptic transmission did not indirectly underpin this effect (n=6). Control membrane potential and spontaneous firing rate values here are more hyperpolarized than stated in section 4.2.1 as membrane potential was held down to around -50 mV control for voltage-sensitive conductances.

4.2.4 Ionic mechanism underlying glucose-induced excitation of NPY eGFP neurons under fed and fasted conditions

Of the 'fed' population of NPY neurons, glucose-induced excitatory (GE) responses were associated with membrane depolarization from -48.94 ± 2.46 mV to -43.80 ±

2.78 mV without any associated changes in spontaneous firing rate. Thus the GE response of neurons recorded in slices from animals fed *ad libitum* failed to reach threshold for firing. This response was associated with a decrease in input resistance from 1668 ± 291 MΩ to 1564 ± 252 MΩ (n=9). In the 'fasted' population of NPY neurons, GE responses were observed as a mean membrane depolarization from -49.07 ± 1.44 mV to -44.12 ± 1.32 mV, associated with an increase in firing rate from 0.00 ± 0.00 Hz to 0.01 ± 0.01 Hz, and an increase in input resistance from 1143 ± 68 MΩ to 1431 ± 127 MΩ (n=29) (figure 4.6).

When comparing GE responses of fed and fasted groups, no statistical significance was observed in the magnitude of responses, measured in terms of membrane potential, action potential firing rate and input resistance (see figure 4.6F).

The increased input resistance associated with glucose-induced excitation in the fasted state was accompanied by a reversal potential around -90 mV. Reversal potentials associated with excitatory responses to glucose varied between neurons tested here, ranging from -63.00 mV to -95.00 mV with a mean of -78.50 ± 2.14 mV (n=20). This is indicative of the inhibition of a potassium conductance by glucose under our recording conditions (figure 4.4Biii). The GE effect in NPY eGFP neurons persisted in the presence of TTX suggesting activity-dependent synaptic transmission did not indirectly underpin this effect (n=6). Bath application of the K_{ATP} channel blocker tolbutamide (200 μM) induced membrane excitation similar to that observed with increased extracellular glucose. Repolarization of the membrane potential in these neurons to pre-tolbutamide levels and subsequent application of 5 mM glucose from 1 mM, in the presence of tolbutamide, failed to induce membrane excitation. Thus block of K_{ATP} channels

with tolbutamide was sufficient to prevent the glucose-induced excitation of NPY eGFP neurons (n=4). In one NPY eGFP neuron, 5 mM glucose application induced a reversible membrane potential depolarization, whilst subsequent application of 5 mM glucose in the presence of 200 μM tolbutamide induced membrane hyperpolarization (n=1) (figure 4.7A). Control membrane potential and spontaneous firing rate values here are more hyperpolarized than stated in section 4.2.1 as membrane potential was held down to around -50 mV control for voltage-sensitive conductances.

4.2.5 The effects of adenosine receptor antagonists on glucose-induced responses in NPY eGFP neurons

To probe the potential role for non-neuronal glia/tannycytes in glucose-sensing by NPY neurons, the effect of adenosine receptor antagonists were tested on glucose-induced responses, adenosine being released from astroglia directly, or produced by extracellular, nucleotidase-dependent catalysis of glia-derived ATP.

Incubation of brain slices prepared from 'fasted' animals, in the adenosine A_1 receptor antagonist DPCPX (1 μM), did not affect the percentage of glucose-induced inhibitions, relative to the control 'fasted' population (34% vs. 35% respectively) but markedly decreased the percentage of excitations induced by glucose from 40% in control to 24% in the presence of DPCPX. An increase in the percentage of non-responders from 26% to 41% was also apparent (n=29) (figure 4.5C). Chi-square analysis did not reveal any significant response redistribution, when comparing 'fasted' to 'fasted, DPCPX' (p=0.2189).

Incubation of brain slices prepared from 'fasted' animals, in the adenosine A_{2A} receptor antagonist istradefylline (50 nM) did not alter the percentage of

glucose-induced inhibitions, compared to the 'fasted' control population, but decreased the percentage of GE-NPY neurons from 40% to 13%. The percentage of non-responders increased from 26% to 40% (n=23) (figure 4.5D). Chi-square analysis revealed significant response redistribution, when comparing 'fasted' to 'fasted, Istradefylline' (p=0.0242).

Incubation of brain slices prepared from 'fasted' animals, in the adenosine A_{2B} receptor antagonist PSB-603 (100 nM), slightly increased the percentage of glucose-induced inhibitions, relative to the 'fasted' control population, from 34% to 35%, and slightly decreased the percentage of excitations induced by glucose from 40% in control to 35% in the presence of PSB-603. A small increase in the percentage of non-responders from 26% to 30% was also apparent (n=20) (figure 4.5E). Chi-square analysis did not reveal any significant response redistribution, when comparing 'fasted' to 'fasted, PSB-603' (p=0.9115).

Incubation of brain slices prepared from 'fasted' animals, in the adenosine A_3 receptor antagonist MRS 1523 (300 nM), slightly increased the percentage of glucose-induced inhibitions, relative to the 'fasted' control population, from 34% to 36%, and notably decreased the percentage of excitations induced by glucose from 40% in control to 23% in the presence of MRS 1523. An increase in the percentage of non-responders from 26% to 41% was also apparent (n=22) (figure 4.5F). Chi-square analysis did not reveal any significant response redistribution, when comparing 'fasted' to 'fasted, MRS 1523' (p=0.2649).

4.2.6 The effects of ghrelin on NPY eGFP neurons in fed and fasted conditions

NPY/AgRP neurons from both 'fed 5 mM glucose' and 'fasted 1 mM glucose' groups were sensitive to bath application of 3nM, 10nM and 30nM ghrelin, with excitation associated with an increased action potential, firing rate and input resistance (Figure 4.10).

In the 'Fed 5 mM glucose' NPY eGFP neurons, ghrelin induced a concentration-dependent excitation whereby 40% of NPY eGFP neurons were excited by 3 nM, 60% by 10 nM and 75% by 30 nM (n=15,15,16 respectively).

In the 'fasted 1 mM glucose' NPY eGFP neurons, ghrelin induced a concentration-dependent excitation whereby 42% were excited by 3 nM, 66% by 10 nM and 70% % by 30 nM (n=33, 33, 23 respectively) (figure 4.10).

In the fed group, ghrelin-induced depolarization amounted to 4.10 ± 0.77 mV, 3.37 ± 0.42 mV and 4.27 ± 0.94 mV in the presence of 3, 10 and 30 nM respectively. The corresponding values for the fasted group amounted to 3.96 ± 0.72 mV, 5.01 ± 1.12 mV and 7.30 ± 1.76 mV in the presence of 3, 10 and 30 nM respectively.

In the fed group ghrelin-induced excitation was associated with an increase in action potential firing rate and amounted to 0.29 ± 0.12 Hz, 0.30 ± 0.14 Hz and 0.16 ± 0.16 Hz in the presence of 3, 10 and 30 nM ghrelin, respectively. The corresponding values for the fasted group amounted to 0.05 ± 0.03 Hz, 0.20 ± 0.09 Hz and 0.45 ± 0.28 Hz in the presence of 3, 10 and 30 nM respectively.

Ghrelin-induced depolarization was associated with in increase in neuronal input resistance in the fed population amounting to an increase of 196 ± 131 MΩ, 119 ± 121 MΩ and 56 ± 74 MΩ in the presence of 3, 10 and 30 nM respectively. The

corresponding values for the fasted group amounted to 264 ± 223 MΩ, 541 ± 421 MΩ and 1446 ± 409 MΩ in the presence of 3, 10 and 30 nM respectively.

When comparing the magnitude of ghrelin-induced excitation in NPY eGFP neurons of fed and fasted animals, no significant difference in membrane potential change or firing rate change was observed between groups. Numbers are summarized in figures 4.9Bi and 4.9Bii. However, when comparing the change in input resistance associated with ghrelin-induced excitation, NPY eGFP neurons of the 'fasted 1 mM glucose' group displayed a significantly greater increase in input resistance in response 30 nM ghrelin, compared to neurons of the 'fed 5 mM glucose' group in the presence of 30 nM ghrelin (1446 ± 409 MΩ vs. 56 ± 74, n=3 and 4 respectively, p=<0.05, 2-way ANOVA).

4.2.7 Ionic mechanism underlying ghrelin-induced excitation of NPY eGFP neurons in fasted conditions

Bath application of the K_{ATP} channel blocker tolbutamide (200 μM) induced membrane excitation similar to that observed with ghrelin bath application. Repolarization of the membrane potential in these neurons to pre-tolbutamide levels and subsequent application of 100 nM ghrelin, in the presence of tolbutamide, failed to induce membrane excitation. Thus block of K_{ATP} channels with tolbutamide was sufficient to prevent the ghrelin-induced excitation of NPY eGFP neurons (n=6) (figure 4.8A). The ghrelin-induced excitation of NPY/AgRP neurons can be reversed by lowering the extracellular glucose concentration (n=1) (figure 4.7B).

4.2.8 Effects of ghrelin on glucose inhibited and glucose excited eGFP neurons

There is a subpopulation of NPY eGFP neurons that are excited by ghrelin, are glucose excited and express K_{ATP} channels (figure 4.11A). There is also a subpopulation of NPY eGFP neurons that are excited by ghrelin, are inhibited by glucose, and expresses K_{ATP} channels (figure 4.11B). Of ghrelin-excited NPY eGFP neurons from fasted animals, 37% are GE, 37% are GI whilst 26% are glucose insensitive (n=19). Of ghrelin-excited NPY eGFP neurons from animals fed *ad libitum*, 33% are GE, 50% are GI and 17% are glucose insensitive (n=6).

4.3 Discussion

The principle findings of this study were:

1. NPY neurons demonstrate a remarkable energy-status-dependent functional plasticity whereby fasting and low ambient glucose levels recruit GE neurons. This is the first report of NPY-GE neurons, with previous studies suggesting NPY neurons to be exclusively GI. NPY-GE neurons may be recruited from previously non-glucose sensing NPY neurons, and may also be recruited through the switching of GI to GE. Although a trend was detected towards this effect (p=0.0783), no significant difference was observed between the glucose response distribution of fed and fasted NPY neurons.
2. Glucose-induced excitation in NPY neurons is mediated via an ATP-sensitive potassium channel-dependent mechanism, whereas glucose-induced inhibition is mediated via multiple mechanisms, possibly via the activation of chloride and/or potassium conductances.

3. A role for adenosine in mediating the glucose-induced excitation of NPY neurons is also suggested, via A_{2A} receptors, and possibly also via adenosine A_1, and A_3 receptors. The neuronal/non-neuronal origins of this response remain to be determined.
4. Ghrelin induced a concentration-dependent excitation in both NPY-GE and NPY-GI neurons, and the responsiveness to ghrelin was enhanced in the fasted state.
5. In fasted states, the ghrelin-induced excitation of NPY neurons (including NPY-GE neurons) was mediated via the block of K_{ATP} channels.
6. These data suggest that in the fasted state, glucose and ghrelin converge on a common signal transduction endpoint; the K_{ATP} channel. This indicates an important relationship between glucose and ghrelin at NPY-GE neurons. This may from a mechanism by which in states of hunger, glucose and ghrelin may work synergistically to drive increased food intake to restore depleted glucose levels. Thus NPY-GE neurons may adopt a reward-like phenotype to drive food intake whereas the function of NPY-GI neurons is likely to suppress food intake upon store repletion. Nevertheless these data represents a previously unrecognized and potentially vital functional adaptation for survival in NPY neurons, and also presents a novel role for glucose sensing in the melanocortin system.

4.3.1 NPY/AgRP neuron firing rate is sensitive to extracellular glucose concentration and feeding state

At first glance, results presented here do not appear to fit with our current understanding of the orexigenic NPY neuron. Here, I present results demonstrating that *in vitro,* NPY eGFP neurons have a significantly elevated input resistance and action potential firing rate when taken from mice fed *ad libitum* and incubated in 5 mM glucose, compared to NPY eGFP neurons of brain slices taken from 'fasted' mice, incubated in 1 mM glucose. Elevated input resistance could underpin high(er) frequency discharge however increased EPSPs could also be the cause of elevated NPY eGFP neuron firing rate.

Undoubtedly these activity levels are not representative of arcuate NPY neuron activity *in vivo*, as in situ neuronal activity will be subject to neuronal and hormonal stimulation, variables that are not present when neurons are recorded from during brain slice electrophysiological experiments. These data allow us to generate a deeper understanding of NPY neuron information processing at the molecular and cellular levels.

Here, I propose that the increased firing rate and input resistance observed *in vitro* in relatively positive energy states is the result of increased glucose uptake and metabolism, elevated ATP/ADP ratio, inhibited K_{ATP} channels and membrane depolarization.

Previous *in vitro* slice electrophysiology has described NPY/AgRP neurons to elevate their electrical activity *in vitro* following a fast (Takahashi and Cone, 2005). However this and other work describes neurons from brain slices incubated in 10 mM glucose post-fast. I suggest the elevated firing rate observed in previous studies is due to an acute response to glucose, rather than an effect of the

food deprivation. Consistent with this hypothesis is the observation that fasting increases the percentage of GE NPY/AgRP neurons. It is my contention that in their publication, Takahashi and Cone are mistaking a glucose excitation for a fast-induced activity increase.

4.3.2 Fasting-induced reorganization of glucose sensing in the arcuate NPY/AgRP neuron population

Fasting increased the percentage of glucose-sensing NPY neurons in the ARH. A greater degree of plasticity was observed in the subpopulation of GE neurons, with the percentage of glucose-induced excitations rising by 15%, from 25% in fed conditions to 40% in fasted conditions (figure 4.5). Conversely, the fasting increased the percentage of NPY-GI neurons by 5%, from 29% to 34%.

This fast-induced increase in the proportion of NPY-GE neurons in the ARH could underlie a short-lived positive feedback loop, wherein post-fast consumption of carbohydrate promotes further feeding through elevated NPY neuron activity. This acute excitatory response to elevated central glucose may then be supplanted by lower frequency NPY neuron electrical activity, when long-term signals indicative of a positive energy status are transduced by NPY neurons.

4.3.3 Mechanism of glucose-induced excitation of NPY neurons

The glucose-induced excitation of NPY neurons was via the inhibition of K_{ATP} channels. In the fasted state, glucose-induced excitation was associated with increased neuronal input resistance and reversal potential around -90 mV. This, in addition to the sensitivity of the GE response to the K_{ATP} channel blocker tolbutamide confirms ATP-sensitive potassium channels as the signal transduction

endpoint mediating the excitatory effects of glucose observed here. K_{ATP} channels are expressed in arcuate NPY/AgRP neurons (van den Top et al., 2007). Glucose sensing experiments conducted in the presence of TTX, confirm the glucose-induced excitation of NPY neurons to be direct, not via increased excitatory afferent neuronal innervation. In many instances, the glucose-induced membrane response was not reversible upon 5 mM glucose washout from the recording chamber. As such the preferred experimental design for signal transduction characterization - of repeating the experiment in the presence of receptor antagonists – was deemed unreliable, namely too vulnerable to false positive results. As such the experimental design was adapted to assess the glucose response distribution of NPY neurons after incubation in receptor antagonists prior to recording. These experimental response distributions would then be compared with control data.

Incubation of brain slices in adenosine receptor antagonists decreased the percentage of NPY-GE neurons but had little or no affect upon the proportion of NPY-GI neurons. Whole-cell recordings taken from brain slices of fasted mice demonstrate that antagonism of adenosine receptors A_1, A_{2A}, A_{2B} and A_3 reduces the percentage of NPY-GE neurons from 40% to 24%, 13%, 35% and 23% respectively. This data indicates that the glucose-induced excitation of NPY neurons is via A_1, A_3 and A_{2A} receptors, and perhaps to a lesser degree by A_{2B} receptors.

Further work is required to investigate the neuronal or non-neuronal origin of adenosine mediating glucose sensing in NPY-GE neurons. A potential source of adenosine in the arcuate nucleus is astrocytes. Previous studies have concluded that increased astrocytic activity is associated with a reduction of ghrelin evoked

feeding whilst A_1 receptor antagonism or astrocyte inhibition potentiates ghrelin-induced food intake (Yang et al., 2015). This study found no effect of astrocytic activation or A1 receptor inhibition on post-fast refeeding. The study by Yang et al would suggest A_1 receptors to negatively regulate AgRP neuron activity, whereas data presented here indicates that A_1 receptors transduce excitatory signals in NPY neurons.

K_{ATP} channel activation as a result of adenosine A_1 receptor activation has been identified as a mechanism of hippocampal ischemic tolerance (Heurteaux et al., 1995). The inhibition of hypothalamic K_{ATP} channels by A_1 receptor activation is yet to be definitively demonstrated. Previous reports have linked A_{2A} receptors to K_{ATP} channels via protein kinase A (PKA) (Kleppisch and Nelson, 1995, Tang et al., 1999), however these studies found A_{2A} activation linked to channel activation and neuronal hyperpolarization, rather than the K_{ATP} inhibition and neuronal depolarization, observed here.

4.3.4 Mechanism of glucose-induced inhibition of NPY neurons

The mechanisms of glucose-induced inhibition observed here appeared to be heterogeneous in nature, with reversal potentials indicating multiple mechanisms including potassium and chloride conductance activation. This heterogeneity of inhibitory mechanisms is consistent with previous reports of multiple mechanisms (Oomura et al., 1974, Fioramonti et al., 2007, Burdakov and Gonzalez, 2009, Jordan et al., 2010, Canabal et al., 2007).

Fast-induced plasticity was observed in the GI subpopulation of NPY/AgRP neurons of the ARH, albeit to a lesser degree than the GE subpopulation. Here fasting increased the percentage of GI neurons from 29% to 34%.

Data presented here does not implicate adenosine receptors in mediating the glucose-induced inhibition of arcuate NPY neurons. A 1% increase (from 34% to 35%) in glucose-induced inhibitions was observed in glucose sensing experiments conducted on NPY neurons in the presence of either the adenosine A_1 receptor antagonist DPCPX or the adenosine A_{2B} receptor antagonist PSB-603. No change in the percentage of NPY-GI neurons was observed in glucose sensing experiments conducted in the presence of the adenosine A_{2A} receptor antagonist istradefylline. The largest - but still modest – increase in the percentage of NPY-GI neurons was observed in whole-cell glucose-sensing experiments conducted in the presence of the adenosine A_3 receptor antagonist MRS 1523. Here the percentage of NPY-GI neurons rose by 2%, from 34% in fasted conditions to 36% in fasted conditions, with the A_3 receptor antagonist. This suggests that the glucose-induced inhibition of NPY neurons in the ARH is via adenosine receptor-independent mechanisms.

4.3.5 The mechanism of fast-induced reorganization

Experiments presented here do not concussively prove the mechanism of fast-induced reorganization of NPY neurons. However they do demonstrate that adenosine, and/or adenosine receptor subtypes are required for the fast-induced recruitment of glucose-excited NPY neurons. Mechanisms of plasticity could involve increased ATP release, increased extracellular ectonucleotidase activity, increased adenosine receptor expression, increased uncoupling protein-2 (UCP-2)-dependent mitochondrial fusion / fission, changes in AMPK or PI3K signaling and undoubtedly many more possibilities (Coppola et al., 2007, Toda et al., 2016).

Among further work required is the characterization of NPY neuron adenosine receptor expression in fed and fasted conditions.

4.3.7 NPY-GI and NPY-GE neuron excitation by ghrelin is K_{ATP} channel-dependent

In whole-cell recordings taken from brain slices of fasted animals, bath application of the K_{ATP} channel blocker tolbutamide was sufficient to prevent NPY neuron membrane depolarization by ghrelin. This in addition to the increased input resistance and reversal potential around -90 mV associated with the ghrelin-induced membrane excitation in the presence of TTX confirms the excitatory actions of ghrelin on NPY neurons to be direct, and not via increased excitatory afferent neuron innervation.

Ghrelin induced excitation observed in whole cell recordings taken from brain slices of animals fed *ad libitum* were also associated with increases in neuronal input resistance and reversal potentials around -90 mV. However the 30nM ghrelin-induced excitation of NPY neurons in the fasted state was associated with a significantly greater input resistance elevation, relative to recordings taken from brain slices of fed animals (Δ 966 ± 373 vs. Δ 56 ± 74 MΩ, Figure 4.10 Aiv). The ability of ghrelin to induce large increases in input resistance in the fasted state may be the result of increased basal K_{ATP} channel activity under these conditions.

Ghrelin excited both NPY-GI and NPY-GE neurons from both fed and fasted animals. As both ghrelin and glucose induce membrane depolarization of NPY neurons via K_{ATP} channel inhibition, it follows that the signaling of one these metabolic factors will affect the signaling of the other. In the case of ghrelin-

sensitive NPY-GE neurons, glucose and ghrelin may work synergistically post-fast to increase the acute refeeding response. Conversely glucose sensing in ghrelin sensitive NPY-GI neurons may work have an antagonistic relationship with ghrelin orexigenic ghrelin signaling, functioning to suppress food intake once food intake has resorted a positive energy status. Here we propose that glucose 'sets the gain' for hormonal signaling, in NPY/AgRP neurons, and presumably other neuronal populations.

4.3.8 The convergence of glucose and ghrelin signaling

Previous work has demonstrated the convergence of PI3K signaling and K_{ATP} channel ATP sensitivity (Shyng and Nichols, 1998). Here, PIP_3 stabilizes K_{ATP} channel open state and prevents channel inhibition by ATP, reducing channel ATP sensitivity by orders of magnitude. Multiple hormones – including insulin and leptin - converge on the PI3K pathway, and modulation of cytoplasmic inositide concentrations will affect K_{ATP} channel opens state and ATP sensitivity.

Increased AMPK signaling has been shown to stimulate PI3K signaling (Tao et al., 2010). Fast-induced AMPK activity would elevate PI3K, opening K_{ATP} channels. Subsequent ghrelin application would rapidly inhibit PI3K activity, causing a profound reduction in K_{ATP} channel open probability. The relative change in K_{ATP} channel open probability (before ghrelin vs. after ghrelin) would be greater than that from ghrelin application in a fed (low AMPK activity) state. This mechanism could explain the greater change of input resistance observed in the 'fasted 1 mM' ghrelin dose response. An implication of this finding is that ghrelin sensitivity *in vivo* will be diminished in individuals with elevated central glucose levels, such as obese and diabetic individuals. Increased hormone sensitivity could

potentially be achieved in these individuals by lowering central glucose concentrations.

Figure 4.1: NPY/AgRP neuron membrane potential, firing rate and input resistance is affected by extracellular glucose concentration and feeding state

A: Representative current clamp trace of an NPY/AgRP neuron from a 'fed' mouse, with brain slices incubated in aCSF containing 5 mM glucose (mean spontaneous firing rate: 2.18 ± 0.24 Hz (mean ± SEM), n=70).

B: Representative current clamp trace of an NPY/AgRP neuron from a 'fasted' mouse, with brain slices incubated in aCSF containing 1 mM glucose (mean spontaneous firing rate:1.61 ± 0.11 Hz, n=211).

C: Representative current clamp trace of an NPY/AgRP neuron from a 'fed' mouse, with brain slices incubated in aCSF containing 1 mM glucose (mean spontaneous firing rate:1.33 ± 0.14 Hz, n=41).

Figure 4.1

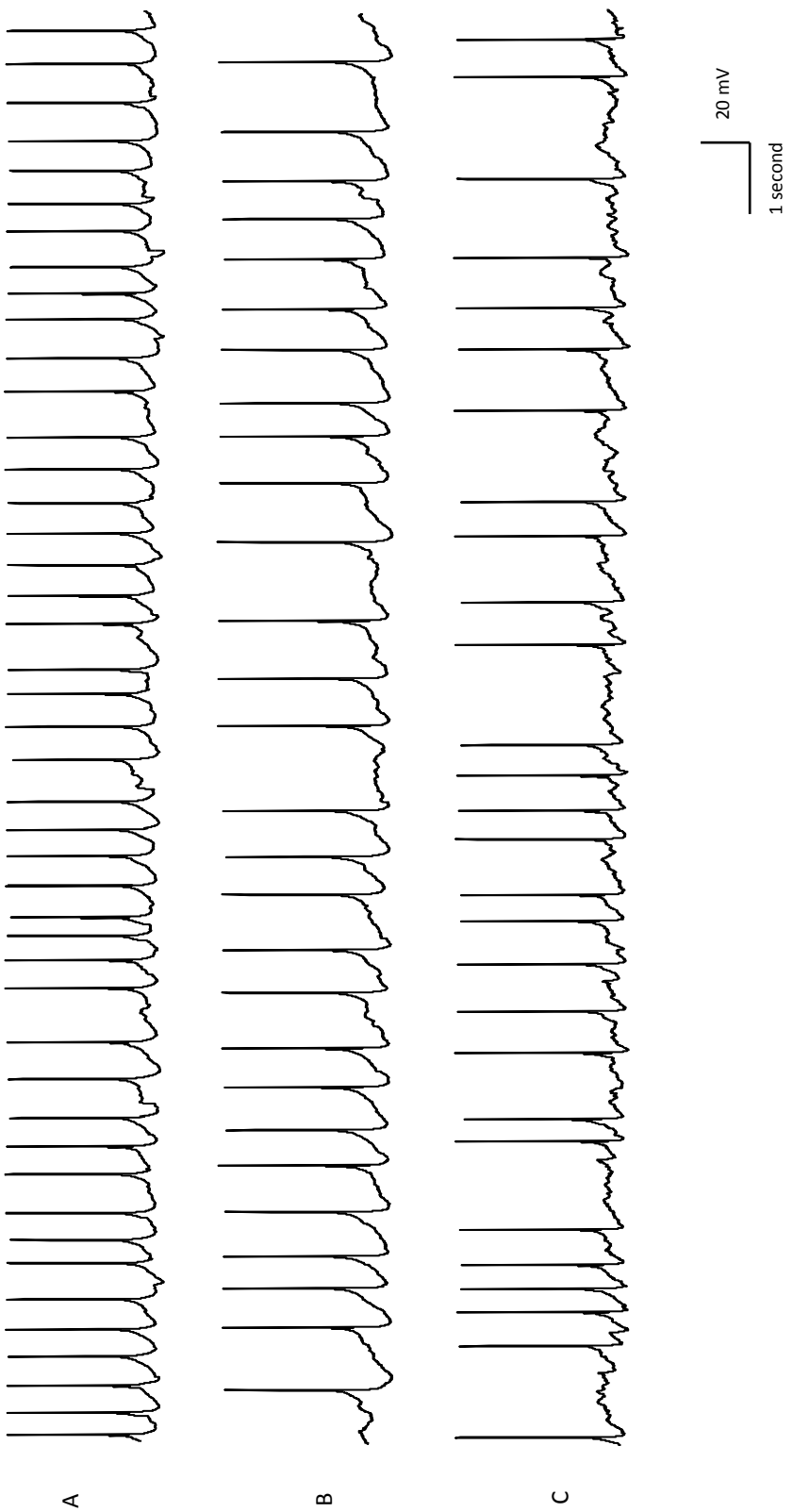

Figure 4.2: NPY/AgRP neuron membrane potential, firing rate and input resistance is modulated by extracellular glucose concentration and feeding state

A: Bar chart summarizing the mean membrane potential of neuronal populations represented in **1A**, **1B** and **1C** (fasted, 1 mM glucose; -41.04 ± 0.57 mV, Fed 1 mM glucose; -38.68 ± 0.63 mV, Fed 5 mM glucose; -39.60 ± 0.84 mV).

B: Bar chart summarizing the mean spontaneous action potential firing rate of neuronal population represented in **1A**, **1B** and **1C** (fasted, 1 mM glucose; 1.61 ± 0.11 Hz, Fed 1 mM glucose; 1.33 ± 0.14 Hz, Fed 5 mM glucose; 2.18 ± 0.24 Hz). (Fasted 1 mM vs. Fed 5 mM, p= <0.05; Fed 1 mM vs. Fed 5 mM, p=<0.05, 2-way ANOVA with post-hoc Bonferroni test)

C: Bar chart summarizing the mean input resistance of neuronal populations represented in **1A**, **1B** and **1C** (Fed 5 mM glucose; 1827 ± 132 MΩ, Fed 1 mM Glucose; 1680 ± 136 MΩ, Fasted 1 mM Glucose; 1538 ± 66 MΩ. (Fasted 1 mM vs. Fed 5 mM, p= <0.05, 2-way ANOVA with post-hoc Bonferroni test)

Figure 4.2

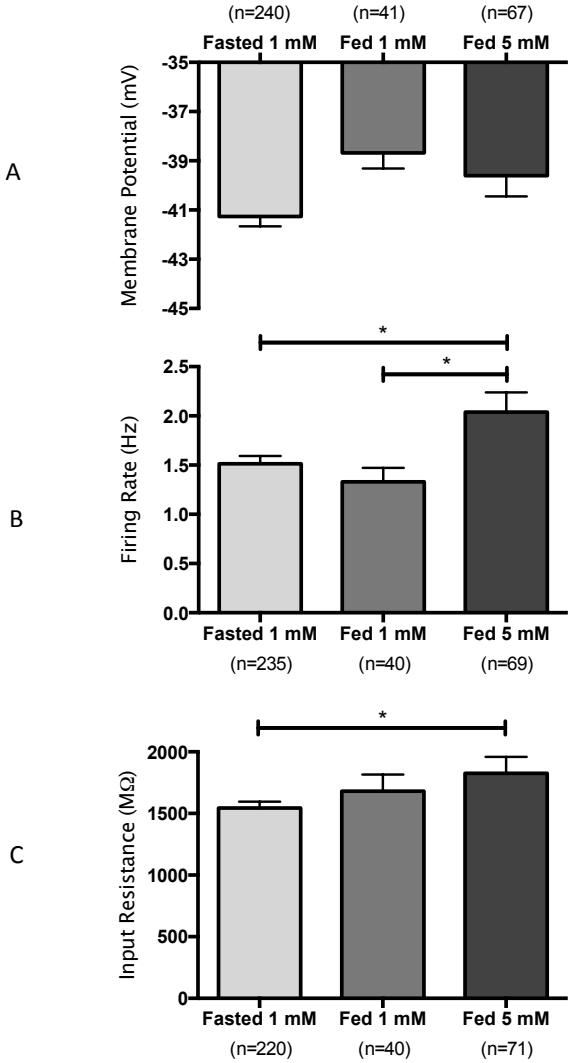
A
B
C
(n=240)
(n=41)
(n=67)
Fasted 1 mM
Fed 1 mM
Fed 5 mM
Membrane Potential (mV)
-35
-37
-39
-41
-43
-45
*
*
Firing Rate (Hz)
2.5
2.0
1.5
1.0
0.5
0.0
Fasted 1 mM
Fed 1 mM
Fed 5 mM
(n=235)
(n=40)
(n=69)
*
Input Resistance (MΩ)
2000
1500
1000
500
0
Fasted 1 mM
Fed 1 mM
Fed 5 mM
(n=220)
(n=40)
(n=71)

Figure 4.3: Glucose-Inhibited NPY-eGFP neurons

A: A representative current-clamp recording taken from an NPY-eGFP neuron showing glucose-induced inhibition. Briefly increasing extracellular glucose induced a reversible membrane hyperpolarization.

Bi: Superimposed sweeps of a current clamp recording taken from a glucose-inhibited NPY eGFP neuron, showing the membrane current-voltage relationship in 1 mM glucose aCSF.

Bii: Superimposed sweeps of a current clamp recording taken the same glucose inhibited NPY eGFP neuron shown in **Bi.** Sweeps show the membrane current-voltage relationship in the presence of 5 mM glucose aCSF.

Biii: Representative current-voltage relationship plots of glucose-induced inhibition. Note the decreased slope of the membrane response to current injection and reversal potential around -70 mV. Taken together these indicate membrane hyperpolarization via the activation of a chloride conductance, and decreased neuronal input resistance.

Figure 4.3

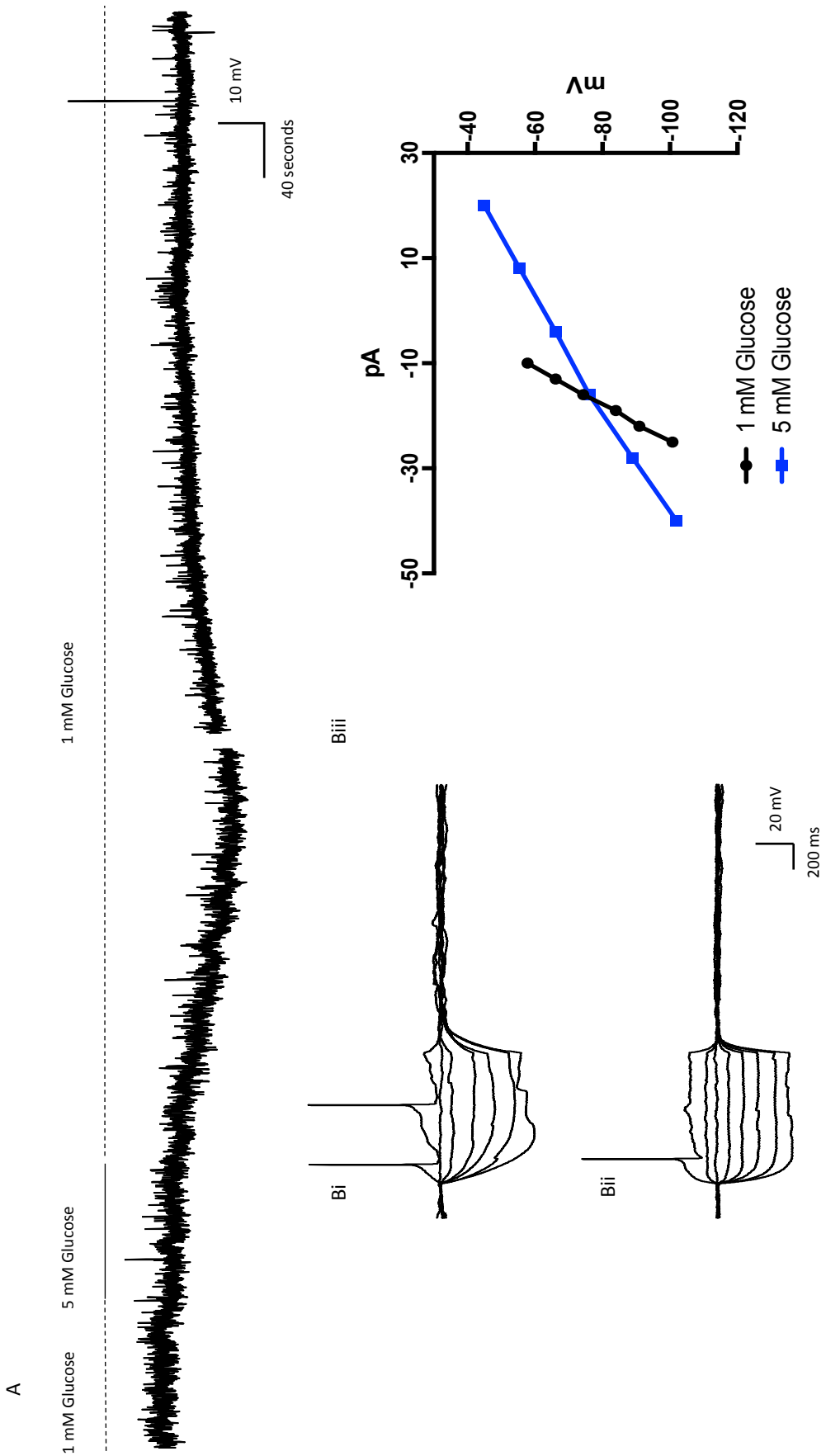
A
1 mM Glucose
5 mM Glucose
1 mM Glucose
10 mV
40 seconds
Bi
Bii
Biii
20 mV
200 ms
pA
mV
30
10
-10
-30
-50
-40
-60
-80
-100
-120
1 mM Glucose
5 mM Glucose

Figure 4.4: Glucose-Excited NPY-eGFP neurons

A: A representative current-clamp recording taken from an NPY-eGFP neuron showing glucose-induced excitation. Increasing extracellular glucose concentration from 1 mM to 5 mM induced membrane depolarization and increased action potential firing frequency.

Bi: Superimposed sweeps of a current clamp recording taken from a glucose-excited NPY eGFP neuron, showing the membrane current-voltage relationship in 1 mM glucose aCSF.

Bii: Superimposed sweeps of a current clamp recording taken from the same glucose excited NPY eGFP neuron shown in **Bi.** Sweeps show the membrane current-voltage relationship in the presence of 5 mM glucose aCSF.

Biii: Representative current-voltage relationship plots of glucose excitation. Note the increased slope of the membrane response to current injection and reversal potential around -90 mV. Taken together these indicate membrane depolarization via the inhibition of a potassium conductance, and increased neuronal input resistance.

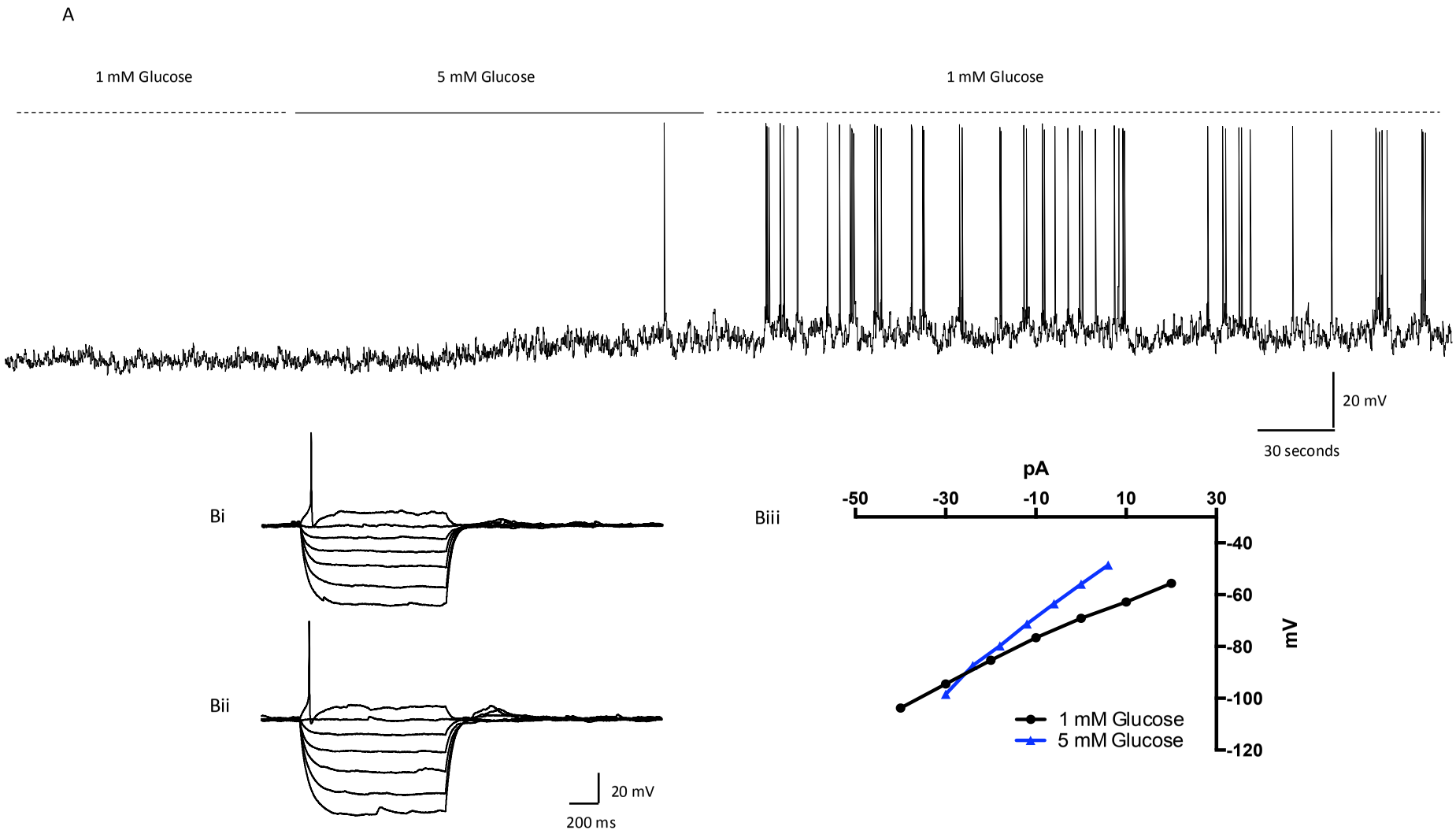
A
1 mM Glucose
5 mM Glucose
1 mM Glucose
20 mV
30 seconds
Bi
Bii
20 mV
200 ms
Biii
pA
-50
-30
-10
10
30
-40
-60
-80
-100
-120
mV
1 mM Glucose
5 mM Glucose

Figure 4.4

Figure 4.5: Fasting-induced reorganization of glucose sensing in the NPY/AgRP neurons of the ARH: Effects of adenosine receptor antagonists

A: Pie chart showing the response distribution of NPY eGFP neurons from mice fed *ad libitum* prior to culling. Increasing extracellular glucose concentration from 1 mM to 5 mM caused membrane excitation in 26% of neurons, membrane inhibition in 29% of neurons, whilst 46% of neurons did not respond (n=35).

B: Pie chart showing the response distribution of NPY eGFP neurons from mice subjected to an 18-hour fast prior to culling. Increasing extracellular glucose concentration from 1 mM to 5 mM caused membrane excitation in 40% of neurons, membrane inhibition in 34% of neurons, whilst 26% of neurons did not respond (n=73).

C: Pie chart showing the response distribution of NPY eGFP neurons incubated in the adenosine A_1 receptor antagonist DPCPX (1 μM), from mice subjected to an 18-hour fast prior to culling. Increasing extracellular glucose concentration from 1 mM to 5 mM caused membrane excitation in 24% of neurons, membrane inhibition in 35% of neurons, whilst 41% of neurons did not respond (n=29).

D: Pie chart showing the response distribution of NPY eGFP neurons incubated in the adenosine A_{2A} receptor antagonist Istradefylline (50 nM), from mice subjected to an 18-hour fast prior to culling. Increasing extracellular glucose concentration from 1 mM to 5 mM caused membrane excitation in 13% of neurons, membrane inhibition in 34% of neurons, whilst 52% of neurons did not respond (n=23).

E: Pie chart showing the response distribution of NPY eGFP neurons incubated in the adenosine A_{2B} receptor antagonist PSB-603 (100 nM), from mice subjected to an 18-hour fast prior to culling. Increasing extracellular glucose concentration

from 1 mM to 5 mM caused membrane excitation in 35% of neurons, membrane inhibition in 35% of neurons, whilst 30% of neurons did not respond (n=20).

F: Pie chart showing the response distribution of NPY eGFP neurons incubated in the adenosine A_3 receptor antagonist MRS 1523 (300 nM), from mice subjected to an 18-hour fast prior to culling. Increasing extracellular glucose concentration from 1 mM to 5 mM caused membrane excitation in 23% of neurons, membrane inhibition in 36% of neurons, whilst 41% of neurons did not respond (n=22).

G: Table summarizing the *p*-values resulting from Chi-square analysis of population data displayed in A – F.

Figure 4.5

A. Fed

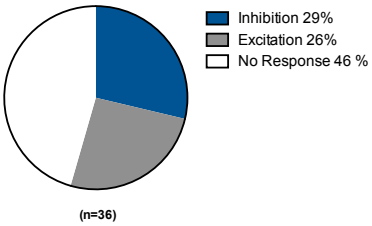

B. Fasted

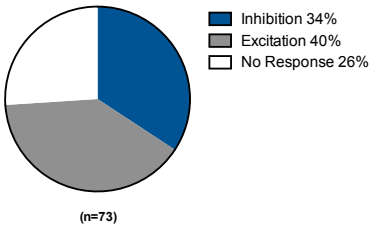

C. Fasted, DPCPX (A_1)

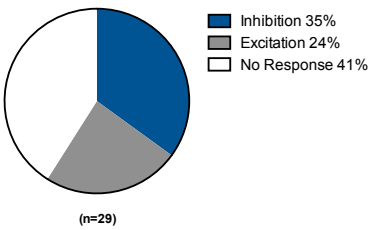

D. Fasted, Istradefylline (A_{2A})

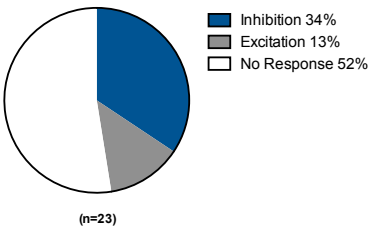

E. Fasted, PSB-603 (A_{2B})

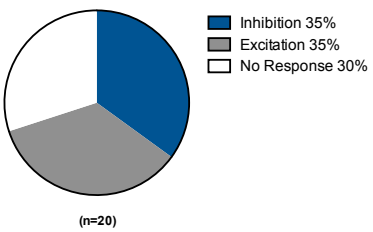

F. Fasted, MRS 1523 (A_3)

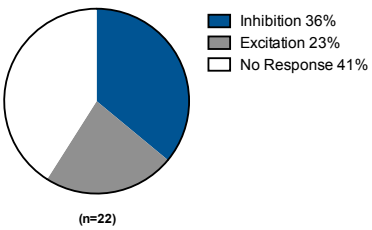

G.

Population Comparison	***p***
Fed Vs. Fasted	0.0783
Fasted Vs. DPCPX	0.2189
Fasted Vs. Istradefylline	**0.0242**
Fasted Vs. PSP-603	0.9115
Fasted Vs. MRS 1523	0.2649

Figure 4.6: Magnitude of glucose-induced responses in NPY neurons in fed and fasted states

A: Bar chart outlining the mean change in membrane potential of the glucose-induced inhibition of NPY eGFP neurons. Data is from animals fed *ad libitum* prior to culling and from animal subjected to an 18-hour fast prior to culling. Of glucose-induced inhibitions recorded from mouse tissue prepared from fed animals, neurons were hyperpolarized -6.66 ± 1.63 mV from a mean control level of -52.73 ± 1.54 mV to a peak of -59.39 ± 1.76 mV (n=10) (p=0.003). Of glucose-induced inhibitions recorded from mouse tissue prepared from fasted animals, neurons were hyperpolarized by -6.26 ± 0.87 mV from a mean control level of -49.79 ± 1.41 mV to a peak of -55.90 ± 1.73 mV (n=17) (p=0.000002), (paired students t-test).

B: Bar chart outlining the mean change in neuronal input resistance associated with glucose-induced inhibition of NPY eGFP neurons. Data is from neurons of glucose-induced inhibition in NPY eGFP neurons from animals fed *ad libitum* prior to culling and from animal subjected to an 18-hour fast prior to culling. Of glucose-induced inhibitions observed in the 'fed' state, neuronal input resistance fell by 785 ± 355 MΩ from a mean control level of 1759 ± 318 MΩ to a peak of 1410 ± 342 MΩ (n=6) (p=0.090). In the 'fasted' state, neuronal input resistance associated with glucose-induced inhibition fell by 308 MΩ ± 143 MΩ from a mean control level of 1559 ± 165 MΩ to a peak of 1150 ± 174 MΩ (n=14) (p=0.049), (paired students t-test).

C: Bar chart outlining the mean change in membrane potential of the glucose-induced excitation of NPY eGFP neurons. Data is from animals fed *ad libitum* prior to culling and from animal subjected to an 18-hour fast prior to culling. Of the glucose-induced excitatory responses observed in the 'fed' state, neurons were

depolarized by 5.13 mV ± 1.00 from a mean control level of -48.94 ± 2.46 mV to a new peak of -43.80 ± 2.78 mV (n=6) (p=0.001). Of 'fasted' excitations, NPY eGFP neurons were depolarized by 4.65 ± 0.52 mV from a mean control level of -49.07 ± 1.44 mV to a peak of -44.12 ± 1.32 mV (n=12) (p=0.0000001; paired students t-test).

D: Bar chart outlining the mean change in neuronal input resistance of the glucose-induced excitation of NPY eGFP neurons. Data is from neurons of glucose excitation in NPY eGFP neurons from animals fed *ad libitum* prior to culling and from animal subjected to an 18-hour fast prior to culling. Of the glucose-induced excitatory responses observed in the 'fed' state, neuronal input resistance decreased by 188 ± 234 MΩ from a mean control level of 1668 ± 291 MΩ to a peak of 1263 ± 213 MΩ (n=6) (p=0.459). Of 'fasted' excitation, neuronal input resistance increased by 398 ± 249 MΩ from a mean control level of 1143 ± 68 MΩ to a peak of 1431 ± 127 MΩ (n=12) (p=0.138), (paired students t-test).

E: Table comparing the magnitude of glucose-induced inhibitions in 'fed' and 'fasted' groups. Measured in terms of change in membrane potential (mV), action potential firing rate (Hz) and neuronal input resistance (MΩ). Statistical values expressed are results of unpaired students t-test.

F: Table comparing the magnitude of glucose-induced excitations in 'fed' and 'fasted' groups. Measured in terms of change in membrane potential (mV), action potential firing rate (Hz) and neuronal input resistance (MΩ). P values expressed are results of unpaired students t-test.

Figure 4.6

A

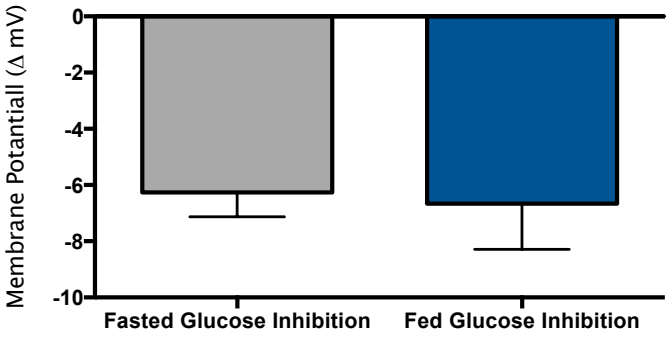

B

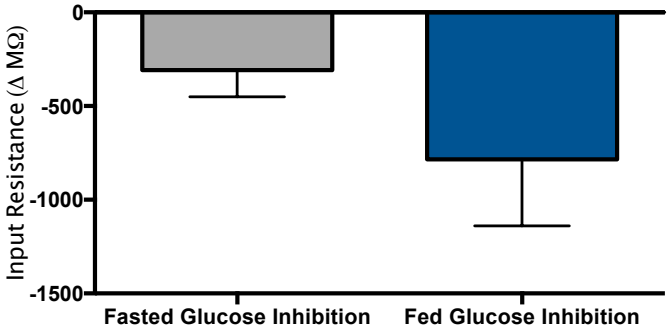

C

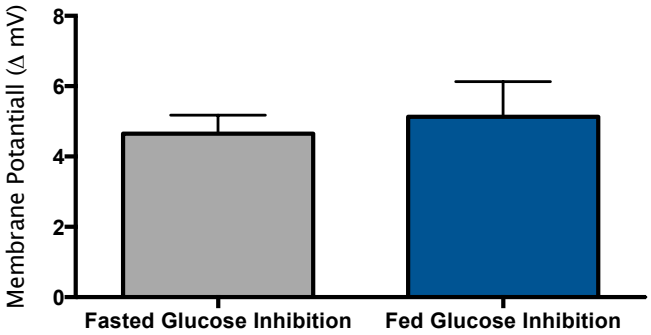

D

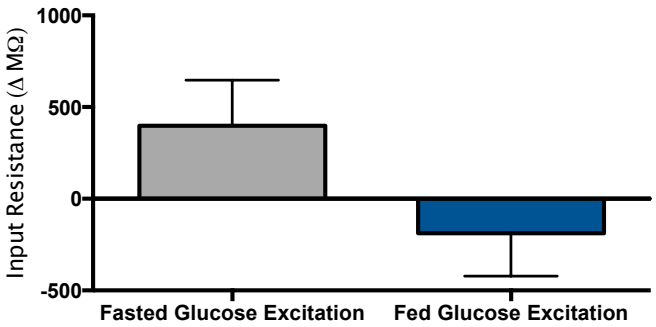

E

	Fed Glucose Inhibition vs. Fasted Glucose Inhibition		
	mV	Hz	MΩ
p	0.814	0.682	0.147

F

	Fed Glucose Excitation vs. Fasted Glucose Excitation		
	mV	Hz	MΩ
p	0.640	1.000	0.154

Figure 4.7: K_{ATP} channels mediate the glucose-induced excitation of NPY eGFP neurons

A: Current-clamp recording taken from an NPY-eGFP neuron. Increasing extracellular glucose concentration from 1 mM to 5 mM induced membrane depolarization. Subsequent washout of glucose and application of 200 μM tolbutamide mimicked and blocked the depolarizing response induced by D-glucose (n=4). In one NPY eGFP neuron (shown), blocking K_{ATP}-dependent glucose-induced excitation revealed a glucose-induced inhibition. Arrow indicates the point in peak response to tolbutamide at which neuron membrane voltage was clamped back to the pre-response resting level by manual constant current injection.

B: Plot of current-voltage relationship of neuron shown in **A**, in 1mM glucose and in 5 mM extracellular glucose. Note the increased slope of the membrane response to current injection and reversal potential around -70 mV. However, as glucose-induced excitation can mask simultaneous glucose-induced inhibitory responses, attempts to extrapolate reversal potentials may have been confounded by the simultaneous activation of another, opposing conductance.

C: Plot of current-voltage relationship of neuron shown in **A.** Plots of IVs in 1mM glucose, 1 mM glucose and tolbutamide and 5 mM and tolbutamide are shown. Note increased slope of the membrane response to current injection, and reversal around -90 mV upon tolbutamide application. Also note the decreased slope in the membrane response to current injection upon 5 mM glucose application in the presence of tolbutamide. Here an extrapolated reversal potential around -70 mV indicates membrane hyperpolarization via the activation of a chloride conductance.

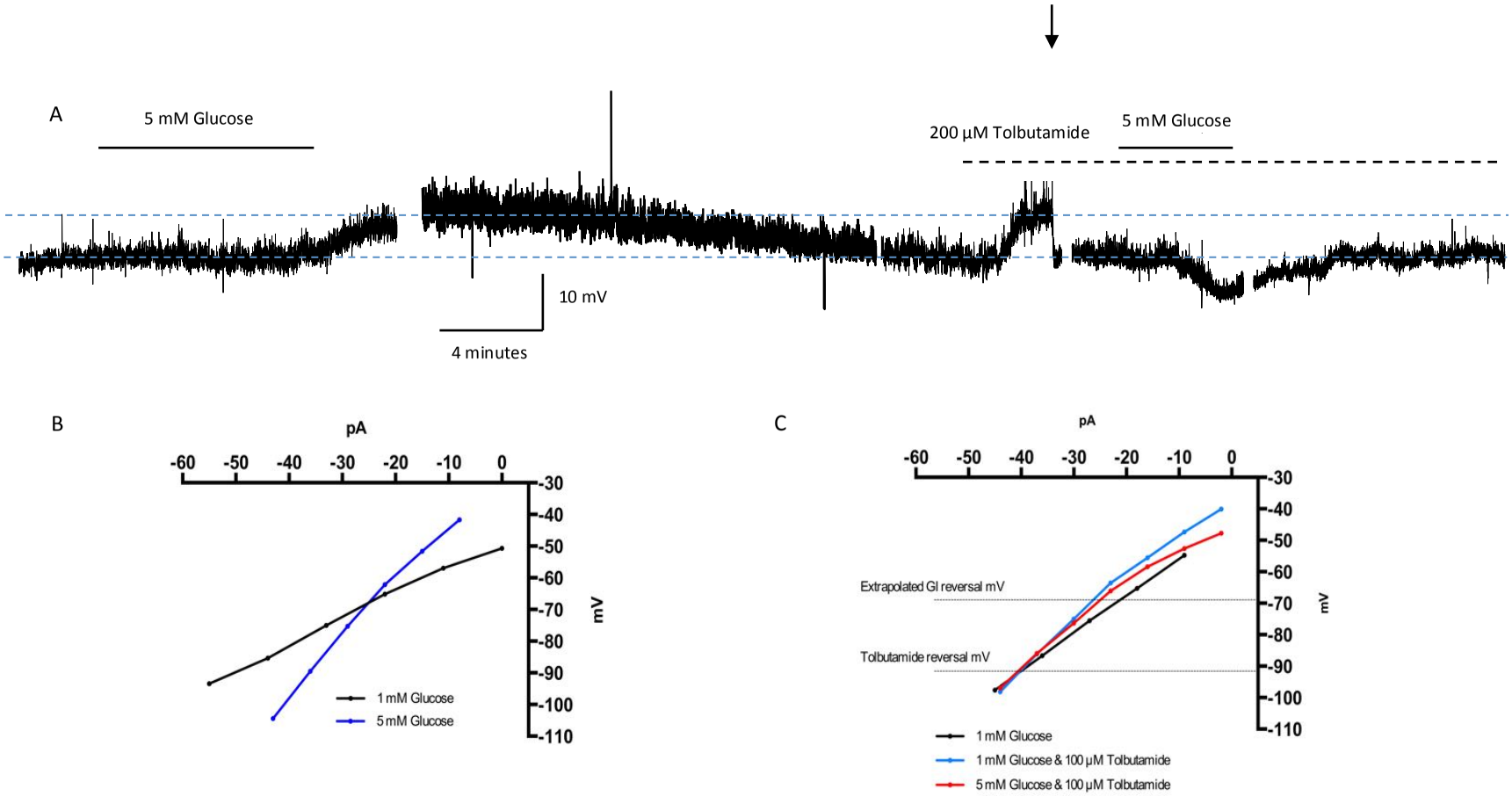
A
5 mM Glucose
200 µM Tolbutamide
5 mM Glucose
10 mV
4 minutes
B
pA
-60 -50 -40 -30 -20 -10 0
-30 -40 -50 -60 -70 -80 -90 -100 -110
mV
1 mM Glucose
5 mM Glucose
C
pA
-60 -50 -40 -30 -20 -10 0
-30 -40 -50 -60 -70 -80 -90 -100 -110
mV
Extrapolated Gl reversal mV
Tolbutamide reversal mV
1 mM Glucose
1 mM Glucose & 100 µM Tolbutamide
5 mM Glucose & 100 µM Tolbutamide

Figure 4.7

Figure 4.8: K_{ATP} channels mediate ghrelin-induced excitation of NPY eGFP neurons

A: Current-clamp recording taken from a NPY-eGFP neuron. Bath application of 100 nM ghrelin-induced reversible membrane depolarization and increased action potential firing rate. This effect of ghrelin was mimicked and blocked by bath application of 200μM tolbutamide. Arrow indicates the point in peak response to tolbutamide at which neuron membrane voltage was clamped back to the pre-response resting level by manual constant current injection.

Bi: Superimposed sweeps of a current clamp recording taken from a ghrelin-sensitive NPY eGFP neuron showing the current-voltage relationship before bath application of 100 nM ghrelin.

Bii: Superimposed sweeps of a current clamp recording taken the same NPY eGFP neuron shown in **Bi.** Sweeps show the membrane current-voltage relationship in the presence of 100 nM ghrelin.

C: Current-clamp recording taken from NPY-eGFP neuron. Bath application of 10 nM ghrelin-induced membrane depolarization. Subsequent decrease of extracellular glucose concentration from 5 mM to 1 mM induces membrane hyperpolarization and the reversal of the ghrelin-induced excitation.

Figure 4.8

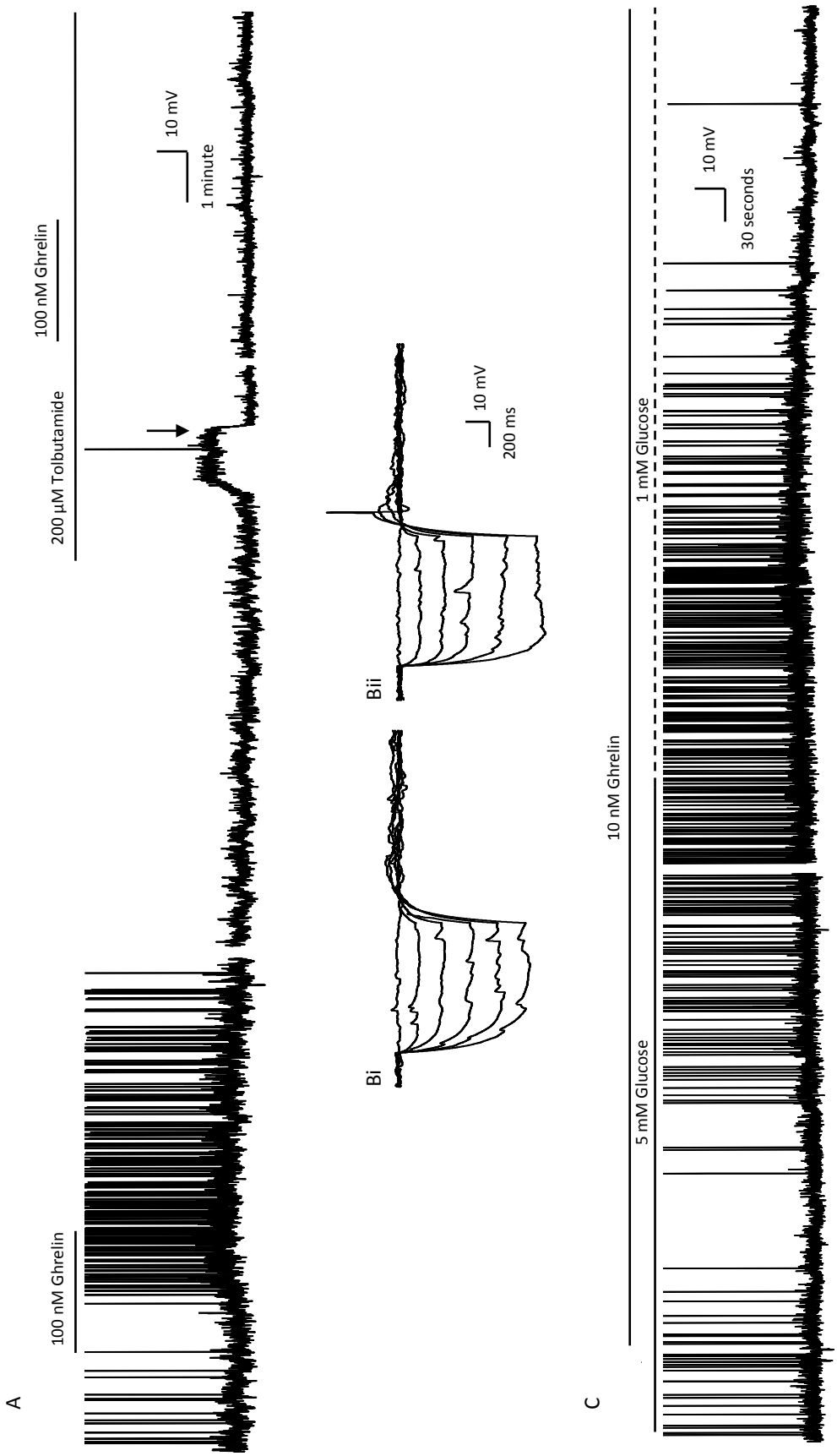
A
100 nM Ghrelin
200 µM Tolbutamide
100 nM Ghrelin
10 mV
1 minute
Bi
Bii
10 mV
200 ms
C
10 nM Ghrelin
5 mM Glucose
1 mM Glucose
10 mV
30 seconds

Figure 4.9: The excitatory effect of ghrelin on NPY eGFP neurons is amplified in low glucose conditions

A: Current clamp recording take from NPY eGFP neuron, from a mouse fed *ad libitum* prior to culling, with brain slices incubated in aCSF containing 5 mM glucose. Bath application of 100 nM ghrelin caused a reversible membrane depolarization and increase in action potential firing frequency.

B: Current clamp recording take from a NPY eGFP neuron, from a mouse subjected to an 18-hour fast prior to culling, with brain slices incubated in aCSF containing 1 mM glucose. Bath application of 100 nM ghrelin, in the presence of 1 μM TTX induces a reversible membrane depolarization. At peak response, membrane hyperpolarization through constant negative current injection revealed subthreshold membrane potential oscillations (shown in expanded timescale; bottom panel).

Figure 4.9

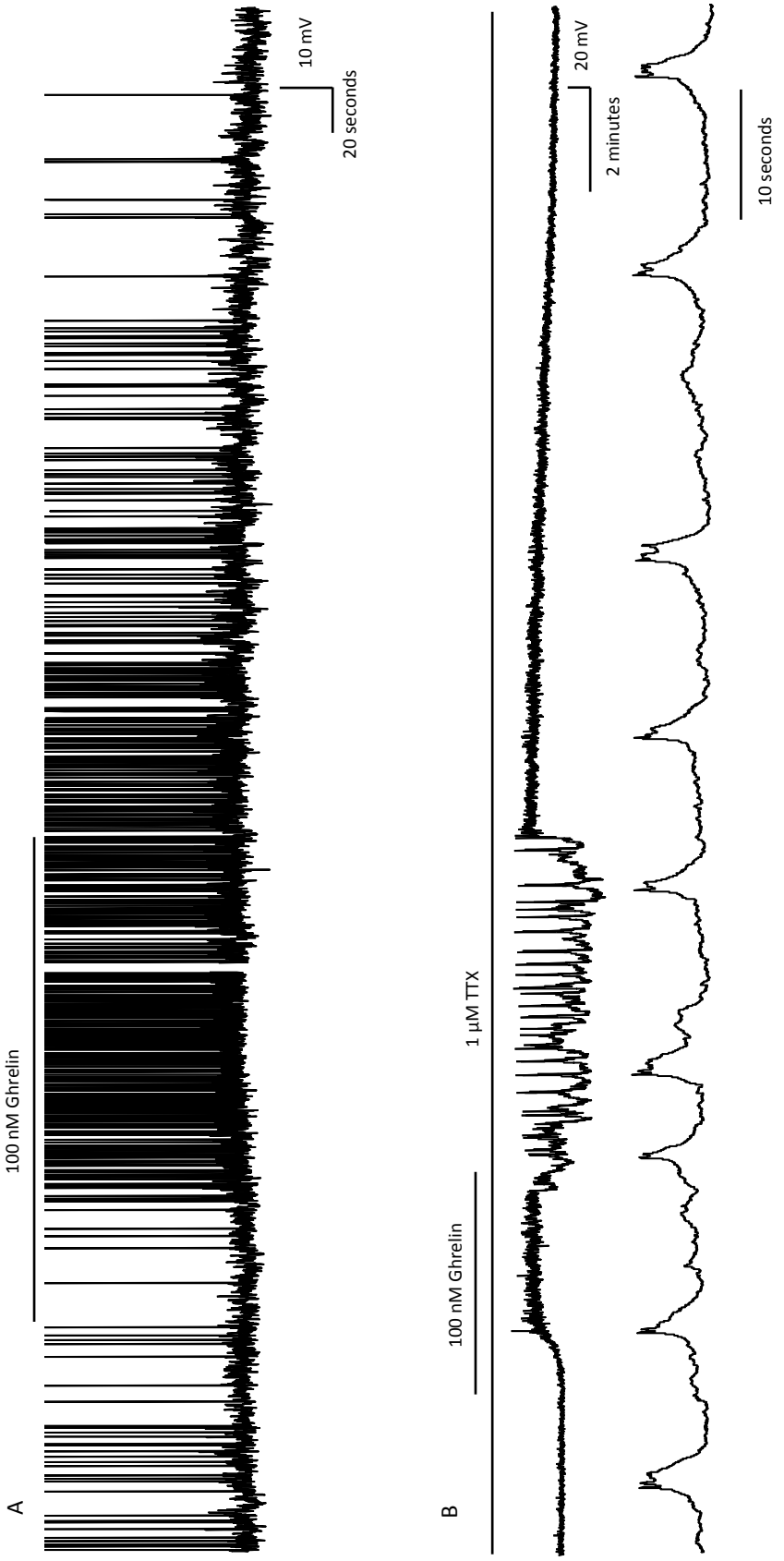
A
100 nM Ghrelin
10 mV
20 seconds
B
100 nM Ghrelin
1 µM TTX
20 mV
2 minutes
10 seconds

Figure 4.10: The excitatory effect of ghrelin on NPY eGFP neurons is amplified in low glucose conditions

Ai: Graph summarizing the percentage of NPY-eGFP neurons sensitive to bath application of ghrelin at concentrations of 3, 10 and 30 nM in the following conditions: Fed, 5 mM glucose group; 40% (n=15), 60% (n=15), 75% (n=16); Fasted, 1 mM glucose group: 42.4% (n=33), 65.5% (n=33), 69.6% (n=23) (Control/wash vs. ghrelin).

Aii: Graph summarizing the mean change in membrane potential induced by bath application of ghrelin at 3, 10 and 30 nM (Data summarized in **Bi**).

Aiii: Graph summarizing the mean change action potential firing frequency induced by bath application of ghrelin at 3, 10 and 30 nM (Data summarized in **Bii**).

Aiv Graph summarizing the mean change in input resistance induced by bath application of ghrelin at 3, 10 and 30 nM (Data summarized in **Biii**).

Bi: Table summarizing data shown in **Ai**.

Bii: Table summarizing data shown in **Aii**.

Biii: Table summarizing data shown in **Aiii**.

Figure 4.10

Ai

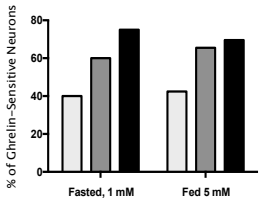

Aii

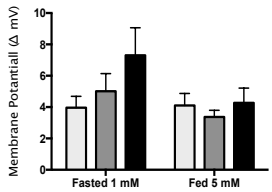

Aiii

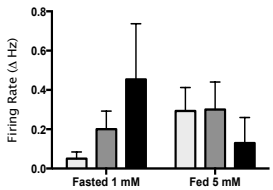

Aiv

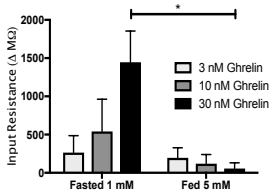

Bi

	Ghrelin Dose Response: Membrane Potential								
	3 nM Ghrelin			10 nM Ghrelin			30 nM Ghrelin		
	Δ mV	n	SEM	Δ mV	n	SEM	Δ mV	n	SEM
Fasted 1 mM	3.96	6.00	0.72	5.01	6	1.12	7.30	7	1.76
Fed 5 mM	4.10	14.00	0.77	3.37	12	0.42	4.27	5	0.94

Bii

	Ghrelin Dose Response: Action Potential Firing Rate								
	3 nM Ghrelin			10 nM Ghrelin			30 nM Ghrelin		
	Δ Hz	n	SEM	Δ Hz	n	SEM	Δ Hz	n	SEM
Fasted 1 mM	0.05	6	0.03	0.20	6	0.09	0.45	7	0.28
Fed 5 mM	0.29	14	0.12	0.30	12	0.14	0.16	4	0.16

Biii

	Ghrelin Dose Response: Neuronal Input Resistance								
	3 nM Ghrelin			10 nM Ghrelin			30 nM Ghrelin		
	Δ MΩ	n	SEM	Δ MΩ	n	SEM	Δ MΩ	n	SEM
Fasted 1 mM	264	5	223	541	6	421	1446	3	409
Fed 5 mM	196	12	131	119	9	121	56	4	74

Figure 4.11: Ghrelin excites both glucose inhibited and glucose excited NPY eGFP neurons

A: Current clamp recording taken from a NPY eGFP neuron from a mouse subjected to an 18 hour fast prior to culling. Bath application of 100 nM ghrelin induced membrane depolarization and increased action potential firing rate. After ghrelin washout from the recording chamber and membrane repolarization, increasing extracellular glucose concentration from 1 mM to 5 mM induced membrane depolarization and an increase in action potential firing rate. Further membrane excitation was induced by subsequent bath application of 200μM tolbutamide, the latter confirming the expression of functional K_{ATP} channels in this neuron.

B: Current clamp recording taken from a NPY eGFP neuron from a mouse subjected to an 18 hour fast prior to culling. Bath application of 100 nM ghrelin induced membrane depolarization and increased action potential firing rate. After ghrelin washout from the recording chamber and membrane repolarization, increasing extracellular glucose concentration from 1 mM to 5 mM induced membrane hyperpolarization. Membrane excitation by subsequent bath application of 200μM tolbutamide confirmed the expression of functional K_{ATP} channels in this neuron.

Figure 4.11

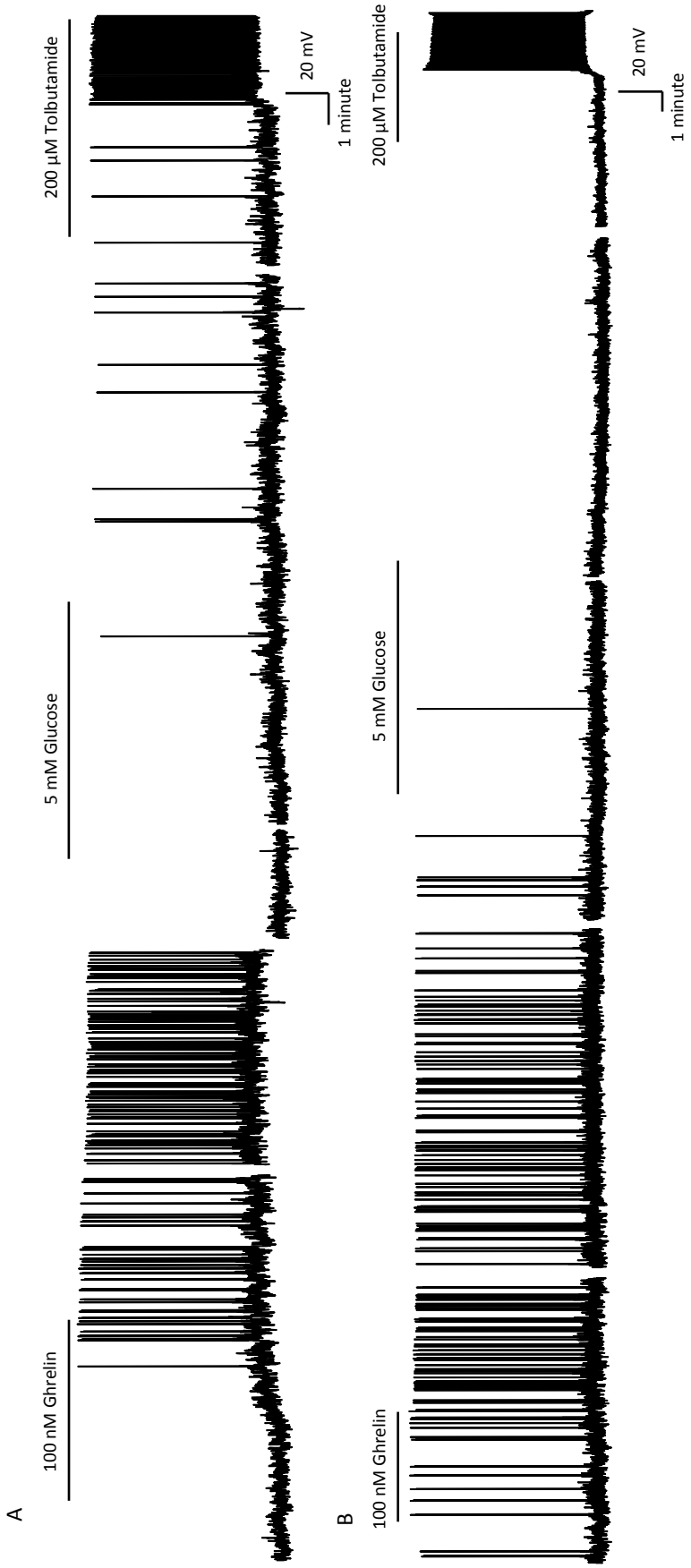
A
100 nM Ghrelin
5 mM Glucose
200 µM Tolbutamide
20 mV
1 minute
B
100 nM Ghrelin
5 mM Glucose
200 µM Tolbutamide
20 mV
1 minute

Chapter 5: The contribution of TCPTP, PTP1B and PI3-kinase to insulin signaling in POMC neurons

5.1 Introduction

Obesity is increasing in prevalence, especially in western societies. Intervention strategies aimed at reducing appetite and increasing energy expenditure would reduce death attributed to obesity-related diseases. Increased fat mass is associated with a number of co-morbidities including cardiovascular disease, cancer and type-2 diabetes mellitus (T2DM). In 2016, 1 in 11 adults worldwide were affected by diabetes and between 1980 and 2014, the prevalence of diabetes rose to from 108 million to 422 million (WHO, 2016). Elevated blood sugar is linked to 3.7 million deaths annually (WHO, 2016). T2DM reduces life expectancy by 7 years, increases the risk of cardiovascular disease, peripheral artery disease, retinopathy, nephropathy and neuropathy (NICE, 2015). The underlying metabolic disorders of T2DM are insulin insensitivity and insulin deficiency (NICE, 2015).

Insulin is secreted from pancreatic β-cells in response to elevated plasma glucose (Rorsman and Braun, 2013). The insulin receptor (IR) is a hormone-activated protein tyrosine kinase, expressed ubiquitously in all mammalian tissues (Desbuquois et al., 1993). Insulin-IR binding initiates insulin receptor substrate (IRS) tyrosine residue phosphorylation and signal transduction (Watanabe et al., 1998). Functional peripheral and central insulin signaling is required for normal glucose homeostasis (Plum et al., 2006a). Peripheral organs mediate the physiological effects of insulin on blood glucose. The liver and kidneys regulate plasma glucose through glycogenesis and gluconeogenesis whilst glucose uptake

by muscle and adipose tissue is also critical to glucose homeostasis (Patti and Kahn, 1998). Elevated plasma insulin decreases hepatic glycogenolysis and gluconeogenesis whilst also increasing glucose uptake to fat and muscle tissue. Central insulin signaling affects glucose homeostasis through the regulation of hepatic glucose production, appetite and energy expenditure (Pocai et al., 2005).

Insulin elicits significant physiological effects through signaling in neurons of the arcuate nucleus of the hypothalamus (ARH), including neuropeptide Y/agouti-related peptide (NPY/AgRP) and proopiomelanocortin/ cocaine and amphetamine-regulated transcript (POMC/CART) neurons (Dodd et al., 2015, Konner et al., 2007). POMC neurons of the ARH are sensitive to both insulin and leptin (Cowley et al., 2001, Qiu et al., 2014, Williams et al., 2010). Leptin and insulin signaling in POMC neurons increases brown adipose tissue (BAT) thermogenesis and also converts white adipose tissue (WAT) to BAT. BAT is a key effector of energy expenditure; it is highly metabolic, dense with mitochondria and the BAT-specific protein, uncoupling protein-1 (UCP-1) (Dodd et al., 2015). UCP-1 uncouples fatty acid oxidation and ATP production by catalyzing ATP synthase-independent proton transport across the inner mitochondrial membrane (Rosen and Spiegelman, 2014). Increased UCP-1 activity increases BAT thermogenesis and energy expenditure (Rosen and Spiegelman, 2014). The attenuation of leptin and insulin signal transduction blunts these effects (Dodd et al., 2015).

POMC neurons of the ARH are anorexigenic, with increased electrical activity promoting satiety and increasing energy expenditure via elevated αMSH release onto second order neurons, including those in the PVH (Huszar et al., 1997). Insulin exerts inhibitory effects on some POMC neurons, whilst on others it induces membrane excitation (Williams et al., 2010, Qiu et al., 2014). Insulin

excites a subpopulation of POMC neurons via transient receptor potential channel (TRPC) activation (Qiu et al., 2014). The proportion of insulin-inhibited POMC neurons varies greatly and has been reported to be 25%, 50%, and 80% of the population (Choudhury et al., 2005, Claret et al., 2007, Williams et al., 2010). POMC neurons express functional K_{ATP} channels and insulin has been shown to inhibit arcuate neurons via a K_{ATP} channel and PI3K-dependent mechanism (Spanswick et al., 2000, Claret et al., 2007, Plum et al., 2006b). Both TRPC and K_{ATP} channel activation is dependent upon PI3K signal transduction: Increased POMC PI3K activity has been associated with elevated K_{ATP} channel activation, and obesity (Plum et al., 2006b). The PI3K inhibitor wortmannin has been shown to block insulin-induced POMC neuron excitation (Qiu et al., 2014).

Insulin signal transduction (see Figure 1.2) is initiated by the binding and activation of the IR, initiating IRS2 phosphorylation. IRS2 recruits PI3K, increasing intracellular PIP_3 concentration. PI3K activates K_{ATP} channels in arcuate NPY/AgRP and POMC neurons, and also activates TRPC channels in POMC neurons (Spanswick et al., 2000, Williams et al., 2010, Qiu et al., 2014). Increased PIP_3 activates the serine/threonine protein kinase AKT, which phosphorylates FOX01, increasing POMC expression, promoting the anorexigenic axis of the melanocortin system. Central insulin-IRS-PI3K signaling is required for normal energy homeostasis. Knock-out or inhibition of hypothalamic insulin signaling results in obesity, insulin resistance and impaired gonadotroph secretion, whilst increased hypothalamic PI3K signaling enhances central glucose sensitivity (Bruning et al., 2000, Kubota et al., 2004, Gelling et al., 2006).

The protein tyrosine phosphatases, T-cell protein tyrosine phosphatase (TCPTP) and protein tyrosine phosphatase 1B (PTP1B), attenuate central insulin

signaling and are expressed in distinct and overlapping subpopulations of arcuate POMC neurons (Zhang et al., 2015). PTP1B is expressed in 75% of arcuate POMC neurons, with highest POMC expression in the central and caudal ARH (Dodd et al., 2015). TCPTP is expressed in 40% of ARH POMC neurons, with increased POMC-TCPTP localization in the rostral ARH (Dodd et al., 2015). PTP1B dephosphorylates Y1162 and Y1163 of the IR (Zhang et al., 2015). Hypothalamic PTP1B knockdown reduces food intake and body weight and is protective against obesity (Picardi et al., 2008, Goldstein, 2002). However, specific PTP1B knockout in arcuate POMC neurons does not affect insulin signaling and energy homeostasis (Dodd et al., 2015). TCPTP also dephosphorylates Y1162 and Y1163 of the IR, and knockout of this phosphatase in ARH POMC neurons increases AKT-induced POMC expression, and improves glucose homeostasis (Dodd et al., 2015, Galic et al., 2003).

Intact PI3K signal transduction is required for insulin to affect arcuate POMC neuron electrical activity, and TCPTP is recognized as a negative regulator of insulin signaling. The aims of this study were to use the visualized whole-cell patch clamp technique to determine the effects of TCPTP and PI3K activity on insulin-induced changes in electrical activity of POMC neuron

5.2 Results

5.2.1 The effects of insulin on POMC eGFP neurons

Whole-cell recordings were obtained from 53 POMC eGFP neurons in hypothalamic brain slices prepared from POMC eGFP transgenic mice. Application of 100 nM insulin induced membrane depolarization and/or an increase in spontaneous action potential firing rate in 9.4% (n=5) of recorded neurons;

membrane hyperpolarization in 51.0% (n=27) of recorded neurons, and the remaining 39.6% (n=21) of neurons did not respond to bath application of 100 nM insulin (Figure 5.1A).

Insulin induced a mean peak amplitude depolarization of 6.29 ± 1.74 mV from a mean resting potential of −44.39 ± 2.27 mV to a new steady-state membrane potential of −38.11 ± 1.74 mV (p=0.023, n=5). Insulin-induced excitation was associated with an increase in firing rate from a mean control basal level of 0.79 ± 0.35 Hz to 1.35 ± 0.57 Hz in the presence of insulin (p=0.093, n=5), Spontaneous firing rate in the presence of insulin amounted to 173.2 ± 22.3 % of activity observed in control conditions (n=3).

Insulin induced a mean peak amplitude membrane hyperpolarization of 2.58 ± 0.45 mV: from a mean resting potential of −41.04 ± 0.97 mV to a new steady-state membrane potential of −43.70 ± 1.40 mV (p=0.00001, n=27). Insulin-induced inhibition was associated with a reduction in firing rate from a mean control basal level of 0.90 ± 0.20 Hz to 0.16 ± 0.06 Hz in the presence of insulin (p=0.00007, n = 27). Spontaneous firing rate in the presence of insulin amounted to 21.2 ± 4.8 % of activity observed in control conditions (n=15).

5.2.2 The effects of insulin on POMC-eGFP neurons, in the presence of a TCPTP inhibitor

Whole-cell recordings were obtained from 58 POMC eGFP neurons, with the TCPTP inhibitor 'Compound 8' included in the pipette solution at a concentration of 20 nM. Compound 8 is a menthoxyacetic acid derivative (Zhang et al., 2009). Bath application of 100 nM insulin was performed at least 15 minutes after whole-

cell access was achieved. Here, insulin induced membrane depolarization and/or an increase in spontaneous action potential firing rate in 32.7% (n=19) of recorded neurons; membrane hyperpolarization in 12.1% (n=7) of recorded neurons, and the remaining 55.2% (n=32) of neurons did not respond to bath application of 100 nM insulin (Figure 5.1B).

Insulin induced a mean peak amplitude depolarization of 5.91 ± 0.79 mV from a mean resting potential of −48.25 ± 1.60 mV to a new steady-state membrane potential of −42.33 ± 1.20 mV (p=0.0000007, n=19). Insulin-induced excitation was associated with an increase in firing rate from a mean control basal level of 0.51 ± 0.21 Hz to 0.81 ± 0.27 Hz in the presence of insulin (p=0.094, n=19). Of neurons firing in control conditions, spontaneous firing rate in the presence of insulin amounted to 160 % of activity observed in control conditions (n=10).

Insulin induced a mean peak amplitude hyperpolarization of 4.00 ± 0.50 mV from a mean resting potential of −46.98 ± 3.89 mV to a new steady-state membrane potential of −50.98 ± 4.22 mV (p=0.0002, n=7). Insulin-induced inhibition was associated with a reduction in firing rate from a mean control basal level of 0.11 ± 0.09 Hz to 0.01 ± 0.00 Hz in the presence of insulin (p=0.27, n=7). Of neurons firing in control conditions spontaneous firing rate in the presence of insulin amounted to 7.4 ± 2.6 % of activity observed in control conditions (n=2).

5.2.3 The effects of insulin on POMC neurons lacking TCPTP

Whole-cell recordings were obtained from 33 POMC Z/EG TCPT $^{lox/lox}$ neurons. Application of 100 nM insulin induced membrane depolarization and/or an increase in spontaneous action potential firing rate in 36.4% (n=12) of recorded neurons, membrane hyperpolarization in 36.4% (n=12) of recorded neurons, and

the remaining 27.2% (n=9) of neurons did not respond to bath application of 100 nM insulin (Figure 5.1C).

Insulin induced a mean peak amplitude depolarization of 4.24 ± 0.67 mV from a mean resting potential of −42.11 ± 1.84 mV to a new steady-state membrane potential of −37.87 ± 1.66 mV (p=0.00006). Insulin-induced excitation was associated with an increase in firing rate from a mean control basal level of 0.35 ± 0.19 Hz to 0.79 ± 0.39 Hz in the presence of insulin (p=0.14; n = 12; paired students t-test). Spontaneous firing rate in the presence of insulin amounted to 366.6 ± 113.9 % of activity observed in control conditions (n=6).

Insulin induced a mean peak amplitude hyperpolarization of 3.75 ± 0.89 mV from a mean resting potential of −43.04 ± 1.77 mV to a new steady-state membrane potential of −46.78 ± 2.30 mV (p=0.001). Insulin-induced inhibition was associated with a reduction in firing rate from a mean control basal level of 0.32 ± 0.15 Hz to 0.05 ± 0.03 Hz in the presence of insulin (p=0.058; n = 12; paired students t-test). Spontaneous firing rate in the presence of insulin amounted to 11.2 ± 4.1 % of activity observed in control conditions (n=6).

5.2.4 The effects of inhibition of PI3kinase on insulin-induced responses in POMC eGFP neurons

Whole-cell recordings were obtained from 58 POMC eGFP neurons. Application of 100 nM insulin was preceded by bath application of the PI3K inhibitor LY294002 (10μM). Insulin induced membrane depolarization and/or an increase in spontaneous action potential firing rate in 36.6% (n=21) of recorded neurons, membrane hyperpolarization in 11.6% (n=7) of recorded neurons, and the

remaining 51.6% (n=30) of neurons did not respond to 100 nM insulin (Figure 5.1).

Insulin induced a mean peak amplitude depolarization of 4.04 ± 0.39 mV from a mean resting potential of −45.38 ± 0.67 mV to a new steady-state membrane potential of −41.34 ± 0.68 mV (p=0.00001). Insulin-induced excitation was associated with an increase in firing rate from a mean control basal level of 0.72 ± 0.13 Hz to 1.03 ± 0.19 Hz in the presence of insulin (n = 22, p=0.89; paired students t-test). Spontaneous firing rate in the presence of insulin amounted to 115.7 ± 17.7 % of activity observed in control conditions (n=18).

Insulin induced a mean peak amplitude membrane hyperpolarization of 3.60 ± 1.22 mV from a mean resting potential of −39.76 ± 3.60 mV to a new steady-state membrane potential of −43.35 ± 4.75 mV (p=0.008). Insulin-induced inhibition was associated with a reduction in firing rate from a mean control basal level of 0.40 ± 0.17 Hz to 0.07 ± 0.07 Hz in the presence of insulin (n = 7, p=0.055; paired students t-test). Spontaneous firing rate in the presence of insulin amounted to 5.6 ± 5.6 % of activity observed in control conditions (n=4).

5.3 Discussion

Here I show an increased proportion of insulin-induced excitations when TCPTP is inhibited or knocked out, or when PI3K is inhibited, compared to POMC eGFP controls. I also show that the magnitude of the insulin-induced excitation is significantly increased in the presence of a TCPTP inhibitor, relative to insulin-induced excitations in the presence of a PI3K inhibitor. Here, the response distribution of insulin's effect on POMC EGFP neurons was found to be significantly different to the effect of insulin in the presence of a TCPTP inhibitor (p=<0.0001),

the effect of insulin on POMC Z/EG neurons lacking TCPTP (p=0.0095) and POMC EGFP neurons in the presence of a PI3K inhibitor (p=<0.0001). The insulin response distribution of the TCPTP inhibitor and PI3K inhibitor groups were not statistically different (p=0.9041). Response distributions of the TCPTP inhibitor and TCPTP knockout groups were found to be significantly different (p=0.008).

Taken together, this data indicates that TCPTP attenuates insulin-induced excitation of POMC neurons. This data is generally in agreement with physiological studies that demonstrated attenuation of insulin signaling by TCPTP *in vivo* (Tiganis, 2013). Thus TCPTP has an important role in mediating insulin-induced excitation in POMC neurons.

Previous studies have suggested Insulin depolarizes arcuate POMC neurons via the PI3K-dependent activation of TRPC channels (Qiu et al., 2014). TCPTP dephosphorylates Y1162 and Y1163 residues of the IR (Galic et al., 2003), downstream effects of which are the reduced phosphorylation of IRS2 and reduced activation of PI3K. Thus, disinhibition of PI3K signaling, via inhibition of TCPTP, may promote POMC neuron excitation via TRPC channels. This notion is further supported by the observations here of the significantly elevated magnitude of the excitatory membrane potential response to insulin, in the presence of a TCPTP inhibitor, relative to a PI3K inhibitor.

These data indicate that the inhibition of TCPTP in arcuate POMC neurons promotes an increased proportion of insulin-induced excitations possibly via disinhibition of the IR-PI3K-TRPC pathway. The larger proportion of insulin-induced inhibitions observed in the control POMC population, compared to eGFP plus TCPTP inhibitor population suggests that TCPTP signaling promotes insulin-induced inhibition of POMC neurons. Paradoxically the similarity between TCPTP

and PI3K inhibitor group response distributions would suggest that the same insulin response distribution can be generated through both the inhibition and disinhibition of PI3K signaling. Previous work has demonstrated K_{ATP} channel activation to result from elevated intracellular PIP3 (Harvey et al., 2000). Presumably PI3K inhibition would decrease cytosolic PIP3, whilst TCPTP inhibition would increase intracellular PIP3. How blocking TCPTP and PI3-kinase results in a similar population and distribution of insulin-sensitive POMC neurons is currently unclear. However, as indicated above, increased excitation through disinhibition of PI3-kinase could explain increased excitation whilst inhibition of PI3-kinase could promote insulin-induced excitation by suppressing a PI-3-kinase-dependent inhibition that effectively masks concomitant excitation. Such a notion is supported here by observations that PI3-kinase inhibition alone induced depolarization, suggesting a tonic inhibitory drive via PI3 kinase exists in some POMC neurons. Furthermore, PI3 kinase has been clearly shown to activate K_{ATP} channels in pancreatic beta cells (Khan et al., 2001) and hypothalamic neurons (Spanswick et al., 2000) including POMC (Plum et al., 2006b). PI3-kinase can also be activated via many routes other than tyrosine kinase-dependent pathways including via G-protein coupled receptors, for example adenosine A_2 and A_3 receptors (Gavi et al., 2006). Thus, the reduced incidence of insulin-induced inhibitions in the PI3K inhibitor population is explainable in that neurons are no longer competent of K_{ATP} channel activation and membrane hyperpolarization. One final point worthy of note is the fact that the selectivity of the TCPTP inhibitor may be questionable, although introducing the inhibitor via the patch pipette enabled drug application at a reported selective concentration. The fact that some inhibitions remain in the PI3K inhibitor group also suggests PI3K-independent

mechanisms may contribute to insulin-induced hyperpolarization in some POMC neurons.

TCPTP and PI3K inhibitor groups have comparable proportions of insulin-induced inhibitory responses in POMC neurons. However the TCPTP knockout population had a notably higher proportion of insulin inhibited neurons and less insulin-insensitive neurons. These observations may be indicative of the presence of redundant compensatory mechanisms arising in POMC neurons, in response to TCPTP knockout.

POMC neurons can be hyperpolarized via a PI3K-K_{ATP} channel-dependent mechanism (Plum et al., 2006b). Increased PI3K activity is associated with activated K_{ATP} channels and membrane hyperpolarization. Therefore one could hypothesize that the control population would have the smallest percentage of insulin-inhibited neurons due to TCPTP attenuation of PI3K signaling. However this is not the case. A smaller proportion of POMC neurons are inhibited in the TCPTP knockout compared to control and to a greater degree in the presence of a TCPTP or PI3K inhibitor. Thus TCPTP also appears important fro insulin-induced inhibition, at least in a subpopulation of POMC neurons

These results indicate that TCPTP can drive inhibitory insulin signaling through the attenuation of PI3K signaling. Blocking the ability of TCPTP to attenuate signaling gives rise to a greater proportion of insulin excited and smaller proportion of insulin-inhibited POMC neurons. This net increase in membrane excitation is associated with increased innervation of the sympathetic nervous system (SNS) by POMC neurons, measured in terms of BAT thermogenesis and increased browning of white adipose tissue (Dodd et al., 2015).

Blocking the effects of TCPTP at these neurons generates an increase in excitatory output. A net increase in the electrical activity of arcuate POMC neurons is associated with reduced food intake, elevated energy expenditure and the reduction of adiposity (Claret et al., 2007, Zhan et al., 2013). Insulin acts at POMC neurons to increase energy expenditure by promoting the conversion of WAT to BAT, in addition to increasing BAT thermogenesis, an effect enhanced by the knock out of PTP1B and TCPTP (Dodd et al., 2015). POMC neuron specific TCPTP knockout has been shown to increase PI3K-pAKT signaling. *In vivo* Inhibition of TCPTP with the selective inhibitor used in electrophysiological experiments outlined here and described by Zhang et al., results in a 2.5 fold increase in POMC mRNA expression (Dodd et al., 2015, Zhang et al., 2009). Thus, data described here, at least in part, agree with physiological observations made in vivo. One final point worthy of note here is the heterogeneity of insulin-induced responses. This almost certainly reflects heterogeneity of POMC neuronal function (Sohn and Williams, 2012) in relation to functional anatomical organization, target neuron, organ and behavioral output. Future work would benefit from identifying insulin responses in relation to target organ and function to fully understand the heterogeneity of insulin-induced responses in these neurons and their associated signal transduction pathways. In summary, data presented here provide insight of the mechanisms by which insulin-dependent signaling regulates POMC neurons and how future pharmaceuticals could attenuate obesity, through the inhibition of POMC protein tyrosine phosphatases, and the disinhibition of insulin signal transduction. However it must be noted that TCPTP expression is ubiquitous, with especially high expression found in hematopoietic tissue (Ibarra-Sanchez et al., 2001). As such, the effects on food intake and energy expenditure are unlikely to

the only impact of phosphatase manipulation. Furthermore, current pharmacological agents - such as Compound 8 used here - although effective at nanomolar concentrations, also inhibit other phosphatases - such as PTP1B – at the same order of magnitude concentration. There is a need for more specific and selective pharmacological agents.

Figure 5.1: Distribution of insulin-induced responses in POMC neurons and the effects of TCPTP and PI3K inhibition

A: Pie chart summarizing POMC eGFP neuron responses to bath application of insulin (100nM). 51.0% of neurons were inhibited by insulin; 9.4% were excited by insulin and in 39% of neurons, no membrane response was detected (n=53).

B: Pie chart summarizing POMC eGFP neuron responses to bath application of insulin (100nM) in the presence of a selective TCPTP inhibitor, Compound 8 (20 nM), introduced from the patch pipette. 12.1% of neurons were inhibited by insulin, 32.7% were excited by insulin and in 55.2% of neurons, no membrane response was detected (n=58).

C: Pie chart summarizing the effects of insulin (100nM), applied by bath application, in hypothalamic slices prepared from POMC Z/EG TCPTP knockout transgenic mice. Under these conditions, TCPTP was selectively knocked-out of POMC neurons. 36.4% of neurons were inhibited by insulin, 36.4% were excited by insulin and 27% did not respond to this hormone.

D: Pie chart summarizing POMC eGFP neuron responses to bath application of insulin (100nM) following inhibition of PI3K by incubating hypothalamic slices in the PI3K inhibitor LY294002 (10μM). 11.66% of neurons were excited by insulin, 36.66% of neurons were inhibited by insulin and 51.66% of neurons did not respond to insulin in the presence of LY294002 (10μM).

E. Table summarizing comparative analysis of population data shown in A – D. *p*-values shown are the result of Chi-square population analysis.

Figure 5.1

A

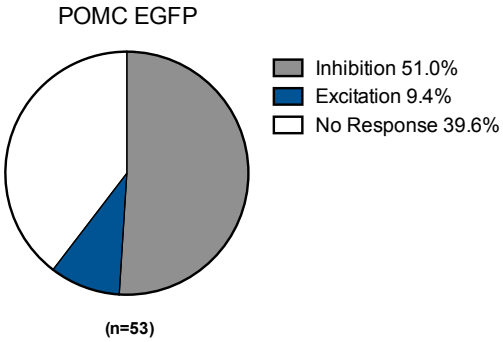

B

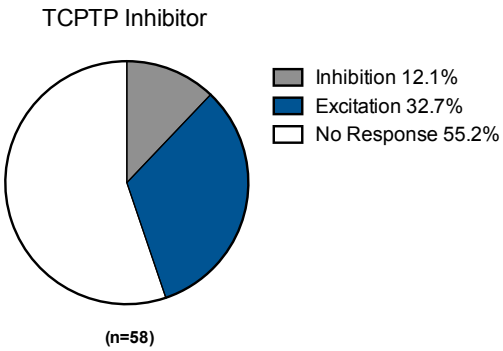

C

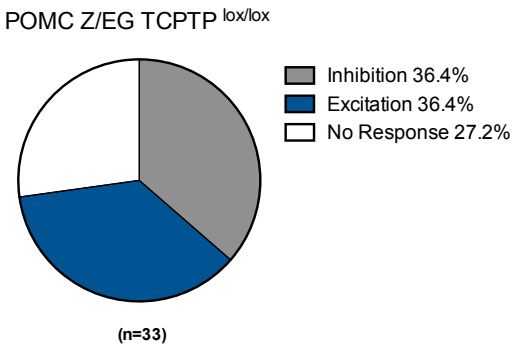

D

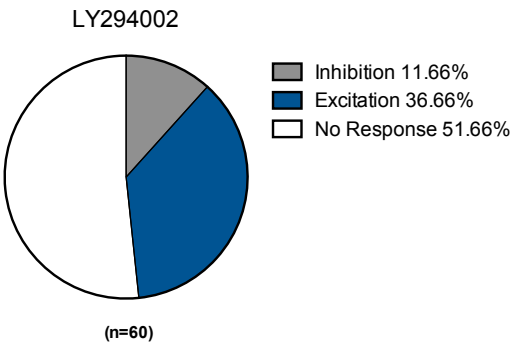

E

Population Comparison	*p*
POMC EGFP Vs. TCPTP Inhibitor	**<0.0001**
POMC EGFP Vs. POMC Z/EG TCPTP lox/lox	**0.0095**
POMC EGFP Vs. LY294002	**<0.0001**
TCPTP Inhibitor Vs. LY294002	0.9041
TCPTP Inhibitor Vs. POMC Z/EG TCPTP lox/lox	**0.008**

Figure 5.2: Magnitude of insulin-induced POMC neuron membrane responses

A: Bar chart summarizing the mean membrane potential change to insulin in all four experimental groups. Both insulin-induced inhibition and insulin-induced excitation are shown. Of POMC eGFP neurons tested, mean insulin-induced membrane depolarization was 6.29 ± 1.74 mV (n=5), whilst mean insulin-induced membrane hyperpolarization was 2.58 ± 0.45 mV (n=27). Of POMC eGFP neurons tested in the presence of a TCPTP inhibitor, mean insulin-induced depolarization was found to be 5.91 ± 0.79 mV (n=19), whilst mean insulin-induced hyperpolarization was 4.00 ± 0.50 mV (n=7). Of POMC Z/EG TCPTP $^{lox/lox}$ neurons, mean insulin-induced depolarization was 4.24 ± 0.67 mV (n=12), whilst mean insulin-induced hyperpolarization was 3.75 ± 0.89 mV (n=12). Of POMC eGFP neurons tested in the presence of a PI3K inhibitor, mean insulin-induced membrane depolarization was 4.04 ± 0.39 mV (n=22), whilst mean insulin-induced membrane hyperpolarization was 3.60-± 1.22 mV (n=7). Of insulin-induced membrane depolarisations, those of the TCPTP inhibitor population were of a significantly greater magnitude than those of the PI3K inhibitor (p=<0.05, 2-way ANOVA).

B: Bar chart summarizing the mean percentage decrease in spontaneous action potential firing rate, of inhibitory responses from all four experimental groups (with control as 100%). Of insulin-inhibited POMC eGFP neurons tested, action potential firing rate in the presence of insulin was 21.2 ± 4.8 % that of control levels (n=15). Of insulin-inhibited POMC eGFP neurons tested in the presence of a TCPTP inhibitor, action potential firing rate in the presence of insulin was 7.4 ± 2.6 % that of control levels (n=2). Of insulin-inhibited POMC Z/EG TCPTP $^{lox/lox}$ neurons tested, action potential firing rate in the presence of insulin was 11.2 ± 4.1

% that of control levels (n=6). Of insulin-inhibited POMC eGFP neurons tested in the presence of a PI3K inhibitor, action potential firing rate in the presence of insulin was 5.6 ± 5.6 % that of control levels (n=4).

C: Bar chart summarizing the mean percentage increase in spontaneous action potential firing rate, of excitatory responses from all four experimental groups (with control as 100%). Of insulin-excited POMC eGFP neurons tested, action potential firing rate in the presence of insulin was 173.2 ± 22.3 % that of control levels (n=3). Of insulin-excited POMC eGFP neurons tested in the presence of a TCPTP inhibitor, action potential firing rate in the presence of insulin was 923.3 ± 678.5 % that of control levels (n=10). Of insulin-excited POMC Z/EG TCPTP $^{lox/lox}$ neurons tested, action potential firing rate in the presence of insulin was 366.6 ± 113.9 % that of control levels (n=6). Of insulin-excited POMC eGFP neurons tested in the presence of a PI3K inhibitor, action potential firing rate in the presence of insulin was 115.7 ± 17.7 % that of control levels (n=18).

Figure 5.2

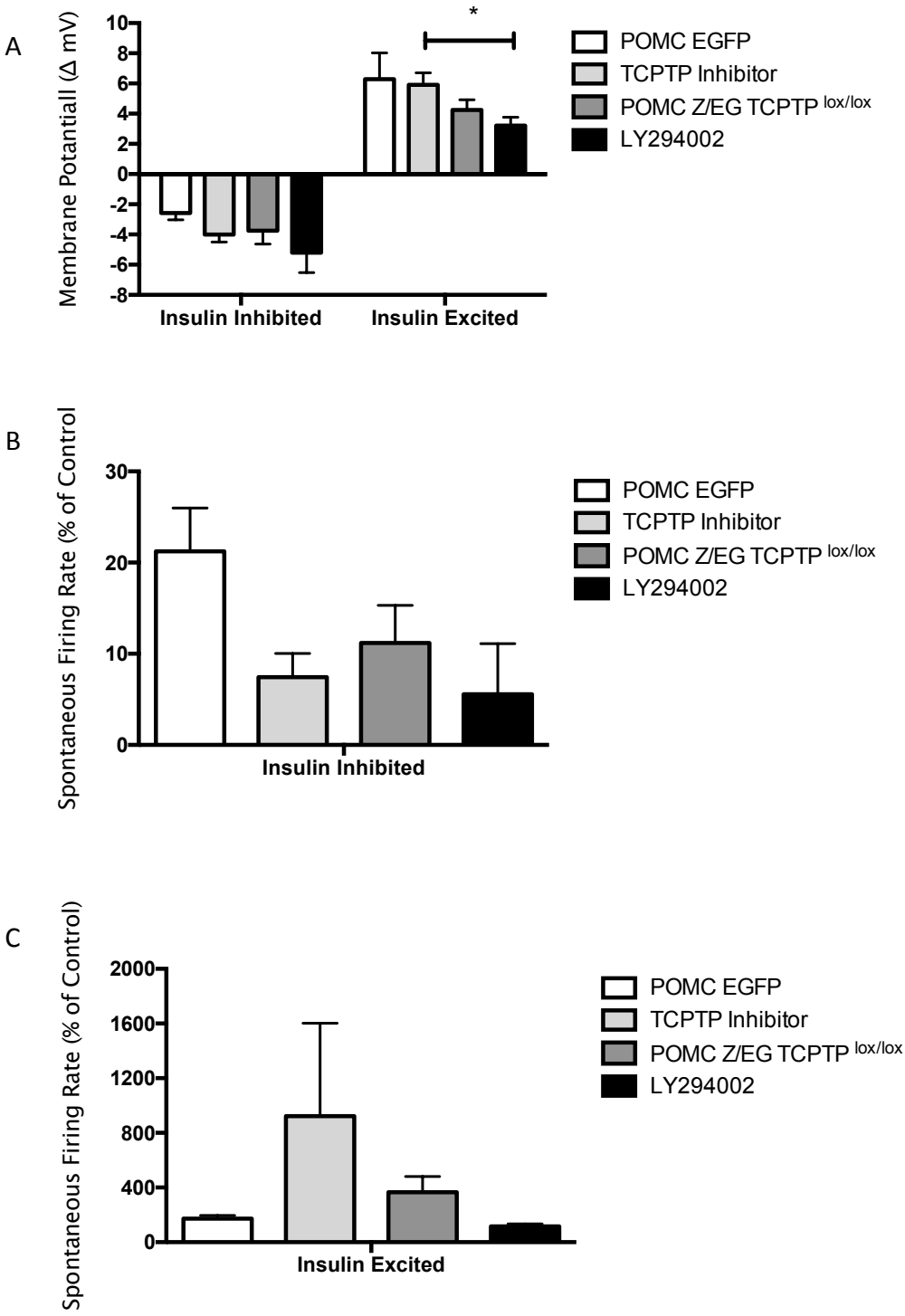
A
Membrane Potantiall (Δ mV)
10
8
6
4
2
0
-2
-4
-6
-8
*
Insulin Inhibited
Insulin Excited
POMC EGFP
TCPTP Inhibitor
POMC Z/EG TCPTP lox/lox
LY294002
B
Spontaneous Firing Rate (% of Control
30
20
10
0
Insulin Inhibited
POMC EGFP
TCPTP Inhibitor
POMC Z/EG TCPTP lox/lox
LY294002
C
Spontaneous Firing Rate (% of Control)
2000
1600
1200
800
400
0
Insulin Excited
POMC EGFP
TCPTP Inhibitor
POMC Z/EG TCPTP lox/lox
LY294002

Figure 5.3: POMC eGFP neurons are insulin-inhibited and insulin-excited

A: Samples of a continuous current-clamp recording of a POMC eGFP neuron, showing insulin induced membrane depolarization and an increase in action potential firing rate. Right panel; samples of the record from **A** shown on a faster time-base to highlight increased firing rate in the presence of insulin compared to control pre-insulin bath application.

B: Samples of a continuous current-clamp recording of a POMC eGFP neuron, showing insulin induced a reversible membrane hyperpolarization and cessation of action potential firing.

Figure 5.3


A
Insulin 100 nM
10 mV
15 seconds
B
100 nM Insulin
10 mV
40 seconds

Figure 5.4: TCPTP-inhibited POMC eGFP neurons have insulin-inhibited and insulin-excited subpopulations

A: Samples of a continuous current-clamp recording of a POMC eGFP neuron with the selective TCPTP inhibitor compound 8 (20 nM) 'loaded' into the patch pipette. Insulin-induced membrane depolarization and increase in action potential firing rate.

B: Samples of a continuous current-clamp recording of a POMC eGFP neuron with the selective TCPTP inhibitor 'loaded' into the patch pipette. Insulin induced a partially reversible membrane hyperpolarization and reduction in action potential firing rate under these recording conditions.

Figure 5.4

Figure 5.5: Insulin-induced excitation and inhibition in POMC Z/EG TCPTP knockout transgenic mice in which TCPTP was selectively knocked-out from POMC neurons

A: Samples of a continuous current-clamp recording of a POMC Z/EG TCPT $^{lox/lox}$ neuron showing insulin induced reversible membrane depolarization.

B: Samples of a continuous current-clamp recording of a POMC Z/EG TCPT $^{lox/lox}$ neuron, showing insulin induced membrane hyperpolarization and reduction of action potential firing rate.

Figure 5.5


A
Insulin 100 nM
10 mV
2 minutes
B
Insulin 100 nM
10 mV
2 minutes

Figure 5.6: Insulin induced excitation in POMC eGFP neurons, incubated in the PI3K inhibitor LY294002

A: Samples of a continuous current-clamp recording of a POMC eGFP neuron showing the PI3K inhibitor LY294002 (10μM) induced membrane depolarization associated with an increase in spontaneous firing rate.

B: Samples of the same continuous current-clamp recording as that shown in A. In the presence of the PI3K inhibitor LY294002 (10μM), insulin induced a further increase in spontaneous firing rate.

Figure 5.6

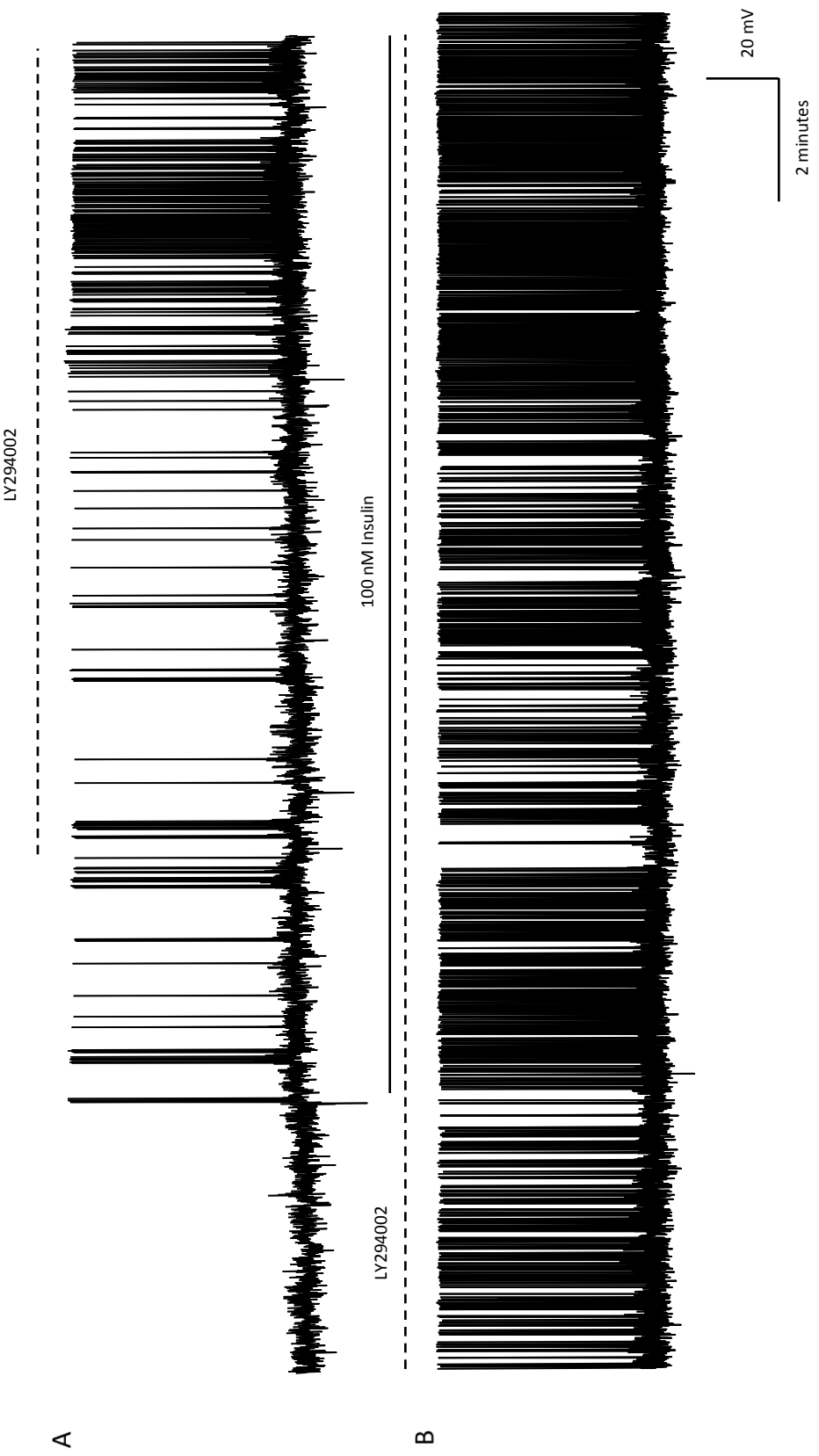

Chapter 6: Effects of leptin on leptin receptor-expressing neurons in the dorsomedial hypothalamus

6.1 Introduction

In 2008 the World Health Organization (WHO) reported that worldwide, 35% of adults were overweight, of these, 10% of men and 14% of women were obese (Bastien et al., 2014). An individual is considered obese if their BMI exceeds 30. A BMI of 30 is representative of a person standing 5 feet and 10 inches high (178 cm) and weighing 97.7 Kg. BMI is calculated as body weight (kg) divided by height^2 (m^2) (Must et al., 1999). Obesity is a disease of significantly elevated fat mass, however elevated adiposity does not kill directly. Secondary, obesity-associated diseases cause morbidity and mortality. These diseases include type II diabetes, osteoporosis, cancer and cardiovascular disease. The incidence of cardiovascular diseases including hypertension is significantly increased in obese populations (Must et al., 1999, Bastien et al., 2014). Cardiovascular diseases are the number 1 cause of death globally and it has been estimated that as much as 70% of cardiovascular disease is associated with elevated fat mass. Hypertension is a major risk factor for stroke, myocardial infarction, heart failure and renal disease. In 2000 it was estimated that 24% of the adult population in the USA were hypertensive or taking medication to reduce blood pressure (Carretero and Oparil, 2000). In addition to obesity, risk factors for hypertension include insulin resistance, high alcohol and or salt consumption, aging and stress, and in many cases, risk factors are additive (Cutler, 1996, Luft, 1998, Sever and Poulter, 1989). In humans, clinical hypertension is defined as blood pressure exceeding 140

mmHg systolic and 90 mmHg diastolic (140/90 mmHg), whilst a normal blood pressure sits around 120/80 mmHg (Carretero and Oparil, 2000).

In 1950, Jackson Laboratory scientists reported mice that quickly gained fat mass from birth, with obese adult mice weighing as much as three times that of age-matched controls (Ingalls et al., 1950). Breeding of heterozygotic mice generated a lean/obese ratio of 3 to 1 indicating the phenotype was due to a recessive gene mutation (Furney et al., 2006). This gene was named the obese gene, and to it was designated the symbol *ob* (Ingalls et al., 1950). Parabiosis experiments, wherein obese mice rapidly lost weight when conjoined to lean mice, indicated the product of the *ob* gene to be a circulatory factor, negatively regulating energy homeostasis (Coleman, 1978). Coleman identified another strain of mice, with an identical obese phenotype, also due to an autosomal recessive mutation. Here, parabiosis experiments of obese and lean mice with connected circulation resulted in starvation of the lean animal due to cessation of food intake, but no weight loss in the obese mouse (Coleman, 1973). The etiology of the metabolic disorder was concluded to be distinct from that of ob mice and the mutation was named diabetic, or db. It was later discovered that the *db* gene encoded the leptin receptor (Coleman, 1973, Tartaglia et al., 1995).

In 1994 the mouse *ob* gene and its human homologue were cloned (Zhang et al., 1994). The sequenced protein was highly conserved, localized to white fat and had an N-terminus signal sequence indicating that it was secreted from adipocytes (Tsuchiya et al., 2003, Zhang et al., 1994). Leptin is a 16kDa, 167 amino acid protein, secreted from white adipose cells into the plasma in proportion to body fat mass. In obesity, circulatory leptin levels are as high as 10 times that of lean mice (Maffei et al., 1995, Zhang et al., 1994). Leptin receptors (LepR) are

expressed ubiquitously in virtually all tissues and high expression levels are found in multiple central nervous system (CNS) regions (Tune and Considine, 2007). To date, six LepRs have been identified (ObRa through ObRf), and they belong to the class-I cytokine receptor family (Scott et al., 2009). ObRa receptors have been attributed to the trafficking of leptin into the brain. ObRb receptors are the only LepR to effectively couple to signal transduction cascades, including Janus kinase 2/ signal transducer and activator of transcription 3 (JAK2/STAT3), mitogen-activated protein kinase (MAPK) and phosphoinositide 3-kinase (PI3K) pathways, and are thus thought to be the only LepRs that mediate the physiological outputs of leptin signaling (Hileman et al., 2002, Fruhbeck, 2006). ObRb is expressed in multiple hypothalamic nuclei critical to energy homeostasis, including the arcuate nucleus of the hypothalamus (ARH), lateral hypothalamus (LH), ventromedial hypothalamus (VMH) and dorsomedial hypothalamus (DMH) (Scott et al., 2009, Minokoshi et al., 1999, Leinninger et al., 2009).

Leptin signaling in the hypothalamus excites anorexigenic neurons and inhibits orexigenic neurons (with the exception of a population of leptin-excited NPY neurons in the DMH (Lee et al., 2013)), eliciting increases in energy expenditure and reductions in food intake (Cowley et al., 2001, Cone, 2005). In doing so an increase in body fat mass will exert negative feedback on the brain, preventing excessive weight gain (Maffei et al., 1995). In obesity, leptin loses its ability to signal in the ARH, and similarly loses its ability to elicit its anorexigenic effects; this is termed leptin resistance (Enriori, 2007). Intracerebroventricular (ICV) administration of leptin to obese animals, although capable of generating acute reductions in food intake and weight loss, is unable to elicit sustained reductions in adiposity (Enriori et al., 2007).

The long form of the LepR, ObRb is structurally associated to JAK2. ObRb activation initiates JAK2 autophosphorylation. pJAK2 then phosphorylates tyrosine (Y) 985, Y1077 and Y1138 on the ObRb. Phosphorylated Y1138 results in the phosphorylation of cytoplasmic STAT3, which then translocates to the nucleus to regulate transcription. Y985 phosphorylation stimulates the MAPK pathway via SHP2. PI3K signaling is also stimulated via JAK2-mediated phosphorylation of IRS2. Leptin also activates the PI3K pathway activation, affecting neuronal electrical activity through ion channel regulation. For example PIP_3 activates ATP-sensitive potassium (K_{ATP}) channels in neuropeptide Y/agouti-related peptide (NPY/AgRP) neurons whilst PI3K stimulated phospholipase-C (PLC) activates transient receptor potential channels (TRPC) in proopiomelanocortin/ cocaine and amphetamine - regulated transcript (POMC/CART) neurons (Niswender and Schwartz, 2003, Qiu et al., 2010).

The etiology of the leptin resistance that develops in obesity is two-fold, 1: BBB leptin trafficking becomes saturated in obesity resulting in low central leptin concentrations relative to plasma levels (Banks, 1996). 2: Central desensitization to leptin; proposed mechanisms underlying central leptin resistance include the inhibition of leptin signal transduction by the protein tyrosine phosphatases protein tyrosine phosphatase 1B (PTP1B) and T-cell protein tyrosine phosphatase (TCPTP), expressed in hypothalamic neurons (Zhang et al., 2015). PTP1B attenuates leptin signaling by dephosphorylating Y1007 and Y1008 in the JAK2 activation loop of the ObRb (Bence et al., 2006). PTP1B knock out in neurons and glia generates diet-induced obese (DIO)-resistant mice, with increased central leptin sensitivity and elevated energy expenditure (Bence et al., 2006). TCPTP inhibits leptin signaling via dephosphorylating nuclear pSTAT3, curtailing its

ability to regulate gene expression. Knockout of neuronal TCPTP elevates POMC and reduces AgRP mRNA expression (Loh et al., 2011). SOCS3 also negatively regulates leptin signaling by dephosphorylating JAK2, reducing STAT, MAPK and PI3K signal transduction (Bjorbaek et al., 1999). Mice lacking neuronal SOCS3 are DIO resistant (Kievit et al., 2006).

In the arcuate nucleus of the hypothalamus (ARH), both NPY/AgRP and POMC/CART neurons express leptin receptors (Spanswick et al., 1997, Cowley et al., 2001). Orexigenic NPY/AgRP neurons are hyperpolarized by increased extracellular leptin via the activation of K_{ATP} channels (Spanswick et al., 1997). Anorexigenic POMC/CART neurons are depolarized by leptin through two mechanisms; (a) direct excitation via the activation of a non-selective cation channel (NSCC) and (b) POMC/CART neuron disinhibition via NPY/AgRP neuron hyperpolarization and reduction of GABAergic transmission (Cowley et al., 2001, Qiu et al., 2010).

Leptin elicits much of its physiological effects through the regulation of sympathetic output, in part through the melanocortin system; increasing brown adipose tissue (BAT) thermogenesis, blood pressure (BP) and heart rate (HR) (Enriori et al., 2007, Simonds et al., 2014). Melanocortin agonists increase BP and HR in both lean and HFD mice whilst antagonists decrease BP (Enriori et al., 2007, da Silva et al., 2006, da Silva et al., 2004). However some leptin-mediated sympathetic nerve activity (SNA) would appear to be melanocortin-independent as BAT temperature elevations are still observed in obese MC4 KO mice (Enriori et al., 2011).

Leptin resistance develops in the ARH of obese mammals, however LepR-expressing neurons in other hypothalamic nuclei remain leptin-sensitive (Enriori

et al., 2011, Rezai-Zadeh et al., 2014). Local injection of leptin into the VMH and DMH elevates blood pressure and heart rate *in vivo*. DMH neurons project to the paraventricular nucleus of the hypothalamus (PVH), raphe pallidus nucleus (RPa) and rostral ventrolateral medulla (RVLM), all premotor nuclei, directly regulating sympathetic tone (Cao and Morrison, 2003, Horiuchi et al., 2004). DMH-RPa efferents regulate leptin-induced BAT thermogenesis (Zhang et al., 2011). DMH-RVLM efferents regulate BP (Horiuchi et al., 2006). To date, a thorough characterization of the molecular, pharmacological and electrophysiological profile of LepR-expressing DMH neurons has not been performed. The DMH is known to be a critical hypothalamic nucleus, regulating physiological processes including stress, circadian rhythm, food intake, energy expenditure and cardiovascular function (Bernardis, 1972, Coolen et al., 1996, Gallo, 1981, Inglefield et al., 1994, Keim and Shekhar, 1996, Bellinger et al., 1976, Enriori et al., 2011).

The aims of this study are to use the visualized whole-cell patch clamp technique to characterize the electrophysiological properties of leptin receptor-expressing neurons in the DMH of a transgenic LepR-YFP mouse. I aimed to determine the electrophysiological effects of leptin and the mechanism(s) by which leptin affects the electrical activity of this neuronal population.

6.2 Results

6.2.1 Leptin-induced depolarization of LepR-expressing neurons in the DMH

Whole-cell recordings were obtained from 34 DMH neurons expressing LepR. Application of 100 nM leptin induced membrane depolarization and/or an

increase in spontaneous action potential firing rate in 38.2% of recorded neurons (n=13, see figure 6.1A), membrane hyperpolarization in 14.7% of recorded neurons (n=5; see figure 6.4A) and the remaining 47.1% (n=16) of neurons did not respond to bath application of 100 nM leptin.

Leptin induced a mean peak amplitude depolarization of 4.9 ± 1.0 mV from a mean resting potential of −49.9 ± 3.1 mV to a new steady-state membrane potential of −45.0 ± 2.7 mV ($p = 0.0004$). Leptin-induced excitation was associated with an increase in firing rate from a mean control basal level of 0.48 ± 0.28 Hz to 0.64 ± 0.34 Hz in the presence of leptin ($n = 5$), effects that were at least in part reversible after washout of leptin ($p = 0.59$). In two neurons, leptin induced sub- and suprathreshold oscillations in membrane potential (Figure 6.2). Voltage-current relations, generated in response to a range of depolarizing and hyperpolarizing rectangular-wave current pulses (−150 to +100 pA, 1,000 ms duration) revealed that leptin-induced excitation was principally associated with a trend for a decrease ($p = 0.86$) in neuronal input resistance from 841 ± 111 MΩ in the absence to 743 ± 138 MΩ in the presence of leptin. Plots of the voltage-current relations revealed extrapolated reversal potentials for leptin-induced excitation around −35 mV (Figure 6.1E). Taken together, these data suggest that leptin-induced excitation is mediated via activation of a non-selective cation conductance. In addition to these effects on membrane input conductance, leptin also induced modulation of intrinsic subthreshold active conductance in a subpopulation of DMH neurons. In DMH neurons, membrane depolarization from negative holding potentials (< −65 mV) or rebound depolarization at the offset of the membrane response to hyperpolarization from potentials close to resting potential (−45 to −50 mV) evoked a transient depolarizing potential consistent with activation of a

low-threshold T-type calcium conductance. In the presence of leptin, this potential was prolonged (Figures 6.1B, C and D), the half-time to decay increasing from 132 ± 59 ms in the absence to 179 ± 61 ms in the presence of leptin. These data are consistent with leptin modulating intrinsic active conductances in a subpopulation of DMH neurons.

In addition to these postsynaptic effects, leptin induced an increase in spontaneous excitatory postsynaptic potentials (EPSPs) in a subpopulation (n = 2) of DMH neurons (Figure 6.3). The mean frequency of spontaneous EPSPs increased from 0.07 ± 0.02 Hz to 0.31 ± 0.11 Hz in the presence of leptin. These EPSPs could be of sufficient magnitude to reach threshold for firing, suggesting that indirect presynaptic effects of leptin on DMH neurons can contribute to leptin-induced increases in neuronal excitability.

6.2.2 Leptin-induced hyperpolarization of DMH LepR-expressing neurons

Application of 100 nM leptin induced membrane hyperpolarization (Figure 6.4A) and/or a decrease in spontaneous action potential firing rate in 14.7% of recorded neurons (n=5). Leptin induced a mean peak amplitude hyperpolarization of -15.5 ± 2.3 mV from a mean resting potential of −46.4 ± 3.0 mV to a new steady-state membrane potential of −61.9 ± 3.3 mV (p = 0.0009). Leptin-induced inhibition was associated with a decrease and abolition of spontaneous firing rate from a mean control basal level of 0.30 ± 0.30 Hz to 0.00 ± 0.00 Hz in the presence of leptin (n = 5). Voltage-current relations, generated in response to a range of depolarizing and hyperpolarizing rectangular-wave current pulses (−150 to +100 pA, 1,000 ms duration) revealed that leptin-induced inhibition was principally associated with a

significant decrease (p = 0.005) in neuronal input resistance from 962 ± 125 MΩ in the absence to 421 ± 67 MΩ in the presence of leptin (Figure 6.4B and C). Plots of the voltage-current relations revealed reversal potentials for leptin-induced inhibition around −90 mV (Figure 6.4D). Taken together, these data suggest that leptin-induced inhibition is mediated via activation of a potassium conductance.

6.2.3 Differential active conductance expression in DMN neurons

In experiments described here, voltage-dependent conductance expression was determined during voltage-current relations experiments, whereby a range of hyperpolarizing and depolarizing square-phase current pulses were injected into the neuron of interest, at equal integers. Here, transient outward rectification (I_{TOR}) was observed as a delayed return to rest at the offset of membrane response to negative current injection. Low-threshold t-type calcium conductances (I_T) were observed as transient membrane depolarization from negative holding potentials (< −65 mV) or transient depolarization at the offset of the membrane response to hyperpolarization from potentials close to resting potential (−45 to −50 mV). Instantaneous or anomalous inward rectification ($I_{AN)}$ was observed as voltage-dependent decrease in membrane response and decrease in input resistance to negative current injection at membrane potentials greater than around -75mV. Hyperpolarization-activated non-selective cation conductances (I_H) were observed as a time- and voltage-dependent repolarization of the membrane potential during the membrane response to negative current injection and a rebound excitation at the offset of the response to hyperpolarising current injection (see Fig 6.4). Of the leptin excited neurons 23% (n=3) of neurons expressed I_{TR}, 54% (n=7) expressed

I_T, 8% expressed $I_{AN\ (n=1)}$ and 15% expressed I_H (n=2). Of leptin inhibited neurons 60% expressed I_{TR}, 60% (n=3) expressed I_T, 40% (n=3) expressed I_{AN} and 40% (n=2) expressed I_H. Of non-responsive neurons 50% (n=8) expressed I_{TOR}, 44% (n=7) expressed I_T, 44% (n=7) expressed I_{AN} and 25% (n=4) expressed I_H (Figure 6.5A). No significant difference in active conductance profile was found between leptin-excited, leptin-inhibited and no response groups when analysed with Chi-squared tests.

6.3 Discussion

6.3.1 Leptin-induced excitation of DMH LepR-expressing neurons

Here I show leptin to depolarize a population of LepR-expressing DMH neurons via the activation of a non-selective cation conductance, consistent with previous research examining the mechanism of leptin-induced depolarization of arcuate POMC neurons (Cowley et al., 2001, Qiu et al., 2010).

Increased EPSP frequency in a subset of DMH LepR-expressing neurons indicates the existence of leptin-sensitive excitatory afferent neurons. DMH neurons receive afferent innervation from other CNS areas including the forebrain and brainstem in addition to local inputs from other hypothalamic nuclei including the ARH and PVH and probably other DMH neurons themselves (Chou et al., 2003, Bagnol et al., 1999, Thompson and Swanson, 1998). Consistency of leptin-induced EPSP rise time kinetics in these experiments may indicate but does not confirm that elevated EPSP frequency is due to the activation of spatially restricted input and most likely from a common source or origin. Further work is required to

identify the source of these inputs and whether leptin effects are mediated at the level of the presynaptic terminal or elsewhere in the presynaptic network. The neuroanatomical location of this leptin-excited/disinhibited afferent neuron could be within the DMH and may be indicative of reciprocal connectivity between LepR neurons of the DMH. Cholera toxin B (CTB) retrograde tracing studies would be a valuable tool to investigate the molecular identity of afferent neurons in this network (Llewellyn-Smith et al., 1990).

In a subpopulation of leptin-excited neurons, oscillatory membrane activity was induced and was associated with the modulation of a low threshold t-type calcium conductance. T-type calcium conductances have been described as necessary for pacemaker-like activity in other hypothalamic neurons (van den Top et al., 2004). Burst-firing activity patterns have been suggested to mediate increased peptide release relative to tonic firing (Poulain and Wakerley, 1982). Leptin-induced oscillatory activity was associated with a prolonged t-type calcium conductance. Whether this effect was mediated via a direct effect on T-type calcium conductance biophysical properties and properties of activation/inactivation requires clarification. Other possible mechanisms that could account for this are inhibition of calcium-activated potassium conductances, activated by calcium influx via the T-type channels. Subsequent activation of the calcium activated potassium conductance could curtail T-type calcium conductance activity. Thus, leptin-induced inhibition of a calcium-activated potassium conductance could indirectly result in prolonged T-type-mediated activity. Again, further studies are required to clarify this mechanism of action of leptin.

6.3.2 Leptin-induced inhibition of DMH LepR-expressing neurons

Of DMH LepR neurons tested, 14.7% were inhibited by leptin, via the activation of a potassium conductance. This is consistent with the mechanism of NPY/AgRP neuron hyperpolarization by leptin in the ARH and other hypothalamic neurones where leptin inhibits cells via activation of ATP-sensitive potassium channels (Spanswick et al., 1997). However as I did not use sulphonamides in a pharmacological characterization of the specific potassium channels involved, further work is therefore required to determine whether leptin inhibits these neurons via K_{ATP} channels. The physiological function of this population of leptin-inhibited DMH neurons is unclear, but retrograde and anterograde tracing from these neurons or trans-synaptic viral tracing from identified target organs would be worthwhile pursuing to identify the functional significance of these neurons. If cellular mechanisms of leptin resistance differentially affect signal transduction pathways, further work would do well to determine if in obesity, any change occurs in the percentage of leptin-excited-leptin-inhibited and leptin-insensitive DMH LepR neurons.

6.3.3 Response distribution

Ostensibly the physiological effect of activation of leptin-excited neurons in the DMH is the elevation of BAT thermogenesis, BP and HR (Enriori et al., 2011, Simonds et al., 2014). Future work will undoubtedly focus on the signal integration at PVH, RPa and RVLM neurons in order to gain a deeper understanding of the neurocircuitry involved in the regulation of sympathetic output. It would be of interest to determine the physiological significance of leptin-inhibited DMH

neurons; anterograde and trans-synaptic viral-tracing studies would be useful to determine the targets of these neurons. DMH-LepR neurons express the ObRb receptor, which is the only leptin receptor coupled to signal transduction pathways. Whether the lack of electrophysiological responsiveness reported here is representative of leptin-insensitive neurons is yet to be determined. In 47.1% of neurons tested here, the absence of electrophysiological response to leptin does not confirm leptin insensitivity. It may be that the leptin-induced effects are delayed and due to time constraints attached to whole cell recording, we are unable to observe effects. Alternatively in these neurons, leptin-effects could involve STA3-mediated gene expression changes, rather than PI3K signalling that likely underlies both the excitation and inhibitions observed in other hypothalamic neurons (Mesaros et al., 2008, Plum et al., 2006b). As the LepRb-CreYFP mouse model has not yet been demonstrated to express false positive YFP neurons, it would appear more likely that ostensible leptin insensitivity is due to either experimental time constrains or signal transduction with a purely transcriptional endpoint.

6.3.4 Differential active conductance expression

Voltage-sensitive subthreshold active conductances inherent to DMH-LepR neurons included I_{TR}, I_{IH}, I_{IT} and I_{AN}. Voltage-sensitive conductances affect neuronal processing of afferent synaptic inputs as well as regulating membrane potential, action potential firing rate and firing pattern. I_{TR} is observed as a delay in the return to rest immediately following the removal of membrane response to negative current injection. In other neuron populations I_{TR} has been shown to

regulate firing frequency by delaying membrane depolarization and are activated during the afterhyperpolarisation potential (AHP), following an action potential (AP) (Whyment et al., 2011). I_T is observed as a rebound depolarization following the removal of membrane response to negative square-phase current injection or as a transient depolarization following depolarization from a hyperpolarized state. I_{IT} is required for the generation of pacemaker-like activity in other hypothalamic neurons (van den Top et al., 2004). Similarly in this study, cells expressing T-type conductance could be induced to oscillate in the presence of leptin suggesting some DMN neurons can act as conditional pacemakers, conditional on the presence of leptin, and underlie and drive pacemaker-like activity. I_H is observed as a time- and voltage-dependent depolarization following the injection of negative square-phase current. I_H has been shown to be required for rhythmic firing in other neuronal populations and can generate membrane depolarization, following IPSP-mediated membrane hyperpolarization (Maccaferri and McBain, 1996, McCormick and Pape, 1990). I_{AN} is observed as an instantaneous reduction in membrane input resistance following hyperpolarization to potentials more negative than around -75mV. This membrane conductance can contribute to resting neuronal membrane potential and input resistance, for example as exemplified by medium spiny neurons (MSN) in the striatum (Mermelstein et al., 1998). It has also been suggested to function to prevent cells becoming too hyperpolarized and maintain neurons within a functional operational window. The inward rectifier family of potassium channels is an extensive group made up of 7 families and includes the weakly rectifying ATP-sensitive potassium channels and g-protein coupled inwardly rectifying subfamily (Hibino et al., 2010). The effects of many neurotransmitters can be mediated through the modulation of I_{AN} properties.

These include 5-HT, a transmitter important in the regulation of stress, the role of 5-HT in the control of BP and HR at these DMH neurons is worth investigating (Horiuchi et al., 2006, Lambe and Aghajanian, 2001, Chaouloff et al., 1999).

Although not statistically significant when compared to leptin-inhibited or no responders, we observed a distinct profile of subthreshold voltage-sensitive active conductances in leptin excited DMH neurons tested here. Conversely, profiles of conductances expressed in leptin-inhibited and leptin-insensitive neurons were relatively similar. Here we find that the greatest predictor of a leptin-excited neuron is the absence of I_{AN} and I_{TR}. Although I_T conductance modulation was associated with leptin-induced excitation, a similar percentage of both inhibited and insensitive DMH neurons express I_T. Thus, these properties are not predictive of a leptin-excited DMH neuron. However the homogeneity in terms of % I_{TOR} expression between groups may indicate that the majority of DMH LepR neurons are competent for leptin-excitation, and that acute application of leptin is insufficient to generate increases in firing rate. Studies in obese animals should further this work.

Populations of leptin inhibited and non-responsive neurons exhibited a similar profile of active conductances. There was a notably low percentage of leptin-excited neurons expressing I_{TOR} and I_{AN}, indicating that these potassium conductances are not necessarily involved in the excitatory effect of leptin in the DMH, consistent with I/V relationships of these neurons indicating the activation of a non-selective cation conductance as mediating the leptin-induced excitation of these neurons. However, upon inspection of active conductance expression, the absence of I_{TOR} would appear to be the best predictor of leptin excitation, rather

than I_H and I_T conductances. Finally, the extensive differential expression of these active conductances between DMN neurons argues strongly for this population being heterogeneous in electrophysiological properties. Further work combining retrograde labelling from known target areas with electrophysiological, morphological and chemical phenotype profiling is needed to fully understand the functional and topographic significance of this heterogeneity.

6.3.5 Physiological significance of leptin-excited LepR-expressing DMH neurons

My research examining the electrophysiological characteristics of LepR neurons in the mouse DMH has contributed to a publication investigating the physiological significance of leptin-excited DMH neurons in obesity-associated hypertension (Simonds et al., 2014). This work outlines the physiological significance of increased leptin-DMH signalling in obesity. Results generated here describe obesity to be associated with elevated plasma leptin, HR and BP. Increased BP is not observed in in *ob/ob* or *db/db* mice and increased cardiovascular parameters can be reversed with leptin antagonists injected into DMH. Additional evidence is provided by the use of engineered pharmacologically selective chimeric ion channels to hyperpolarize LepR neurons *in vivo,* this being associated with reductions in BP. Conversely the depolarization of these neurons *in* vivo increases BP. Human data supports the hypothesis that leptin increases BP as leptin deficient adults have reduced BP, regardless of extreme obesity.

Future studies should determine the molecular profile of DMH LepR neurons, and investigate the physiological significance of leptin-inhibited and

leptin-insensitive neurons described here. Further study of LepR DMH neurons may uncover potential target for antihypertensive drugs.

6.3.6 Leptin resistance

In obesity, neurons of the ARH develop leptin resistance (Enriori et al., 2007). Work outlined in chapter 3 of this thesis would support the notion of reduced K_{ATP} channel-dependent signalling in high extracellular glucose conditions. Elevated central glucose concentrations, as is the case in obesity and diabetes, leads to an elevated neuronal ATP/ADP ratio and the closure of K_{ATP} channels. In NPY/AgRP and POMC/CART neurons, both leptin and insulin hyperpolarize membrane potential via the activation of K_{ATP} channels (Spanswick et al., 1997). Further work is required to investigate the hypothesis, but elevated central glucose may prevent leptin and insulin signalling via this mechanism. Arcuate POMC/CART neurons are excited by leptin via a TRPC channel (Qiu et al., 2010); this in addition to NPY/AgRP neuron hyperpolarization promotes MC4 release, MC4R agonism, reduced food intake, increased hepatic gluconeogenesis and increased energy expenditure. Perhaps glucose-induced NPY/AgRP neuron K_{ATP} channel closure is sufficiently strong that it prevents channel opening by insulin and/or leptin. In this case increased AgRP-mediated MC4R antagonism would prevent optimal melanocortin agonism and its associated physiological affects. Indeed, DMH LepR neurons do not develop leptin resistance in obesity. Perhaps this is reflective of a non K_{ATP}-dependent mechanism or efferent neuron innervation. Further work is required to test this hypothesis.

Figure 6.1: A subpopulation of DMH LepR-expressing neurons are excited by leptin

A: Samples of a continuous whole-cell recording taken from DMH LepR neuron showing an increase in spontaneous action potential firing rate following bath application of 100 nM leptin.

B: Samples of a continuous whole-cell recording showing superimposed responses to rectangular-wave current injection: the current-voltage relationship of a DMH LepR neuron in control conditions.

C: same neuron as **B** showing the voltage-current relations taken at the peak of leptin-induced excitation.

D: Superimposed current-voltage relations of neuron shown in **A, B** and **C** before and in the presence of leptin. Note the prolonged transient rebound depolarization at the offset of membrane response to negative current injection in the presence of leptin compared to control (in red).

E: Plot of current voltage relations shown in **B** and **C**. Note the decrease in slope of the voltage-current relations in the presence of leptin and extrapolated reversal potential around -30 mV. Taken together these data indicate a decrease in neuronal input resistance and the activation of a non-selective cation conductance.

Figure 6.1

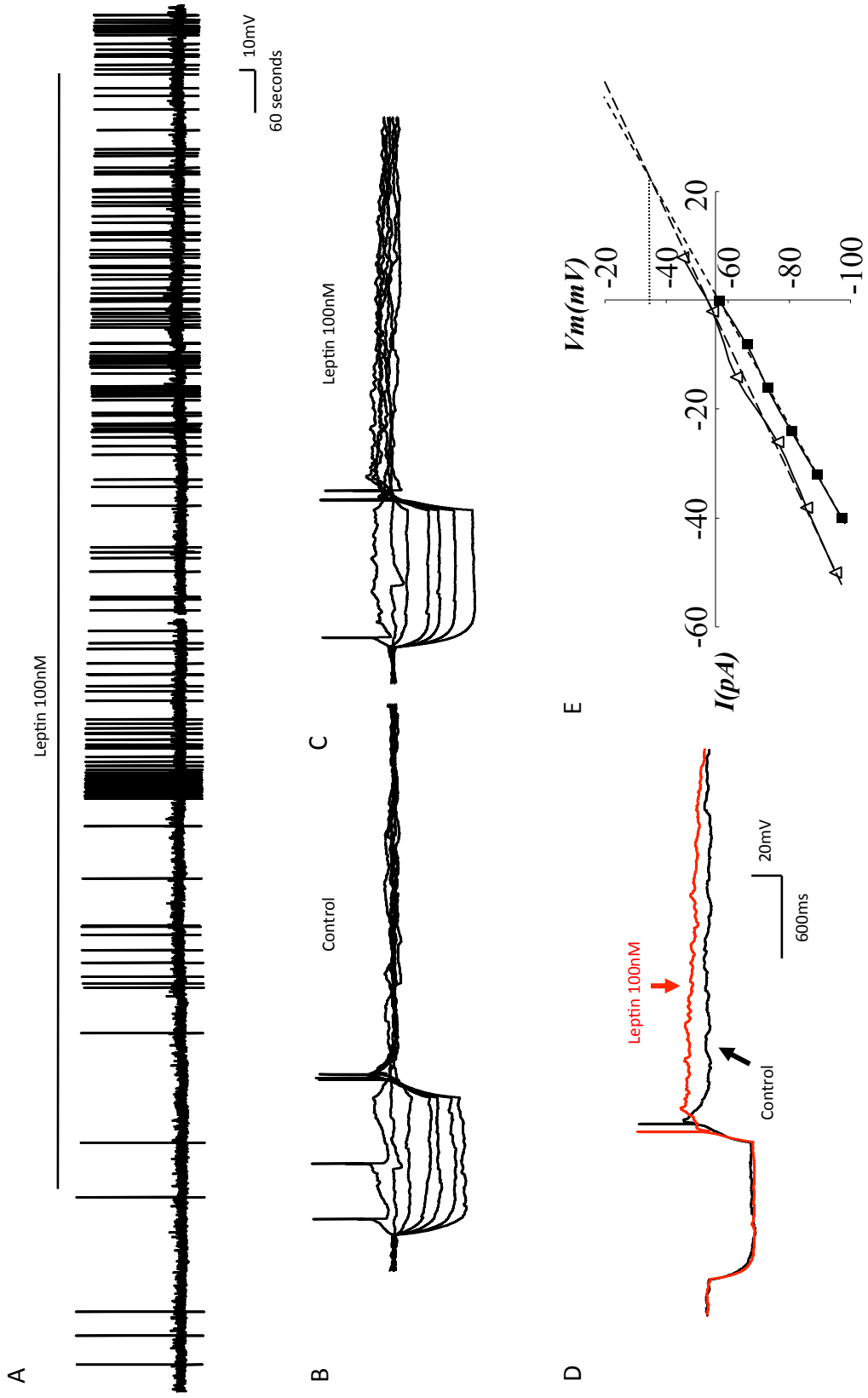
A
Leptin 100nM
10mV
60 seconds
B
Control
C
Leptin 100nM
D
Leptin 100nM
Control
20mV
600ms
E
Vm(mV)
-20
-40
-60
-80
-100
20
-60
-40
-20
I(pA)

Figure 6.2: A subpopulation of DMH LepR-expressing neurons are excited by leptin

A: Samples of a continuous whole-cell current clamp recording taken from a DMH LepR neuron in which membrane potential oscillations were induced by bath application of 100 nM leptin.

B: 1 highlights membrane activity from **A** before leptin application, **2** highlights membrane oscillations on an extended time scale and **3** shown the abolition of membrane oscillations by membrane hyperpolarization.

Figure 6.2

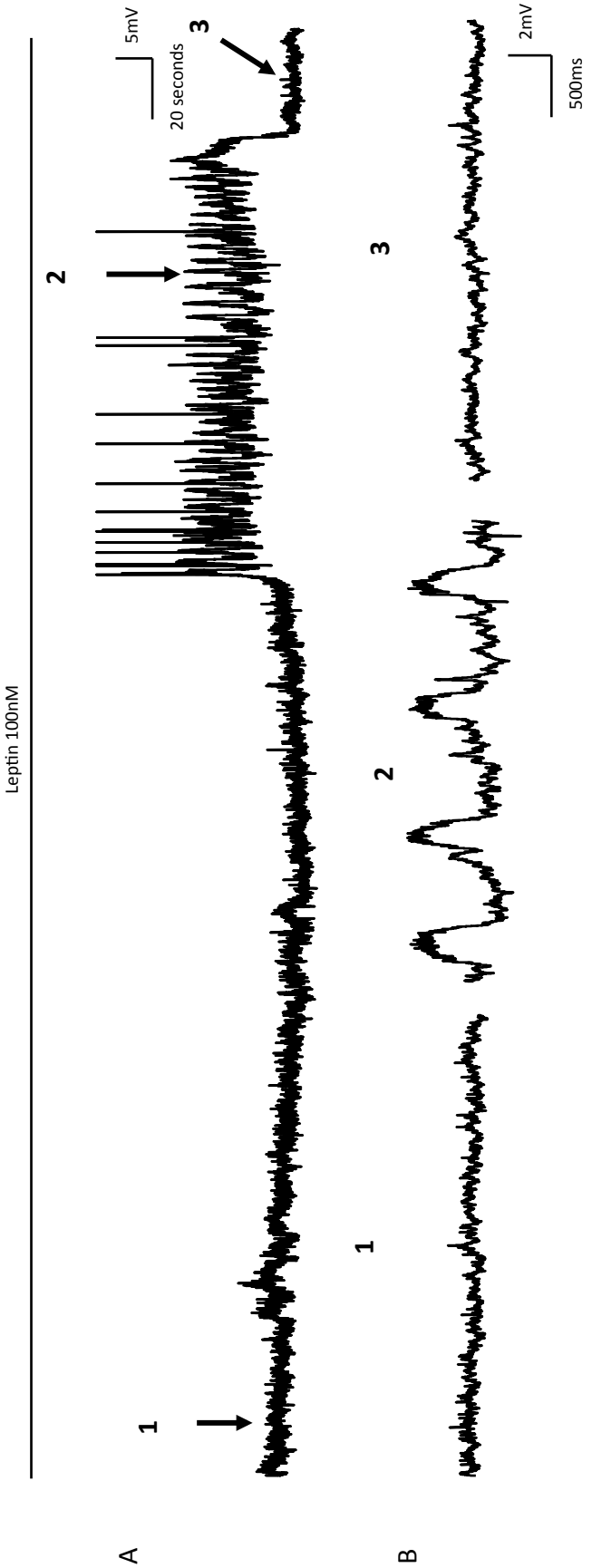

Figure 6.3: Indirect excitation of DMH LepR neurons by leptin

A: Current-camp recording of a DMH LepR neuron showing membrane depolarization and increased frequency of EPSPs in the presence of 100 nM leptin.

B: Extracts of the current clamp recording shown in **A**, before leptin application, on an expanded time base.

C: Extracts of the current clamp recording shown in **A**, in the presence of leptin, shown, on an expanded time base, highlighting the increased frequency of EPSPs. Shown in lower panel are superimposed EPSPs. Note the consistent rise times, indicating a likely single origin of excitatory synaptic potentials.

Figure 6.3

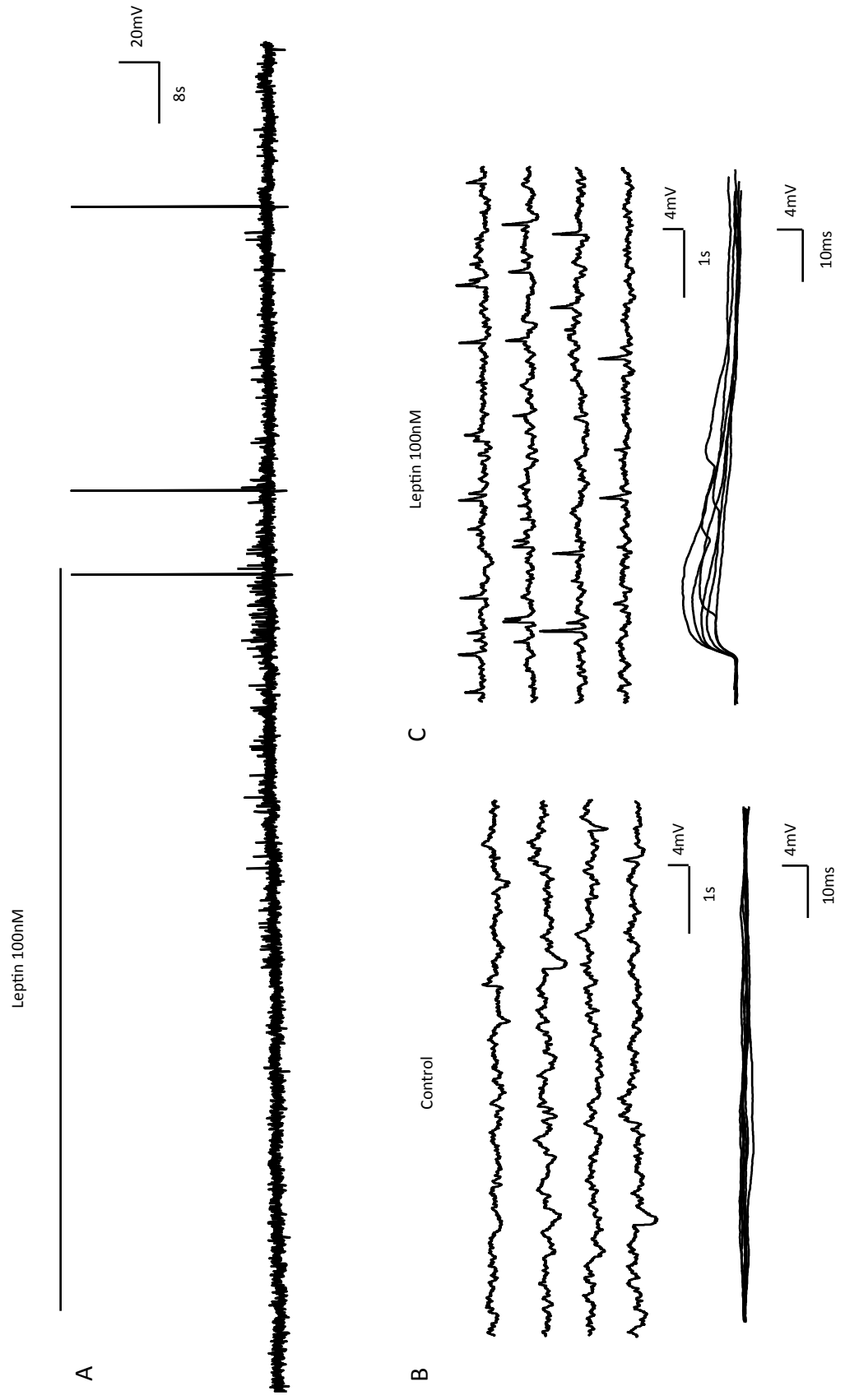
A
Leptin 100nM
20mV
8s
B
Control
4mV
1s
4mV
10ms
C
Leptin 100nM
4mV
1s
4mV
10ms

Figure 6.4: A subpopulation of DMH LepR neurons are inhibited by leptin

A: Samples of a continuous whole-cell current clamp recording of a DMH LepR neuron, showing bath application of leptin induced a membrane hyperpolarization, reversible upon washout of the peptide.

B: Same neuron as **A** showing samples of a continuous whole-cell current clamp recording and superimposed membrane potential responses to rectangular-wave current injection in control, before leptin application.

C: Same neuron as **A** and **B** showing current-voltage relations in the presence of leptin. This data was obtained at the point in the record indicated by ***** in **A**.

D: Plot of current-voltage relations shown in **B** and **C**. Note the decrease in slope of the voltage-current relations in the presence of leptin and reversal potential around -90 mV. Taken together these data indicate a decrease in neuronal input resistance and the activation of a potassium conductance.

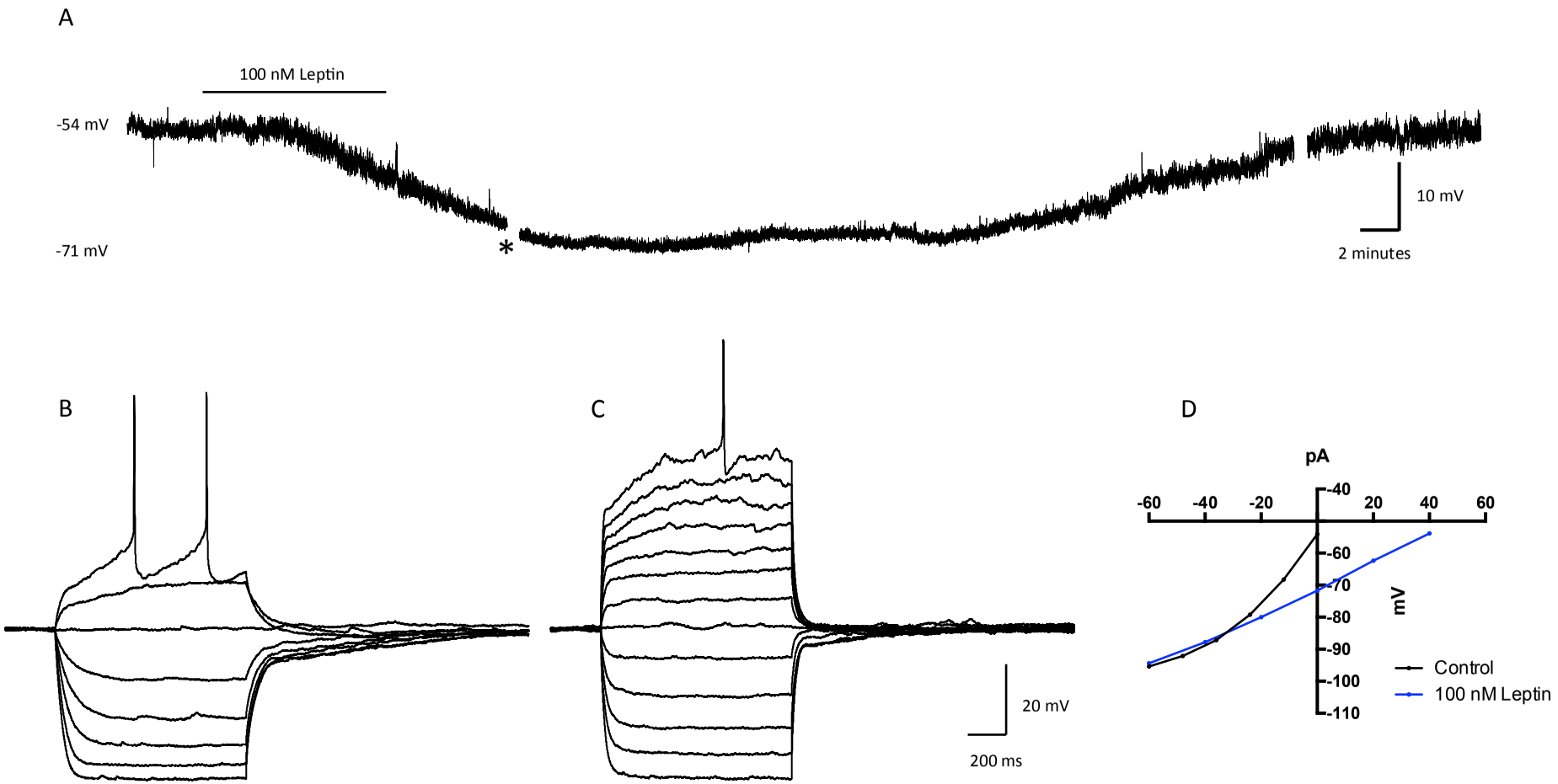
A
100 nM Leptin
-54 mV
-71 mV
*
10 mV
2 minutes
B
C
20 mV
200 ms
D
pA
-60
-40
-20
-40
20
40
60
-60
-70
-80
-90
-100
-110
mV
Control
100 nM Leptin

Figure 6.4

Figure 6.5: Differential expression of subthreshold active conductances in LepR-expressing DMH neurons

A: Samples of a continuous whole-cell current clamp recording of a DMH LepR neuron, ostensibly lacking any subthreshold active conductance expression.

B: Samples of a continuous whole-cell current clamp recording of a DMH LepR neuron, expressing a low threshold T-type calcium conductance (I_T), observed as an overshoot in membrane potential following the offset of membrane hyperpolarization and in response to the highest depolarizing pulse tested here.

C: Samples of a continuous whole-cell current clamp recording of a DMH LepR neuron, expressing a hyperpolarization-activated non-selective cation conductance I_H, observed as a time- and voltage-dependent reduction in neuron input resistance, upon membrane hyperpolarization and a rebound depolarization at the offset of the response to current injection.

D: Samples of a continuous whole-cell current clamp recording of a DMH LepR neuron, expressing transient outward rectification (I_{TOR}), observed as a delayed return to resting membrane potential and action potential firing following the offset of membrane hyperpolarization.

E: Samples of a continuous whole-cell current clamp recording of a DMH LepR neuron, expressing both I_{TOR}, observed here as a delay in reaching threshold of the membrane response to depolarizing current injection from a relatively negative resting potential

F: Samples of a continuous whole-cell current clamp recording of a DMH LepR neuron, expressing instantaneous anomalous inward rectification (I_{AN}) and I_T. I_{AN} is observed as an immediate or instantaneous reduction in neuronal input resistance upon membrane hyperpolarization to negative membrane potentials.

G: Samples of a continuous whole-cell current clamp recording of a DMH LepR neuron, expressing I_{AN} and I_{TOR}.

H: Samples of a continuous whole-cell current clamp recording of a DMH LepR neuron, expressing I_{H} and I_{TOR}.

I: Samples of a continuous whole-cell current clamp recording of a DMH LepR neuron, expressing I_{H} and I_{T}.

J: Samples of a continuous whole-cell current clamp recording of a DMH LepR neuron, expressing I_{AN}, and I_{TOR}.

Figure 6.5

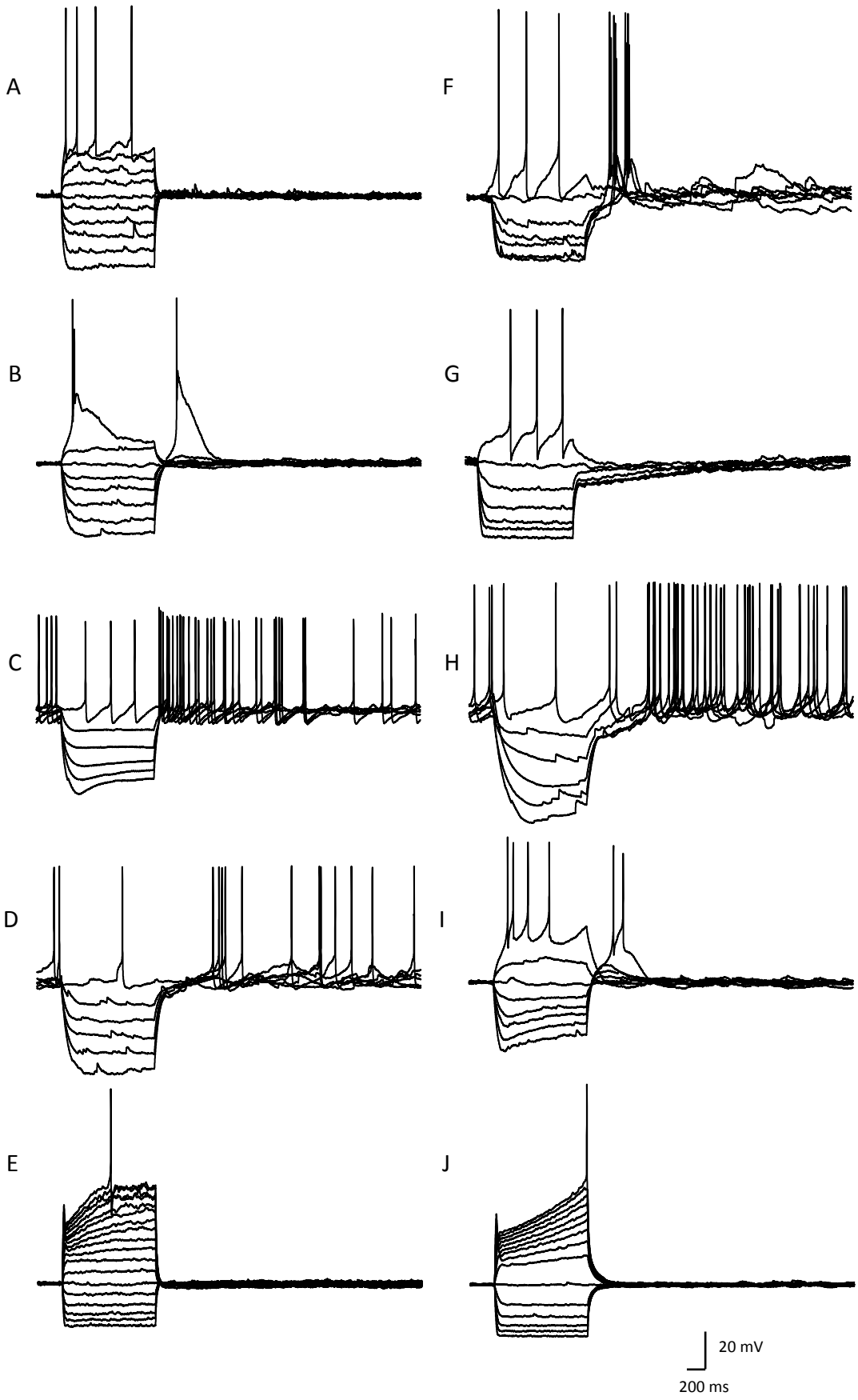

Figure 6.6: Differential subthreshold active and passive properties of DMH LepR neurons and the effects of leptin

A: Pie chart illustrating the response distribution of DMH LepR neurons to bath application of 100 nM leptin. In 47.1% of neurons, bath application of 100 nM leptin does not alter membrane excitability. In 14.7% of neurons, leptin application induced an inhibitory response whilst in 38.2% of DMH LepR neurons bath application of leptin induced membrane excitation (n=34)

B: Bar chart illustrating the differential expression profile of active conductances expressed in leptin-inhibited, leptin-excited and leptin-insensitive DMH LepR neurons.

C: Table summarizing the statistical analysis of data shown in B. *p* values are of Chi-square statistical tests.

Figure 6.6

A

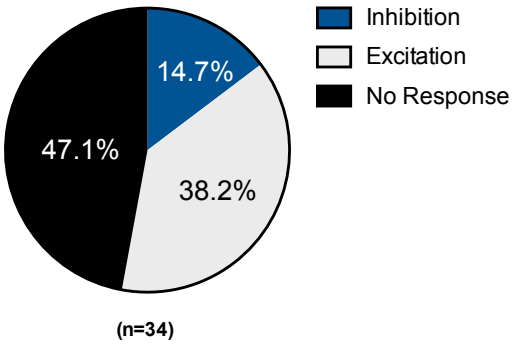

B

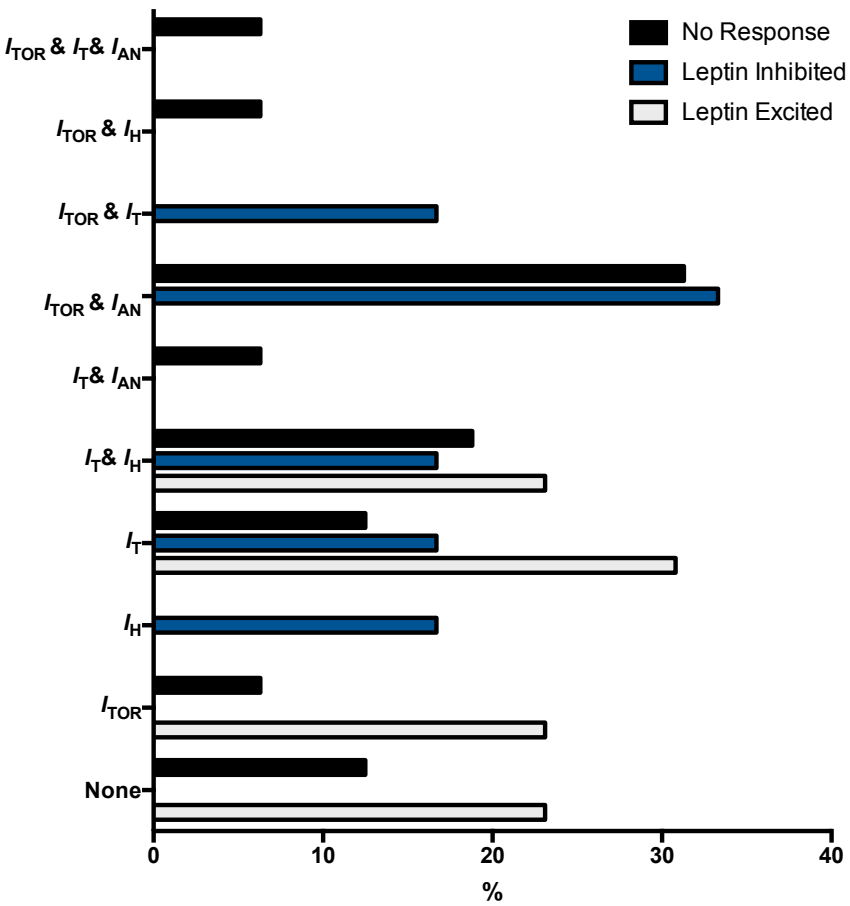

C

Population Comparison	*p*
leptin-Excited Vs. Leptin-Inhibited	0.066
Leptin-Excited Vs. No Response	0.2087
Leptin-inhibited Vs. No Response	0.5692

Chapter 7: Electrophysiological and pharmacological profile of Gonadotropin Inhibitory hormone-expressing neurons of the rat *in vitro*

7.1 Introduction

Reproductive function is critical to the survival of any species. For mammals it is closely controlled by an interacting signaling matrix of hypothalamic, pituitary and gonadal hormones. The hypothalamic pituitary gonadal (HPG) axis consists of multiple negative feedback loops, coordinating the pattern of the estrus (or menstrual) cycle.

Three distinct hypothalamic neuronal populations are key regulators of the reproductive axis; gonadotrophin-releasing hormone (GnRH) neurons, kisspeptin neurons, and gonadotropin-inhibitory hormone (GnIH) neurons. The GnRH neuron is the key stimulator of luteinizing hormone (LH) and follicle-stimulating hormone (FSH) secretion from the pituitary (Amoss et al., 1971, Matsuo et al., 1971, Schally et al., 1971). GnIH and kisspeptin neurons are afferent to GnRH neurons, and exert significant influence over GnRH neuron excitability. Unlike GnRH neurons, both kisspeptin and GnIH neurons express sex steroid receptors (Smith et al., 2006, Soga et al., 2014). A cartoon of the hypothalamic neuronal network, key to reproductive and metabolic function is outlined in figure 7.1.

Kisspeptin neurons express the estrogen receptor ERα and are a conduit through which estrogen excites GnRH neurons and initiates the preovulatory LH surge (Smith et al., 2006, Wintermantel et al., 2006). Kisspeptin neurons of the arcuate nucleus of the hypothalamus (ARH) coexpress neurokinin B and

dynorphin and are termed KNDy neurons (Cheng et al., 2010). In addition to ERα, KNDy neurons express the progesterone receptor (Foradori et al., 2002). Kisspeptin signaling is required for normal sexual development and function (de Roux et al., 2003). Kisspeptin acts centrally, stimulating gonadotroph secretion via actions at GnRH neuron GPR54 receptors, rather than via release into hypophysial portal blood (Messager et al., 2005, Smith et al., 2008, Han et al., 2005, Irwig et al., 2004). Function-specific subpopulations of kisspeptin neurons exist. Not all kisspeptin neurons express ERα and kisspeptin neurons of the Anteroventral periventricular nucleus (AVPV) increase their activity in the preovulatory period whilst the opposite is true for KNDy neurons (Smith, 2009). Ostensibly, some kisspeptin neurons integrate reproductive and metabolic signals, indicated by observations that kisspeptin neurons have reciprocal connections with neuropeptide-Y/agouti-related peptide (NPY/AgRP) and proopiomelanocortin/ cocaine and amphetamine-regulated transcript (POMC/CART) neurons, and are sensitive to the adipokine leptin (Backholer et al., 2010).

GnIH is a hypothalamic peptide that exerts an inhibitory tone on pituitary gonadotroph secretion (Tsutsui et al., 2000). In mammals, two GnIH variants are translated; GnIH-related peptide (RP)-1 and GnIH-RP-3 (Tsutsui et al., 2010). In the rat, GnIH is produced within neurons of the dorsomedial hypothalamus (DMH) and tuberomamillary nucleus (TMN) (Johnson et al., 2007). Extrahypothalamic GnIH neuron projection fibers are found throughout the amygdala, bed nucleus of the stria terminalis (BnST), septal nuclei and the paraventricular thalamic nucleus (PVT) (Johnson et al., 2007). GnIH projections within the hypothalamus include the medial preoptic area (MPOA) and to other neurons within the DMH (Johnson et al., 2007). In the rat 75% of GnIH projections in the MPOA have been shown to co-

localize with GnRH cell bodies whilst in sheep and primates GnIH immunoreactive terminals have been observed in the neurosecretory zone of the median eminence (Clarke et al., 2008, Ubuka et al., 2009a, Ubuka et al., 2009b, Johnson et al., 2007), some of these projection targets are highlighted in figure 7.2.

The lack of interspecies consistency in GnIH neuron projection sites suggests a degree of variation in the specific regulatory mechanisms of gonadotropin secretion. GnIH is the endogenous agonist of the GPR147 receptor, expressed in both the gonads and CNS (Ubuka et al., 2013). In the ovine brain, GPR147 is expressed in the suprachiasmatic nucleus, supraoptic nucleus, periventricular nucleus and the pars tuberalis of the anterior pituitary (Clarke, 2011). In the Siberian hamster over 85% of GnRH-expressing neurons in the POA express GPR147 (Ubuka et al., 2012). In the mouse, application of GnIH-3 has been found to inhibit a subset of GnRH neurons (Ducret et al., 2009). Wu et al. demonstrated the inhibitory mechanism of GnIH at GnRH neurons to be via potassium conductance activation (Wu et al., 2009).

Stress is a known negative regulator of reproductive function and sexual behavior, as such the hypothalamic-pituitary-adrenal (HPA) axis exerts an inhibitory influence upon the HPG axis. Quail GnIH neurons express α2A-adrenoreceptor mRNA and norepinephrine has been demonstrated to increase GnIH secretion *in vitro* (Tobari et al., 2014). Central administration of glucocorticoids suppresses plasma LH whist hypothalamic corticotropin-releasing hormone (CRH) reduces plasma GnRH and LH *in vivo* (Petraglia et al., 1987, Rivier et al., 1986, Dubey and Plant, 1985, Sakakura et al., 1975). CRH receptor-1 (CRH-R1) and the glucocorticoid receptor (GCR) are expressed on 12.8 ± 1.1% and 53.1 ± 11.4% of rat GnIH neurons respectively (Kirby et al., 2009). GnIH mRNA

expression is elevated upon both acute (2.3 ± 0.3 fold) and chronic (1.8 ± 0.1 fold) immobilization stress; an effect that can be prevented by adrenalectomy (Kirby et al., 2009). In rats, genetic knockdown of GnIH can prevent stress-induced reproductive dysfunction, suggesting that these neurons are key regulators of the reproductive axis (Geraghty et al., 2015).

Stress and glucocorticoids are known to regulate the central serotonergic system. 5-HT 1A, 1D, 1F, 2A, 2B, 3A, 5A, 5B, 6 and 7 receptors (but not 2C, 3B or 4) are expressed on all GnIH neurons and the selective serotonin reuptake inhibitor (SSRI) citalopram can cause sexual dysfunction (de Jong et al., 2005, Soga et al., 2010). Citalopram treatment is associated with reduced GnRH and elevated GnIH mRNA expression (Soga et al., 2010, Prasad et al., 2015). These data suggest the central serotonergic system to exert an excitatory effect upon GnIH neurons and an inhibitory tone upon the HPG axis.

The aim of this study was to use the visualized whole-cell patch clamp technique to characterize the electrophysiological properties of GnIH neurons in the GnIH-EGFP rat. Herein I investigate the intrinsic membrane and extrinsic fast synaptic properties of GnIH neurons, and the membrane receptor profile of a number of putative GnIH-regulating neurotransmitters, including noradrenaline, 5-HT, ghrelin and TRH. These studies highlight the importance of mechanisms that regulate the electrical excitability and output of GnIH neurons.

7.2 Results

7.2.1 Electrophysiological profile of GnIH neurons

A total of 32 GnIH neurons within the DMH were recorded from and included in this study. Whole-cell current clamp recordings revealed a mean resting

membrane potential of -39.54 ± 0.74 mV (range: -32.6 to -52.6 mV), a spontaneous firing rate of 0.92 ± 0.19 Hz (range; 0 to 4.2 Hz), input resistance of 1596 ± 122 MΩ (range 691 to 3245 MΩ), with 25% (n=8) of neurons displaying an absence of action potential firing at rest. Of female rats (n=17), whole-cell current clamp recordings revealed a mean resting membrane potential of -40.48 ± 1.05 mV, whilst mean control action potential firing rate was 0.79 ± 0.19 Hz and basal input resistance was 1469 ± 125 MΩ. Of male rats (n=15), whole-cell current clamp recordings revealed a mean resting membrane potential of -38.49 ± 1.00 mV, whilst mean control action potential firing rate was 1.07 ± 0.36 Hz and basal input resistance was 1750 ± 233 MΩ. No significant difference in membrane potential, firing rate or input resistance was observed between male and female rats (p=0.18, 0.49 and 0.25 respectively, (Students unpaired t-test)). The estrus phase of female rats was not determined on the day of culling.

7.2.2 Sub-threshold active conductances

57% (n=18 of 32) of neurons expressed a Cs^+ (500μM) sensitive hyperpolarization-activated non-selective cation conductance (I_H) defined by a delayed depolarizing sag in membrane potential at the peak of large amplitude membrane hyperpolarizations evoked in response to negative current injection (Figure 7.3A).

74% (n=24 of 32) of neurons expressed a Ni^{2+} (1 mM) sensitive rebound depolarization observed at the break of the response to membrane hyperpolarization, this being consistent with the activation of a T-type Ca^{2+} conductance. 91% (n=29 of 32) of neurons expressed a 4-aminopyridimine (1 mM) sensitive transient outwardly rectifying K^+ conductance (I_{TOR}) defined by a delayed

return to resting membrane potential at the break of the response to hyperpolarizing current injection or as a delay in reaching threshold for action potential firing in response to depolarizing current injection from a hyperpolarized resting potential (Figure 7.3C).

7.2.3 Synaptic inputs

Under control conditions, both excitatory and inhibitory postsynaptic events were detectable (n=8 of 8), (Figure 7.4). At rest, spontaneous EPSPs were observed at a frequency of 1.88 ± 0.47 Hz. EPSPs were sensitive to the AMPA receptor antagonist NBQX (5 μM). At rest spontaneous IPSPs were observed at a frequency of 0.19 ± 0.07 Hz and were sensitive to the $GABA_A$ receptor antagonist Bicuculine (20 μM) (Figure 7.4B).

7.2.4 Noradrenaline depolarizes GnIH neurons

Bath application of 40 μM noradrenaline induced membrane depolarization in all GnIH neurons tested (n=5) (Figures 7.5 and 7.6). Noradrenaline induced membrane depolarization from a mean resting potential of -46.90 ± 2.19 mV to a peak membrane potential of -45.84 ± 3.12 mV. Depolarization was associated with an increase in action potential firing rate, from 0.40 ± 0.19 Hz at rest, to a peak rate of 0.68 ± 0.41 Hz in the presence of NA. The NA induced excitation was associated with a reduction in neuronal input resistance from 1230 ± 196 MΩ to 884 ± 244 MΩ. Following washout of NA from the recording chamber, membrane potential, firing rate and input resistance returned to basal levels. The NA-induced excitation persisted in the presence of 1 μM TTX (n=3) indicating a direct effect on the postsynaptic membrane (Figure 7.5B). I/V relationships plotted for this group

revealed an extrapolated reversal potential around 0 mV indicating that the activation of a non-selective cation conductance most likely underpins this response to NA (Figure 7.6).

7.2.5 5-HT induced effects on GnIH neurons

7.2.5.1 Inhibition

15.8 % (n=3 of 19) of neurons were inhibited upon bath application of 50 μM 5-HT, observed as a hyperpolarization of the membrane potential from a mean control of -48.08 ± 8.67 mV to peak inhibition of -55.27 ± 8.00 mV (p=0.032). This effect persisted in the presence of 1 μM TTX (n=3) and was associated with a reduction in input resistance from a basal level of 1213 ± 270 MΩ to a peak of 1021 ± 124 MΩ (p=0.415). Current-voltage relationships plotted for this group revealed a reversal potential of around -90 mV indicating the activation of a K^+ conductance (n=3) (Figure 7.7 Biii). Furthermore voltage-current relations in the presence of 5-HT revealed a rectification at negative membrane potentials suggesting 5-HT-induced inhibition at least in part involves the activation of an inwardly rectifying potassium conductance.

7.2.5.2 Excitation

42.1 % (n=8 of 19) of neurons were excited upon bath application of 5-HT (Figure 7.7Ai) Membrane potential depolarized from a baseline of -47.45 ± 1.52 mV to a peak of -41.68 ± 1.73 mV (p=0.001). This was associated with a decrease in input resistance from a baseline of 912 ± 229 MΩ to a peak of 862 ± 209 MΩ (p=0.163). This effect persisted in the presence of TTX (n=8). Current-voltage relationships

indicated that at least two mechanisms were involved in the 5-HT-induced excitation of GnIH neurons. Of the eight 5-HT-induced excitations, five were associated with a reduction in neuronal input resistance and reversal potential around 0 mV. Two excitations were associated with an increase in input resistance and reversal potential around -90 mV. In the one remaining neuron, input resistance in the presence of 5-HT was not determined. These data indicate that 5-HT-induced excitation of GnIH neurons is via at least two mechanisms, the inhibition of a potassium conductances and the activation of one or a cation conductance.

7.2.5.3 Biphasic inhibitory/ excitatory responses

42.1 % (n=8 of 19) of neurons responded to 5-HT with a biphasic response observed as a transient inhibition followed by a delayed depolarization (Figures 7.7 and 7.8Aii). 5-HT initially induced membrane hyperpolarization from a control level of -46.30 ± 1.51 mV to -56.17 ± 3.65 mV (p=0.005), which was followed by depolarization, which peaked at -39.53 ± 1.17 mV (p=0.0001 vs. control). Transient membrane hyperpolarization was associated with a decrease in input resistance from 1665 ± 287 MΩ to 1213 ± 261 MΩ (p=0.16). Subsequent depolarization was associated with reduced input resistance compared to control, peaking at 1027 ± 333 MΩ (p=0.51).

7.2.5.4 Pharmacological characterization of 5-HT-induced responses in GnIH neurons

A combination of the 5-HT1A receptor antagonist (S)-WAY 100135 (100 nM) and the 5-HT1B receptor antagonists SB224289 (10 μM) reduced 5-HT-induced

membrane hyperpolarization by 78% in GnIH neurons. Under control conditions, 5-HT induced a membrane hyperpolarization of -5.24 ± 1.00 mV. Subsequently in the presence of 5-HT1A and 5-HT1B receptor antagonists, 5-HT induced a membrane hyperpolarization of -1.17 ± 1.43 mV (p=0.09) (n=3) (Paired students t-test).

In one neuron, the 5-HT7 receptor antagonist SB-269970 hydrochloride (100nM) reduced 5-HT induced depolarization by 39%. Under control conditions, 5-HT induced a membrane depolarization of 7.75 mV. Subsequently in the presence of the 5HT7 receptor antagonist, 5-HT induced a membrane hyperpolarization of 4.73 mV.

7.2.6 Thyrotropin-releasing hormone excites GnIH neurons

Bath application of 400 nM thyrotropin releasing hormone (TRH) induced an excitation in all neurons tested (n=7) (Figures 7.9 and 7.10) TRH induced membrane depolarization from a resting membrane potential of -48.07 ± 1.95 mV to a peak of -33.43 ± 1.19 mV in the presence of TRH (p=0.0001). Action potential firing was induced in previously silent GnIH neurons reaching a peak firing frequency of 1.52 ± 1.23 Hz (p=0.03). This effect persisted in the presence of TTX (n=3) (Figure 7.9B) and TRH-induced depolarization of the membrane potential was associated with a reduction in input resistance from 1699 ± 338 MΩ to 1053 ± 203 MΩ at peak response (p=0.02). I/V relationships plotted for this group revealed an extrapolated reversal potential around 0 mV, indicating the activation of a non-selective cation conductance most likely underlies this effect of TRH (Figure 7.10).

7.2.7 Ghrelin excites GnIH neurons

Bath application of 100 nM ghrelin induced a membrane excitation in half of GnIH neurons tested (4 of 8). Ghrelin-induced excitation was associated with a membrane potential depolarization from -53.3 ± 3.21 mV to a peak of -46.05 mV (n=4) (p=0.13) (Figure 7.11). This effect was associated with an increase in action potential firing rate from 0.46 ± 0.33 Hz to a peak of 0.62 ± 0.39 Hz (p=0.15) in the presence of ghrelin. Membrane depolarization was associated with an increase in input resistance from a baseline of 2348 ± 1002 MΩ to 3347 ± 1723 MΩ in the presence of ghrelin (p=0.15). I/V relationships plotted for this group revealed a reversal potential of around -90 mV, which under our recording conditions is indicative of ghrelin inducing excitation via the closure of a resting potassium conductance (Figure 7.11B).

7.2.8 β-estradiol and corticosterone

400 nM β-estradiol was bath applied to 5 GnIH neurons, without any ostensible effect on membrane potential, action potential firing frequency or input resistance. The effect of corticosterone (400 nM) upon GnIH neurons was also investigated. Here, bath application of corticosterone to 4 GnIH neurons was without any clear effect on membrane potential, action potential firing frequency or input resistance.

7.3 Discussion

7.3.1 Electrophysiological properties

GnIH neuronal activity and ultimately peptide release can be modulated by intrinsic voltage-dependent membrane properties. Active conductances modulate

the mechanisms by which neurons compute afferent inputs and generate functional outputs partly through regulating the amplitude and time course of post-synaptic currents but also by affecting basic membrane characteristics such as membrane potential, input resistance, action potential firing rate and firing pattern (Zhu et al., 1999). In this context, these parameters ultimately impact GnIH release, GnRH secretion, and the tone of the HPG axis.

91% of GnIH neurons displayed transient outward rectification. Transient potassium conductances (I_{TR}) are a conduit through which neurons delay membrane depolarization, opposing excitation (Whyment et al., 2011). I_{TOR} are voltage-dependent conductances, and become activated during the afterhyperpolarisation potential (AHP) that follows an action potential (AP), delaying membrane depolarization and in doing so regulating action potential firing frequency and firing pattern (Whyment et al., 2011, van den Top et al., 2004). Modulation of this conductance by central and peripheral factors would likely influence neuronal firing rate and GnIH release.

74% of GnIH neurons tested expressed a Ni^{2+}-sensitive low-threshold T-type Ca^{2+} conductance. T-type calcium conductances are observed as a rebound depolarization in response to negative current injection and are required for the generation of pacemaker-like activity in other hypothalamic neuronal populations (van den Top et al., 2004). 57% of GnIH neurons expressed a Cs^{+}-sensitive hyperpolarization-activated conductance (I_h). I_h has been demonstrated to be required for rhythmic firing and pacemaker-like activity in other neuronal populations (Maccaferri and McBain, 1996, McCormick and Pape, 1990). No rhythmic or pacemaker-like firing was observed in the GnIH neurons tested here. However further experiments may clarify endogenous and exogenous factors

capable of generating this activity type, which may be required for significant elevations of GnIH secretion from these neurons.

Active conductance expression was remarkably conserved amongst GnIH neurons tested here. Variations in active conductance expression may be indicative of functional heterogeneity within this population of neurons. No sex differences were observed in terms of active conductance expression in this study. It remains unclear as to whether these conductances are under temporal or steroidal regulation.

7.3.2 Pharmacology

Here we demonstrate that rat DMH GnIH neurons express $GABA_A$ receptors and AMPA glutamate receptors, activated at rest under our recording conditions. The DMH is known to receive afferents from the telencephalon including the ventral subiculum, infralimbic area of the prefrontal cortex, lateral septal nucleus, and bed nuclei of the stria terminalis (Thompson and Swanson, 1998). Brainstem afferents originate in the periaqueductal gray, parabrachial nucleus (PBN), and ventrolateral medulla (Thompson and Swanson, 1998). Intrahypothalamic inputs are received from the suprachiasmatic nucleus (SCN), subparaventricular zone (SPZ), VMH, and both NPY/AgRP and POMC/CART neurons of the ARH (Chou et al., 2003, Bagnol et al., 1999, Thompson and Swanson, 1998). Local DMH glutamate/TRH neurons could be a source of glutamatergic transmission in the rat (Chou et al., 2003). GnIH neuron sensitivity to TRH would suggest this to be likely. DMH neurons are known to receive GABAergic afferents from SCN neurons and NPY/AgRP neurons of the ARH (Kalsbeek et al., 1996, Bellinger et al., 1976, Bagnol et al., 1999). It is evident that there are a multitude of neuronal populations terminating at DMH neurons,

and probably GnIH neurons. Cholera toxin B (CTB) retrograde tracing studies would be a valuable tool to investigate the molecular identity of afferent neurons in this network (Llewellyn-Smith et al., 1990).

7.3.3 Noradrenaline

Here we show that the catecholamine noradrenaline directly excites GnIH neurons via the activation of a non-selective cation conductance, consistent with α_1 adenoreceptor (AR) activation (Ishibashi et al., 2003). α_1 adrenoceptors are expressed in the rat DMH (Day et al., 1997). α-1B receptors are also expressed in rat GnRH neurons (Hosny and Jennes, 1998) and α_1 receptor activation has been shown to increase LH secretion (Gearing and Terasawa, 1991, Heaulme and Dray, 1984). These data indicate a complex integration of noradrenergic signals upstream of gonadotroph secretion. Further work should further clarify the influence of NA and NA receptor subtypes on the electrophysiological activity of these neuronal populations.

Quail GnIH neurons express α2A receptors and are innervated by noradrenergic afferents (Tobari et al., 2014). This is associated with increased noradrenergic innervation of the male quail PVH following the viewing of a female. This mechanism has been proposed to mediate the decrease in plasma T observed in male quail following visualization of a female (Delville et al., 1984, Cornil et al., 2009). It is clear that noradrenergic innervation of GnIH neurons is conserved between species. The DMH is well characterized as a hypothalamic nucleus involved in stress signal integration. In non-mammalian vertebrates both restraint stress and central administration of corticotropin releasing hormone (CRH) and corticosterone have been shown to elevate adrenaline, noradrenaline, dopamine

and 5-HT tissue concentration in the DMH (Lowry et al., 2001). Catecholaminergic excitation of GnIH neurons may represent a central mechanism by which the HPA axis inhibits gonadotroph release (Inglefield et al., 1994, Keim and Shekhar, 1996, Bellinger et al., 1976).

7.3.4 Serotonin

A significant degree of variation was observed in the 5-HT responses of GnIH neurons. 31.6% were inhibited, 26.3% excited and 42.1% biphasic responses. This differential responsiveness may be indicative of functional heterogeneity within the GnIH neuron population, or perhaps 5-HT receptor expression in under temporal control, and the proportion of excitations and inhibitions changes during estrus. The diversity of 5-HT-induced responses observed in these studies is no doubt reflective of the complex profile of 5-HT receptor expression on these neurons. It has previously been demonstrated that all rat GnIH neurons contain mRNA for multiple 5-HT receptor subtypes 1A, 1D, 1F, 2A, 2B, 3A, 5A, 5B, 6 and 7, but not 2C, 3B or 4 (Soga et al., 2010). This complexity of receptor expression may account for the somewhat incomplete pharmacological characterization of responses reported here.

Previous research into the effects of serotonin on the HPG axis has garnered disparate results, with some studies reporting 5-HT to have a stimulatory effect upon gonadotroph, whilst others have observed 5-HT to exert an inhibitory effect upon the release of both GnRH and LH secretion (Chen et al., 1981, Donnelly and Dailey, 1991, Hery et al., 1976, Johnson and Crowley, 1986, Vitale et al., 1985, Fink et al., 1999, Gore and Terasawa, 2001, Arendash and Gallo, 1978, Lynch et al., 1984, Schneider and McCann, 1970).

Whilst Gore *et al* found 5-HT antagonists to inhibit LH secretion, the 5-HT receptor agonist quipazine did not increase LH pulse amplitude but did induce a more erratic LH pulse pattern (Gore and Terasawa, 2001). Perhaps this data, in addition to observations of the plethora of 5-HT receptor subtypes expressed on hypothalamic neurosecretory cells, implies a more intricate regulation of gonadotroph release by 5-HT. Considering serotonergic control of reproductive function as either 'on' or 'off' is presumably too reductive to be helpful.

The differential effect of specific 5-HT receptor agonists and antagonists on gonadotroph secretion *in vivo* (and at different points of estrus) needs to be determined in order for us to better understand the serotonergic control of the HPG axis.

7.3.5 TRH

Here we demonstrate that TRH reliably depolarizes GnIH neurons in the rat via the activation of a non-selective cation conductance. This is consistent with activation of the TRH-receptor TRHR (Gershengorn and Osman, 1996). This receptor is $Gq_{/11}$-coupled, and ligand binding stimulates phosphoinositide-specific phospholipase C, which in turn increases intracellular IP_3, DAG and calcium store mobilization (Aragay et al., 1992, Hsieh and Martin, 1992, Gershengorn and Osman, 1996). Further work to determine the specific TRHR subtype(s) expressed on GnIH neuron membranes is needed to characterize this population.

Previous studies have shown TRH to increase prolactin secretion (Donnelly and Dailey, 1991), and also increase LH and FSH secretion in humans (Lamberts et al., 1987, Snyder et al., 1984, Kwekkeboom et al., 1989). Perhaps TRH excitation of GnIH neurons is indicative of a negative feedback mechanism, regulating the

degree to which TRH stimulates gonadotroph secretion. Further work is needed to clarify this. TRH responsiveness may indicate the existence of a PVN-GnIH synaptic contact, therefore it would be worthwhile for future studies to investigate the effects of other PVH neuropeptides such as corticotropin-releasing hormone (CRH), arginine vasopressin and oxytocin on the electrical activity of GnIH neurons.

7.3.6 Ghrelin

These studies demonstrate that ghrelin excites GnIH neurons through the inhibition of a resting potassium conductance, this being similar to previous reports of a direct effect of ghrelin upon the neuron, via binding to the growth hormone secretagogue receptor (GHSR) and ATP-sensitive potassium (K^{+}_{ATP}) channel inhibition (see chapter 4 of this thesis) (van den Top et al., 2007).

These results suggest a cellular mechanism by which ghrelin inhibits GnRH and LH pulse frequency as described in previous work (Fernandez-Fernandez et al., 2004, Lebrethon et al., 2007). It also provides more evidence that GnIH neurons exist within both reproductive and feeding circuitry in the hypothalamus.

It is well known that the reproductive axis is inhibited during negative energy states (Bronson, 1986, Sisk and Bronson, 1986, Schneider et al., 2013). It would seem unsurprising that a peptide, with increased plasma concentrations during negative energy states would exert a negative effect upon the HPG axis, however perhaps it would be considered more appropriate for long-term signaling hormones such as leptin to affect GnIH neuron electrical activity. However leptin did not result in membrane depolarization in neurons tested here despite the high concentration of LepR in the DMH (Elmquist et al., 1998).

Reports indicate that GnIH has an orexigenic effect *in vivo* with ICV GnIH stimulating food intake in rats and chicks (Johnson et al., 2007, Tachibana et al., 2005). GnIH has been shown to inhibit POMC neurons via the activation of a potassium conductance (Fu and van den Pol, 2010). GnIH terminals are in close apposition to ARH NPY/AgRP neurons, although there is not yet any direct electrophysiological evidence demonstrating NPY neuron excitation, ICV GnIH does increase arcuate NPY mRNA expression (McConn et al., 2014, Jacobi et al., 2013). If the endpoint of ghrelin signaling in these neurons is K_{ATP} channels, it may be that the electrical excitability of the GnIH neuron is directly coupled to the metabolic state of the organism, introducing another mechanism by which the HPG axis is modulated by central homeostatic factors.

This study looked into the effects of both estradiol and corticosterone on GnIH neurons activity, with no ostensible effects observed. However this result may be more indicative of time restrictions whist performing whole-cell recordings. Perhaps steroids regulate GnIH neuronal excitability over durations in excess of those we were able to study here. Additionally these steroids are cyclical and phasic in their expression levels, as are their receptors. These factors were not accounted for in these experiments however they warrant investigation. Nevertheless the absence of any clear corticosterone or estrogen indicates that these hormones do not regulate electrical excitability directly and more likely change the functional operation and sensitivity of the GnIH circuit through changes in gene expression and protein synthesis in the longer term.

7.3.7 Conclusions

These studies demonstrate the basal electrophysiological profile of rat GnIH neurons, the pharmacology of afferent synaptic connections within the hypothalamic circuit and reveal the manner by which they respond to a number of neurotransmitters and hormones allowing us to further contextualize the GnIH neuron within the HPG axis. From the data presented here, GnIH neurons would appear to integrate multiple signals including stress and metabolic secretagogues. Observations that central factors known to stimulate GnRH and LH secretion *in vivo* also excite GnIH neurons suggests a highly complex central regulation of gonadotroph secretion, that should be investigated further. It must be noted that a significant caveat of this work is that the estrus phase of female rats was not determined on the day of culling and until this sort of work is performed we are unable to associate electrophysiological characteristics to specific female reproductive functions.

Figure 7.1: Functional organization of the hypothalamic reproductive circuit

Both GnIH and kisspeptin neuron project to GnRH neurons; kisspeptin neurons send additional projections to arcuate NPY and POMC neurons. This connectivity is likely indicative of a neuronal circuit, linking metabolic energy status to reproductive function. Adapted from (Fu and van den Pol, 2010).

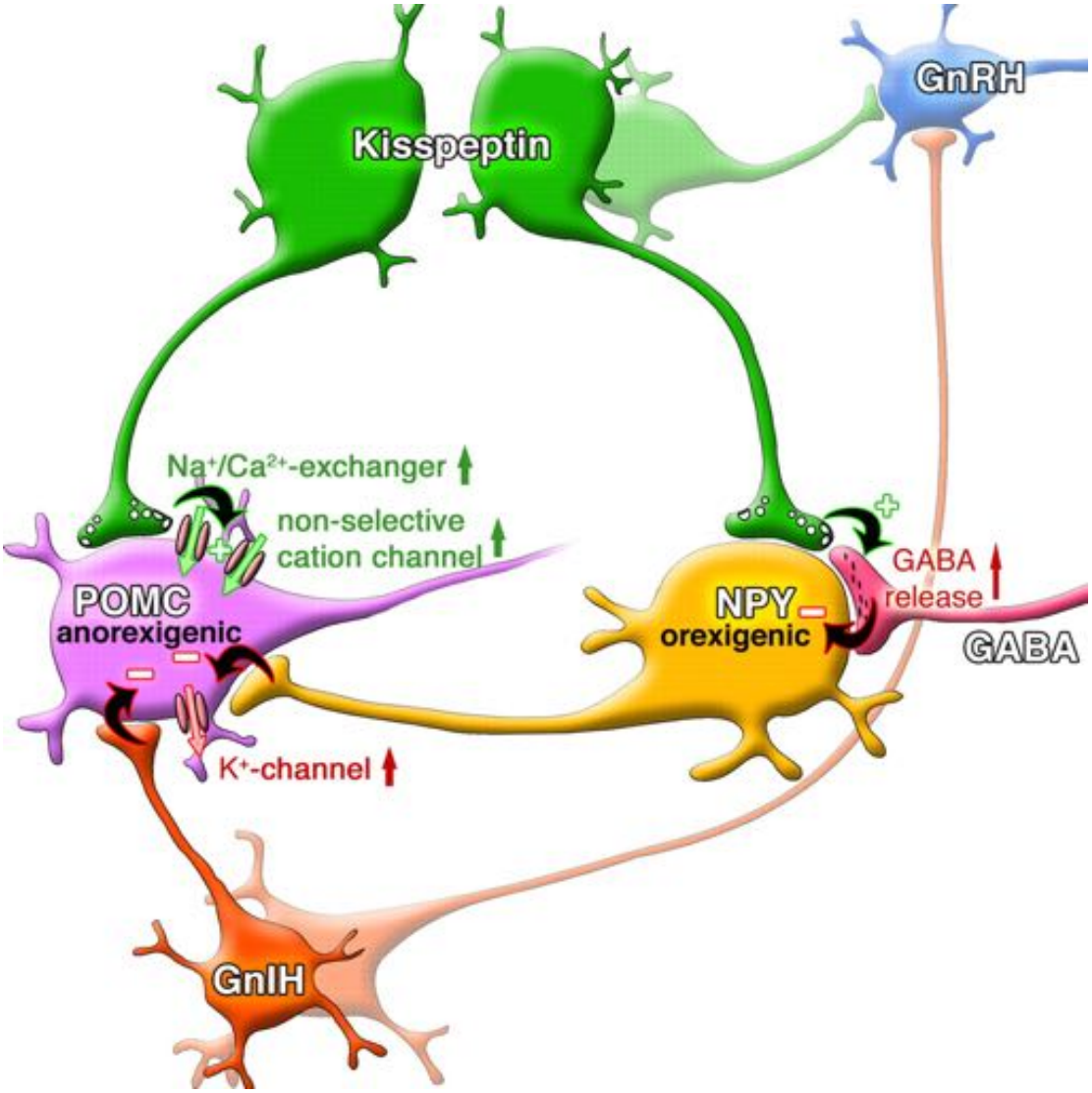
Kisspeptin
GnRH
Na+/Ca2+-exchanger
non-selective
cation channel
POMC
anorexigenic
NPY
orexigenic
GABA
release
GABA
K+-channel
GnIH

Figure 7.2: GnIH neuron projection sites from the rat dorsomedial hypothalamus

Sagittal section of an adult mouse brain with DMH GnIH neuron projection sites highlighted; these include the amygdala, PVT, BnST and MPOA.

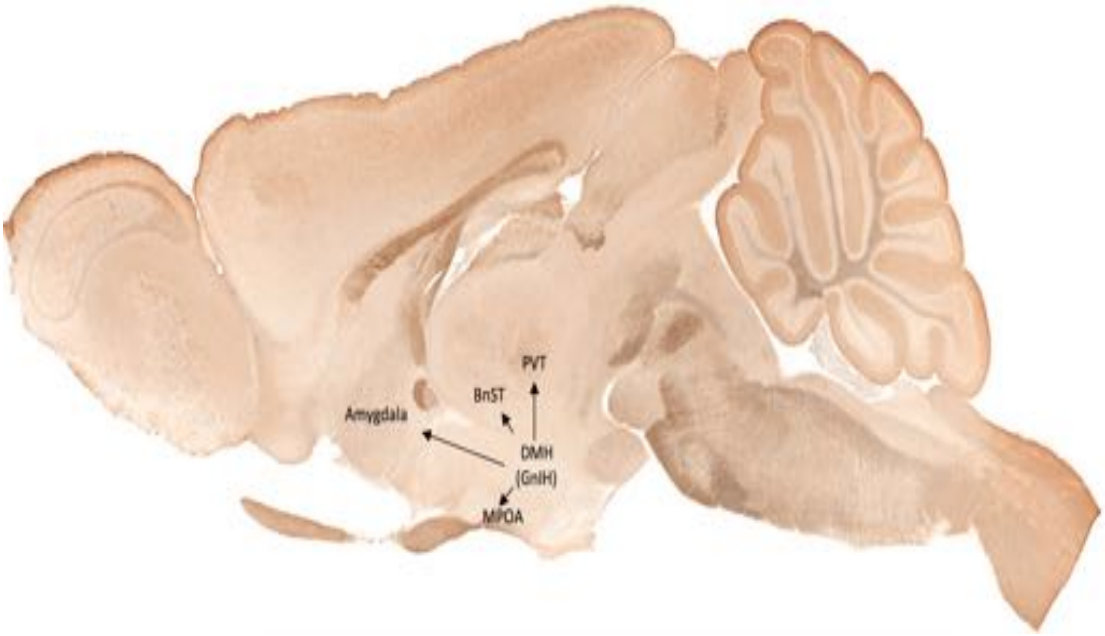
PVT
BnST
Amygdala
DMH
(GnIH)
MPOA

Figure 7.3: Characteristic electrophysiological properties of GnIH neurons

A: Representative current-voltage relationship of a GnIH neuron recorded in current-clamp mode. Here, superimposed sweeps show membrane potential deflections in response to the injection of square-wave current steps of decreasing magnitude and constant integer. A hyperpolarization-activated cation conductance (I_H) is expressed by this neuron. I_H is observed as a depolarizing sag in the larger amplitude hyperpolarizing responses to negative current injection.

B: The current-voltage relationship of the same cell as shown in **Ai**, in the presence of CsCl (500μM), which blocked I_H. Note the linear relationship in the membrane response to hyperpolarizing current steps, in the presence of CsCl.

C: The current-voltage relationship of a GnIH neuron that was characterized by a transient-outward rectifying conductance (I_{TR}). In this instance I_{TR} was activated in response to depolarizing current pulses from a negative resting membrane potential, and is seen as a delay in the neuron membrane potential reaching threshold for firing. This conductance was sensitive to 4-AP (1mM) (data not shown).

Figure 7.3

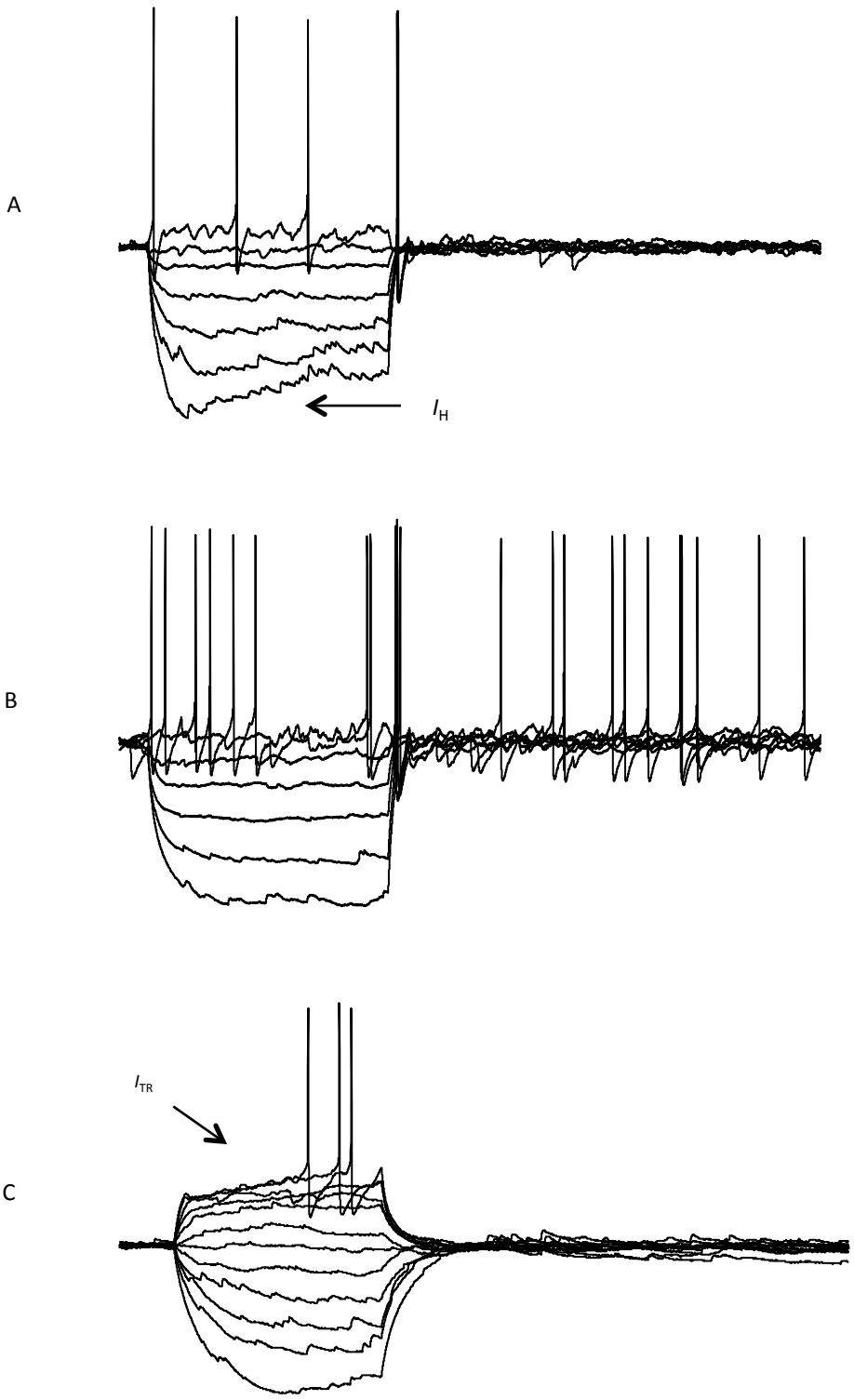

Figure 7.4: Synaptic properties of GnIH neurons

A: Representative voltage clamp recording from a GnIH neuron, with membrane potential 'clamped' at -60 mV. Upward deflections from the trace are inhibitory postsynaptic currents (IPSCs) and downward deflections are excitatory postsynaptic currents (EPSCs).

B: Voltage clamp recording from the same neuron as in **Bi** after bath application of NBQX and bicuculine, blocking AMPA and $GABA_A$ membrane currents respectively. Note the total abolition of synaptic currents.

C: Superimposed EPSPs from **Bi**. Note the similar rise-times of the post-synaptic currents, suggesting a common spatial origin of these inputs.

D: Superimposed EPSPs from a GnIH neuron voltage clamp recording. Note the similar rise-times of the post-synaptic currents, suggesting a common spatial origin of these inputs.

Figure 7.4

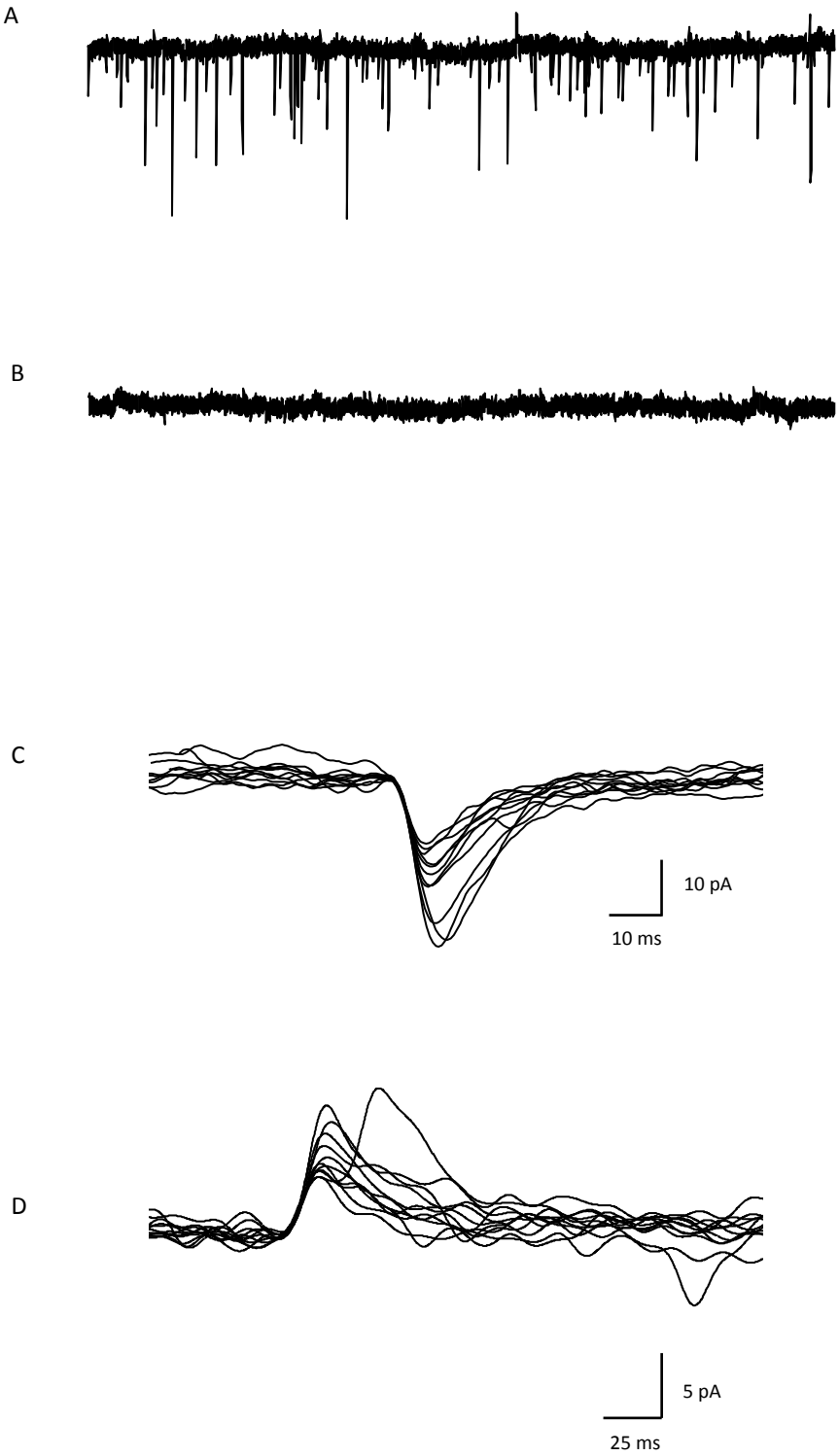

Figure 7.5: Noradrenaline excites GnIH neurons via a direct postsynaptic mechanism of action

A: Current-clamp recording from a GnIH neuron. Bath application of 40 μM noradrenaline (NA) induced a membrane depolarization that was sufficient to reach threshold for action potential firing, an effect that was reversible upon washout of NA.

B: Noradrenaline-induced excitation persisted in the presence of 1 μM TTX, the latter applied to eliminate activity dependent synaptic inputs and potential indirect effects of NA. This data suggests a direct postsynaptic site and mechanism of action.

Figure 7.5

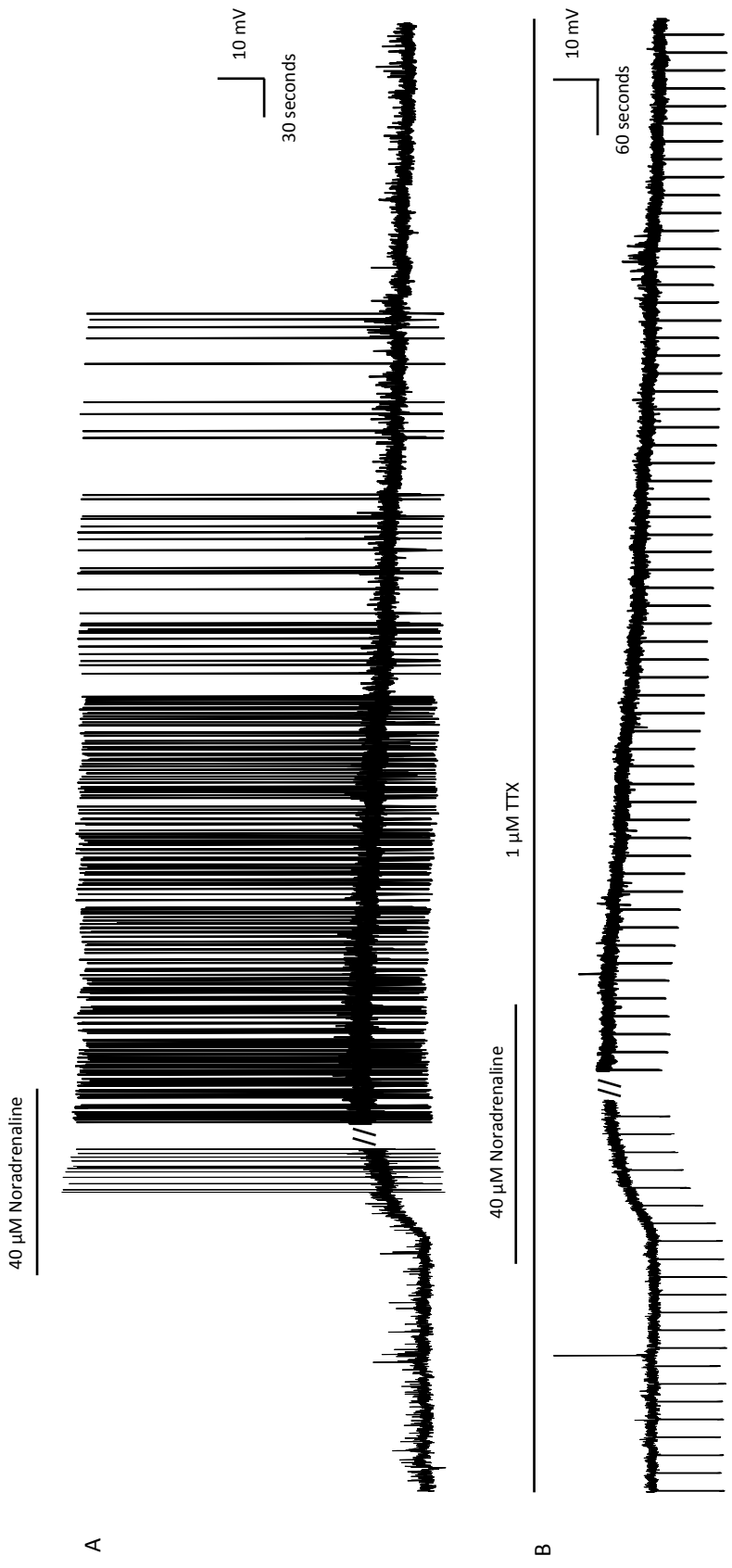
10 mV
30 seconds
40 µM Noradrenaline
A
10 mV
60 seconds
1 µM TTX
40 µM Noradrenaline
B

Figure 7.6: Direct excitation of GnIH neurons by noradrenaline.

A: Samples of a continuous record showing superimposed current clamp recordings of the current-voltage relations of a GnIH neuron in control conditions.

B: Superimposed current clamp recording showing the current-voltage relationship of the same neuron as in **A** during the peak response to NA.

C: Plots of the current-voltage relationships shown in **A** and **B**. Note the reduced slope of the membrane potential response to current injection in the presence of noradrenaline. Also note the extrapolated reversal potential around 0 mV, indicating GnIH neuron NA-induced depolarization to be via the activation of a non-selective cation conductance, and a reduction in neuronal input resistance.

Figure 7.6

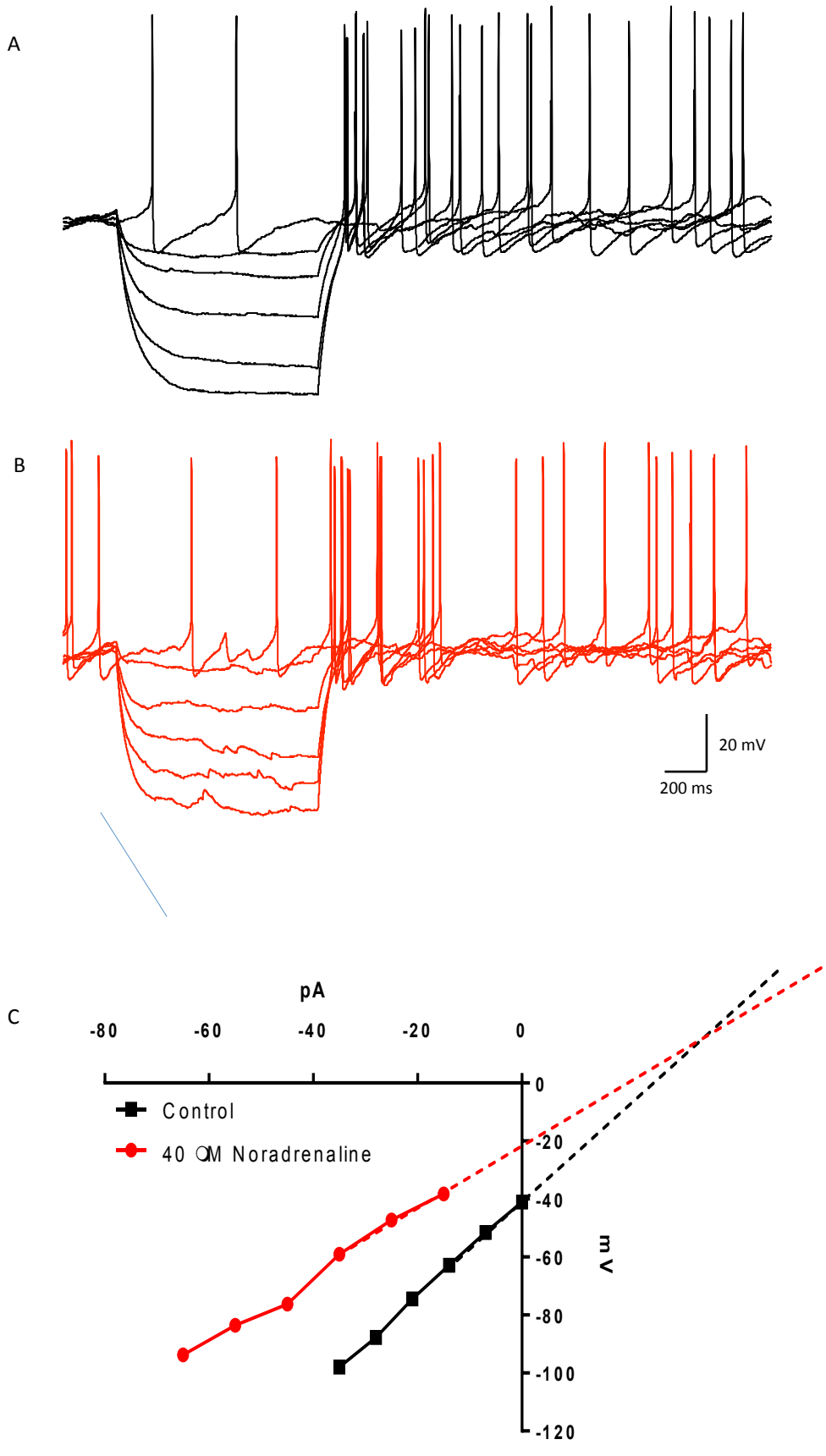
A
B
20 mV
200 ms
C
pA
-80
-60
-40
-20
0
Control
40 OM Noradrenaline
0
-20
-40
-60
-80
-100
-120
mV

Figure 7.7: Differential effects of 5-HT on GnIH neurons

Ai: Current clamp recording of a GnIH neuron. Bath application of 50 μM 5-HT induced a biphasic response, with an initial transient membrane potential hyperpolarisation followed by a membrane depolarisation, associated with an increase in action potential firing rate. These effects were reversed upon washout of 5-HT.

Aii: The same neuron as that shown in **Ai,** in the presence of 1μM TTX to block activity-dependent transmission and indirect effects of 5-HT. Bath application of 50 μM 5-HT induced a primarily inhibitory response with the excitatory response observed previously in this cell, significantly diminished.

Bi: Superimposed current clamp recording showing the current-voltage relationship of a GnIH neuron in control conditions.

Bii: Superimposed current clamp recording showing the current-voltage relationship of same GnIH neuron shown in **Bi,** recorded at the peak of 5-HT-induced inhibition.

Biii: The plots of current-voltage relationships shown in **Bi** and **Bii.** Note the reduced slope of the membrane response to current injection in the presence of 5-HT and the distinct non-linear deviation (rectification) at more negative membrane potentials. Also note the reduction in neuronal input resistance and reversal potential around -90 mV. Taken together these data indicate that 5-HT-induced GnIH neuron hyperpolarization is via the activation of a potassium conductance, most likely involving an inwardly rectifying potassium conductance

Figure 7.7

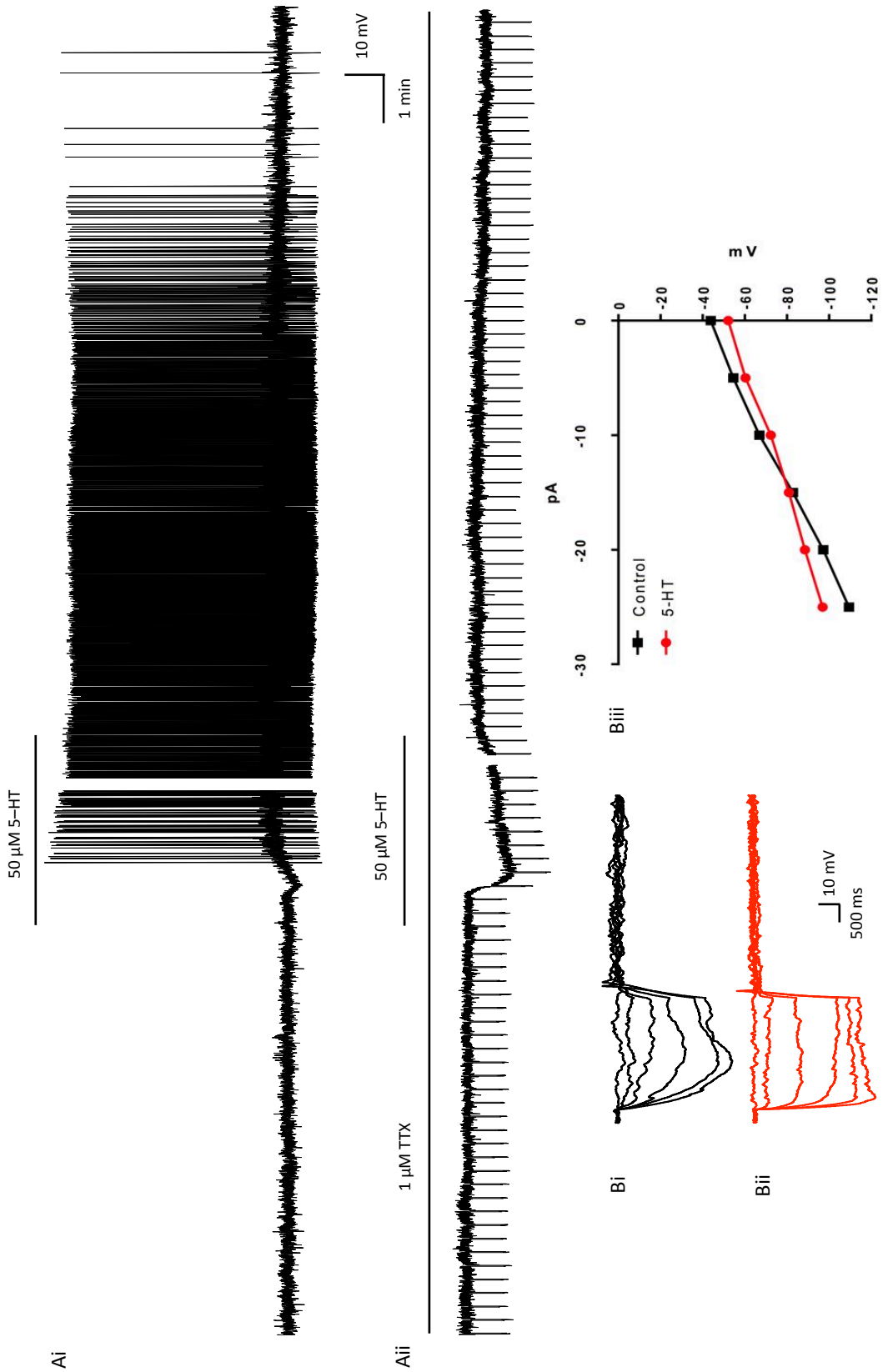
Ai
50 µM 5–HT
10 mV
1 min
Aii
1 µM TTX
50 µM 5–HT
Bi
Bii
10 mV
500 ms
Biii
pA
0
-10
-20
-30
mV
0
-20
-40
-60
-80
-100
-120
Control
5-HT

Figure 7.8: Differential effects of 5-HT on GnIH neurons

Ai & **Aii:** Two simultaneous current-clamp recordings of GnIH neurons, both held at a membrane potential of -50 mV by injection of constant current. Bath application of 50 μM 5-HT induced a membrane depolarization in the cell shown in **Ai** and biphasic inhibition-excitation in the cell shown in **Aii**.

B: Pie chart showing the proportion of GnIH neurons excited, inhibited and responding with a biphasic (inhibited-excited) response to bath application of 5-HT. Here, 42.1% of 5-HT-induced responses were biphasic, 15.8% of neurons were inhibited whilst the remaining 42.1% were excited (n=19).

Figure 7.8

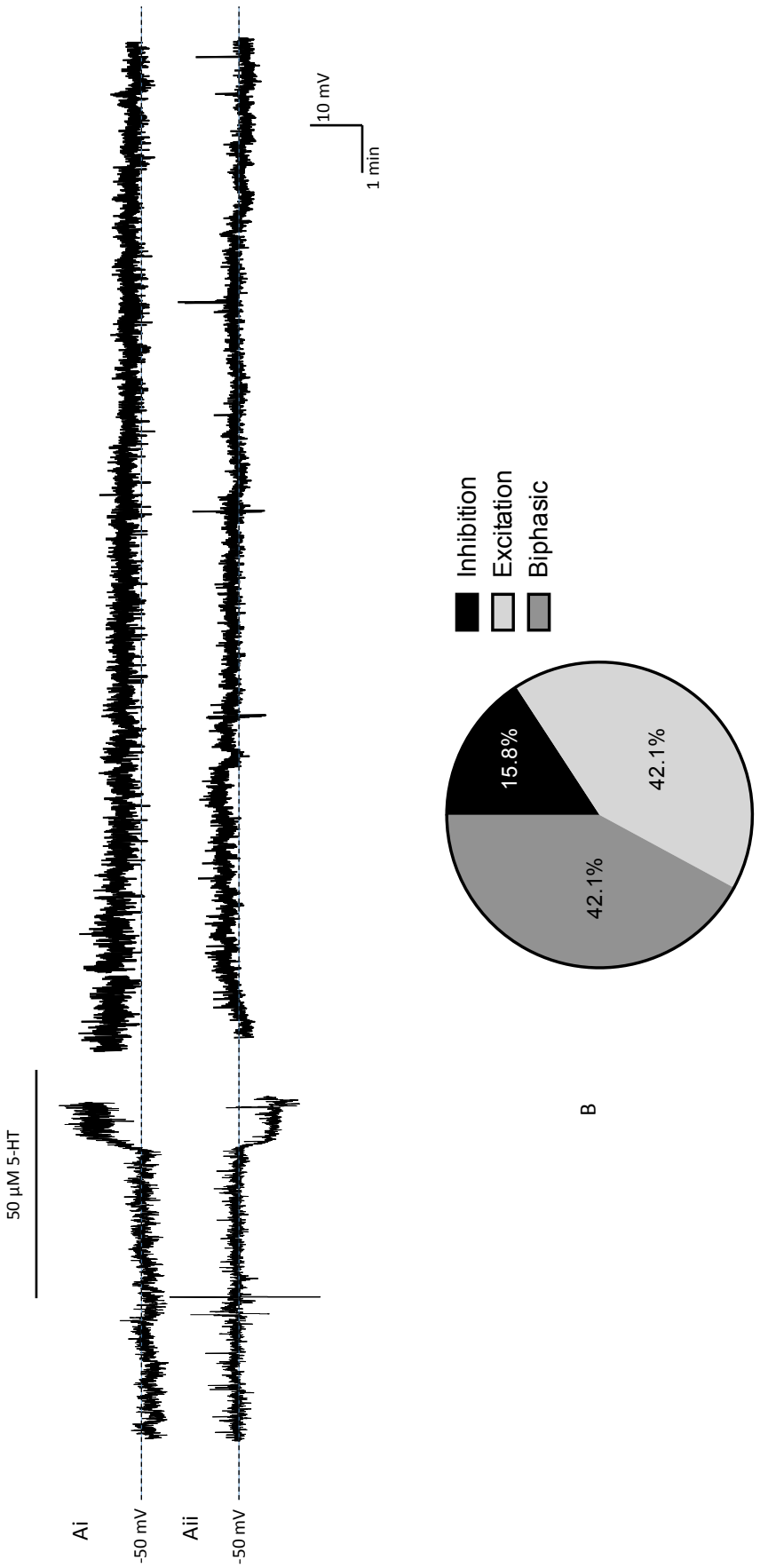
Ai
Aii
-50 mV
-50 mV
50 µM 5-HT
10 mV
1 min
Inhibition
Excitation
Biphasic
15.8%
42.1%
42.1%
B

Figure 7.9: TRH-induced direct post-synaptic excitation of GnIH neurons

A: Samples of a continuous current clamp recording from a GnIH neuron. Bath application of 400 nM TRH induced a reversible membrane depolarization and increase in action potential firing rate.

B: Current clamp recording of the same neuron as shown in **A**, in the presence of 1μM TTX. TRH-induced depolarization persisted in the presence of TTX indicating a direct post-synaptic site of action. Note also the fall in amplitude of the electronic potentials (downward deflections of the record), evoked in response to regular square-wave negative current pulses, indicating a reduction in neuronal input resistance underlies TRH-induced excitation.

Figure 7.9

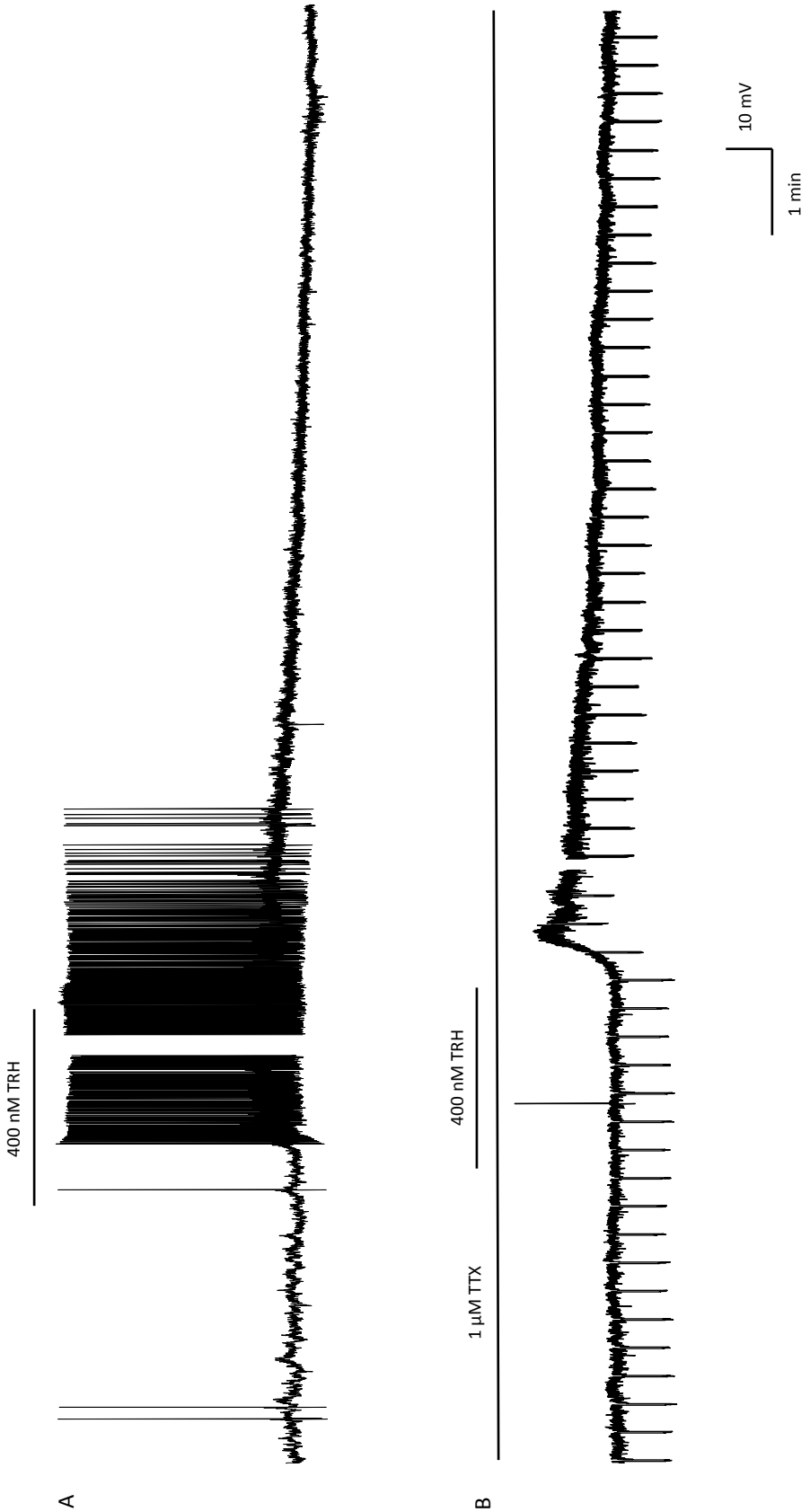

Figure 7.10: TRH-induced direct post-synaptic excitation of GnIH neurons

A: Superimposed current clamp recordings showing the current-voltage relationship of a GnIH neuron in control conditions.

B: Superimposed current clamp recording showing the current-voltage relationship of the same GnIH neuron shown in **A,** taken at the peak of the TRH-induced excitation.

C: The plots of current-voltage relationships shown in **A** and **B.** Note the reduced slope of the membrane response to current injection in the presence of TRH. Also note the extrapolated reversal potential around 0 mV. Taken together these data indicate that GnIH neuron TRH-induced depolarization is via the activation of a non-selective cation conductances, and a reduction in neuronal input resistance.

Figure 7.10

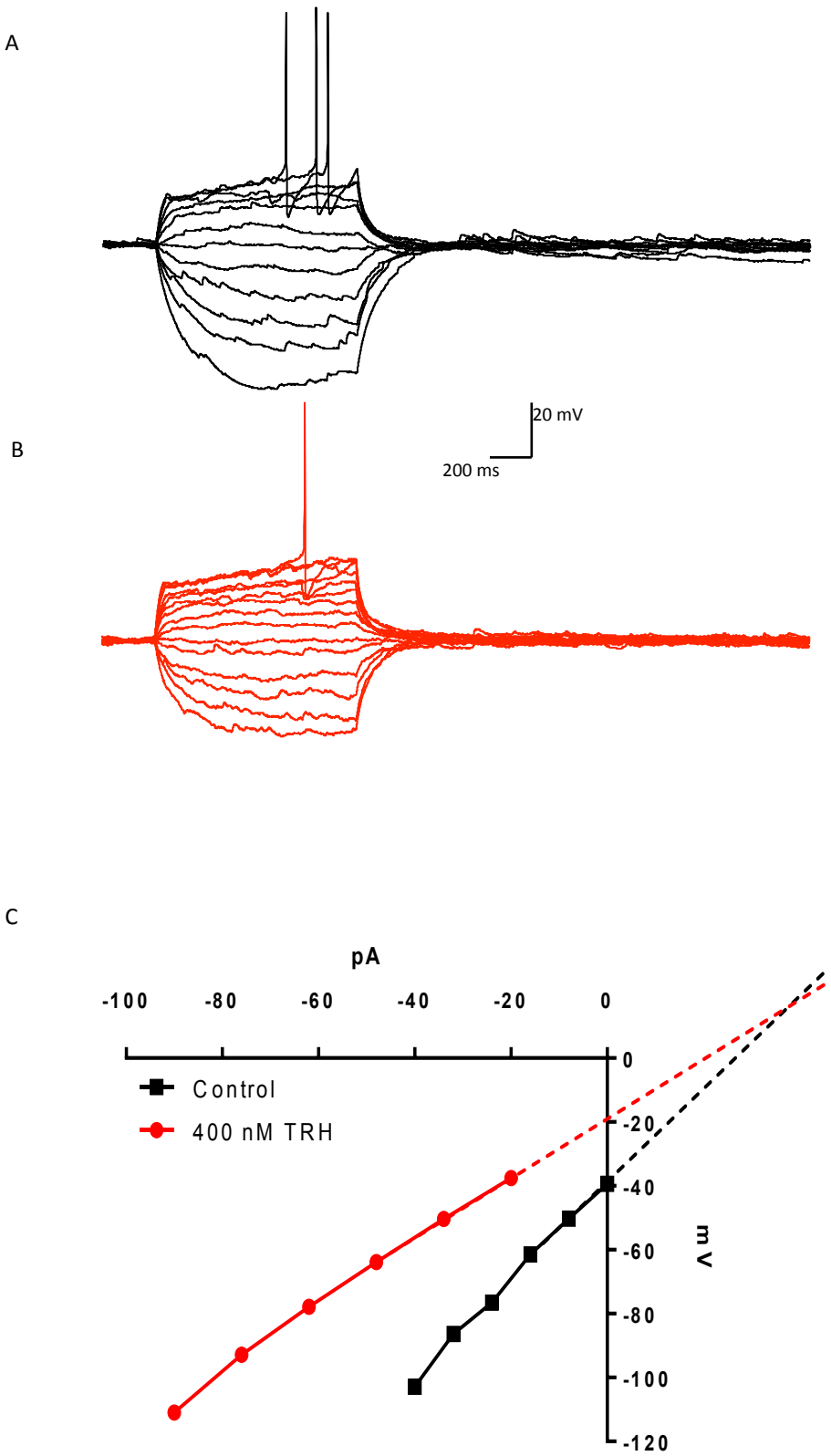
A
B
20 mV
200 ms
C
pA
-100
-80
-60
-40
-20
0
Control
400 nM TRH
0
-20
-40
-60
-80
-100
-120
mV

Figure 7.11: Ghrelin excites GnIH neurons.

A: Current clamp recording taken from a GnIH neuron. Bath application of 100 nM ghrelin induced membrane depolarization.

B: Plot of GnIH neuron current-voltage relationships in control conditions and in the presence of 100 nM ghrelin. Note the increased slope of the membrane response to current injection and reversal potential around -90 mV. Taken together these indicate membrane depolarization is via inhibition of a resting potassium conductance.

Figure 7.11

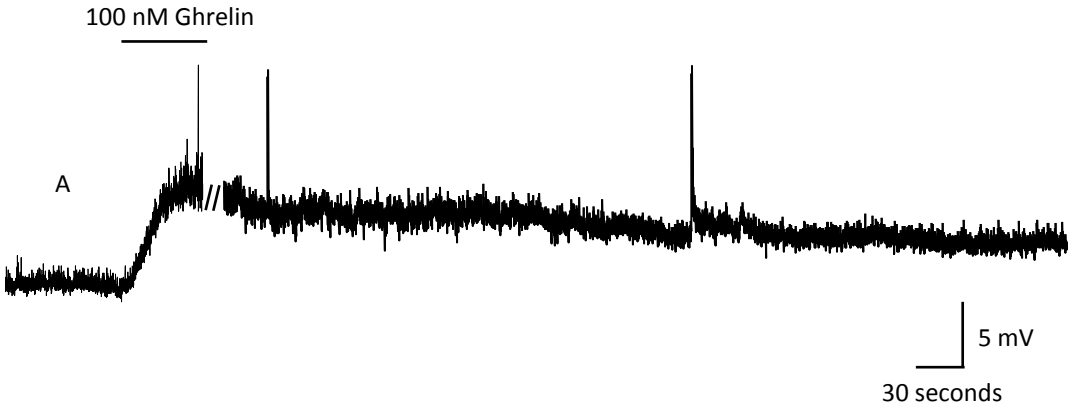
100 nM Ghrelin
A
5 mV
30 seconds

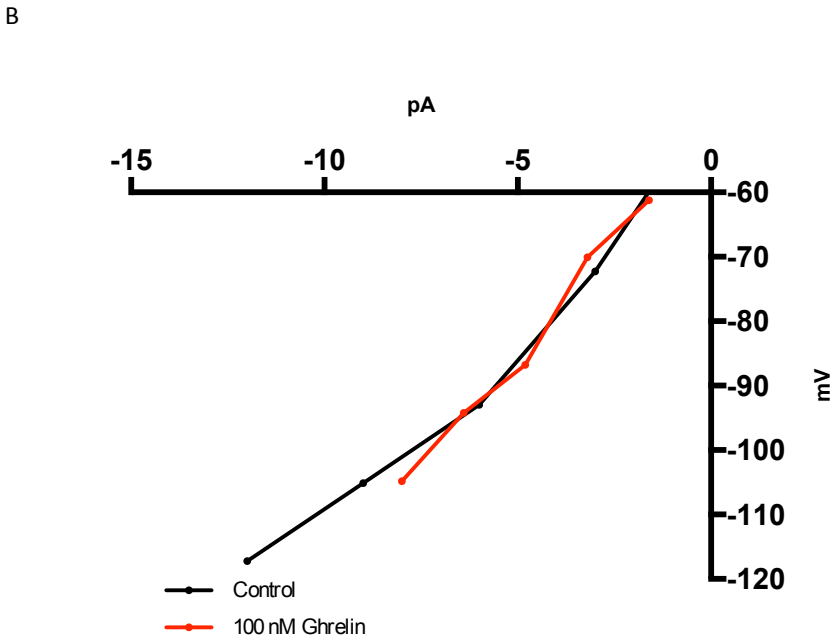
B
pA
-15
-10
-5
0
-60
-70
-80
-90
-100
-110
-120
mV
Control
100 nM Ghrelin

Chapter 8: Electrical synaptic transmission in layer 1 cortical interneurons

8.1 Introduction

Gap-junctions are conduits through which ions and metabolites can move between apposing mammalian cells, including neurons. A gap-junction plaque is composed of a number of intercellular channels, ranging from just a few to hundreds. Each of these intercellular channels is made up of two hemichannels, covalently docked to one another via their extracellular moieties (Harris, 2001). Each hemichannel is a hexamer of connexin subunits and 20 connexin genes have been identified in mice (Sohl and Willecke, 2004). In the central nervous system (CNS), 11 connexin isoforms are differentially expressed in glia and neurons and throughout development (Harris, 2001). To date only connexin 36 (Cx36) has been clearly identified to mediate neuron-to-neuron gap junction communication (Bargiotas et al., 2012, Beaumont and Maccaferri, 2011). Cx36 is found throughout the CNS but with a discrete distribution in specific cell types. Direct electrotonic coupling and electrical synaptic transmission has been demonstrated in the cerebral cortex, hippocampus, locus coeruleus, suprachiasmatic nucleus, olfactory bulb, inferior olive and spinal cord (Meier and Dermietzel, 2006, Nolan et al., 1999, Galarreta and Hestrin, 2001, Leznik and Llinas, 2005, Long et al., 2005, Kosaka et al., 2005, Fukuda and Kosaka, 2000). It is becoming increasingly evident that electrical synaptic transmission plays a more widespread role in CNS information processing in development and adulthood, in health and disease, than previously recognized. Whilst the precise role of these synapses is still far from clear, one function of

electrotonic coupling in neurons is to synchronize the electrical activity of neuronal networks (Meier and Dermietzel, 2006, Harris, 2001, Leznik and Llinas, 2005, Logan et al., 1996).

Aberrant gap-junctional intercellular communication is associated with a number of neurological diseases including cerebrovascular disease, Alzheimer's disease, Parkinson's disease, and epilepsy (Nakase and Naus, 2004). Epilepsy is the most common neurological disorder worldwide (Jacoby et al., 2005). Seizures result from the aberrant spread of synchronized neuronal depolarization, either spreading within a CNS structure, or throughout the entire forebrain, resulting in a tonic-clonic seizure (Beghi, 2016). Connexin-based electrical synapses are known to synchronize electrical activity across neuronal networks and as such the neuronal gap junction is a potential target for anti-epileptic drugs (Meldrum and Rogawski, 2007).

Specific pharmacological tools for experimental and therapeutic manipulation of gap junctions are still lacking. This is in part due to a shortage of high throughput screening protocols, as well as poor knowledge of the intricacies and idiosyncrasies of connexin channel structure and conformation, irrespective of some successful crystallographic studies (Maeda et al., 2009). A number of relatively non-specific gap-junction blockers are available. Carbenoxolone is among the most widely used (Juszczak and Swiergiel, 2009). Carbenoxolone is a glycyrrhetinic acid derivative used as a non-specific gap junction blocker in *in vitro* experiments, however it's mechanism of action at gap junctions remains unclear (Connors, 2012). Major drawbacks of the use of carbenoxolone in experiments are off-target effects. In addition to gap-junctions, carbenoxolone blocks voltage gated Ca^{2+} channels, P2X7 receptors, NMDA, and $GABA_A$ currents (Connors, 2012, Vessey

et al., 2004, Suadicani et al., 2006, Chepkova et al., 2008). Carbenoxolone also stimulates glucocorticoid signaling, elevating cortisol and coritcosterone levels by inhibiting 11-β hydroxysteroid dehydrogenase (Juszczak and Swiergiel, 2009). In addition to carbenoxolone, quinine, quinidine and mefloquine are commonly used gap-junction blockers, however none are selective for a single connexin isoform, and all have off target effects, including well documented effects on other ion channels (Juszczak and Swiergiel, 2009). Novel, selective gap junction blockers are required for a thorough and accurate characterization of gap-junction functions *in vitro* and *in vivo*.

Tonabersat (SB-220453) and Carabersat (SB-204269) are structurally related benzoylamino-benzopyran compounds that have been studied in preclinical and clinical trials as potential antimigraine and anticonvulsant therapeutics (Dahlof et al., 2009, Goadsby et al., 2009, Hauge et al., 2009, Bradley et al., 2001, Parsons et al., 2001, Upton et al., 1997, Upton and Thompson, 2000). Carabersat is an effective anticonvulsant when used in a number of *in vivo* seizure models, including the maximal electroshock seizure threshold (MEST) test, the maximal electroshock (MES) test, and in a pentylenetetrazole (PTZ) infusion-evoked tonic extension seizure model (Upton et al., 1997). Treatment with carabersat is not associated with depressive side effects (Upton et al., 1997). In an *in vitro* model of hippocampal seizure induced by elevated extracellular potassium, Carabersat is a more effective anticonvulsant than carbamazepine and lamotrigine (Upton et al., 1997). Data indicates that the mechanism of action of benzoylamino-benzopyran compounds on epileptiform activity is independent of sites affected by current anticonvulsants including phenobarbitone, phenytoin, sodium valproate, carbamazepine, diazepam, ethosuximide, lamotrigine, vigabatrin, gabapentin and

levetiracetam (Herdon et al., 1997). Tonabersat has been shown to reduce cortical spreading depression (CSD), inhibit nitric oxide release and antagonize gap junction glia-neuron communication (Durham and Garrett, 2009, Damodaram et al., 2009, Read et al., 2000). The effect of these compounds on neuron-to-neuron gap-junctional communication is unknown and is of significant interest given the therapeutic potential of this compound family. Data may provide a definitive explanation of the mechanism(s) of anticonvulsant action.

The International Federation of Societies for Electroencephalographers (IFSECN) define epileptiform activity as "*Distinctive waves or complexes, distinguished from background activity, and resembling those recorded in a proportion of human subjects suffering from epileptic disorders*" (IFESCN, 1974). This activity, measured *in vivo* using the electroencephalogram (EEG), can be replicated *in vitro* using whole-cell patch clamp recording techniques, and is observed as aberrant depolarizing potentials, synchronized throughout neuronal populations (Kantrowitz et al., 2005, Bikson et al., 2002, Carlen et al., 2000). Electrotonic coupling of neuronal networks facilitates the generation of synchronous activity in *in vitro* models of hippocampal and cortical seizure (Perez Velazquez and Carlen, 2000). Gap-junction blockers such as quinine, reduce epileptiform activity *in vitro*, cortical seizure *in vivo,* and protect against PTZ-induced seizure (Srinivas et al., 2001, Bikson et al., 2002, Gajda et al., 2005, Nassiri-Asl et al., 2009). Conversely, some studies have concluded that gap-junctions do not contribute significantly to synchronized epileptiform activity: *In vitro* studies of brain slices obtained from Cx36 knockout mice, demonstrate that synchronous epileptiform activity can generated in response to Mg^{2+}-free aCSF (Voss et al., 2014). This activity can be decoupled by the application of either the anaesthetic

etomidate or carbenoxolone. Glycyrrhizic acid, a compound similar to carbenoxolone that does not affect gap junctions, does not decouple epileptiform activity (Voss et al., 2014). These results suggest that non-Cx36 gap junctions may synchronize epileptiform activity, or that the antiepileptic actions of carbenoxolone are not at all mediated via gap-junction inhibition (Voss et al., 2014). Muddying the waters further - in terms of the role of gap-junctions and epilepsy - is data indicating that electrical synapses are actually protective against seizure. Quinine and carbenoxolone have been found to exert a proconvulsive effect in rat cortical slices, increasing both the frequency and amplitude of seizure-like events (Voss et al., 2009). Moreover Cx36 knockout mice have a lower threshold for PTZ-induced generalized tonic-clonic seizures, compared to wild-type controls (Jacobson et al., 2010).

In vitro experimental models of epileptiform activity aim to closely resemble the neuronal activity underlying epileptic phenomena. As such they generally concentrate on pathophysiological neuronal activity within hippocampal and cortical networks; two neuroanatomical structures affected by epilepsy *in vivo*. The rodent prefrontal cortex (PFC) consists of six layers. Layer 1 is the most superficial, and contains the apical dendrites of pyramidal neurons originating in deeper cortical layers. The few cell bodies that exist in layer 1 include neurogliaform interneurons that extend inhibitory projections to deeper pyramidal neurons (Puig and Gulledge, 2011). Layers 2 and 3 contain pyramidal neurons, fast spiking and non-fast spiking interneurons. Layers 5 and 6 contain pyramidal neurons with large somata, relative to those originating in more superficial layers. Also in layers 5 and 6 are several interneuron subtypes, including fast spiking and non-fast spiking interneurons (Puig and Gulledge, 2011).

The prefrontal cortex is innervated by serotonergic fibers originating in the dorsal and median raphe (O'Hearn and Molliver, 1984, Puig and Gulledge, 2011). Fourteen 5-HT receptor subtypes have been identified (5-HT_{1A} through 5-HT_7). All but one of the 5-HT receptor subtypes are G-protein coupled receptors, the exception is the 5-HT_3 receptor which is a ligand-gated ion channel (Derkach et al., 1989). Cortical pyramidal neurons express 5-HT_{1A} and 5-HT_{2A} receptors (Martin-Ruiz et al., 2001, Puig et al., 2003, Pompeiano et al., 1992). Unpublished data from the Spanswick laboratory also indicates the expression of $5HT_{2B}$, $5HT_{2C}$ and $5HT_7$ receptors on rat layer 5 pyramidal neurons, all of which contribute to the excitatory effects of 5-HT on prefrontal pyramidal neurons (unpublished data). Cortical interneurons express 5-HT_{1A}, 5-HT_{2A} and 5-HT_3 receptors (Puig and Gulledge, 2011). In cortical interneurons, 5-HT_3 receptors are found coexpressed with cholecystokinin (CCK) and calretinin (CR) but not parvalbumin (PV) or somatostatin (SOM), and are preferentially expressed in layers 2, 3, 5 and 6 (Morales and Bloom, 1997). In cortical CCK and CR neurons, the inward currents gated by 5-HT_3 receptors elicit rapid membrane depolarization, and in doing so modulate GABAergic output and the activity of efferent cortical neurons (Ferezou et al., 2002). 5-HT_3 receptors are widely expressed throughout the CNS and in the periphery (Thompson and Lummis, 2007). In the CNS, in addition to the cortex, 5-HT_3 receptors are found in the hippocampus, entorhinal cortex, cingulate cortex, amygdala, nucleus accumbens, substantia nigra ventral tegmental area and hypothalamus (Thompson and Lummis, 2007). 5-HT_3 receptor antagonism has been proposed as a potential therapeutic strategy for the treatment of a number of neurological diseases including anxiety, schizophrenia and bipolar disorder (Niesler et al., 2001, Kelley et al., 2003, Thompson and Lummis, 2007).

In the cortex, Cx36-dependent electrotonic coupling is ostensibly exclusive to interneuron networks (Galarreta and Hestrin, 2002, Galarreta and Hestrin, 1999, Lee et al., 2014). Layer 1 (L1) of the rat somatosensory cortex contains no principal neurons. Here 20% of GABAergic neurons contain CR/VIP/CCK/ChAT whilst the remaining neurons are positive for α-actinin2 (Ma et al., 2011). In L1, 49% of Cx36 positive neurons are positive for α-actinin2, whilst in L2 and L3, 13% of Cx36 positive neurons are α-actinin2 positive (Ma et al., 2011). In addition to α-actinin2 cell bodies, L1 contains the dendritic arbors of principal cells originating in deeper cortical layers, it does not contain pyramidal cell somata (Vogt, 1991).

L1 receives glutamatergic, GABAergic, noradrenergic and serotonergic innervation (Llinas et al., 2002). Axons terminating in L1 include thalamic afferents and cortical afferents originating in L2 to L6. As such, L1 is thought of as a site of cortical and thalamic signal integration (Llinas et al., 2002, Vogt, 1991). In L1, networks of electrotonically coupled late spiking (LS) interneurons receive glutamatergic innervation from L2 and L3 pyramidal neurons and have efferent GABAergic connections with other GABAergic neurons of L1. In L1 83% of electrotonic coupling is between LS neurons (Chu et al., 2003). Electrical stimulation of L1 can evoke EPSPs in L5 pyramidal neuron apical dendrites and evoke action potentials at the soma of L5 principle neurons (Larkum and Zhu, 2002, Helmchen et al., 1999). A thorough functional characterization of electronically coupled networks in L1 of the cortex is yet to be completed. However, electrical synapse-dependent network synchronization may be critical to the maintenance GABAergic tone to layer 5 pyramidal cells.

The aims of this study were to characterize the electrophysiological properties of electrotonically coupled interneurons of L1 of the cortex. Investigate

the effect of serotonin (5-HT) on the membrane excitability of these neurons and determine the utility of carbenoxolone, tonabersat and carabersat as neuronal gap junction modulators.

8.2 Results

Whole cell patch clamp recordings were obtained from 25 pairs of electrotonically coupled interneurons in L1 of the adult mouse (> 6 weeks) PFC. These neurons had a mean resting membrane potential and neuronal input resistance of -63.98 ± 0.98 mV and 570 ± 60 MΩ respectively. Of the 50 L1 interneurons recorded, 8 were classified as fast spiking (FS), and 42 were classified as non-fast spiking (NFS). FS interneurons were defined by their ability to discharge rapidly at frequencies between 12 and 29 Hz in response to a depolarizing current step, with little obvious spike frequency accommodation. NFS interneurons were characterized by slower frequencies of firing in response to depolarizing current injection, and marked spike frequency accommodation. Simultaneous paired recordings were obtained from >60 pairs of L1 interneurons. Of these, direct electrotonic coupling was detected between 25 pairs and the latter were experimented upon.

8.2.1 Biophysical properties of L1 electrical synapses

A pair of cells were defined as electrotonically coupled by the demonstration of direct current transfer between cells following injection of rectangular-wave current pulses from one of a pair (figure 8.2). From these paired recordings and injected current steps quantification of membrane properties allowed estimates of junctional conductance (gj), using a model in which each neuron was represented by a single compartment joined by a resistor representing the electrical synapse:

g12 = R1k12 / ((R1R2) (R1k12)) (see Nolan et al., 1999; Logan et al., 1996) where R1 and R2 are input resistances of pre- and postsynaptic cells, respectively, and k12 is the coupling coefficient. Using this approach, electrotonically coupled interneurons originating in L1 of the PFC recorded here had a mean coupling coefficient (cc) of 0.07 ± 0.01, and junctional conductance of 0.16 ±0.01 nS (n=25) (figure 8.5). In the majority of electrotonically coupled pairs recorded here coupling was bidirectional and symmetrical in that current passed equally well in either direction (See table 8.1). Any ostensible asymmetric junction rectification can be explained as a product of unequal neuronal input resistance. Figure 8.5C demonstrates the negative correlation of junction symmetry to input resistance asymmetry.

8.2.2 Interneuron subtype

Of the 25 pairs of electrotonically coupled neurons discussed here, electrotonic coupling between L1 interneurons was predominantly between non fast spiking (NFS) interneurons (80%, n=20 pairs), with 12% of coupling observed between two fast spiking (FS) neurons (n=3 pairs) and 8% between one FS neuron and one NFS neuron (n=2 pairs) (figure 8.5B).

8.2.3 Electrical synaptic transmission and low pass filters

Action potentials in one neuron, discharged in response to depolarizing current injection, evoked simultaneous oscillations (spikelets) in the neighboring coupled cell. These, 'spikelets' or electrical postsynaptic potentials constituted low-pass filtered action potentials from the presynaptic neuron, the rapid spike component of the action potential being more markedly filtered than the subsequent

inhibitory afterhyperpolarisation (AHP). Thus, electrical postsynaptic potentials were biphasic, with rapid depolarizing transients (electrical excitatory postsynaptic potentials (eEPSPs)) followed by electrical inhibitory PSPs (eIPSPs). Examples of the low pass filtering properties conferred unto FS and NFS neurons by gap-junctions are shown in figure 8.3. Mean presynaptic action potential to postsynaptic spikelet time-lag was 2.04 ± 0.20 ms (n=12).

8.2.4 Dual electrical and chemical synaptic transmission in L1 PFC interneurons

Electrical synaptic transmission was demonstrated by positive current injection into the presynaptic neuron and evoked membrane depolarization and discharge of a train of action potentials in the presynaptic neuron. Simultaneous membrane depolarization was also observed in the postsynaptic neuron, with biphasic membrane potential oscillations or 'spikelets' observed in the postsynaptic neuron. In 4 of 25 pairs, chemical postsynaptic currents were also observed evoked in response to presynaptic action potential firing. These electrotonically-coupled cells were connected unidirectionally with IPSPs only evoked by action potential firing in one of the pair, which in all instances was a NFS neuron (n=4). Inhibitory postsynaptic currents (IPSCs) and potentials (IPSPs) were observed in response to depolarisation and action potential discharge in the presynaptic neurone. Chemical IPSPs and IPSCs manifest with a simple monophasic waveform characterised by a relatively rapid rising phase followed by a slower decay, unlike their electrical counterparts. Bath application of the $GABA_A$ receptor antagonist bicuculine (10-20mM) blocked IPSPs and IPSCs in all neurones tested (n=2) and

was without effect on the electrical postsynaptic currents, confirming dual chemical and electrical innervation of these neurons (figure 8.7).

8.2.5 Carbenoxolone blocks gap junctions

The effects of the putative gap junction and hemichannel blocker carbenoxolone were tested on electrotonic coupling between L1 interneurons. Carbenoxolone (100 μM) suppressed electrotonic coupling between all cells tested (n=5 pairs). Carbenoxolone induced a mean peak reduction in neuronal coupling coefficient from 0.11 ± 0.04 to 0.03 ± 0.01 (p=0.055) (Figure 8.6A). Junctional conductance was reduced from a control value of 0.23 ± 0.06 nS to a peak of 0.11 ± 0.02 (p=0.021) in the presence of carbenoxolone (Figure 8.6B). However this effect of carbenoxolone was associated with a reduction in neuronal input resistance, from control levels of 494 ± 67 MΩ to a peak of 260 ± 21 MΩ in the presence of carbenoxolone (p=0.008) (figures 8.8 and 8.9) (n=10). This change in neuronal input resistance was not consistent with a block of ion channels, despite a clear reduction in electrotonic coupling. Plots of current-voltage relations in the absence and presence of carbenoxolone revealed a reversal potential around -60 mV (Figure 8.8C). Taken together these data indicate that the effects of carbenoxolone on these neurons is in part a product of gap-junction blockade, but also a product of the activation of a chloride conductance. The mean peak reduction in cc and JC was observed around 16 minutes after the onset of application of carbenoxolone (Figures 8.9A and 8.9B), whereas the mean peak reduction in input resistance was observed 24 minutes after the onset of bath application of carbenoxolone (Figure 8.9C). Taken together, these differences in the temporal effects of carbenoxolone suggest that this compound targets independent signalling pathways.

8.2.6 Novel gap junction blockers: Effects on electrical synaptic transmission

Carabersat and Tonabersat, anticonvulsant and anti-migraine agents, respectively, have been suggested as putative gap-junction/ hemichannel blockers (Damodaram et al., 2009, Durham and Garrett, 2009). Thus we investigated the effects of these agents on electrotonically coupled PFC L1 interneurons. Bath application of Tonabersat (10 μM) induced a mean peak reduction in neuronal coupling coefficient from a control value of 0.08 ± 0.02 to 0.07 ± 0.02 (n=8 pairs). Subsequent application of carabersat further reduced cc to 0.05 ± 0.01 (n=8 pairs) (Figures 8.12 and 8.13). This slight reduction in coupling coefficient by Tonabersat corresponded with a mean peak reduction in junctional conductance from 0.26 ± 0.05 nS to 0.22 ± 0.05 nS (p=0.03) (n=8 pairs). Subsequent application of carabersat further reduced the junctional conductance to 0.17 ± 0.04 (p=0.02 (vs. control)) (Figures 8.12 and 8.13). These effects of Tonabersat were associated with a mean peak increase in neuronal input resistance from 392 ± 40 MΩ to 409 ± 46 MΩ. However, subsequent application of carabersat reduced mean input resistance to 370 ± 28.81 (n=12) (Figures 8.12 and 8.13).

8.2.7 5-HT-induced depolarization of fast spiking layer 2 interneurons

Bath application of 5-HT (50 μM) induced membrane depolarization in all FS neurons tested (n=6). 5-HT-induced depolarization had a mean peak amplitude of 6.7 ± 1.8 mV, from a mean resting potential of −48.7 ± 1.4 mV to a new steady-state membrane potential of −42.0 ± 1.9 mV (p=0.014) (n=6) (figures 8.14 and 8.15). 5-HT-induced excitation was associated with an increase in action potential firing

rate from a mean control level of 0.02 ± 0.01 Hz to 1.54 ± 0.90 Hz in the presence of 5-HT (p=0.14) (Figures 8.14 and 8.15). Voltage-current relations, generated in response to a range of depolarizing and hyperpolarizing rectangular-wave current pulses (−250 to +100 pA, 1,000 ms duration) revealed that 5-HT-induced excitation was principally associated with a trend for a decrease in neuronal input resistance from a mean control value of 384 ± 43 MΩ to a peak of 365 ± 29 MΩ in the presence of 5-HT (p=0.52) (Figures 8.14 and 8.15). Plots of the voltage-current relations revealed reversal potentials for 5-HT-induced excitation around -50 mV (n=3) (figure 8.13D), -90 mV (n=2) and in one instance, 5-HT-induced FS interneuron excitation was not associated with any clear conductance change. In the case of excitations associated with a reversal potential of -90 mV, input resistance actually increased, from a control value of 233 MΩ to 287 MΩ at the peak of excitation. Taken together, these data suggest that 5-HT-induced excitation is mediated via either the activation of a non-selective cation conductance and in some cells the inhibition of a potassium conductance.

8.3 Discussion

Data presented here demonstrate for the first time electrical synaptic transmission between L1 interneurons of the PFC. Furthermore these interneurons not only communicate via direct electrical synaptic transmission, but also chemically, utilizing GABA as a neurotransmitter. Thus, interneurons in L1 of PFC show similar properties to those described for layer 1 neurons in the neocortex (Chu et al., 2003) and other layers in various regions of the cortex (Galarreta and Hestrin, 2002, Simon et al., 2005, Tamas et al., 2000).

8.3.1 Biophysical properties of L1 electrical synapses

Electrotonic coupling between L1 interneurons in the PFC was demonstrated in 25 pairs of cells. Coupling for the main part was bidirectional and symmetrical i.e. current passed equally well in either direction regardless of which cell was designated pre- or post-synaptic. Any ostensible rectification could be explained as a result of differences in neuronal input resistance on either side of the junction rather than a rectifying property of the junction itself.

The mean coupling coefficient of electrotonically-coupled neurons recorded here was 0.07 ± 0.01. This is compared to a value of 0.09 ± 0.06 observed in α-actinin-positive neurogliaform neurons of the rat hippocampus (Price et al., 2005). The mean junctional conductance of coupled neurons observed in this study was 0.16 ±0.01 nS. This is somewhat weaker than coupling reported between other rodent cortical interneuron populations. Of layer 2/3 basket cells of the rat somatosensory cortex, mean junctional conductance is 0.334 ± 0.086 nS (Tamas et al., 2000), whilst murine L5, PV-positive FS interneurons exhibit a mean junctional conductance of 0.203 ± 0.044 nS (Galarreta and Hestrin, 2002).

The mean junctional conductance observed here was 0.16 ± 0.01 nS. If one assumes the coupling described here is mediated via Cx36 and the mean unitary conductance of Cx36-based gap junctions to be 15 pS (Harris, 2001), and assumes that under control conditions, gap junctions connecting layer 1 interneurons are fully open, one can estimate that around 10.66 Cx36-based channels are responsible for the electrotonic coupling observed here. Conversely if the number of connexin channels interconnecting neurons described here is comparable to the number between cortical PV-positive interneurons (150 – 380) (Fukuda and Kosaka, 2003), then only 2.81% to 7.11% of channels are open at any one time,

and this minority of open channels is responsible for the electrotonic coupling observed. An ultrastructural study of the gap junction plaques in these neurons is required to fully address this issue.

8.3.2 Low-pass filtering by gap junctions

Of neurons recorded in layer 1, electrotonic coupling was most commonly detected between non-fast spiking interneurons (80%), whilst coupling between fast spiking interneurons was observed in 12% of pairs recorded and coupling between fast spiking and non-fast spiking interneurons was observed between 8% of cortical pairs. Previous studies have reported an absence of fast spiking interneurons in layer 1 of the cortex (Puig et al., 2010) and coupling in the neocortex layer 1 has previously been suggested mediated via late spiking interneurons (Chu et al., 2003). The report of their existence in layer 1 here may simply be the result of a lack of a definitive anatomical boundary between the superficial edge of layer two, and the deep border of layer 1.

Synchronized discharge of action potentials in fast spiking coupled neurons was not observed in these experiments. The filtering properties of the gap junction truncated the action potentials of fast spiking interneurons to a greater degree than that of slow spiking interneurons, reflecting the low-pass filtering properties of these connections. Synchronous action potential firing was not observed under control conditions in data presented here, I attribute this to action potential waveform rather than conductance limitations of electrical synapses. Synchronous firing was observed in a pair of coupled interneurons when patch pipettes were 'loaded' with cesium chloride (Figure 8.4). CsCl has the effect of inhibiting membrane potassium channels, broadening the action potential repolarization

phase. Synchronous firing of gap junction coupled neurons is apparent in neurons with broad, slow, relatively long duration action potentials such as sympathetic preganglionic neurons, the action potentials of which have a characteristic calcium shoulder, making them ideal for transmission across an electrical synapse (Nolan et al., 1999). The function of neuronal gap junctions between cortical interneurons is yet to be determined, however unless yet-unknown endogenous factors manipulate gap junction open state or action potential waveform, it would seem unlikely that their primary function is to synchronize discharge of individual action potentials in these neurons. However, in the event that rhythmic patterns of activity, as seen in epileptiform-like patterns of activity, where bursts of action potentials superimpose on slow depolarizing shifts, the coupling described here would and indeed does contribute to synchronization of bursts of activity.

8.3.3 Electrical and chemical synaptic transmission

Electrotonically coupled NFS interneurons reported here have similar electrophysiological characteristics to coupled α-actinin2-positive neurogliaform neurons of the hippocampal CA1 area (Price et al., 2005) and layer 1 interneurons reported in neocortex of rat (Chu et al., 2003). In the study by Price et al., 85% of neurons were electrotonically coupled and 70% were connected by GABAergic synapses. Similar recordings in the present study revealed chemical GABA-mediated synaptic interactions between electrotonically-coupled interneurons. It must be noted that ostensible chemical transmission observed here did have a remarkably high failure rate and as such data presented here (Figure 8.7) is of limited value. At present the numbers included in the present study are insufficient to draw definitive conclusions regarding the extent of chemical interactions

between these electrically coupled cells and to relate circuit structure and organization to function. More recordings from layer 1 pairs are needed to determine fully the role of dual electrical and chemical communication between these cells, although it is tempting to hypothesize that one function may be to modulate the synchronization and timing of GABA output commands from these interneurons, in order to affect target pyramidal neuron output. Strength of electrotonic coupling here could be an important determinant of GABAergic output drive and could constitute an important form of synaptic plasticity regulating this output.

Although the filtering properties of electrical synapses ostensibly did not drive the generation of synchronized action potential discharge in these neurons, it is likely that they would increase the probability of synchronizing activity in the *in vivo* situation. Alternatively, perhaps gap junctional coupling here is more suited to the electrotonic dissemination of slower events, such as GABAergic or other chemical inputs. If this is indeed a function of coupling between cortical interneurons, it provides a mechanism by which the activity and input resistance of coupled networks could be modulated *in vivo*, affecting efferent pyramidal function and cortical output.

8.3.4 Fast spiking layer 2 interneurons are depolarized by 5-HT

Here I show that 5-HT rapidly and reversible depolarizes fast spiking interneurons of layer 2 of the prefrontal cortex. In experiments described here, membrane depolarization was associated with either a reduction of neuronal input resistance and reversal potential around -30 mV, or an increase in input resistance and reversal potential around -90 mV. The former is consistent with the activation of a

non-selective cation conductance, whilst the latter is consistent with the inhibition of a potassium conductance. With the exception of 5-HT_3 receptors, all 5-HT receptors are coupled to G-proteins. Previous studies have found 5-HT_3 receptors to be restricted to non-fast spiking interneurons, whist the excitation of fast spiking interneurons by 5-HT was mediated by 5-HT_{2A} receptors (Puig et al., 2010). Further work is required to clarify the specific receptors mediating the effects of 5-HT, as described in the present study.

8.3.5 Rundown of coupling following patching

In the first 10 minutes following the onset of dual whole-cell recording, a steady reduction in junctional conductance and coupling coefficient was observed. This may be reflect dialysis or washout of cytoplasmic factors that affect the gating of gap junctions. Washout occurs due to the high volume of pipette solution relative to neuronal capacitance. A decrease in coupling between pairs would indicate the washout of a positive regulator of these electrical synapses, or the introduction of a negative regulator in the pipette solution itself. Likely mechanisms for this change in gap junction properties are alterations in phosphorylation state, pH or calcium binding (Harris, 2001).

8.3.6 Carbenoxolone

Here I show 100μM carbenoxolone to significantly inhibit electrotonic coupling between cortical interneurons, taking around 16 minutes to elicit peak gap junction block ($p=<0.05$). The effect and time course of carbenoxolone gap junction block are consistent with previous reports (Verselis and Srinivas, 2013). The mechanism for gap junction block by carbenoxolone has not been confirmed but

antagonism through connexin dephosphorylation has been suggested (Guan et al., 1996). Another suggested mechanism is via insertion into the membrane and reduction in junctional conductance via connexin conformational change. This is supported by observations that other lipophilic compounds such as testosterone and estrogen also block gap junctions, however some steroids, such as progesterone, do not (Herve, 2002, Bodendiek and Raman, 2010).

Many previous studies have demonstrated the generation of cortical and hippocampal epileptiform activity through the removal of Mg^{2+} from, and addition of 4-AP to aCSF (Lamsa and Kaila, 1997, Ziburkus et al., 2006, Beaumont and Maccaferri, 2011). Previous studies have shown epileptiform activity to rely upon depolarizing GABAergic transmission with gabazine application reducing epileptiform activity (Kantrowitz et al., 2005, Zsiros et al., 2007). In these experiments, bicuculine application did not have an inhibitory effect, instead it increased event frequency. The synaptic pharmacology of induced cortical epileptiform activity can be deconstructed with the use of GABA and glutamate receptor antagonists. Removing the GABAergic drive disinhibits the circuit, increasing the frequency of epileptiform events. AMPA receptor blockade inhibits the network activity, reducing frequency of events whilst NMDA receptor block eliminates spontaneous discharge in L1 neurons.

In the cortex electrical synapses would appear to exist predominantly within interneuronal networks, although coupling between pyramidal cells has been reported (Wang et al., 2010). Two theses could be put forward with regards to the effect of interneuronal coupling on epileptiform activity: 1. Interneuronal gap junctions provide a conduit through which epileptiform activity can be synchronized throughout vast neuronal networks, predisposing the network to

epileptigenesis. 2. Increased synchronicity of GABAergic neurons coordinates the inhibitory cortical drive, protecting against epileptiform activity. Results from these experiments would suggest that blocking gap junctions does indeed have a protective effect against cortical epileptiform activity. However due to the non-specific nature of CBX, I cannot be sure that these effects are due to those on gap junctions or at other targets within the network.

Here, I show carbenoxolone to decouple synchronous epileptiform activity and block gap junctions. Whether antiepileptic effects observed are due to gap junction inhibition or via the gap junction-independent mechanisms described by Beaumont and Maccaferri is unclear. For confirmation either way, we would need to perform control experiments on Cx36 knockout mice (Beaumont and Maccaferri, 2011). It is clear from my experiments that carbenoxolone is a 'dirty' pharmacological tool. In addition to the reduction in baseline synaptic noise after its application and elimination of inward rectifying conductances (not quantified but frequently observed), carbenoxolone reliably activated chloride conductances in these experiments.

8.3.7 Tonabersat and Carabersat

Here I show both 10 μM Carabersat and of 10 μM Tonabersat are capable of significantly inhibiting ($p=<0.05$) the conductance between L1 cortical interneurons, without significantly affecting input resistance. This is consistent with the specific inhibition of gap junctional channels. These effects on L1 interneurons provide evidence that the anticonvulsant properties of these benzoylamino-benzopyran compounds may be at least in part via gap junction block, and not through actions at molecular sites targeted by other extant antiepileptic compounds. This class of compound may therefore be useful in the

treatment of medication-resistant forms of epilepsy. Conclusions drawn from this data set are nonetheless limited due to two caveats in particular. One; that tonabersat and carabersat were applied sequentially without a wash period and two; that no time-control experiment was performed in order to account for the rundown of electrotonic coupling observed in the minutes immediately following the onset of dual whole-cell recording.

Figure 8.1: Basic schematic of L1 interneuron functional organization

Subsets of L1 interneurons express Cx36 and α-actinin 2. L1 interneurons release GABA into other L1 interneurons and onto distal dendritic tufts of pyramidal neurons originating in deep cortical layers.

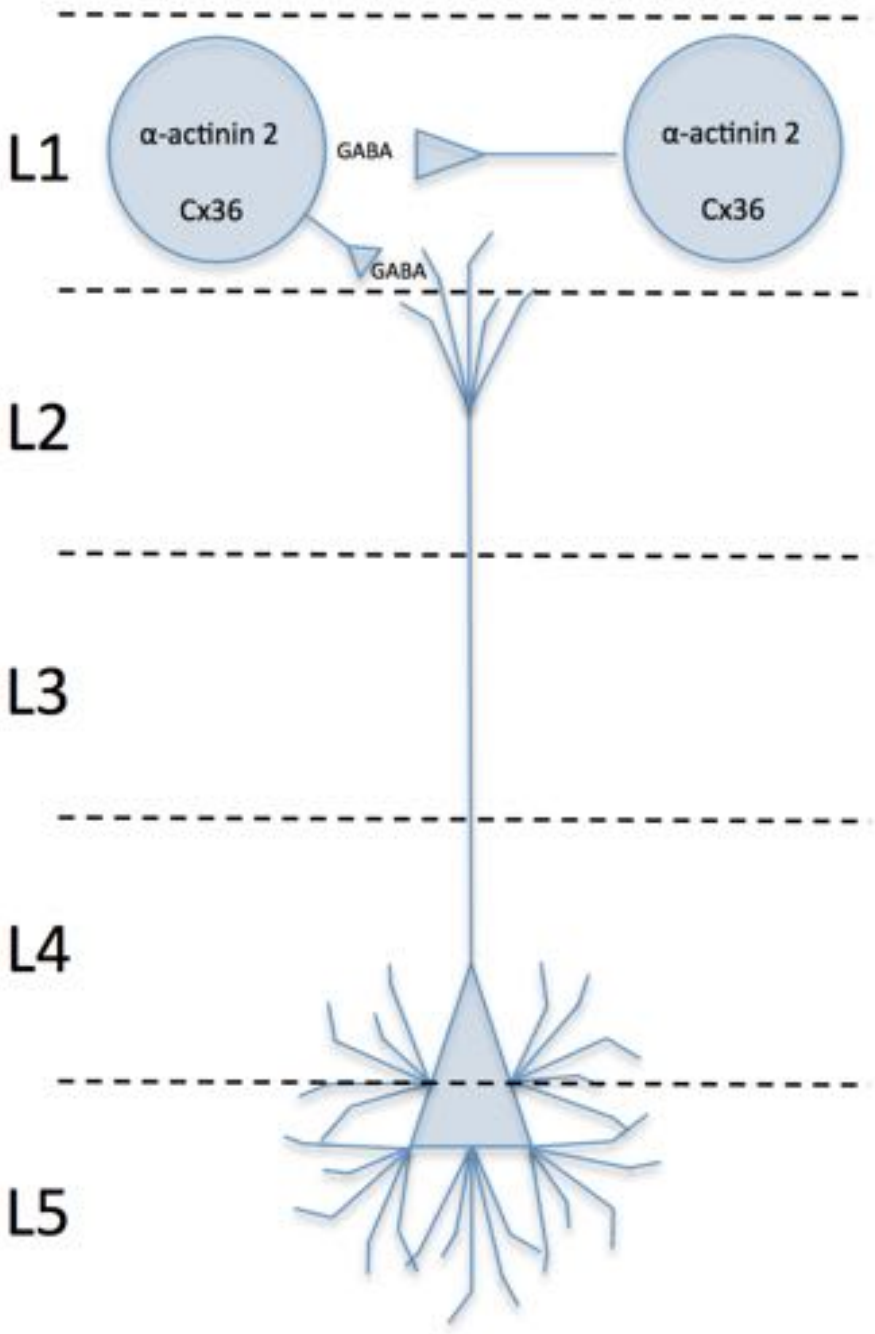
L1
α-actinin 2
Cx36
GABA
α-actinin 2
Cx36
GABA
L2
L3
L4
L5

Figure 8.2: Electrotonic coupling between layer 1 cortical interneurons

A: An example of electrotonic coupling between two non-fast spiking interneurons in layer 1 of the prefrontal cortex. Left: injection of a range of hyperpolarizing (downward) and depolarizing (upward) current pulses injected into one of a simultaneously recorded pair of neurons evoked membrane responses in the injected cell (top) and the simultaneously recorded cell (bottom). Right: The injection of a rectangular-wave current pulse into the presynaptic neuron, evoked a membrane potential change in both the presynaptic (top) and postsynaptic (bottom) neuron.

B: Differential interference contrast (DIC) photomicrograph of two simultaneously recorded electrotonically coupled interneurons of layer 1 or the prefrontal cortex, taken at 157.5-X magnification.

Figure 8.2

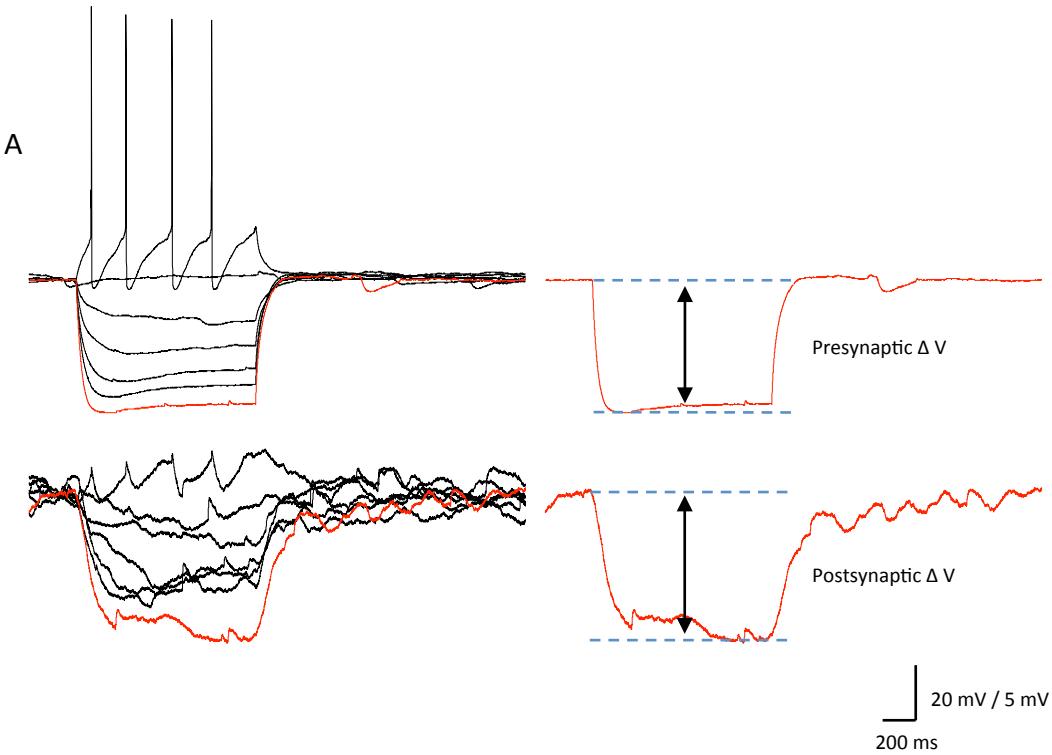

B

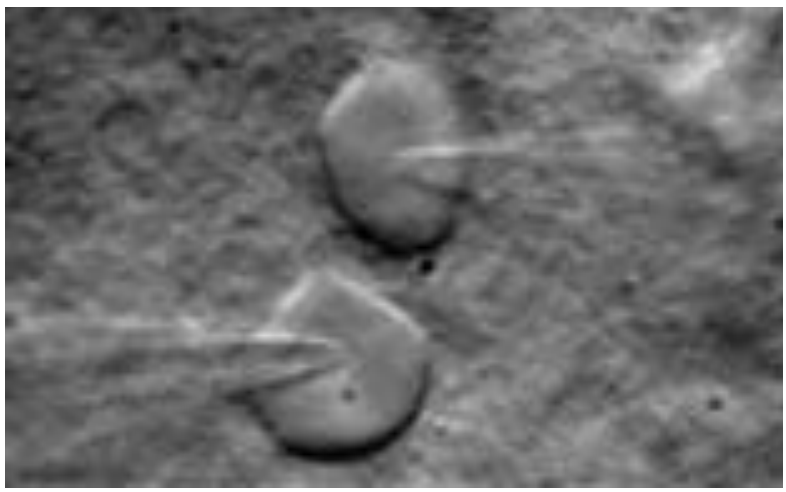

Figure 8.3: Layer I neuronal electrical synapses act as low-pass filters

A: Electrotonically coupled non fast-spiking interneurons highlighting low pass filtering of action potentials across the gap junction. Action potentials evoked in the presynaptic neuron (black) are detected in the postsynaptic neuron (red) as truncated biphasic membrane potential oscillations.

B: Electrotonically coupled fast-spiking interneurons highlighting low pass filtering of action potentials across the gap junction. Action potentials evoked in the presynaptic neuron (black) are detected in the postsynaptic neuron (red) as truncated biphasic membrane potential oscillations.

Figure 8.3

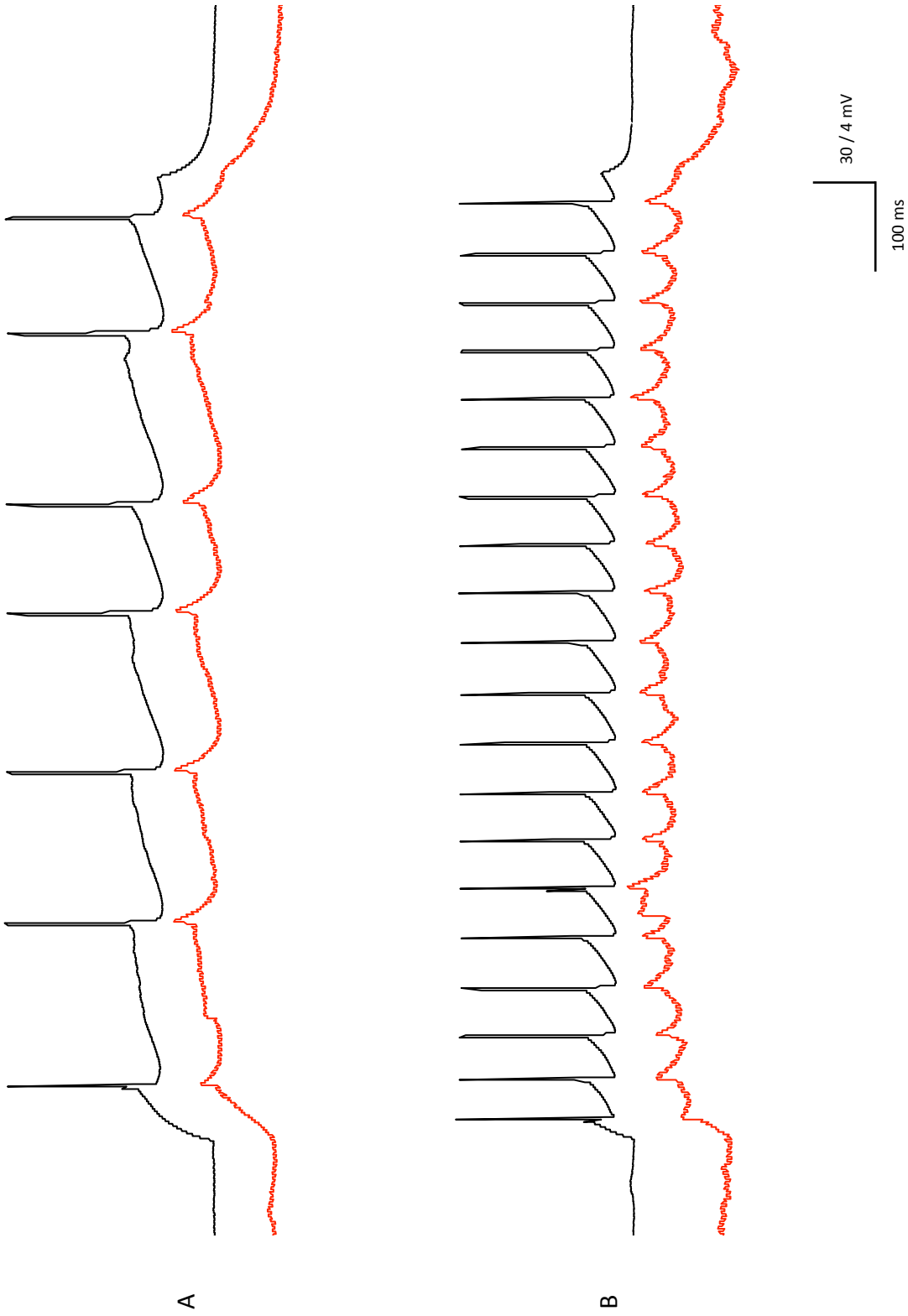

Figure 8.4: Layer I interneuron-based electrical synapses act as low-pass filters; cesium chloride loading of cells facilitates synchronous action potential firing

A: Current clamp recording taken from an electrotonically coupled pair of layer 1 interneurons, with CsCl included in the patch pipette solution. Note synchronous spontaneous action potential firing in cell 1 (top) and cell 2 (bottom).

B: Action potential and membrane potential oscillation recorded from the same neurons shown in **A**. Note the narrow waveform of 'cell 1' action potential associated with asynchronous discharge. An action potential is not evoked in 'cell 2', however a biphasic membrane potential oscillation is observed.

C: Action potential and membrane potential oscillation of the neurons shown in **A**. Note the broad waveform of 'cell 1' action potential associated with synchronous action potential discharge.

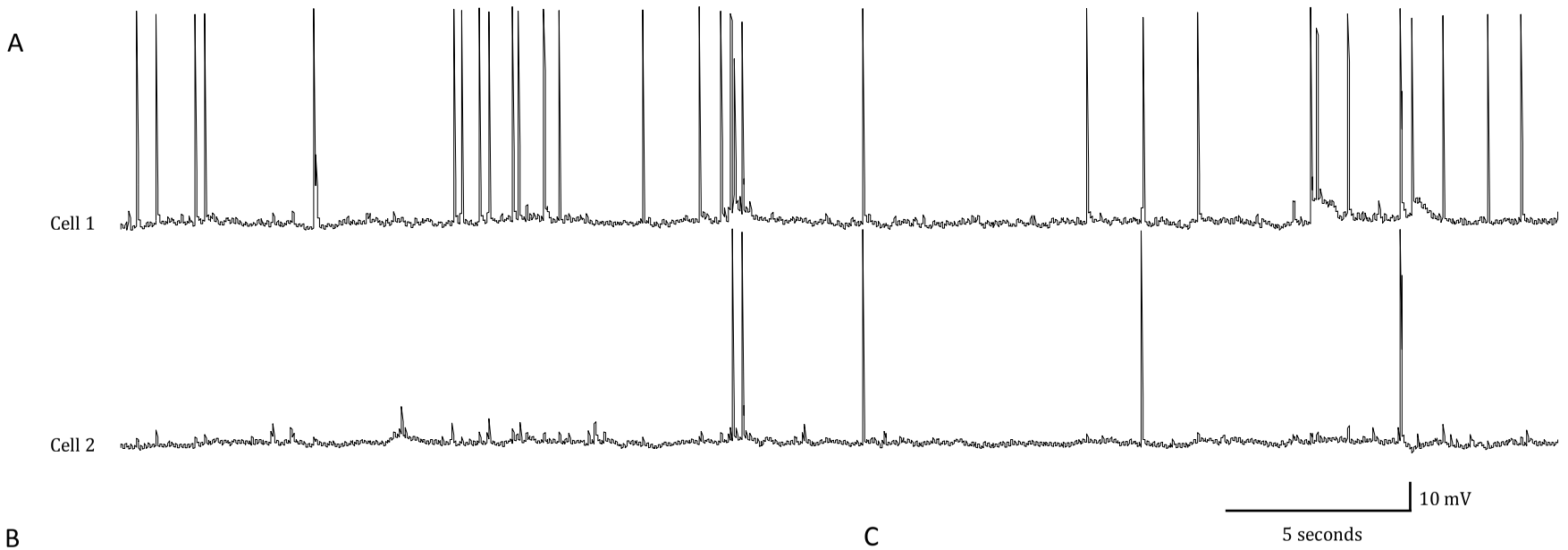
A
Cell 1
Cell 2
10 mV
5 seconds
B
Cell 1
Cell 2
20 mV / 3 mV
10 ms
C
Cell 1
Cell 2

Figure 8.4

Figure 8.5: Properties of electrical synaptic transmission between interneurons of layer 1 of the cortex

Ai: Bar chart showing mean coupling coefficient 0.07 ± 0.01 (n=25).

Aii: Bar chart showing mean junctional conductance 0.16 ±0.01 nS (n=25).

Aiii: Bar chart showing mean neuronal input resistance 570 ± 60 MΩ (n=25).

B: Electrotonic coupling is predominantly between non-fast spiking (NFS) interneurons (80%), with 12% of coupling observed between two fast spiking (FS) neurons and between one (8%) FS neuron and one NFS neuron (total n=25).

C: Graph showing normalized Cell 2 input resistance against Normalized cell2 to cell 1 coupling coefficient, demonstrating the negative correlation between the two. This graph highlights the directionality and symmetrical nature of layer 1 based electrical synapses. Any ostensible channel rectification is a product of differences in neuronal input resistance on either side of the junction.

Figure 8.5

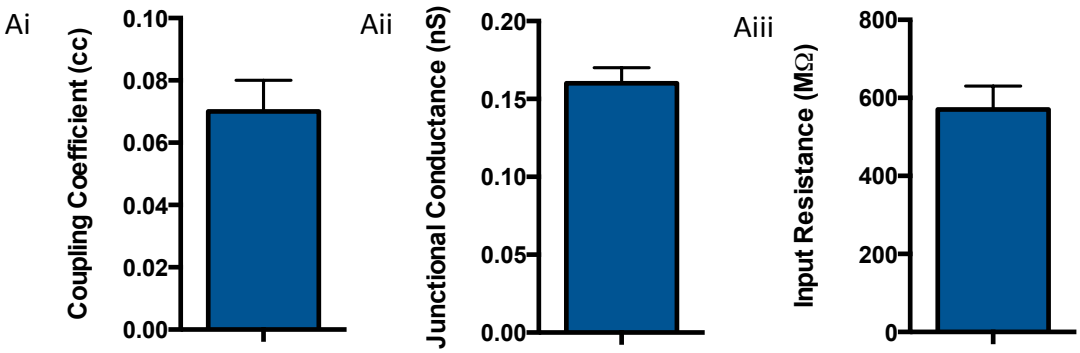
Ai
Coupling Coefficient (cc)
0.10
0.08
0.06
0.04
0.02
0.00
Aii
Junctional Conductance (nS)
0.20
0.15
0.10
0.05
0.00
Aiii
Input Resistance (MΩ)
800
600
400
200
0

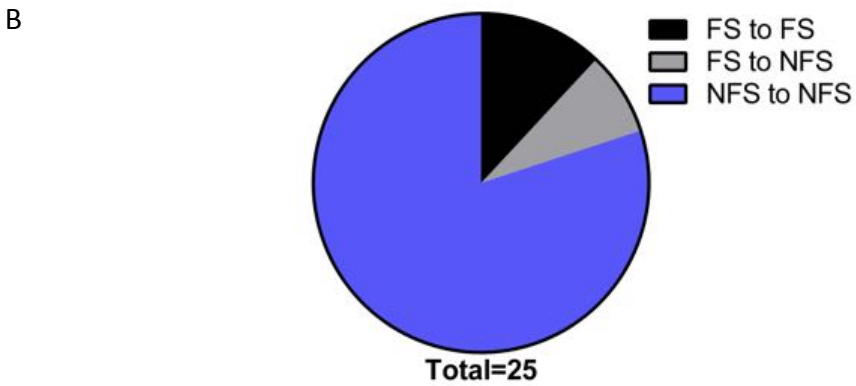
B
FS to FS
FS to NFS
NFS to NFS
Total=25

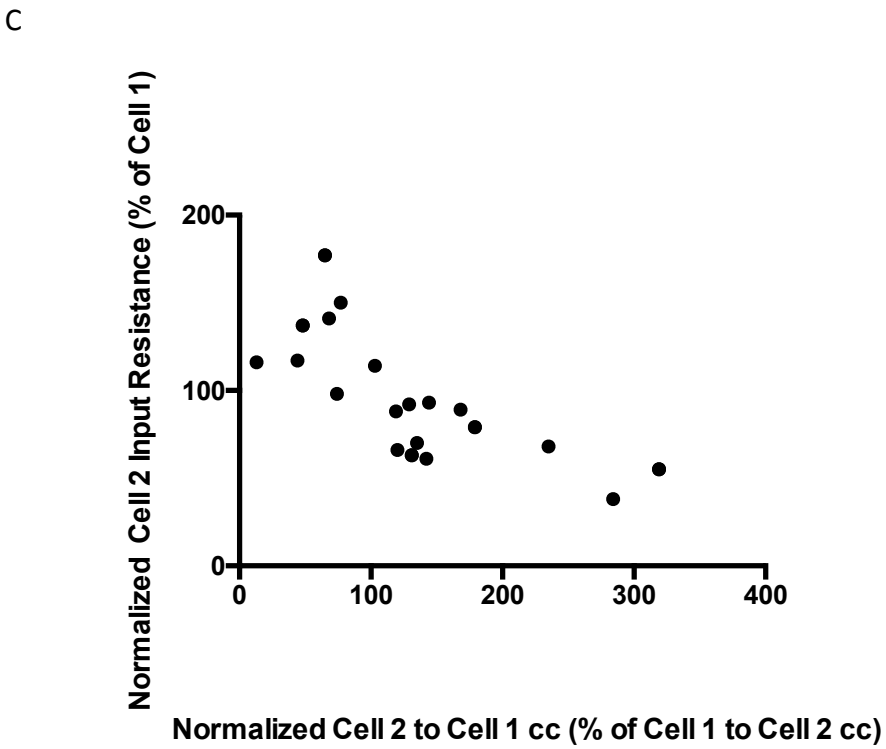
C
Normalized Cell 2 Input Resistance (% of Cell 1)
200
100
0
0
100
200
300
400
Normalized Cell 2 to Cell 1 cc (% of Cell 1 to Cell 2 cc)

Figure 8.6: Summary of coupling coefficient and neuronal input resistance values for each electrotonically-coupled pair of cortical interneurons included in this study

Figure 8.6

	Cell 1 Input Resistance (MΩ)	Cell 2 Input Resistance (MΩ)	Cell 1 Normalized Input Resistance	Cell 2 Normalized Input Resistance (% of Cell 1)
Par 1	687	263	100	38
Par 2	778	343	100	75
Par 3	340	315	100	93
Par 4	339	354	100	117
Par 5	233	214	100	92
Par 6	345	401	100	116
Par 7	453	288	100	66
Par 8	435	417	100	96
Par 9	400	271	100	68
Par 10	484	430	100	89
Par 11	404	438	100	114
Par 12	713	1009	100	141
Par 13	411	361	100	88
Par 14	325	487	100	150
Par 15	783	481	100	61
Par 16	972	765	100	79
Par 17	1132	724	100	63
Par 18	854	1172	100	137
Par 19	231	410	100	177
Par 20	388	212	100	55
Par 21	873	765	100	79
Par 22	1134	724	100	63
Par 23	836	1172	100	137
Par 24	231	410	100	177
Par 25	388	212	100	55

Figure 8.7: Mixed electrical and chemical synaptic transmission

A: Action potentials evoked in the presynaptic neuron (top, red) were detected in the postsynaptic neuron (bottom, red) as truncated biphasic membrane potential oscillations. The initial biphasic membrane oscillation is likely the result of a combination of electrical synaptic transmission combined with chemical GABAergic inhibitory synaptic transmission, whereas subsequent oscillations are mediated by electrical synaptic transmission alone.

B: The same neuron as shown in **A**. Presynaptic neuron (top) recorded in current clamp configuration, postsynaptic neuron (bottom) recorded in voltage-clamp configuration, held at -50 mV. Presynaptic action potentials can evoke an inhibitory postsynaptic current (IPSC) in the postsynaptic neuron.

C: The same neuron as shown in **A** and **B**. Bath application of the $GABA_A$ receptor antagonist bicuculine (20μM), inhibits postsynaptic IPSC's, induced by presynaptic action potential firing. Note downward deflections shown in the bottom record represent spontaneous EPSC's.

Figure 8.7

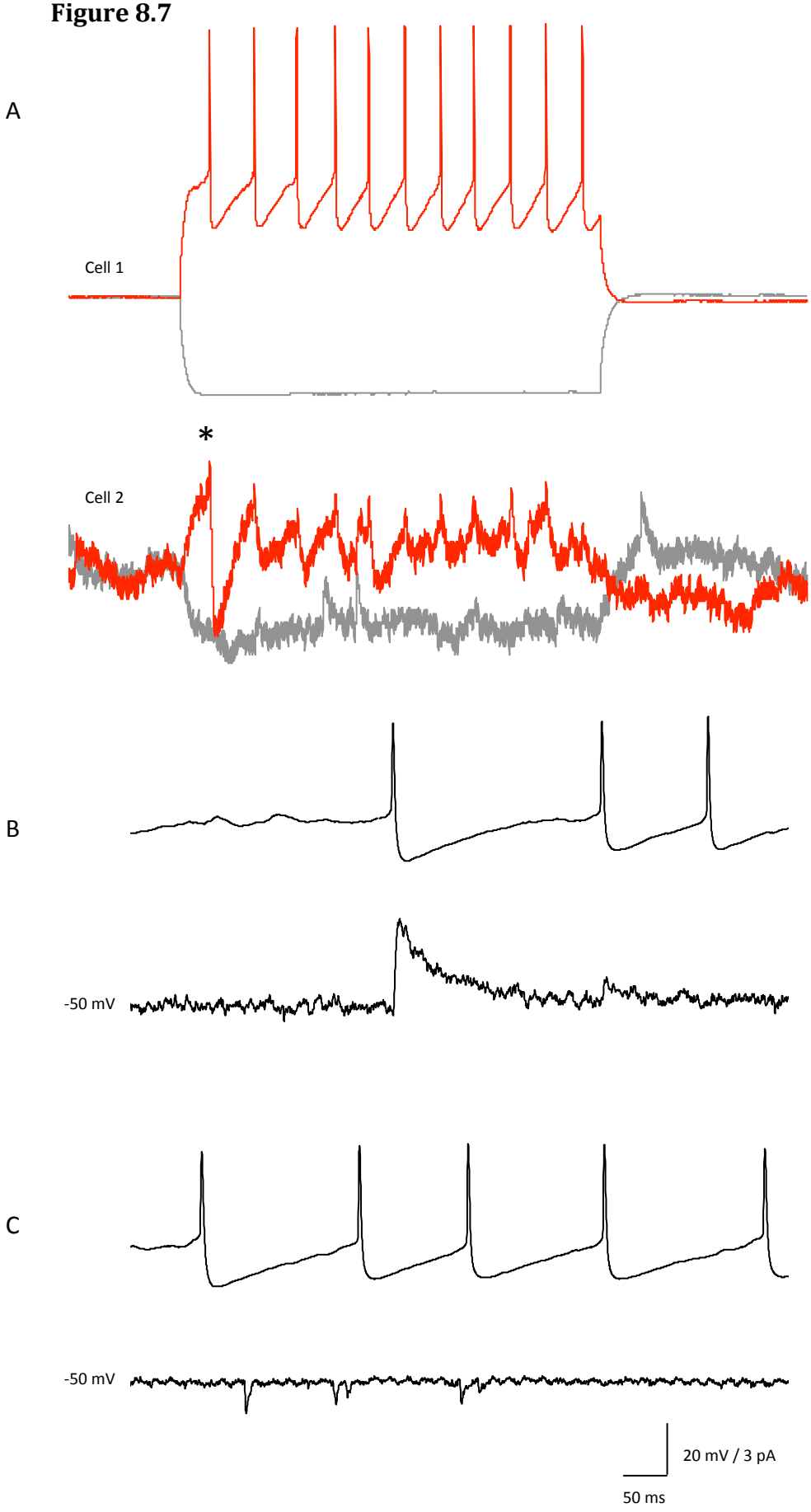

Figure 8.8: Carbenoxolone suppresses electrotonic coupling and induces a reduction in neuronal input resistance

A: A pair of electrotonically coupled non-fast spiking interneurons of layer 1 of the cortex. Current injected into the presynaptic neuron (top) results in membrane potential change in both the presynaptic and the postsynaptic (bottom) neurons.

B: The same pair of electrotonically-coupled neurons as shown in **A,** after bath application of 100μM carbenoxolone. Electrotonic coupling was reduced, shown as a reduced membrane potential change in the postsynaptic neuron, in response to current injection into the presynaptic neuron.

C: Plot of current voltage relations of a layer 1 interneuron in control conditions and in the presence of 100μM carbenoxolone. Note the decreased slope of the membrane response to current injection in the presence of carbenoxolone, indicating a decrease of neuronal input resistance. Also note the reversal potential around -70 mV indicating the activation of a chloride conductance under our recording conditions.

Figure 8.8

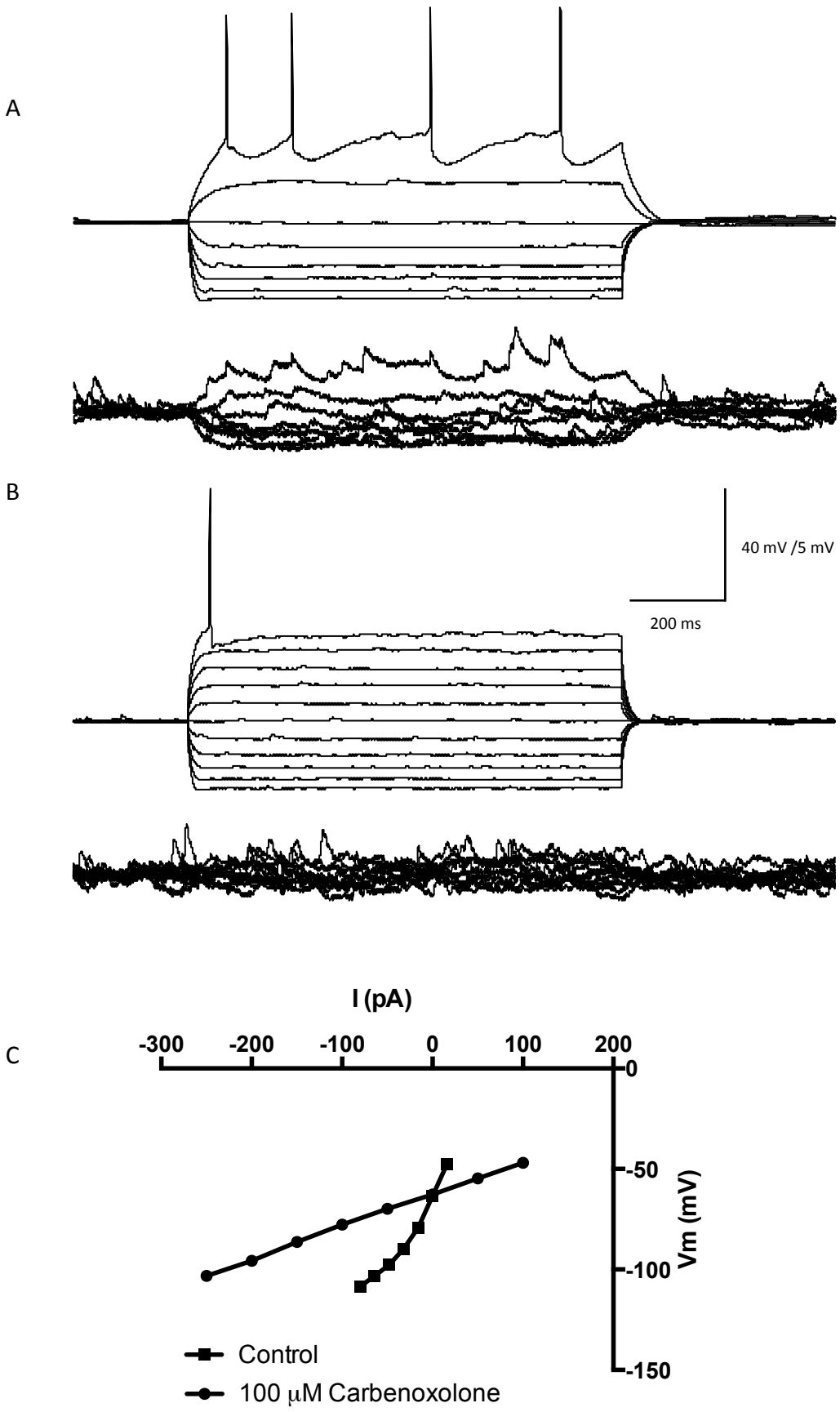
A
B
40 mV /5 mV
200 ms
C
I (pA)
-300
-200
-100
0
100
200
0
-50
-100
-150
Vm (mV)
Control
100 μM Carbenoxolone

Figure 8.9: Carbenoxolone suppresses electrotonic coupling and induced a reduction of input resistance

A: Carbenoxolone reduces the neuronal coupling coefficient (mean peak response on top panel, time plot on bottom panel), from a mean control value of 0.07 ± 0.02 to 0.03 ± 0.01 in the presence of 100μM carbenoxolone (n=10) (p=0.055; paired students t-test).

B: Carbenoxolone significantly reduces the neuronal junctional (mean peak response on top panel, time plot on bottom panel), from a mean control value of 0.2 ± 0.04 nS to 0.14 ± 0.04 nS in the presence of 100μM carbenoxolone (n=10) (p=0.021; paired students t-test).

C: Carbenoxolone significantly reduces the neuronal input resistance (mean peak response on top panel, time plot on bottom panel), from a mean control value of 383 ± 25 MΩ to 239 ± 27 MΩ in the presence of 100μM carbenoxolone (n=10) (p=0.008; Paired students t-test).

Figure 8.9

A

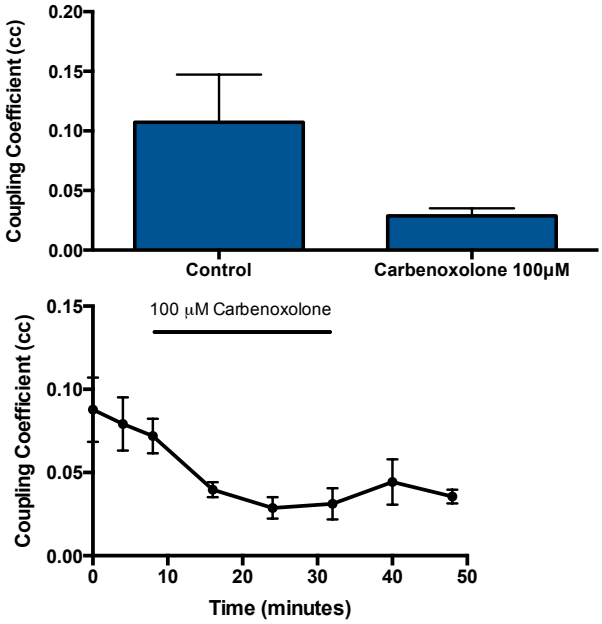

B

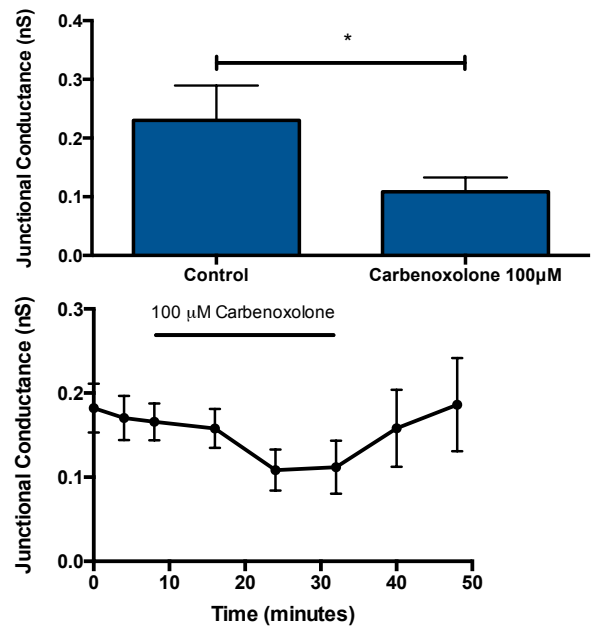

C

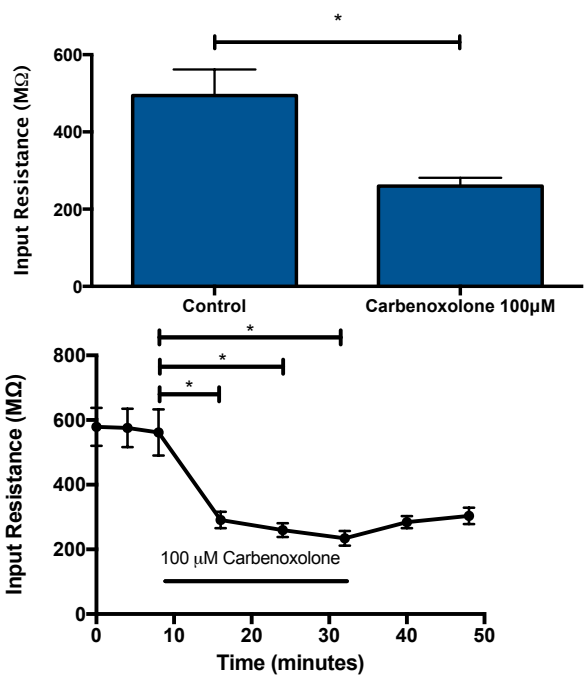

Figure 8.10: Tonabersat and Carabersat inhibit electrotonic coupling between cortical interneurons

A: Example of steady-state electrotonic coupling between a pair of layer 1 interneurons. With current transfer from cell 1 to cell two (top panel) and from cell two to cell 1 (bottom panel).

B: Electrotonic coupling between the same neurons shown in **A,** after bath application of 10μM Tonabersat.

C: Electrotonic coupling between the same neurons shown in **A** and **B,** after bath application of 10μM Carabersat.

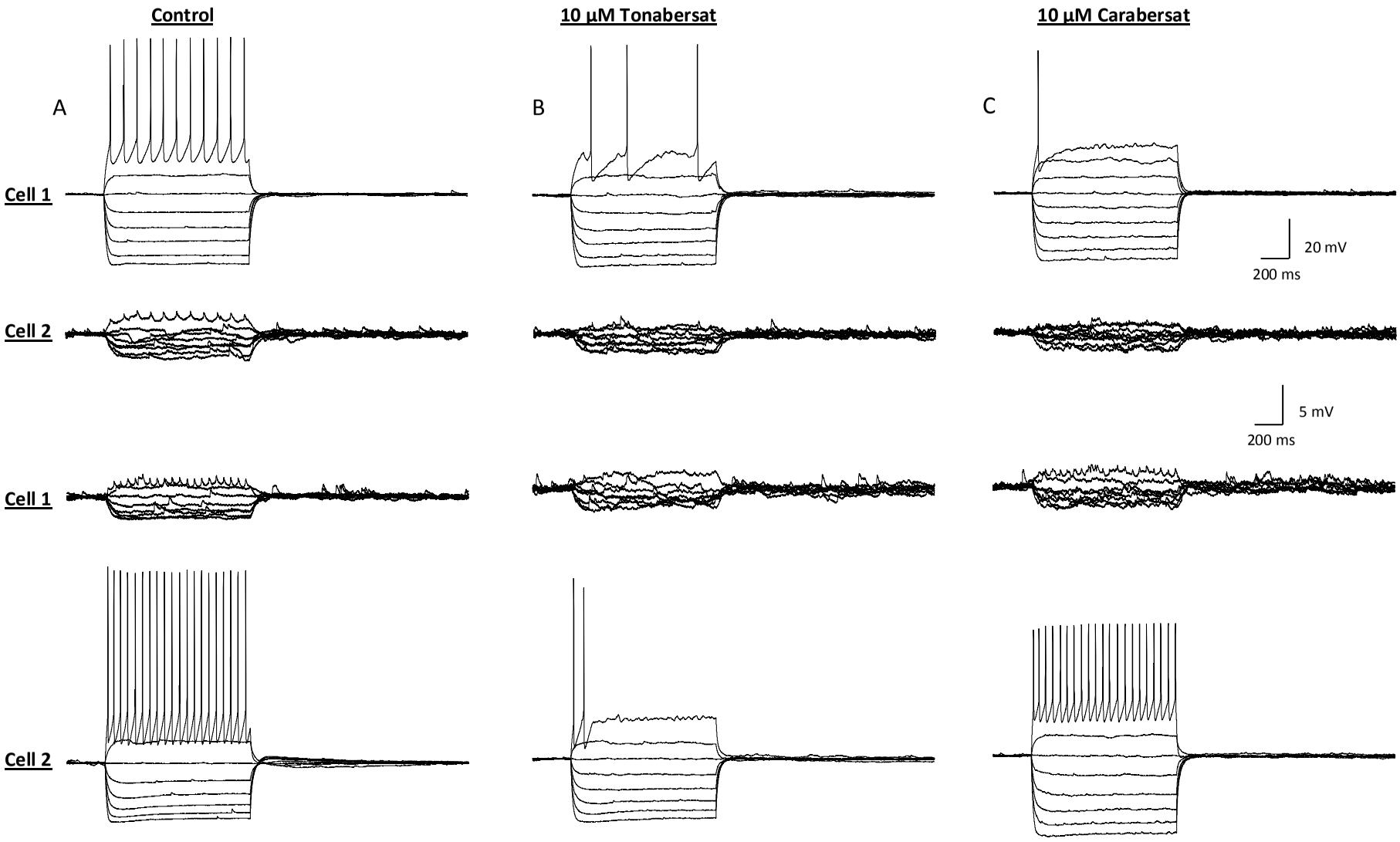
Control
10 µM Tonabersat
10 µM Carabersat
A
B
C
Cell 1
Cell 2
Cell 1
Cell 2
20 mV
200 ms
5 mV
200 ms

Figure 8.10

Figure 8.11: Tonabersat and Carabersat inhibit electrotonic coupling between cortical interneurons. (Mean peak inhibition; left panel, time plot; right panel)

Ai & Aii: Bath application of 10 μM Tonabersat reduced neuronal coupling coefficient from a control level of 0.08 ± 0.02 to a peak inhibition of 0.07 ± 0.02 (p=0.402), subsequent bath application of 10 μM Carabersat further reduced neuronal coupling coefficient to 0.05 ± 0.01 (p=0.080 vs. control; n=16; Paired students t-test).

Bi & Bii: Bath application of 10 μM tonabersat inhibits neuronal junctional conductance from a mean control level of 0.26 ± 0.05 nS to 0.22 ± 0.05 nS (p=0.032). Subsequent bath application of 10 μM Carabersat further reduced junctional conductance to 0.17 ± 0.04 nS (p=0.022 vs. control; n=16; Paired students t-test).

Ci & Cii: Bath application of 10 μM Tonabersat increased neuronal input resistance from a mean control level of 392 ± 40 MΩ to a peak of 409 ± 46 MΩ (p=0.242). Subsequent application of 10 μM Carabersat reduced neuronal input resistance to 370 ± 28.81 (P=0.454; n=16; Paired students t-test).

Figure 8.11

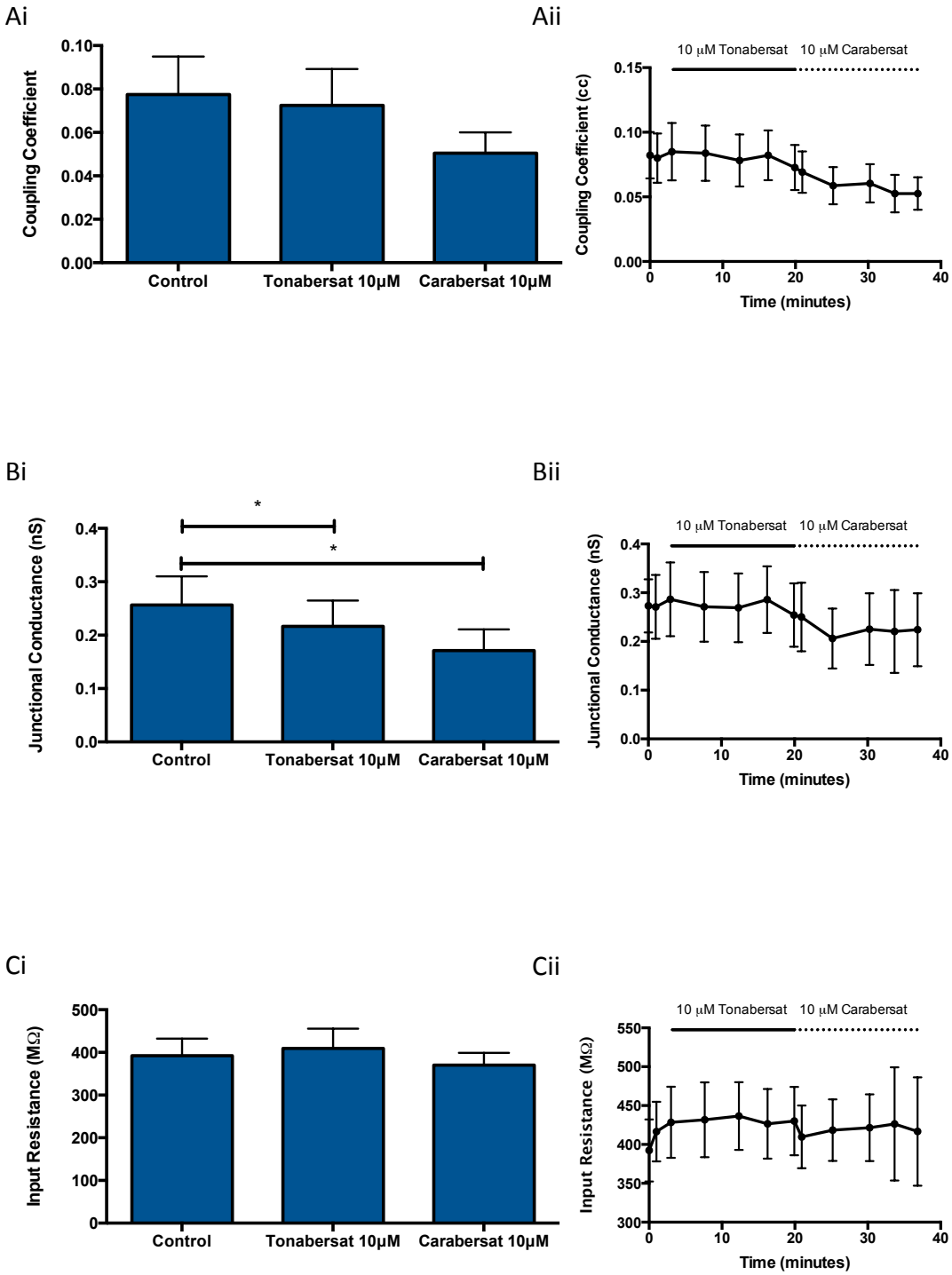
Ai
Coupling Coefficient
0.10
0.08
0.06
0.04
0.02
0.00
Control
Tonabersat 10μM
Carabersat 10μM
Aii
10 μM Tonabersat
10 μM Carabersat
Coupling Coefficient (cc)
0.15
0.10
0.05
0.00
0
10
20
30
40
Time (minutes)
Bi
Junctional Conductance (nS)
*
*
0.4
0.3
0.2
0.1
0.0
Control
Tonabersat 10μM
Carabersat 10μM
Bii
10 μM Tonabersat
10 μM Carabersat
Junctional Conductance (nS)
0.4
0.3
0.2
0.1
0.0
0
10
20
30
40
Time (minutes)
Ci
Input Resistance (MΩ)
500
400
300
200
100
0
Control
Tonabersat 10μM
Carabersat 10μM
Cii
10 μM Tonabersat
10 μM Carabersat
Input Resistance (MΩ)
550
500
450
400
350
300
0
10
20
30
40
Time (minutes)

Figure 8.12: Layer 2 fast-spiking interneurons are excited by 5-HT

A: Bath application of 50 μM 5-HT induced membrane excitation of layer 2 fast spiking interneurons.

B: Superimposed current clamp recordings showing membrane current-voltage relationship of a fast spiking interneuron before 5-HT bath application.

C: Superimposed current clamp recordings showing membrane current-voltage relationship of the same fast spiking interneuron as shown in B following 5-HT-induced membrane depolarization.

D: Plot of membrane current-voltage relationships shown in figures 8.3B and 8.3C. Note the reduced slope of the membrane response to current injection in the presence of 5-HT indicating a reduction of neuronal input resistance. Also note the reversal potential around -30 mV. Taken together these data are indicative of 5-HT-induced activation of a non-selective cation conductance, consistent with 5-HT3 receptor activation.

Figure 8.12

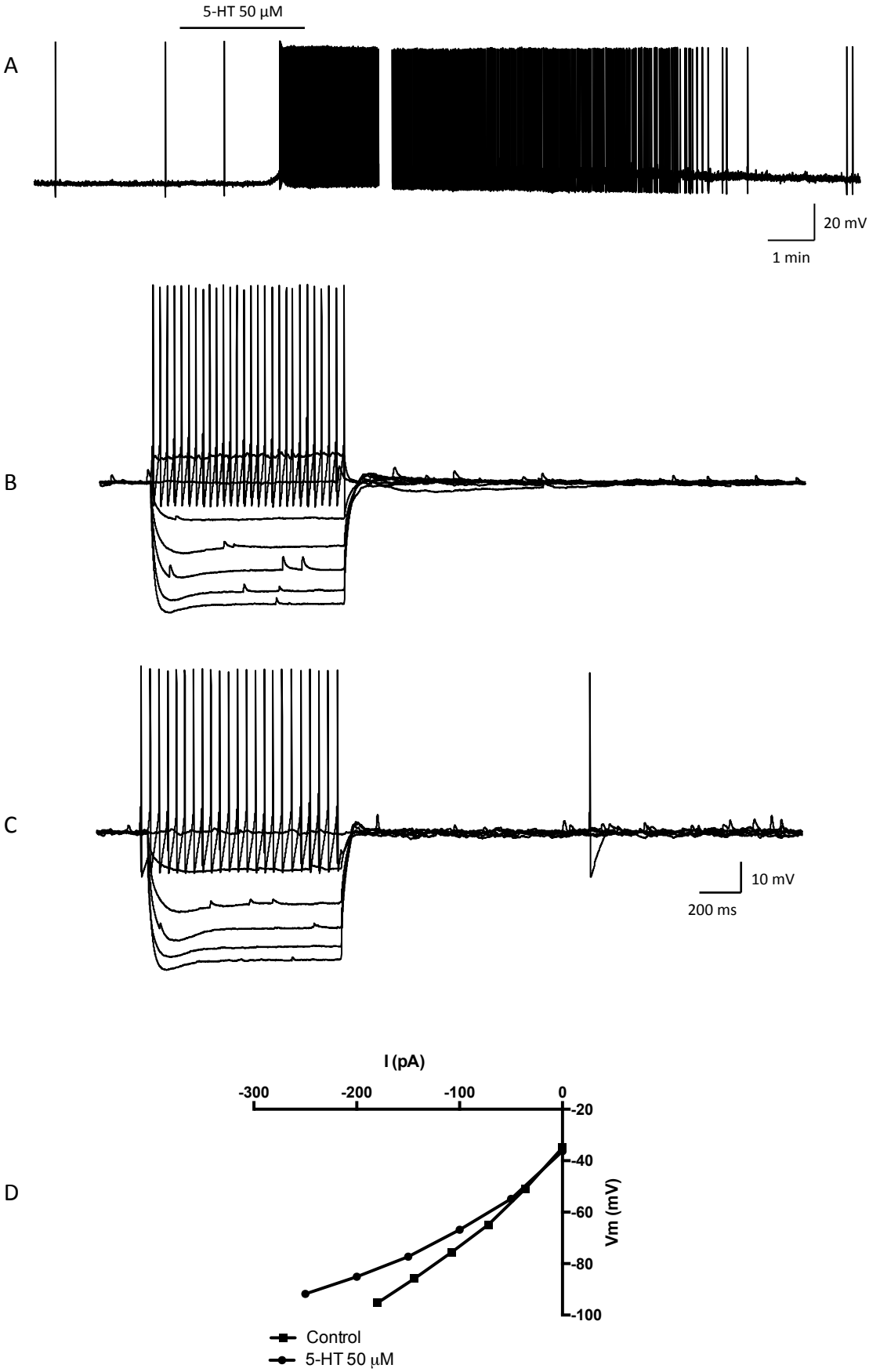
A
5-HT 50 μM
20 mV
1 min
B
C
10 mV
200 ms
D
I (pA)
-300
-200
-100
0
-20
-40
-60
-80
-100
Vm (mV)
Control
5-HT 50 μM

Figure 8.13: Layer 2 fast-spiking interneurons are excited by 5-HT

A: Bath application of 50 μM 5-HT induced a mean membrane depolarization of 6.7 ± 1.8 mV from a mean resting potential of −48.7 ± 1.4 mV to a new steady-state membrane potential of −42.0 ± 1.9 mV (p=0.014; n=6; Paired students t-test).

B: Bath application of 50 μM 5-HT increased action potential firing rate from a mean control basal level of 0.02 ± 0.01 Hz to 1.54 ± 0.90 Hz in the presence of 5-HT (p=0.14; n=6; Paired students t-test).

C: Fast spiking neuron excitation was associated with a reduction in the mean neuronal input resistance from 384 ± 43 MΩ in control conditions to 365 ± 29 MΩ in the presence of 5-HT (p=0.522; Paired students t-test).

Figure 8.13

A

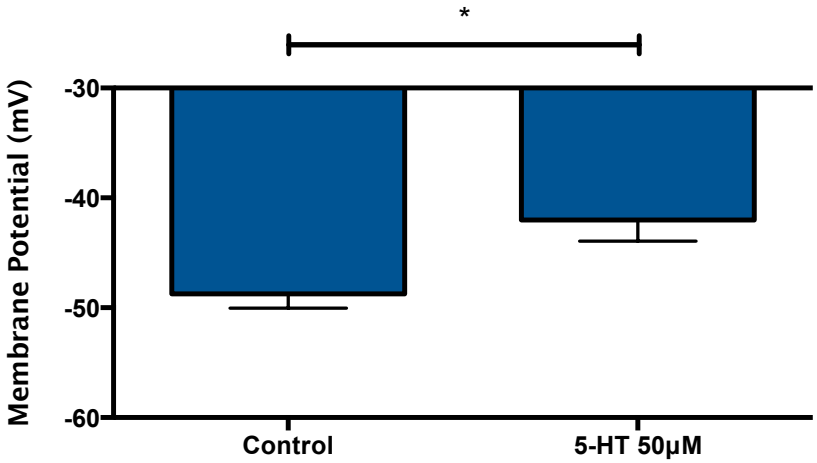

B

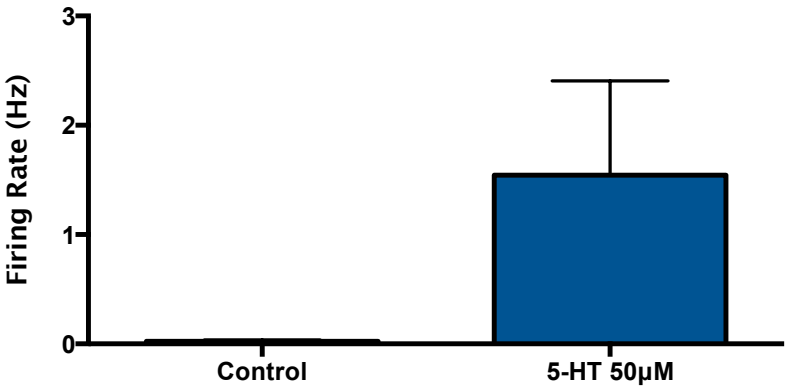

C

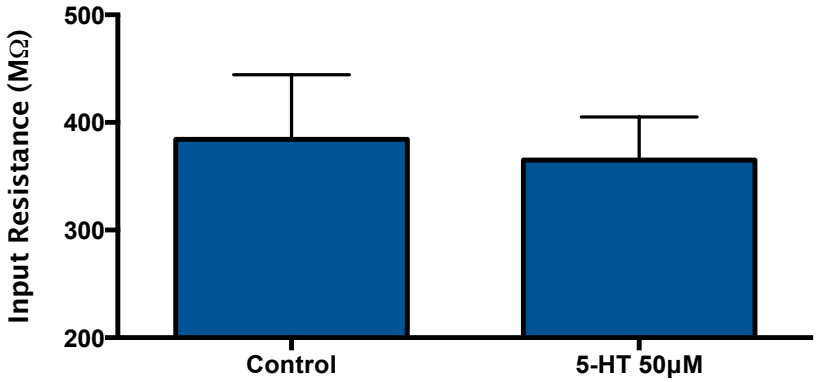

Chapter 9: General Discussion

Multiple, distinct populations of hypothalamic neurons, defined in terms of neuroanatomical location, chemical phenotype, molecular profile and efferent target, are required for the maintenance of normal neurological and physiological function. Work described here investigated the electrophysiological and pharmacological profile of a number of hypothalamic neuronal populations, yielding a deeper and broader understanding of their functional significance. Hypothalamic neurons investigated here include neuropeptide-Y/agouti-related peptide (NPY/AgRP) and proopiomelanocortin / cocaine and amphetamine-regulated transcript (POMC/CART) neurons of the arcuate nucleus of the hypothalamus (ARH), leptin receptor (LepR) and gonadotropin inhibitory hormone (GnIH)-expressing neurons of the dorsomedial hypothalamus (DMH). Also explored in this thesis, are the electrophysiological characteristics of electrotonically-coupled interneurons of the prefrontal cortex (PFC). This latter work focused on neuron and network properties of coupled interneurons. Additionally the sensitivity of these neurons to 5-hydroxytryptamine (5-HT) was investigated, as were the effects of the gap junction blocker carbenoxolone and the novel benzoylamino-benzopyran anticonvulsant compounds Tonabersat and Carabersat.

9.1 An electrophysiological characterization of NPY neurons of the hypothalmic arcuate nucleus *in vitro*

NPY/AgRP neurons of the ARH are known to have an important physiological role in the regulation of food intake, body weight and glucose homeostasis (Aponte et al., 2011, Hahn et al., 1998, Konner et al., 2007, Luquet et al., 2005, Muroya et al., 1999, Takahashi and Cone, 2005). These neurons are sensitive to a number of metabolic signals and secretagogues, including glucose, fatty acids, insulin, leptin and ghrelin. NPY/AgRP neurons compute these peripheral physiological signals, in addition to central afferent neurochemical signals, and generate functional outputs, including driving food intake and influencing energy expenditure (Belgardt et al., 2009, Hahn et al., 1998, Luquet et al., 2005, van den Top et al., 2004, Takahashi and Cone, 2005). Neurosecretion is known to positively correlate with action potential firing frequency, the linearity of this relationship varying between neurons and depends on the transmitter or peptide in question (Brown et al., 2013). Within the *in vivo* context of the melanocortin system, low central glucose and high central orexigen concentrations are known to elevate NPY neuron firing rate, the output of which is NPY GABA and AgRP (Cowley et al., 2001). Ostensibly GABA primarily functions to inhibit POMC neurons whilst AgRP antagonizes MC4Rs at second order neurons. It is this neuronal output that correlates to functional outputs such as elevated food intake and reduced energy expenditure (Cone, 2005). Here multidisciplinary research has demonstrated the physiological effects of neuronal firing frequency fluctuations.

This study represents one of the first electrophysiological characterizations of identified NPY neurons in positive and negative energy states. Previous studies have used the 'blind' whole-cell patch clamp technique to investigate the active

and passive electrophysiological properties of hypothalamic neurons, however these studies have grouped neurons in terms of their neuroanatomical location and/or voltage-sensitive conductance expression, rather that molecular expression profile (Burdakov and Ashcroft, 2002, Armstrong, 1995, Tasker and Dudek, 1991, Stern, 2001, Pennartz et al., 1998, Gonzalez et al., 2012).

This investigation uncovered significant fed-state dependent changes in passive and active membrane properties. NPY neurons of fasted animals, with brain slices incubated in fasted levels of glucose (1 mM), had a significantly shorter mean action potential duration - both when measured from threshold and at action potential half-height – than NPY neurons of fed animals, with brain slices incubated in 1 mM glucose-containing aCSF. A reduced action potential refractory period, resulting from faster action potential kinetics could theoretically increase the upper limits of neuronal firing frequency, and therefore could be a means of influencing neurotransmitter release rate, however this may be unlikely to have any significant effect at the low frequencies observed here. This may be a mechanism by which NPY neurons elevate NPY, AgRP and GABA release in negative energy states.

Action potential firing frequency, membrane potential and input resistance did not show significant state-dependent variation. However this could reflect the small sample size relative to that discussed in Chapter 4 of this thesis.

In these studies, active conductance expression displayed a degree of fed-state-dependent plasticity. Of particular note was the variation in the expression of T-type calcium (I_T), and hyperpolarization-activated non-selective cation (I_H) conductances. I_T was identified most frequently in NPY neurons of fed mice, incubated in 5 mM glucose-containing aCSF, and least frequently observed in

neurons of fasted animals, with brain slices incubated in 1 mM glucose-containing aCSF. Conversely, I_H was identified most frequently in the fasted 1 mM glucose population and least frequently in slices reflecting the fed-state: 5 mM glucose-containing population. Previous studies have linked I_T but not Ih to orexin and ghrelin-induced pacemaker-like activity in arcuate NPY neurons (van den Top et al., 2004). The increased expression of the Ih conductance in negative energy states therefore may have a critical role in generating and patterning activity of NPY neurons in states of hunger and negative energy balance and thus driving increased food intake. As I_T is also implicated in pacemaker-like activity in NPY neurons in fed states and 10mM glucose (van den Top et al., 2004), the functional significance of the differential expression of these conductances depending on energy status is unclear. However, given that the biophysical properties of Ih and I_T and their modes of activation - Ih being hyperpolarization activated versus hyperpolarization-inactivated and depolarization-activated, as seen with T-type conductances - differ, changes in expression of these conductances could significantly modulate electrical excitability and computational capability of neurons and thus modify neurotransmitter release. In relation to this point, NPY/AgRP neuron-derived GABA NPY and AgRP clearly have differences in function and can be differentially released, therefore a relationship between neuron electrical coding and specific chemical release would seem likely (Krashes et al., 2013). Further work would do well to further investigate the relationship between fed state, extracellular glucose and orexigen concentration, upon active conductance expression and the functional significance of Ih and T-type calcium conductances *in vivo* in NPY neurons.

9.2 Energy status-dependent plasticity of arcuate NPY neurons

NPY neurons of the ARH express ATP-sensitive potassium (K_{ATP}) channels, and are sensitive to both glucose and ghrelin (van den Top et al., 2004, van den Top et al., 2007, Willesen et al., 1999, Muroya et al., 1999). To-date NPY neurons have been characterized as exclusively glucose-inhibited, although the fundamental ionic mechanisms underlying this response are unclear. Furthermore, the ability of these neurons to detect changes in extracellular glucose in different physiological states- such as a fasted versus fed, - has never been explored.

In experiments discussed here, the effect of increasing extracellular glucose concentration was investigated on NPY neurons of brain slices obtained from fed and fasted animals. Also investigated were the effects of ghrelin on NPY neurons, using *in vitro* conditions approximating the fed and fasted states found *in vivo*. Action potential firing frequency and neuronal input resistance were significantly elevated in NPY neurons of fed mice, with brain slices incubated in 5 mM glucose – containing aCSF, compared to neurons of fasted mice, with slices incubated in 1 mM glucose-containing aCSF. This is the first report of elevated electrical activity of NPY neurons in positive energy states. Previous *in vitro* work has reported elevated NPY electrical activity in negative energy states, which is possibly due to the use of supraphysiological glucose concentration used in aCSF (Takahashi and Cone, 2005, Burdakov and Gonzalez, 2009). Other work has reported afferent, excitatory PVH neurons to regulate energy-status-dependent NPY/AgRP output (Krashes et al., 2014, Yang et al., 2011). Work described here unequivocally supports the notion that NPY/AgRP neurons are intrinsic energy sensors, with increased system computational power introduced by afferent NPY neuron innervation.

The reduced electrical activity of fasted NPY neurons observed here is likely not representative of *in vivo* activity levels where NPY neurons are driven to higher levels of excitability in fasted hunger states. This most likely reflects the presence of other factors *in vivo*, such as ghrelin. However these data inform us of the manner in which energy status-signals are integrated at the level of the NPY neuron, and the critical role of K_{ATP} channels - open when glucose levels are low and vice-versa. Future work would do well to bear this in mind when designing experiments investigating glucose-sensing neurons.

These experiments also unveiled an increased proportion of glucose responsive (GR) NPY neurons in brain slices of mice fasted for 18-hours prior to culling, relative to the proportion of GR neurons observed in brain slices of animals fed *ad libitum*. This work is the first report of glucose excited (GE) arcuate NPY neurons, which have previously been presumed to be universally glucose inhibited (GI) (Burdakov and Gonzalez, 2009). Fasting increased the proportion of both GE and GI NPY neurons, compared to a fed control, however the greatest degree of plasticity was observed in the GE population. The GE response was mediated via adenosine A_1, A_{2A} and A_3 receptors, and K_{ATP} channel inhibition, whereas the GI response was via the activation of a chloride conductance. These data suggest a physiological role for GE NPY neurons in post-fast refeeding, and future work should focus on the physiological effects of NPY neuron adenosine receptor antagonism. Interestingly, in one neuron tested, K_{ATP} channel antagonism was capable of converting a glucose-induced excitation to a glucose-induced inhibition. This data indicates that there exists a subpopulation of NPY neurons that are both GE and GI competent and can shift depending on fed and glucose status. It also suggests GE can be recruited from both previously non-glucose sensing NPY

populations and from GI populations. The functional significance of this remarkable energy-status-dependent plasticity requires further study to fully understand the functional and physiological significance. *In vivo* pharmacological manipulation of this could be of therapeutic benefit to metabolic disorders.

The excitatory effect of ghrelin on NPY neurons was shown to be a direct post-synaptic action, via K_{ATP} channel inhibition. Ghrelin induces the greatest excitatory effect upon NPY neurons, under fasted, low extracellular glucose conditions. These data suggest that glucose 'sets the gain' for ghrelin at NPY neuron membranes, with low ambient glucose concentrations – as found during fasting conditions – amplifying the orexigenic effects of ghrelin, whilst inevitably reducing the physiological effect of K_{ATP} channel openers, such as leptin and insulin. This data also suggest a synergistic relationship between ghrelin and glucose in certain states of energy balance. For example, following a period of hunger, or fasting when glucose levels are low, an initial spike in glucose levels with food intake may operate synergistically with ghrelin to drive further, excessive food intake to maximize the opportunity to restore energy levels following fasting. This scenario may also be important in excess food intake and increased bodyweight that often follows calorie-restriction based diets. Further work is required to clarify this suggestion.

9.3 The contribution of TCPTP and PTP1B and PI3-kinase to insulin signaling in POMC neurons

POMC neurons of the ARH are sensitive to insulin, yet in obesity, hypothalamic neurons fail to respond accordingly to changes in extracellular insulin (Williams et al., 2010, Spanswick et al., 2000). In arcuate POMC neurons, phosphoinositide 3-

kinase (PI3K)–dependent insulin signal transduction promotes the browning of white adipose tissue (WAT), and elevates energy expenditure (Dodd et al., 2015, Qiu et al., 2014). Inhibition of PI3K-dependent insulin signal transduction by T-cell protein tyrosine phosphatase (TCPTP) is associated with obesity and type-2 diabetes mellitus (T2DM). Conversely, disinhibition of the PI3K pathway - through TCPTP inhibition - is protective against metabolic disease (Zhang et al., 2015, Tiganis, 2013, Dodd et al., 2015, Loh et al., 2011). Hence we investigated the neuronal, electrophysiological mechanisms underlying these physiological phenomena.

Whole-cell patch clamp experiments revealed that of arcuate POMC neurons, insulin-excited, insulin-inhibited, and insulin-insensitive subpopulations exist. Of the insulin-excited POMC subpopulation, a significantly greater insulin-induced membrane depolarization was observed when brain slices were incubated in a TCPTP inhibitor, relative to insulin-induced excitations observed in brain slices incubated in a PI3K inhibitor. These results concur with previous research, and suggest that TCPTP does indeed diminish the extent to which insulin is able to depolarize POMC neurons, and promote energy expenditure. Manipulation of this pathway may be a viable anti-obesity strategy and hence further investigation is of value.

Comparison of the TCPTP inhibitor and control population indicates that TCPTP acts to impede excitatory insulin signal transduction, whilst also promoting the transduction of signals leading to POMC neuron hyperpolarization. A comparison of the control population with the POMC neuron-specific TCPTP knockout group also suggests that TCPTP acts to reduce excitatory signal transduction. Here, unlike the TCPTP inhibitor population, over a third of POMC

neurons remain inhibited by insulin – compared to only around 10% in the inhibitor group. Whether the TCPTP-inhibitor or the TCPTP-knockout is a more appropriate model is yet to be determined. Anomalies could be introduced in either group, resulting from off target-effects of the TCPTP inhibitor, and from compensatory mechanisms arising in the TCPTP knockout mouse model. Future research should look in to this. Finally, when comparing the control population of POMC neurons to those of brain slices pretreated with a PI3K inhibitor, results indicate that PI3K-dependent insulin signaling in POMC neurons, differentially promotes neuron hyperpolarization, over depolarization. This response distribution is remarkably similar to that observed in the TCPTP inhibitor population and the reason for this remains unclear. This result is ostensibly paradoxical, with both inhibition and disinhibition of PI3K-dependent insulin signaling promoting POMC neuron excitation. Of benefit to these experiments would have been independent verification of phosphatase within neurons recorded from in electrophysiological experiments. Future work would do well to use the single-cell polymerase chain reaction (PCR) technique in order to correlate electrophysiological data with a definitive molecular analysis.

9.4 Effects of leptin on leptin receptor-expressing neurons in the dorsomedial hypothalamus

The dorsomedial hypothalamus (DMH) is a hypothalamic nucleus known to exert significant control over energy expenditure, in addition to blood pressure and physiological responses to stress (Horiuchi et al., 2004, Enriori et al., 2011, Guyenet, 2006, Horiuchi et al., 2006). The DMH contains leptin receptor (LepR)-expressing neurons (Enriori et al., 2011). The leptin-induced excitation in 38.2% of

DMH LepR neurons, as observed here, correllates with *in vivo* experiments (not presented here) demonstrating that activation of these neurons using engineered, pharmacologically-selective chimeric ion channels can elevate blood pressure and heart rate, whilst the pharmacological inhibition of these neurons has the opposite effect (Simonds et al., 2014). This hypertensive physiological response to hyperleptinemia underlies the high blood pressure associated with obesity. The evolutionary origin of leptin-induced energy expenditure is easy to explain; it exerts negative feedback upon adipose stores. However the evolutionary origin of the hypertensive effects of leptin are less obvious.

Research outlined here will undoubtedly lead to further work, investigating the cardiovascular effects of DMH leptin signaling, in addition to revealing potential targets for hypertension intervention strategies. Furthermore, subpopulations of leptin receptor-expressing DMN neurons were inhibited by leptin via activation of unidentified potassium channels, similar to previous reports of leptin inhibiting hypothalamic neurons via KATP channels (Spanswick et al., 1997). Further work is required to clarify the physiological role of these DMN neurons.

9.5 Electrophysiological and pharmacological profile of gonadotropin inhibitory hormone-expressing neurons of the rat *in vitro*

Gonadotropin inhibitory hormone (GnIH) exerts a negative tone over the hypothalamic-pituitary-gonadal (HPG) axis. Depending on the species, GnIH inhibits gonadotroph secretion either through release into the hypophyseal blood or at gonadotropin-releasing hormone (GnRH)-expressing neurons (Clarke et al., 2008, Ducret et al., 2009). Stress-induced reproductive dysfunction is associated with elevated GnIH expression (Kirby et al., 2009).

This is the first electrophysiological characterization of GnIH neurons in any animal model. Whole-cell patch clamp experiments demonstrated that GnIH neurons are sensitive to noradrenaline, thyrotropin releasing hormone (TRH), ghrelin and 5-hydroxytryptamine (5-HT). These data indicate that GnIH neurons integrate stress and orexigenic signals, and may be a critical hypothalamic link between stress, reproductive and feeding axes.

These neurons were exclusively excited by TRH, ghrelin and noradrenaline, whilst 5-HT elicited inhibitory, excitatory and biphasic responses. A pharmacological characterization of the contribution of 5-HT receptor subtypes to the 5-HT-induced membrane responses was attempted, however this proved inconclusive at this point. This is likely due to the abundance of 5-HT receptors expressed on these neurons, as reported by Soga et al. (Soga et al., 2010) and the limited number of recordings in the present study. These data suggest that metabolic and orexigenic signals are integrated into the HPG axis, at the level of the GnIH neuron, inevitably influencing physiological function. Further work would do well to determine the physiological significance of noradrenergic and serotonergic GnIH neuron innervation. Some previous work has investigated this, but with insufficient depth and rigor to determine GnIH neuron-specific contributions to reproductive function.

9.6 Electrical synaptic transmission in layer 1 cortical interneurons *in vitro*

Gap-junctions are intercellular channels, conduits allowing the passage of ions and small molecules. The fundamental subunit of the gap-junction is the connexin. A gap-junction plaque is made up of intercellular channels, each channel being

comprised of a dimer of two hemichannels, and each hemichannel is a hexamer of connexin subunits (Harris, 2001). The connexin isoform Cx36 mediates neuron-neuron gap junctional coupling, and forms functional electrical synapses throughout the mammalian central nervous system (CNS) (Rozental et al., 2000).

Interneurons of the mammalian PFC are electrotonically coupled via Cx36-based gap-junctions (Galarreta and Hestrin, 1999, Galarreta and Hestrin, 2001). Aberrant electrotonic coupling is associated with a number of neurological diseases and pathophysiological phenomena including epilepsy, migraine, cortical spreading depression, and glutamatergic excitotoxicity (Bargiotas et al., 2012, de Rivero Vaccari et al., 2007, Durham and Garrett, 2009, Gajda et al., 2005). As such gap-junctions are of interest as a potential therapeutic target for a number of conditions, including epilepsy (Meldrum and Rogawski, 2007). Hence I performed experiments to determine the electrophysiological properties of coupled neurons, and the effects of novel benzoylamino-benzopyran compounds on electrotonic coupling. Additional research focused on the effects of 5-HT on FS neurons of the PFC.

The anti-convulsant benzoylamino-benzopyran compounds tonabersat and carabersat inhibit electrotonic coupling between cortical interneurons, without having significant effects upon neuronal input resistance, implying but not confirming gap-junction-specific actions. These data indicate that these compounds do indeed have, at least in part, a novel antiepileptic mechanism of action via an effect on electrical synapses. Further work investigating the efficacy of these gap-junction blockers, in epilepsy models that more closely mimic the human phenomenon, would be of value.

FS interneurons are sensitive to 5-HT, and are depolarized via the activation of a non-selective cation conductance, consistent with 5-HT_3-receptor activation. As the pharmacological manipulation of the cortical serotonergic system is key to a number of therapeutics including antidepressant and antipsychotic medication, this data may have implications for these fields of research.

9.7 Conclusions and future work

Key findings of studies discussed here amount to a deeper understanding of hypothalamic neuron function. Experimental results presented in this thesis include novel data revealing an energy-status-dependent plasticity within the arcuate NPY neuron population. Additional novel findings presented here include the identification of a subpopulation of GE arcuate NPY neurons, and the identification of a K_{ATP} channel-dependent mechanism of gain control over hormone signal transduction in NPY neurons. This deeper understanding of hypothalamic cell signaling is immediately translational, allowing for the design of pharmacological and lifestyle intervention strategies to curtail obesity.

Other key findings of work presented in this thesis include the quantification of the role of the protein tyrosine phosphatase TCPTP and PI3K-dependent insulin signaling in arcuate POMC neurons. The significance of this work is a deeper understanding of neuronal signal transduction, known to be a key regulator of energy expenditure, which is of particular importance in research focused on combating the global obesity epidemic. Future work should look further into the effects of protein tyrosine phosphatases on central insulin

signaling and body weight management and its potential as a target for diabetes and obesity using diet-induced obese models.

Investigations of LepR neurons of the DMH revealed subpopulations of leptin inhibited and leptin excited neurons. Of leptin-excited neurons, the modulation of a T-type calcium conductance and the induction of oscillatory membrane activity represent novel mechanisms of leptin-induced neuron excitation. This mechanism of excitation is of particular interest, as it provides a potential target for centrally acting hypertensive medication. Future research would do well to pursue this avenue of investigation.

Experiments performed on rat GnIH neurons represent the first electrophysiological characterization of the mammalian GnIH neuron. This work allows us to more accurately contextualize the GnIH neuron within the HPG and HPA axes, in addition to providing us with a deeper appreciation of the integration of neurohormonal signals into the reproductive axis, and vice-versa. Future work should further elucidate the role of GnIH, not only as a reproductive regulator, but also as a central stress and central orexigenic signal.

Investigations of electrotonic coupling in the PFC outline the inhibitory effects of benzoylamino-benzopyran on cortical gap-junctions. This data provides a potential mechanism, underlying the antiepileptic properties of these compounds. Further work should continue to investigate the extent of the pharmaceutical applications of these compounds. Also of note is the excitation of layer 2 FS interneurons by 5-HT, via a non-selective cation conductance. These data allow us to understand cortical network function to a deeper level, and is of particular relevance to psychiatric-disorder research.

Chapter 10: Bibliography

ABASCAL, F. & ZARDOYA, R. 2013. Evolutionary analyses of gap junction protein families. *Biochim Biophys Acta,* 1828**,** 4-14.

AMOSS, M., BURGUS, R., BLACKWELL, R., VALE, W., FELLOWS, R. & GUILLEMIN, R. 1971. Purification, amino acid composition and N-terminus of the hypothalamic luteinizing hormone releasing factor (LRF) of ovine origin. *Biochem Biophys Res Commun,* 44**,** 205-10.

ANAND, B. K. & BROBECK, J. R. 1951. Localization of a "feeding center" in the hypothalamus of the rat. *Proc Soc Exp Biol Med,* 77**,** 323-4.

APONTE, Y., ATASOY, D. & STERNSON, S. M. 2011. AGRP neurons are sufficient to orchestrate feeding behavior rapidly and without training. *Nat Neurosci,* 14**,** 351-5.

ARAGAY, A. M., KATZ, A. & SIMON, M. I. 1992. The G alpha q and G alpha 11 proteins couple the thyrotropin-releasing hormone receptor to phospholipase C in GH3 rat pituitary cells. *J Biol Chem,* 267**,** 24983-8.

ARCUINO, G., LIN, J. H., TAKANO, T., LIU, C., JIANG, L., GAO, Q., KANG, J. & NEDERGAARD, M. 2002. Intercellular calcium signaling mediated by point-source burst release of ATP. *Proc Natl Acad Sci U S A,* 99**,** 9840-5.

ARENDASH, G. W. & GALLO, R. V. 1978. Serotonin involvement in the inhibition of episodic luteinizing hormone release during electrical stimulation of the midbrain dorsal raphe nucleus in ovariectomized rats. *Endocrinology,* 102**,** 1199-206.

ARMSTRONG, W. E. 1995. Morphological and electrophysiological classification of hypothalamic supraoptic neurons. *Prog Neurobiol,* 47**,** 291-339.

ASHCROFT, F. M. 1988. Adenosine 5'-triphosphate-sensitive potassium channels. *Annu Rev Neurosci,* 11**,** 97-118.

ASHCROFT, F. M. 2005. ATP-sensitive potassium channelopathies: focus on insulin secretion. *J Clin Invest,* 115**,** 2047-58.

ASHCROFT, F. M. 2006. K(ATP) channels and insulin secretion: a key role in health and disease. *Biochem Soc Trans,* 34**,** 243-6.

ASHCROFT, F. M. & GRIBBLE, F. M. 2000. New windows on the mechanism of action of K(ATP) channel openers. *Trends Pharmacol Sci,* 21**,** 439-45.

ASHCROFT, F. M., HARRISON, D. E. & ASHCROFT, S. J. 1984. Glucose induces closure of single potassium channels in isolated rat pancreatic beta-cells. *Nature,* 312**,** 446-8.

ASHFORD, M. L., BODEN, P. R. & TREHERNE, J. M. 1990a. Glucose-induced excitation of hypothalamic neurones is mediated by ATP-sensitive K+ channels. *Pflugers Arch,* 415**,** 479-83.

ASHFORD, M. L., BODEN, P. R. & TREHERNE, J. M. 1990b. Tolbutamide excites rat glucoreceptive ventromedial hypothalamic neurones by indirect inhibition of ATP-K+ channels. *Br J Pharmacol,* 101**,** 531-40.

ATASOY, D., BETLEY, J. N., SU, H. H. & STERNSON, S. M. 2012. Deconstruction of a neural circuit for hunger. *Nature,* 488**,** 172-7.

BACKHOLER, K., SMITH, J. T., RAO, A., PEREIRA, A., IQBAL, J., OGAWA, S., LI, Q. & CLARKE, I. J. 2010. Kisspeptin cells in the ewe brain respond to leptin and communicate with neuropeptide Y and proopiomelanocortin cells. *Endocrinology,* 151**,** 2233-43.

BAGNOL, D., LU, X. Y., KAELIN, C. B., DAY, H. E., OLLMANN, M., GANTZ, I., AKIL, H., BARSH, G. S. & WATSON, S. J. 1999. Anatomy of an endogenous antagonist: relationship between Agouti-related protein and proopiomelanocortin in brain. *J Neurosci,* 19**,** RC26.

BANKS, W. A. 2008. The blood-brain barrier as a cause of obesity. *Curr Pharm Des,* 14**,** 1606-14.

BANKS, W. A., KASTIN, A. J., HUANG, W., JASPAN, J. B. & MANESS, L. M. 1996. Leptin enters the brain by a saturable system independent of insulin. *Peptides,* 17**,** 305-11.

BARGIOTAS, P., MUHAMMAD, S., RAHMAN, M., JAKOB, N., TRABOLD, R., FUCHS, E., SCHILLING, L., PLESNILA, N., MONYER, H. & SCHWANINGER, M. 2012. Connexin 36 promotes cortical spreading depolarization and ischemic brain damage. *Brain Res,* 1479**,** 80-5.

BARNES, N. M. N., J.F. 2011. Neuronal 5-HT Receptors and SERT. *Tocris Review,* 34**,** 1-16.

BASTIEN, M., POIRIER, P., LEMIEUX, I. & DESPRES, J. P. 2014. Overview of epidemiology and contribution of obesity to cardiovascular disease. *Prog Cardiovasc Dis,* 56**,** 369-81.

BEAUMONT, M. & MACCAFERRI, G. 2011. Is connexin36 critical for GABAergic hypersynchronization in the hippocampus? *J Physiol,* 589**,** 1663-80.

BEGHI, E. 2016. Addressing the burden of epilepsy: Many unmet needs. *Pharmacol Res,* 107**,** 79-84.

BELANGER, M., ALLAMAN, I. & MAGISTRETTI, P. J. 2011. Brain energy metabolism: focus on astrocyte-neuron metabolic cooperation. *Cell Metab,* 14**,** 724-38.

BELANGER, M. & MAGISTRETTI, P. J. 2009. The role of astroglia in neuroprotection. *Dialogues Clin Neurosci,* 11**,** 281-95.

BELGARDT, B. F., OKAMURA, T. & BRUNING, J. C. 2009. Hormone and glucose signalling in POMC and AgRP neurons. *J Physiol,* 587**,** 5305-14.

BELLINGER, L. L., BERNARDIS, L. L. & MENDEL, V. E. 1976. Effect of ventromedial and dorsomedial hypothalamic lesions on circadian corticosterone rhythms. *Neuroendocrinology,* 22**,** 216-25.

BELLUARDO, N., MUDO, G., TROVATO-SALINARO, A., LE GURUN, S., CHAROLLAIS, A., SERRE-BEINIER, V., AMATO, G., HAEFLIGER, J. A., MEDA, P. & CONDORELLI, D. F. 2000. Expression of connexin36 in the adult and developing rat brain. *Brain Res,* 865**,** 121-38.

BELOUSOV, A. B. & FONTES, J. D. 2013. Neuronal gap junctions: making and breaking connections during development and injury. *Trends Neurosci,* 36**,** 227-36.

BENCE, K. K., DELIBEGOVIC, M., XUE, B., GORGUN, C. Z., HOTAMISLIGIL, G. S., NEEL, B. G. & KAHN, B. B. 2006. Neuronal PTP1B regulates body weight, adiposity and leptin action. *Nat Med,* 12**,** 917-24.

BENNETT, P. A., THOMAS, G. B., HOWARD, A. D., FEIGHNER, S. D., VAN DER PLOEG, L. H., SMITH, R. G. & ROBINSON, I. C. 1997. Hypothalamic growth hormone secretagogue-receptor (GHS-R) expression is regulated by growth hormone in the rat. *Endocrinology,* 138**,** 4552-7.

BENOIT, S. C., AIR, E. L., COOLEN, L. M., STRAUSS, R., JACKMAN, A., CLEGG, D. J., SEELEY, R. J. & WOODS, S. C. 2002. The catabolic action of insulin in the brain is mediated by melanocortins. *J Neurosci,* 22**,** 9048-52.

BERGEN, H. T., MIZUNO, T. M., TAYLOR, J. & MOBBS, C. V. 1998. Hyperphagia and weight gain after gold-thioglucose: relation to hypothalamic neuropeptide Y and proopiomelanocortin. *Endocrinology,* 139**,** 4483-8.
BERNARDIS, L. L. 1972. Hypophagia, hypodipsia and hypoactivity following dorsomedial hypothalamic lesions. *Physiol Behav,* 8**,** 1161-4.
BERRIDGE, C. W. & WATERHOUSE, B. D. 2003. The locus coeruleus-noradrenergic system: modulation of behavioral state and state-dependent cognitive processes. *Brain Res Brain Res Rev,* 42**,** 33-84.
BETLEY, J. N., CAO, Z. F., RITOLA, K. D. & STERNSON, S. M. 2013. Parallel, redundant circuit organization for homeostatic control of feeding behavior. *Cell,* 155**,** 1337-50.
BIKSON, M., ID BIHI, R., VREUGDENHIL, M., KOHLING, R., FOX, J. E. & JEFFERYS, J. G. 2002. Quinine suppresses extracellular potassium transients and ictal epileptiform activity without decreasing neuronal excitability in vitro. *Neuroscience,* 115**,** 251-61.
BILLINGTON, C. J., BRIGGS, J. E., GRACE, M. & LEVINE, A. S. 1991. Effects of intracerebroventricular injection of neuropeptide Y on energy metabolism. *Am J Physiol,* 260**,** R321-7.
BJORBAEK, C., EL-HASCHIMI, K., FRANTZ, J. D. & FLIER, J. S. 1999. The role of SOCS-3 in leptin signaling and leptin resistance. *J Biol Chem,* 274**,** 30059-65.
BLISS, M. 1982. Banting's, Best's, and Collip's accounts of the discovery of insulin. *Bull Hist Med,* 56**,** 554-68.
BLUNDELL, J. E. 1984. Serotonin and appetite. *Neuropharmacology,* 23**,** 1537-51.
BODENDIEK, S. B. & RAMAN, G. 2010. Connexin modulators and their potential targets under the magnifying glass. *Curr Med Chem,* 17**,** 4191-230.
BONAVENTURE, P., ALUISIO, L., SHOBLOCK, J., BOGGS, J. D., FRASER, I. C., LORD, B., LOVENBERG, T. W. & GALICI, R. 2011. Pharmacological blockade of serotonin 5-HT(7) receptor reverses working memory deficits in rats by normalizing cortical glutamate neurotransmission. *PLoS One,* 6**,** e20210.
BORG, W. P., SHERWIN, R. S., DURING, M. J., BORG, M. A. & SHULMAN, G. I. 1995. Local ventromedial hypothalamus glucopenia triggers counterregulatory hormone release. *Diabetes,* 44**,** 180-4.
BOURET, S. G., DRAPER, S. J. & SIMERLY, R. B. 2004. Formation of projection pathways from the arcuate nucleus of the hypothalamus to hypothalamic regions implicated in the neural control of feeding behavior in mice. *J Neurosci,* 24**,** 2797-805.
BRADLEY, D. P., SMITH, M. I., NETSIRI, C., SMITH, J. M., BOCKHORST, K. H., HALL, L. D., HUANG, C. L., LESLIE, R. A., PARSONS, A. A. & JAMES, M. F. 2001. Diffusion-weighted MRI used to detect in vivo modulation of cortical spreading depression: comparison of sumatriptan and tonabersat. *Exp Neurol,* 172**,** 342-53.
BRETON, C. 2013. The hypothalamus-adipose axis is a key target of developmental programming by maternal nutritional manipulation. *J Endocrinol,* 216**,** R19-31.
BROADWELL, R. D. & BRIGHTMAN, M. W. 1976. Entry of peroxidase into neurons of the central and peripheral nervous systems from extracerebral and cerebral blood. *J Comp Neurol,* 166**,** 257-83.
BROBERGER, C., JOHANSEN, J., JOHANSSON, C., SCHALLING, M. & HOKFELT, T. 1998. The neuropeptide Y/agouti gene-related protein (AGRP) brain

circuitry in normal, anorectic, and monosodium glutamate-treated mice. *Proc Natl Acad Sci U S A,* 95**,** 15043-8.
BRODIE, B. B. & SHORE, P. A. 1957. A concept for a role of serotonin and norepinephrine as chemical mediators in the brain. *Ann N Y Acad Sci,* 66**,** 631-42.
BRONSON, F. H. 1986. Food-restricted, prepubertal, female rats: rapid recovery of luteinizing hormone pulsing with excess food, and full recovery of pubertal development with gonadotropin-releasing hormone. *Endocrinology,* 118**,** 2483-7.
BROWN, C. H., BAINS, J. S., LUDWIG, M. & STERN, J. E. 2013. Physiological regulation of magnocellular neurosecretory cell activity: integration of intrinsic, local and afferent mechanisms. *J Neuroendocrinol,* 25**,** 678-710.
BRUINVELS, A. T., LANDWEHRMEYER, B., GUSTAFSON, E. L., DURKIN, M. M., MENGOD, G., BRANCHEK, T. A., HOYER, D. & PALACIOS, J. M. 1994. Localization of 5-HT1B, 5-HT1D alpha, 5-HT1E and 5-HT1F receptor messenger RNA in rodent and primate brain. *Neuropharmacology,* 33**,** 367-86.
BRUNING, J. C., GAUTAM, D., BURKS, D. J., GILLETTE, J., SCHUBERT, M., ORBAN, P. C., KLEIN, R., KRONE, W., MULLER-WIELAND, D. & KAHN, C. R. 2000. Role of brain insulin receptor in control of body weight and reproduction. *Science,* 289**,** 2122-5.
BUKALO, O., CAMPANAC, E., HOFFMAN, D. A. & FIELDS, R. D. 2013. Synaptic plasticity by antidromic firing during hippocampal network oscillations. *Proc Natl Acad Sci U S A,* 110**,** 5175-80.
BUKAUSKAS, F. F. 2012. Neurons and beta-cells of the pancreas express connexin36, forming gap junction channels that exhibit strong cationic selectivity. *J Membr Biol,* 245**,** 243-53.
BUNEMANN, M. & POTT, L. 1995. Down-regulation of A1 adenosine receptors coupled to muscarinic K+ current in cultured guinea-pig atrial myocytes. *J Physiol,* 482 (Pt 1)**,** 81-92.
BURDAKOV, D. & ASHCROFT, F. M. 2002. Cholecystokinin tunes firing of an electrically distinct subset of arcuate nucleus neurons by activating A-Type potassium channels. *J Neurosci,* 22**,** 6380-7.
BURDAKOV, D. & GONZALEZ, J. A. 2009. Physiological functions of glucose-inhibited neurones. *Acta Physiol (Oxf),* 195**,** 71-8.
BUTLER, A. A., KESTERSON, R. A., KHONG, K., CULLEN, M. J., PELLEYMOUNTER, M. A., DEKONING, J., BAETSCHER, M. & CONE, R. D. 2000. A unique metabolic syndrome causes obesity in the melanocortin-3 receptor-deficient mouse. *Endocrinology,* 141**,** 3518-21.
CANABAL, D. D., SONG, Z., POTIAN, J. G., BEUVE, A., MCARDLE, J. J. & ROUTH, V. H. 2007. Glucose, insulin, and leptin signaling pathways modulate nitric oxide synthesis in glucose-inhibited neurons in the ventromedial hypothalamus. *Am J Physiol Regul Integr Comp Physiol,* 292**,** R1418-28.
CAO, W. H. & MORRISON, S. F. 2003. Disinhibition of rostral raphe pallidus neurons increases cardiac sympathetic nerve activity and heart rate. *Brain Res,* 980**,** 1-10.
CARLEN, P. L., SKINNER, F., ZHANG, L., NAUS, C., KUSHNIR, M. & PEREZ VELAZQUEZ, J. L. 2000. The role of gap junctions in seizures. *Brain Res Brain Res Rev,* 32**,** 235-41.

CARRETERO, O. A. & OPARIL, S. 2000. Essential hypertension. Part I: definition and etiology. *Circulation,* 101**,** 329-35.
CHAOULOFF, F., BERTON, O. & MORMEDE, P. 1999. Serotonin and stress. *Neuropsychopharmacology,* 21**,** 28S-32S.
CHEN, H. T., SYLVESTER, P. W., IEIRI, T. & MEITES, J. 1981. Potentiation of luteinizing hormone release by serotonin agonists in ovariectomized steroid-primed rats. *Endocrinology,* 108**,** 948-52.
CHEN, H. Y., TRUMBAUER, M. E., CHEN, A. S., WEINGARTH, D. T., ADAMS, J. R., FRAZIER, E. G., SHEN, Z., MARSH, D. J., FEIGHNER, S. D., GUAN, X. M., YE, Z., NARGUND, R. P., SMITH, R. G., VAN DER PLOEG, L. H., HOWARD, A. D., MACNEIL, D. J. & QIAN, S. 2004. Orexigenic action of peripheral ghrelin is mediated by neuropeptide Y and agouti-related protein. *Endocrinology,* 145**,** 2607-12.
CHENG, G., COOLEN, L. M., PADMANABHAN, V., GOODMAN, R. L. & LEHMAN, M. N. 2010. The kisspeptin/neurokinin B/dynorphin (KNDy) cell population of the arcuate nucleus: sex differences and effects of prenatal testosterone in sheep. *Endocrinology,* 151**,** 301-11.
CHEPKOVA, A. N., SERGEEVA, O. A. & HAAS, H. L. 2008. Carbenoxolone impairs LTP and blocks NMDA receptors in murine hippocampus. *Neuropharmacology,* 55**,** 139-47.
CHOI, Y. H., FUJIKAWA, T., LEE, J., REUTER, A. & KIM, K. W. 2013. Revisiting the Ventral Medial Nucleus of the Hypothalamus: The Roles of SF-1 Neurons in Energy Homeostasis. *Front Neurosci,* 7**,** 71.
CHOU, T. C., SCAMMELL, T. E., GOOLEY, J. J., GAUS, S. E., SAPER, C. B. & LU, J. 2003. Critical role of dorsomedial hypothalamic nucleus in a wide range of behavioral circadian rhythms. *J Neurosci,* 23**,** 10691-702.
CHOUDHURY, A. I., HEFFRON, H., SMITH, M. A., AL-QASSAB, H., XU, A. W., SELMAN, C., SIMMGEN, M., CLEMENTS, M., CLARET, M., MACCOLL, G., BEDFORD, D. C., HISADOME, K., DIAKONOV, I., MOOSAJEE, V., BELL, J. D., SPEAKMAN, J. R., BATTERHAM, R. L., BARSH, G. S., ASHFORD, M. L. & WITHERS, D. J. 2005. The role of insulin receptor substrate 2 in hypothalamic and beta cell function. *J Clin Invest,* 115**,** 940-50.
CHU, Z., GALARRETA, M. & HESTRIN, S. 2003. Synaptic interactions of late-spiking neocortical neurons in layer 1. *J Neurosci,* 23**,** 96-102.
CLARET, M., SMITH, M. A., BATTERHAM, R. L., SELMAN, C., CHOUDHURY, A. I., FRYER, L. G., CLEMENTS, M., AL-QASSAB, H., HEFFRON, H., XU, A. W., SPEAKMAN, J. R., BARSH, G. S., VIOLLET, B., VAULONT, S., ASHFORD, M. L., CARLING, D. & WITHERS, D. J. 2007. AMPK is essential for energy homeostasis regulation and glucose sensing by POMC and AgRP neurons. *J Clin Invest,* 117**,** 2325-36.
CLARK, C. T., WEISSBACH, H. & UDENFRIEND, S. 1954. 5-Hydroxytryptophan decarboxylase: preparation and properties. *J Biol Chem,* 210**,** 139-48.
CLARKE, I. J. 2011. Control of GnRH secretion: one step back. *Front Neuroendocrinol,* 32**,** 367-75.
CLARKE, I. J., SARI, I. P., QI, Y., SMITH, J. T., PARKINGTON, H. C., UBUKA, T., IQBAL, J., LI, Q., TILBROOK, A., MORGAN, K., PAWSON, A. J., TSUTSUI, K., MILLAR, R. P. & BENTLEY, G. E. 2008. Potent action of RFamide-related peptide-3 on pituitary gonadotropes indicative of a hypophysiotropic role in the negative regulation of gonadotropin secretion. *Endocrinology,* 149**,** 5811-21.

COLEMAN, D. L. 1973. Effects of parabiosis of obese with diabetes and normal mice. *Diabetologia,* 9**,** 294-8.
COLEMAN, D. L. 1978. Obese and diabetes: two mutant genes causing diabetes-obesity syndromes in mice. *Diabetologia,* 14**,** 141-8.
CONDORELLI, D. F., PARENTI, R., SPINELLA, F., TROVATO SALINARO, A., BELLUARDO, N., CARDILE, V. & CICIRATA, F. 1998. Cloning of a new gap junction gene (Cx36) highly expressed in mammalian brain neurons. *Eur J Neurosci,* 10**,** 1202-8.
CONE, R. D. 2005. Anatomy and regulation of the central melanocortin system. *Nat Neurosci,* 8**,** 571-8.
CONNORS, B. W. 2012. Tales of a dirty drug: carbenoxolone, gap junctions, and seizures. *Epilepsy Curr,* 12**,** 66-8.
CONSIDINE, R. V., SINHA, M. K., HEIMAN, M. L., KRIAUCIUNAS, A., STEPHENS, T. W., NYCE, M. R., OHANNESIAN, J. P., MARCO, C. C., MCKEE, L. J., BAUER, T. L. & ET AL. 1996. Serum immunoreactive-leptin concentrations in normal-weight and obese humans. *N Engl J Med,* 334**,** 292-5.
COOLEN, L. M., PETERS, H. J. & VEENING, J. G. 1996. Fos immunoreactivity in the rat brain following consummatory elements of sexual behavior: a sex comparison. *Brain Res,* 738**,** 67-82.
COPPOLA, A., LIU, Z. W., ANDREWS, Z. B., PARADIS, E., ROY, M. C., FRIEDMAN, J. M., RICQUIER, D., RICHARD, D., HORVATH, T. L., GAO, X. B. & DIANO, S. 2007. A central thermogenic-like mechanism in feeding regulation: an interplay between arcuate nucleus T3 and UCP2. *Cell Metab,* 5**,** 21-33.
CORNIL, C. A., STEVENSON, T. J. & BALL, G. F. 2009. Are rapid changes in gonadal testosterone release involved in the fast modulation of brain estrogen effects? *Gen Comp Endocrinol,* 163**,** 298-305.
COTECCHIA, S., SCHEER, A., DIVIANI, D., FANELLI, F. & DE BENEDETTI, P. G. 1998. Molecular mechanisms involved in the activation and regulation of the alpha 1-adrenergic receptor subtypes. *Farmaco,* 53**,** 273-7.
COWLEY, M. A., CONE, R., ENRIORI, P., LOUISELLE, I., WILLIAMS, S. M. & EVANS, A. E. 2003. Electrophysiological actions of peripheral hormones on melanocortin neurons. *Ann N Y Acad Sci,* 994**,** 175-86.
COWLEY, M. A., SMART, J. L., RUBINSTEIN, M., CERDAN, M. G., DIANO, S., HORVATH, T. L., CONE, R. D. & LOW, M. J. 2001. Leptin activates anorexigenic POMC neurons through a neural network in the arcuate nucleus. *Nature,* 411**,** 480-4.
CUMMINGS, D. E., PURNELL, J. Q., FRAYO, R. S., SCHMIDOVA, K., WISSE, B. E. & WEIGLE, D. S. 2001. A preprandial rise in plasma ghrelin levels suggests a role in meal initiation in humans. *Diabetes,* 50**,** 1714-9.
CUTLER, J. A. 1996. High blood pressure and end-organ damage. *J Hypertens Suppl,* 14**,** S3-6.
DA SILVA, A. A., KUO, J. J. & HALL, J. E. 2004. Role of hypothalamic melanocortin 3/4-receptors in mediating chronic cardiovascular, renal, and metabolic actions of leptin. *Hypertension,* 43**,** 1312-7.
DA SILVA, A. A., TALLAM, L. S., LIU, J. & HALL, J. E. 2006. Chronic antidiabetic and cardiovascular actions of leptin: role of CNS and increased adrenergic activity. *Am J Physiol Regul Integr Comp Physiol,* 291**,** R1275-82.
DAHLOF, C. G., HAUGE, A. W. & OLESEN, J. 2009. Efficacy and safety of tonabersat, a gap-junction modulator, in the acute treatment of migraine: a double-blind, parallel-group, randomized study. *Cephalalgia,* 29 Suppl 2**,** 7-16.

DAHLSTROM, A. & FUXE, K. 1964. Evidence for the Existence of Monoamine-Containing Neurons in the Central Nervous System. I. Demonstration of Monoamines in the Cell Bodies of Brain Stem Neurons. *Acta Physiol Scand Suppl*, SUPPL 232:1-55.

DAMODARAM, S., THALAKOTI, S., FREEMAN, S. E., GARRETT, F. G. & DURHAM, P. L. 2009. Tonabersat inhibits trigeminal ganglion neuronal-satellite glial cell signaling. *Headache,* 49, 5-20.

DAVIS, P. J., GOGLIA, F. & LEONARD, J. L. 2016. Nongenomic actions of thyroid hormone. *Nat Rev Endocrinol,* 12, 111-21.

DAY, H. E., CAMPEAU, S., WATSON, S. J., JR. & AKIL, H. 1997. Distribution of alpha 1a-, alpha 1b- and alpha 1d-adrenergic receptor mRNA in the rat brain and spinal cord. *J Chem Neuroanat,* 13, 115-39.

DBOUK, H. A., MROUE, R. M., EL-SABBAN, M. E. & TALHOUK, R. S. 2009. Connexins: a myriad of functions extending beyond assembly of gap junction channels. *Cell Commun Signal,* 7, 4.

DE JONG, T. R., PATTIJ, T., VEENING, J. G., DEDEREN, P. J., WALDINGER, M. D., COOLS, A. R. & OLIVIER, B. 2005. Citalopram combined with WAY 100635 inhibits ejaculation and ejaculation-related Fos immunoreactivity. *Eur J Pharmacol,* 509, 49-59.

DE RIVERO VACCARI, J. C., CORRIVEAU, R. A. & BELOUSOV, A. B. 2007. Gap junctions are required for NMDA receptor dependent cell death in developing neurons. *J Neurophysiol,* 98, 2878-86.

DE ROUX, N., GENIN, E., CAREL, J. C., MATSUDA, F., CHAUSSAIN, J. L. & MILGROM, E. 2003. Hypogonadotropic hypogonadism due to loss of function of the KiSS1-derived peptide receptor GPR54. *Proc Natl Acad Sci U S A,* 100, 10972-6.

DEBONS, A. F., SICLARI, E., DAS, K. C. & FUHR, B. 1982. Gold thioglucose-induced hypothalamic damage, hyperphagia, and obesity: dependence on the adrenal gland. *Endocrinology,* 110, 2024-9.

DEL CORSSO, C., IGLESIAS, R., ZOIDL, G., DERMIETZEL, R. & SPRAY, D. C. 2012. Calmodulin dependent protein kinase increases conductance at gap junctions formed by the neuronal gap junction protein connexin36. *Brain Res,* 1487, 69-77.

DELVILLE, Y., SULON, J., HENDRICK, J. C. & BALTHAZART, J. 1984. Effect of the presence of females on the pituitary-testicular activity in male Japanese quail (Coturnix coturnix japonica). *Gen Comp Endocrinol,* 55, 295-305.

DERKACH, V., SURPRENANT, A. & NORTH, R. A. 1989. 5-HT3 receptors are membrane ion channels. *Nature,* 339, 706-9.

DESBUQUOIS, B., TOZZO, E., COLLINET, M., LOPEZ, S., BORTOLI, S. & AMESSOU, M. 1993. [Regulation of insulin receptor expression and its gene]. *Ann Endocrinol (Paris),* 54, 373-84.

DICKEN, M. S., TOOKER, R. E. & HENTGES, S. T. 2012. Regulation of GABA and glutamate release from proopiomelanocortin neuron terminals in intact hypothalamic networks. *J Neurosci,* 32, 4042-8.

DIXON, J. B. 2010. The effect of obesity on health outcomes. *Mol Cell Endocrinol,* 316, 104-8.

DODD, G. T., DECHERF, S., LOH, K., SIMONDS, S. E., WIEDE, F., BALLAND, E., MERRY, T. L., MUNZBERG, H., ZHANG, Z. Y., KAHN, B. B., NEEL, B. G., BENCE, K. K., ANDREWS, Z. B., COWLEY, M. A. & TIGANIS, T. 2015. Leptin and insulin act on POMC neurons to promote the browning of white fat. *Cell,* 160, 88-104.

DONNELLY, P. J. & DAILEY, R. A. 1991. Effects of dopamine, norepinephrine and serotonin on secretion of luteinizing hormone, follicle-stimulating hormone and prolactin in ovariectomized, pituitary stalk-transected ewes. *Domest Anim Endocrinol,* 8**,** 87-98.

DORNONVILLE DE LA COUR, C., BJORKQVIST, M., SANDVIK, A. K., BAKKE, I., ZHAO, C. M., CHEN, D. & HAKANSON, R. 2001. A-like cells in the rat stomach contain ghrelin and do not operate under gastrin control. *Regul Pept,* 99**,** 141-50.

DOSLIKOVA, B., GARFIELD, A. S., SHAW, J., EVANS, M. L., BURDAKOV, D., BILLUPS, B. & HEISLER, L. K. 2013. 5-HT2C receptor agonist anorectic efficacy potentiated by 5-HT1B receptor agonist coapplication: an effect mediated via increased proportion of pro-opiomelanocortin neurons activated. *J Neurosci,* 33**,** 9800-4.

DUBEY, A. K. & PLANT, T. M. 1985. A suppression of gonadotropin secretion by cortisol in castrated male rhesus monkeys (Macaca mulatta) mediated by the interruption of hypothalamic gonadotropin-releasing hormone release. *Biol Reprod,* 33**,** 423-31.

DUCRET, E., ANDERSON, G. M. & HERBISON, A. E. 2009. RFamide-related peptide-3, a mammalian gonadotropin-inhibitory hormone ortholog, regulates gonadotropin-releasing hormone neuron firing in the mouse. *Endocrinology,* 150**,** 2799-804.

DUNWIDDIE, T. V. & MASINO, S. A. 2001. The role and regulation of adenosine in the central nervous system. *Annu Rev Neurosci,* 24**,** 31-55.

DURHAM, P. L. & GARRETT, F. G. 2009. Neurological mechanisms of migraine: potential of the gap-junction modulator tonabersat in prevention of migraine. *Cephalalgia,* 29 Suppl 2**,** 1-6.

DWORAKOWSKA, B. & DOLOWY, K. 2000. Ion channels-related diseases. *Acta Biochim Pol,* 47**,** 685-703.

EBENEZER, I. S. 1990. The effect of intracerebroventricular administration of baclofen on food intake in rats. *Neuroreport,* 1**,** 73-6.

ECWG 2006. Eshre Capri Workshop Group: Nutrition and reproduction in women. *Hum Reprod Update,* 12**,** 193-207.

ELIAS, C. F., LEE, C., KELLY, J., ASCHKENASI, C., AHIMA, R. S., COUCEYRO, P. R., KUHAR, M. J., SAPER, C. B. & ELMQUIST, J. K. 1998. Leptin activates hypothalamic CART neurons projecting to the spinal cord. *Neuron,* 21**,** 1375-85.

ELMQUIST, J. K., AHIMA, R. S., ELIAS, C. F., FLIER, J. S. & SAPER, C. B. 1998. Leptin activates distinct projections from the dorsomedial and ventromedial hypothalamic nuclei. *Proc Natl Acad Sci U S A,* 95**,** 741-6.

ENRIORI, P. J., EVANS, A. E., SINNAYAH, P., JOBST, E. E., TONELLI-LEMOS, L., BILLES, S. K., GLAVAS, M. M., GRAYSON, B. E., PERELLO, M., NILLNI, E. A., GROVE, K. L. & COWLEY, M. A. 2007. Diet-induced obesity causes severe but reversible leptin resistance in arcuate melanocortin neurons. *Cell Metab,* 5**,** 181-94.

ENRIORI, P. J., SINNAYAH, P., SIMONDS, S. E., GARCIA RUDAZ, C. & COWLEY, M. A. 2011. Leptin action in the dorsomedial hypothalamus increases sympathetic tone to brown adipose tissue in spite of systemic leptin resistance. *J Neurosci,* 31**,** 12189-97.

ERDHEIM, J. 1904. Ueber Plattengeschwulste der Hypophysengegend. *Ztschr. j. Augenb.,* 16**,** 530.

FEKETE, C., LEGRADI, G., MIHALY, E., HUANG, Q. H., TATRO, J. B., RAND, W. M., EMERSON, C. H. & LECHAN, R. M. 2000. alpha-Melanocyte-stimulating hormone is contained in nerve terminals innervating thyrotropin-releasing hormone-synthesizing neurons in the hypothalamic paraventricular nucleus and prevents fasting-induced suppression of prothyrotropin-releasing hormone gene expression. *J Neurosci,* 20**,** 1550-8.

FEREZOU, I., CAULI, B., HILL, E. L., ROSSIER, J., HAMEL, E. & LAMBOLEZ, B. 2002. 5-HT3 receptors mediate serotonergic fast synaptic excitation of neocortical vasoactive intestinal peptide/cholecystokinin interneurons. *J Neurosci,* 22**,** 7389-97.

FERNANDEZ-FERNANDEZ, R., TENA-SEMPERE, M., AGUILAR, E. & PINILLA, L. 2004. Ghrelin effects on gonadotropin secretion in male and female rats. *Neurosci Lett,* 362**,** 103-7.

FERNSTROM, J. D. & FERNSTROM, M. H. 2007. Tyrosine, phenylalanine, and catecholamine synthesis and function in the brain. *J Nutr,* 137**,** 1539S-1547S; discussion 1548S.

FINK, G., DOW, R. C., MCQUEEN, J. K., BENNIE, J. G. & CARROLL, S. M. 1999. Serotonergic 5-HT2A receptors important for the oestradiol-induced surge of luteinising hormone-releasing hormone in the rat. *J Neuroendocrinol,* 11**,** 63-9.

FINKELSTEIN, E. A., KHAVJOU, O. A., THOMPSON, H., TROGDON, J. G., PAN, L., SHERRY, B. & DIETZ, W. 2012. Obesity and severe obesity forecasts through 2030. *Am J Prev Med,* 42**,** 563-70.

FINKELSTEIN, E. A., TROGDON, J. G., COHEN, J. W. & DIETZ, W. 2009. Annual medical spending attributable to obesity: payer-and service-specific estimates. *Health Aff (Millwood),* 28**,** w822-31.

FIORAMONTI, X., CONTIE, S., SONG, Z., ROUTH, V. H., LORSIGNOL, A. & PENICAUD, L. 2007. Characterization of glucosensing neuron subpopulations in the arcuate nucleus: integration in neuropeptide Y and pro-opio melanocortin networks? *Diabetes,* 56**,** 1219-27.

FIORAMONTI, X., LORSIGNOL, A., TAUPIGNON, A. & PENICAUD, L. 2004. A new ATP-sensitive K+ channel-independent mechanism is involved in glucose-excited neurons of mouse arcuate nucleus. *Diabetes,* 53**,** 2767-75.

FOOTE, C. I., ZHOU, L., ZHU, X. & NICHOLSON, B. J. 1998. The pattern of disulfide linkages in the extracellular loop regions of connexin 32 suggests a model for the docking interface of gap junctions. *J Cell Biol,* 140**,** 1187-97.

FORADORI, C. D., COOLEN, L. M., FITZGERALD, M. E., SKINNER, D. C., GOODMAN, R. L. & LEHMAN, M. N. 2002. Colocalization of progesterone receptors in parvicellular dynorphin neurons of the ovine preoptic area and hypothalamus. *Endocrinology,* 143**,** 4366-74.

FREDHOLM, B. B., ABBRACCHIO, M. P., BURNSTOCK, G., DALY, J. W., HARDEN, T. K., JACOBSON, K. A., LEFF, P. & WILLIAMS, M. 1994. Nomenclature and classification of purinoceptors. *Pharmacol Rev,* 46**,** 143-56.

FRÖHLICH, A. 1901. Ein Fall von Tumor des Hypophysis cerebri ohne Akromegalie. *Wien. Klin,* 15**,** 906.

FRUHBECK, G. 2006. Intracellular signalling pathways activated by leptin. *Biochem J,* 393**,** 7-20.

FU, L. Y. & VAN DEN POL, A. N. 2010. Kisspeptin directly excites anorexigenic proopiomelanocortin neurons but inhibits orexigenic neuropeptide Y cells by an indirect synaptic mechanism. *J Neurosci,* 30**,** 10205-19.

FUKUDA, T. & KOSAKA, T. 2000. Gap junctions linking the dendritic network of GABAergic interneurons in the hippocampus. *J Neurosci,* 20**,** 1519-28.
FUKUDA, T. & KOSAKA, T. 2003. Ultrastructural study of gap junctions between dendrites of parvalbumin-containing GABAergic neurons in various neocortical areas of the adult rat. *Neuroscience,* 120**,** 5-20.
FURNEY, S. J., ALBA, M. M. & LOPEZ-BIGAS, N. 2006. Differences in the evolutionary history of disease genes affected by dominant or recessive mutations. *BMC Genomics,* 7**,** 165.
GAJDA, Z., SZUPERA, Z., BLAZSO, G. & SZENTE, M. 2005. Quinine, a blocker of neuronal cx36 channels, suppresses seizure activity in rat neocortex in vivo. *Epilepsia,* 46**,** 1581-91.
GALARRETA, M. & HESTRIN, S. 1999. A network of fast-spiking cells in the neocortex connected by electrical synapses. *Nature,* 402**,** 72-5.
GALARRETA, M. & HESTRIN, S. 2001. Electrical synapses between GABA-releasing interneurons. *Nat Rev Neurosci,* 2**,** 425-33.
GALARRETA, M. & HESTRIN, S. 2002. Electrical and chemical synapses among parvalbumin fast-spiking GABAergic interneurons in adult mouse neocortex. *Proc Natl Acad Sci U S A,* 99**,** 12438-43.
GALIC, S., KLINGLER-HOFFMANN, M., FODERO-TAVOLETTI, M. T., PURYER, M. A., MENG, T. C., TONKS, N. K. & TIGANIS, T. 2003. Regulation of insulin receptor signaling by the protein tyrosine phosphatase TCPTP. *Mol Cell Biol,* 23**,** 2096-108.
GALLO, R. V. 1981. Effect of electrical stimulation of the dorsomedial hypothalamic nucleus on pulsatile LH release in ovariectomized rats. *Neuroendocrinology,* 32**,** 134-8.
GAUTRON, L., LAZARUS, M., SCOTT, M. M., SAPER, C. B. & ELMQUIST, J. K. 2010. Identifying the efferent projections of leptin-responsive neurons in the dorsomedial hypothalamus using a novel conditional tracing approach. *J Comp Neurol,* 518**,** 2090-108.
GAVI, S., SHUMAY, E., WANG, H. Y. & MALBON, C. C. 2006. G-protein-coupled receptors and tyrosine kinases: crossroads in cell signaling and regulation. *Trends Endocrinol Metab,* 17**,** 48-54.
GEARING, M. & TERASAWA, E. 1991. The alpha-1-adrenergic neuronal system is involved in the pulsatile release of luteinizing hormone-releasing hormone in the ovariectomized female rhesus monkey. *Neuroendocrinology,* 53**,** 373-81.
GELLING, R. W., MORTON, G. J., MORRISON, C. D., NISWENDER, K. D., MYERS, M. G., JR., RHODES, C. J. & SCHWARTZ, M. W. 2006. Insulin action in the brain contributes to glucose lowering during insulin treatment of diabetes. *Cell Metab,* 3**,** 67-73.
GERAGHTY, A. C., MUROY, S. E., ZHAO, S., BENTLEY, G. E., KRIEGSFELD, L. J. & KAUFER, D. 2015. Knockdown of hypothalamic RFRP3 prevents chronic stress-induced infertility and embryo resorption. *Elife,* 4.
GERSHENGORN, M. C. & OSMAN, R. 1996. Molecular and cellular biology of thyrotropin-releasing hormone receptors. *Physiol Rev,* 76**,** 175-91.
GHAMARI-LANGROUDI, M., VELLA, K. R., SRISAI, D., SUGRUE, M. L., HOLLENBERG, A. N. & CONE, R. D. 2010. Regulation of thyrotropin-releasing hormone-expressing neurons in paraventricular nucleus of the hypothalamus by signals of adiposity. *Mol Endocrinol,* 24**,** 2366-81.

GOADSBY, P. J., FERRARI, M. D., CSANYI, A., OLESEN, J., MILLS, J. G. & TONABERSAT, T. O. N. S. G. 2009. Randomized, double-blind, placebo-controlled, proof-of-concept study of the cortical spreading depression inhibiting agent tonabersat in migraine prophylaxis. *Cephalalgia,* 29**,** 742-50.

GOLDSTEIN, B. J. 2002. Protein-tyrosine phosphatases: emerging targets for therapeutic intervention in type 2 diabetes and related states of insulin resistance. *J Clin Endocrinol Metab,* 87**,** 2474-80.

GONZALEZ, J. A., JENSEN, L. T., FUGGER, L. & BURDAKOV, D. 2012. Convergent inputs from electrically and topographically distinct orexin cells to locus coeruleus and ventral tegmental area. *Eur J Neurosci,* 35**,** 1426-32.

GONZALEZ-NIETO, D., GOMEZ-HERNANDEZ, J. M., LARROSA, B., GUTIERREZ, C., MUNOZ, M. D., FASCIANI, I., O'BRIEN, J., ZAPPALA, A., CICIRATA, F. & BARRIO, L. C. 2008. Regulation of neuronal connexin-36 channels by pH. *Proc Natl Acad Sci U S A,* 105**,** 17169-74.

GOPEL, S. O., KANNO, T., BARG, S. & RORSMAN, P. 2000a. Patch-clamp characterisation of somatostatin-secreting -cells in intact mouse pancreatic islets. *J Physiol,* 528**,** 497-507.

GOPEL, S. O., KANNO, T., BARG, S., WENG, X. G., GROMADA, J. & RORSMAN, P. 2000b. Regulation of glucagon release in mouse -cells by KATP channels and inactivation of TTX-sensitive Na+ channels. *J Physiol,* 528**,** 509-20.

GORE, A. C. & TERASAWA, E. 2001. Neural circuits regulating pulsatile luteinizing hormone release in the female guinea-pig: opioid, adrenergic and serotonergic interactions. *J Neuroendocrinol,* 13**,** 239-48.

GOULD, G. W., THOMAS, H. M., JESS, T. J. & BELL, G. I. 1991. Expression of human glucose transporters in Xenopus oocytes: kinetic characterization and substrate specificities of the erythrocyte, liver, and brain isoforms. *Biochemistry,* 30**,** 5139-45.

GRAY, D. S. & FUJIOKA, K. 1991. Use of relative weight and Body Mass Index for the determination of adiposity. *J Clin Epidemiol,* 44**,** 545-50.

GRIBBLE, F. M., WILLIAMS, L., SIMPSON, A. K. & REIMANN, F. 2003. A novel glucose-sensing mechanism contributing to glucagon-like peptide-1 secretion from the GLUTag cell line. *Diabetes,* 52**,** 1147-54.

GU, J. G., FOGA, I. O., PARKINSON, F. E. & GEIGER, J. D. 1995. Involvement of bidirectional adenosine transporters in the release of L-[3H]adenosine from rat brain synaptosomal preparations. *J Neurochem,* 64**,** 2105-10.

GUAN, X., WILSON, S., SCHLENDER, K. K. & RUCH, R. J. 1996. Gap-junction disassembly and connexin 43 dephosphorylation induced by 18 beta-glycyrrhetinic acid. *Mol Carcinog,* 16**,** 157-64.

GUAN, X. M., YU, H., PALYHA, O. C., MCKEE, K. K., FEIGHNER, S. D., SIRINATHSINGHJI, D. J., SMITH, R. G., VAN DER PLOEG, L. H. & HOWARD, A. D. 1997. Distribution of mRNA encoding the growth hormone secretagogue receptor in brain and peripheral tissues. *Brain Res Mol Brain Res,* 48**,** 23-9.

GUYENET, P. G. 2006. The sympathetic control of blood pressure. *Nat Rev Neurosci,* 7**,** 335-46.

HAGAN, M. M., RUSHING, P. A., SCHWARTZ, M. W., YAGALOFF, K. A., BURN, P., WOODS, S. C. & SEELEY, R. J. 1999. Role of the CNS melanocortin system in the response to overfeeding. *J Neurosci,* 19**,** 2362-7.

HAHN, T. M., BREININGER, J. F., BASKIN, D. G. & SCHWARTZ, M. W. 1998. Coexpression of Agrp and NPY in fasting-activated hypothalamic neurons. *Nat Neurosci,* 1**,** 271-2.

HAN, S. K., GOTTSCH, M. L., LEE, K. J., POPA, S. M., SMITH, J. T., JAKAWICH, S. K., CLIFTON, D. K., STEINER, R. A. & HERBISON, A. E. 2005. Activation of gonadotropin-releasing hormone neurons by kisspeptin as a neuroendocrine switch for the onset of puberty. *J Neurosci,* 25**,** 11349-56.
HARRIS, A. L. 2001. Emerging issues of connexin channels: biophysics fills the gap. *Q Rev Biophys,* 34**,** 325-472.
HARVEY, J., MCKAY, N. G., WALKER, K. S., VAN DER KAAY, J., DOWNES, C. P. & ASHFORD, M. L. 2000. Essential role of phosphoinositide 3-kinase in leptin-induced K(ATP) channel activation in the rat CRI-G1 insulinoma cell line. *J Biol Chem,* 275**,** 4660-9.
HASKELL-LUEVANO, C., CHEN, P., LI, C., CHANG, K., SMITH, M. S., CAMERON, J. L. & CONE, R. D. 1999. Characterization of the neuroanatomical distribution of agouti-related protein immunoreactivity in the rhesus monkey and the rat. *Endocrinology,* 140**,** 1408-15.
HAUGE, A. W., ASGHAR, M. S., SCHYTZ, H. W., CHRISTENSEN, K. & OLESEN, J. 2009. Effects of tonabersat on migraine with aura: a randomised, double-blind, placebo-controlled crossover study. *Lancet Neurol,* 8**,** 718-23.
HEAULME, M. & DRAY, F. 1984. Noradrenaline and prostaglandin E2 stimulate LH-RH release from rat median eminence through distinct 1-alpha-adrenergic and PGE2 receptors. *Neuroendocrinology,* 39**,** 403-7.
HEDLUND, P. B. 2009. The 5-HT7 receptor and disorders of the nervous system: an overview. *Psychopharmacology (Berl),* 206**,** 345-54.
HEIN, L. 2006. Adrenoceptors and signal transduction in neurons. *Cell Tissue Res,* 326**,** 541-51.
HELMCHEN, F., SVOBODA, K., DENK, W. & TANK, D. W. 1999. In vivo dendritic calcium dynamics in deep-layer cortical pyramidal neurons. *Nat Neurosci,* 2**,** 989-96.
HENTGES, S. T., OTERO-CORCHON, V., PENNOCK, R. L., KING, C. M. & LOW, M. J. 2009. Proopiomelanocortin expression in both GABA and glutamate neurons. *J Neurosci,* 29**,** 13684-90.
HERDON, H. J., JERMAN, J. C., STEAN, T. O., MIDDLEMISS, D. N., CHAN, W. N., VONG, A. K., EVANS, J. M., THOMPSON, M. & UPTON, N. 1997. Characterization of the binding of [3H]-SB-204269, a radiolabelled form of the new anticonvulsant SB-204269, to a novel binding site in rat brain membranes. *Br J Pharmacol,* 121**,** 1687-91.
HERNANDEZ-SANCHEZ, C., BASILE, A. S., FEDOROVA, I., ARIMA, H., STANNARD, B., FERNANDEZ, A. M., ITO, Y. & LEROITH, D. 2001. Mice transgenically overexpressing sulfonylurea receptor 1 in forebrain resist seizure induction and excitotoxic neuron death. *Proc Natl Acad Sci U S A,* 98**,** 3549-54.
HERVE, J. C. 2002. Non-genomic effects of steroid hormones on membrane channels. *Mini Rev Med Chem,* 2**,** 411-7.
HERY, M., LAPLANTE, E. & KORDON, C. 1976. Participation of serotonin in the phasic release of LH. I. Evidence from pharmacological experiments. *Endocrinology,* 99**,** 496-503.
HETHERINGTON, A. W. A. R., S. W. 1940. Hypothalamic lesions and adiposity in the rat. *The Anatomical Record,* 78**,** 149–172.
HEURTEAUX, C., LAURITZEN, I., WIDMANN, C. & LAZDUNSKI, M. 1995. Essential role of adenosine, adenosine A1 receptors, and ATP-sensitive K+ channels in cerebral ischemic preconditioning. *Proc Natl Acad Sci U S A,* 92**,** 4666-70.

HIBINO, H., INANOBE, A., FURUTANI, K., MURAKAMI, S., FINDLAY, I. & KURACHI, Y. 2010. Inwardly rectifying potassium channels: their structure, function, and physiological roles. *Physiol Rev,* 90**,** 291-366.

HILEMAN, S. M., PIERROZ, D. D., MASUZAKI, H., BJORBAEK, C., EL-HASCHIMI, K., BANKS, W. A. & FLIER, J. S. 2002. Characterizaton of short isoforms of the leptin receptor in rat cerebral microvessels and of brain uptake of leptin in mouse models of obesity. *Endocrinology,* 143**,** 775-83.

HOFFMAN, R. P. 2007. Sympathetic mechanisms of hypoglycemic counterregulation. *Curr Diabetes Rev,* 3**,** 185-93.

HORIUCHI, J., MCALLEN, R. M., ALLEN, A. M., KILLINGER, S., FONTES, M. A. & DAMPNEY, R. A. 2004. Descending vasomotor pathways from the dorsomedial hypothalamic nucleus: role of medullary raphe and RVLM. *Am J Physiol Regul Integr Comp Physiol,* 287**,** R824-32.

HORIUCHI, J., MCDOWALL, L. M. & DAMPNEY, R. A. 2006. Differential control of cardiac and sympathetic vasomotor activity from the dorsomedial hypothalamus. *Clin Exp Pharmacol Physiol,* 33**,** 1265-8.

HORVATH, T. L., BECHMANN, I., NAFTOLIN, F., KALRA, S. P. & LERANTH, C. 1997. Heterogeneity in the neuropeptide Y-containing neurons of the rat arcuate nucleus: GABAergic and non-GABAergic subpopulations. *Brain Res,* 756**,** 283-6.

HOSNY, S. & JENNES, L. 1998. Identification of alpha1B adrenergic receptor protein in gonadotropin releasing hormone neurones of the female rat. *J Neuroendocrinol,* 10**,** 687-92.

HSIEH, K. P. & MARTIN, T. F. 1992. Thyrotropin-releasing hormone and gonadotropin-releasing hormone receptors activate phospholipase C by coupling to the guanosine triphosphate-binding proteins Gq and G11. *Mol Endocrinol,* 6**,** 1673-81.

HURLEY, P. T., MCMAHON, R. A., FANNING, P., O'BOYLE, K. M., ROGERS, M. & MARTIN, F. 1998. Functional coupling of a recombinant human 5-HT5A receptor to G-proteins in HEK-293 cells. *Br J Pharmacol,* 124**,** 1238-44.

HUSZAR, D., LYNCH, C. A., FAIRCHILD-HUNTRESS, V., DUNMORE, J. H., FANG, Q., BERKEMEIER, L. R., GU, W., KESTERSON, R. A., BOSTON, B. A., CONE, R. D., SMITH, F. J., CAMPFIELD, L. A., BURN, P. & LEE, F. 1997. Targeted disruption of the melanocortin-4 receptor results in obesity in mice. *Cell,* 88**,** 131-41.

IBARRA-SANCHEZ, M. J., WAGNER, J., ONG, M. T., LAMPRON, C. & TREMBLAY, M. L. 2001. Murine embryonic fibroblasts lacking TC-PTP display delayed G1 phase through defective NF-kappaB activation. *Oncogene,* 20**,** 4728-39.

IBRAHIM, N., BOSCH, M. A., SMART, J. L., QIU, J., RUBINSTEIN, M., RONNEKLEIV, O. K., LOW, M. J. & KELLY, M. J. 2003. Hypothalamic proopiomelanocortin neurons are glucose responsive and express K(ATP) channels. *Endocrinology,* 144**,** 1331-40.

IFESCN 1974. A glossary of terms most commonly used by clinical electroencephalographers. *Electroencephalogr Clin Neurophysiol,* 37**,** 538-48.

INAGAKI, N., GONOI, T., CLEMENT, J. P. T., NAMBA, N., INAZAWA, J., GONZALEZ, G., AGUILAR-BRYAN, L., SEINO, S. & BRYAN, J. 1995. Reconstitution of IKATP: an inward rectifier subunit plus the sulfonylurea receptor. *Science,* 270**,** 1166-70.

INGALLS, A. M., DICKIE, M. M. & SNELL, G. D. 1950. Obese, a new mutation in the house mouse. *J Hered,* 41**,** 317-8.

INGLEFIELD, J. R., SCHWARZKOPF, S. B. & KELLOGG, C. K. 1994. Alterations in behavioral responses to stressors following excitotoxin lesions of dorsomedial hypothalamic regions. *Brain Res,* 633**,** 151-61.
IRWIG, M. S., FRALEY, G. S., SMITH, J. T., ACOHIDO, B. V., POPA, S. M., CUNNINGHAM, M. J., GOTTSCH, M. L., CLIFTON, D. K. & STEINER, R. A. 2004. Kisspeptin activation of gonadotropin releasing hormone neurons and regulation of KiSS-1 mRNA in the male rat. *Neuroendocrinology,* 80**,** 264-72.
ISHIBASHI, H., UMEZU, M., JANG, I. S., ITO, Y. & AKAIKE, N. 2003. Alpha 1-adrenoceptor-activated cation currents in neurones acutely isolated from rat cardiac parasympathetic ganglia. *J Physiol,* 548**,** 111-20.
JACOBI, J. S., COLEMAN, H. A., ENRIORI, P. J., PARKINGTON, H. C., LI, Q., PEREIRA, A., COWLEY, M. A. & CLARKE, I. J. 2013. Paradoxical effect of gonadotrophin-inhibiting hormone to negatively regulate neuropeptide Y neurones in mouse arcuate nucleus. *J Neuroendocrinol,* 25**,** 1308-17.
JACOBSON, G. M., VOSS, L. J., MELIN, S. M., MASON, J. P., CURSONS, R. T., STEYN-ROSS, D. A., STEYN-ROSS, M. L. & SLEIGH, J. W. 2010. Connexin36 knockout mice display increased sensitivity to pentylenetetrazol-induced seizure-like behaviors. *Brain Res,* 1360**,** 198-204.
JACOBY, A., SNAPE, D. & BAKER, G. A. 2005. Epilepsy and social identity: the stigma of a chronic neurological disorder. *Lancet Neurol,* 4**,** 171-8.
JOHNSON, M. A., TSUTSUI, K. & FRALEY, G. S. 2007. Rat RFamide-related peptide-3 stimulates GH secretion, inhibits LH secretion, and has variable effects on sex behavior in the adult male rat. *Horm Behav,* 51**,** 171-80.
JOHNSON, M. D. & CROWLEY, W. R. 1986. Role of central serotonin systems in the stimulatory effects of ovarian hormones and naloxone on luteinizing hormone release in female rats. *Endocrinology,* 118**,** 1180-6.
JORDAN, S. D., KONNER, A. C. & BRUNING, J. C. 2010. Sensing the fuels: glucose and lipid signaling in the CNS controlling energy homeostasis. *Cell Mol Life Sci,* 67**,** 3255-73.
JUSZCZAK, G. R. & SWIERGIEL, A. H. 2009. Properties of gap junction blockers and their behavioural, cognitive and electrophysiological effects: animal and human studies. *Prog Neuropsychopharmacol Biol Psychiatry,* 33**,** 181-98.
KALSBEEK, A., DRIJFHOUT, W. J., WESTERINK, B. H., VAN HEERIKHUIZE, J. J., VAN DER WOUDE, T. P., VAN DER VLIET, J. & BUIJS, R. M. 1996. GABA receptors in the region of the dorsomedial hypothalamus of rats are implicated in the control of melatonin and corticosterone release. *Neuroendocrinology,* 63**,** 69-78.
KANG, Y. M., OUYANG, W., CHEN, J. Y., QIAO, J. T. & DAFNY, N. 2000. Norepinephrine modulates single hypothalamic arcuate neurons via alpha(1)and beta adrenergic receptors. *Brain Res,* 869**,** 146-57.
KANTROWITZ, J. T., FRANCIS, N. N., SALAH, A. & PERKINS, K. L. 2005. Synaptic depolarizing GABA Response in adults is excitatory and proconvulsive when GABAB receptors are blocked. *J Neurophysiol,* 93**,** 2656-67.
KARSCHIN, A., BROCKHAUS, J. & BALLANYI, K. 1998. KATP channel formation by the sulphonylurea receptors SUR1 with Kir6.2 subunits in rat dorsal vagal neurons in situ. *J Physiol,* 509 (Pt 2)**,** 339-46.
KEIM, S. R. & SHEKHAR, A. 1996. The effects of GABAA receptor blockade in the dorsomedial hypothalamic nucleus on corticotrophin (ACTH) and corticosterone secretion in male rats. *Brain Res,* 739**,** 46-51.

KELLEY, S. P., BRATT, A. M. & HODGE, C. W. 2003. Targeted gene deletion of the 5-HT3A receptor subunit produces an anxiolytic phenotype in mice. *Eur J Pharmacol,* 461**,** 19-25.
KELLY, T., YANG, W., CHEN, C. S., REYNOLDS, K. & HE, J. 2008. Global burden of obesity in 2005 and projections to 2030. *Int J Obes (Lond),* 32**,** 1431-7.
KHAN, F. A., GOFORTH, P. B., ZHANG, M. & SATIN, L. S. 2001. Insulin activates ATP-sensitive K(+) channels in pancreatic beta-cells through a phosphatidylinositol 3-kinase-dependent pathway. *Diabetes,* 50**,** 2192-8.
KIEVIT, P., HOWARD, J. K., BADMAN, M. K., BALTHASAR, N., COPPARI, R., MORI, H., LEE, C. E., ELMQUIST, J. K., YOSHIMURA, A. & FLIER, J. S. 2006. Enhanced leptin sensitivity and improved glucose homeostasis in mice lacking suppressor of cytokine signaling-3 in POMC-expressing cells. *Cell Metab,* 4**,** 123-32.
KIRBY, E. D., GERAGHTY, A. C., UBUKA, T., BENTLEY, G. E. & KAUFER, D. 2009. Stress increases putative gonadotropin inhibitory hormone and decreases luteinizing hormone in male rats. *Proc Natl Acad Sci U S A,* 106**,** 11324-9.
KISHI, T., ASCHKENASI, C. J., LEE, C. E., MOUNTJOY, K. G., SAPER, C. B. & ELMQUIST, J. K. 2003. Expression of melanocortin 4 receptor mRNA in the central nervous system of the rat. *J Comp Neurol,* 457**,** 213-35.
KLEPPISCH, T. & NELSON, M. T. 1995. Adenosine activates ATP-sensitive potassium channels in arterial myocytes via A2 receptors and cAMP-dependent protein kinase. *Proc Natl Acad Sci U S A,* 92**,** 12441-5.
KLINGER, M., FREISSMUTH, M. & NANOFF, C. 2002. Adenosine receptors: G protein-mediated signalling and the role of accessory proteins. *Cell Signal,* 14**,** 99-108.
KNOWLES, J. R. 1980. Enzyme-catalyzed phosphoryl transfer reactions. *Annu Rev Biochem,* 49**,** 877-919.
KONG, D., DAGON, Y., CAMPBELL, J. N., GUO, Y., YANG, Z., YI, X., ARYAL, P., WELLENSTEIN, K., KAHN, B. B., SABATINI, B. L. & LOWELL, B. B. 2016. A Postsynaptic AMPK-->p21-Activated Kinase Pathway Drives Fasting-Induced Synaptic Plasticity in AgRP Neurons. *Neuron,* 91**,** 25-33.
KONNER, A. C., JANOSCHEK, R., PLUM, L., JORDAN, S. D., ROTHER, E., MA, X., XU, C., ENRIORI, P., HAMPEL, B., BARSH, G. S., KAHN, C. R., COWLEY, M. A., ASHCROFT, F. M. & BRUNING, J. C. 2007. Insulin action in AgRP-expressing neurons is required for suppression of hepatic glucose production. *Cell Metab,* 5**,** 438-49.
KOSAKA, T., DEANS, M. R., PAUL, D. L. & KOSAKA, K. 2005. Neuronal gap junctions in the mouse main olfactory bulb: morphological analyses on transgenic mice. *Neuroscience,* 134**,** 757-69.
KOSHIMIZU, T. A., TANOUE, A. & TSUJIMOTO, G. 2007. Clinical implications from studies of alpha1 adrenergic receptor knockout mice. *Biochem Pharmacol,* 73**,** 1107-12.
KRAJEWSKA, M., BANARES, S., ZHANG, E. E., HUANG, X., SCADENG, M., JHALA, U. S., FENG, G. S. & KRAJEWSKI, S. 2008. Development of diabesity in mice with neuronal deletion of Shp2 tyrosine phosphatase. *Am J Pathol,* 172**,** 1312-24.
KRASHES, M. J., KODA, S., YE, C., ROGAN, S. C., ADAMS, A. C., CUSHER, D. S., MARATOS-FLIER, E., ROTH, B. L. & LOWELL, B. B. 2011. Rapid, reversible activation of AgRP neurons drives feeding behavior in mice. *J Clin Invest,* 121**,** 1424-8.

KRASHES, M. J., SHAH, B. P., KODA, S. & LOWELL, B. B. 2013. Rapid versus delayed stimulation of feeding by the endogenously released AgRP neuron mediators GABA, NPY, and AgRP. *Cell Metab,* 18**,** 588-95.

KRASHES, M. J., SHAH, B. P., MADARA, J. C., OLSON, D. P., STROCHLIC, D. E., GARFIELD, A. S., VONG, L., PEI, H., WATABE-UCHIDA, M., UCHIDA, N., LIBERLES, S. D. & LOWELL, B. B. 2014. An excitatory paraventricular nucleus to AgRP neuron circuit that drives hunger. *Nature,* 507**,** 238-42.

KUBOTA, N., TERAUCHI, Y., TOBE, K., YANO, W., SUZUKI, R., UEKI, K., TAKAMOTO, I., SATOH, H., MAKI, T., KUBOTA, T., MOROI, M., OKADA-IWABU, M., EZAKI, O., NAGAI, R., UETA, Y., KADOWAKI, T. & NODA, T. 2004. Insulin receptor substrate 2 plays a crucial role in beta cells and the hypothalamus. *J Clin Invest,* 114**,** 917-27.

KURATA, H. T., PHILLIPS, L. R., ROSE, T., LOUSSOUARN, G., HERLITZE, S., FRITZENSCHAFT, H., ENKVETCHAKUL, D., NICHOLS, C. G. & BAUKROWITZ, T. 2004. Molecular basis of inward rectification: polyamine interaction sites located by combined channel and ligand mutagenesis. *J Gen Physiol,* 124**,** 541-54.

KWEKKEBOOM, D. J., DE JONG, F. H. & LAMBERTS, S. W. 1989. Gonadotropin release by clinically nonfunctioning and gonadotroph pituitary adenomas in vivo and in vitro: relation to sex and effects of thyrotropin-releasing hormone, gonadotropin-releasing hormone, and bromocriptine. *J Clin Endocrinol Metab,* 68**,** 1128-35.

LAM, T. K. 2010. Neuronal regulation of homeostasis by nutrient sensing. *Nat Med,* 16**,** 392-5.

LAMBE, E. K. & AGHAJANIAN, G. K. 2001. The role of Kv1.2-containing potassium channels in serotonin-induced glutamate release from thalamocortical terminals in rat frontal cortex. *J Neurosci,* 21**,** 9955-63.

LAMBERTS, S. W., VERLEUN, T., OOSTEROM, R., HOFLAND, L., VAN GINKEL, L. A., LOEBER, J. G., VAN VROONHOVEN, C. C., STEFANKO, S. Z. & DE JONG, F. H. 1987. The effects of bromocriptine, thyrotropin-releasing hormone, and gonadotropin-releasing hormone on hormone secretion by gonadotropin-secreting pituitary adenomas in vivo and in vitro. *J Clin Endocrinol Metab,* 64**,** 524-30.

LAMSA, K. & KAILA, K. 1997. Ionic mechanisms of spontaneous GABAergic events in rat hippocampal slices exposed to 4-aminopyridine. *J Neurophysiol,* 78**,** 2582-91.

LARKUM, M. E. & ZHU, J. J. 2002. Signaling of layer 1 and whisker-evoked Ca2+ and Na+ action potentials in distal and terminal dendrites of rat neocortical pyramidal neurons in vitro and in vivo. *J Neurosci,* 22**,** 6991-7005.

LATINI, S. & PEDATA, F. 2001. Adenosine in the central nervous system: release mechanisms and extracellular concentrations. *J Neurochem,* 79**,** 463-84.

LAUF, U., GIEPMANS, B. N., LOPEZ, P., BRACONNOT, S., CHEN, S. C. & FALK, M. M. 2002. Dynamic trafficking and delivery of connexons to the plasma membrane and accretion to gap junctions in living cells. *Proc Natl Acad Sci U S A,* 99**,** 10446-51.

LEBRETHON, M. C., AGANINA, A., FOURNIER, M., GERARD, A., PARENT, A. S. & BOURGUIGNON, J. P. 2007. Effects of in vivo and in vitro administration of ghrelin, leptin and neuropeptide mediators on pulsatile gonadotrophin-releasing hormone secretion from male rat hypothalamus before and after puberty. *J Neuroendocrinol,* 19**,** 181-8.

LECHAN, R. M. & FEKETE, C. 2006. The TRH neuron: a hypothalamic integrator of energy metabolism. *Prog Brain Res,* 153**,** 209-35.
LEE, S. C., PATRICK, S. L., RICHARDSON, K. A. & CONNORS, B. W. 2014. Two functionally distinct networks of gap junction-coupled inhibitory neurons in the thalamic reticular nucleus. *J Neurosci,* 34**,** 13170-82.
LEE, S. J., VERMA, S., SIMONDS, S. E., KIRIGITI, M. A., KIEVIT, P., LINDSLEY, S. R., LOCHE, A., SMITH, M. S., COWLEY, M. A. & GROVE, K. L. 2013. Leptin stimulates neuropeptide Y and cocaine amphetamine-regulated transcript coexpressing neuronal activity in the dorsomedial hypothalamus in diet-induced obese mice. *J Neurosci,* 33**,** 15306-17.
LEIBOWITZ, S. F., SLADEK, C., SPENCER, L. & TEMPEL, D. 1988. Neuropeptide Y, epinephrine and norepinephrine in the paraventricular nucleus: stimulation of feeding and the release of corticosterone, vasopressin and glucose. *Brain Res Bull,* 21**,** 905-12.
LEINNINGER, G. M., JO, Y. H., LESHAN, R. L., LOUIS, G. W., YANG, H., BARRERA, J. G., WILSON, H., OPLAND, D. M., FAOUZI, M. A., GONG, Y., JONES, J. C., RHODES, C. J., CHUA, S., JR., DIANO, S., HORVATH, T. L., SEELEY, R. J., BECKER, J. B., MUNZBERG, H. & MYERS, M. G., JR. 2009. Leptin acts via leptin receptor-expressing lateral hypothalamic neurons to modulate the mesolimbic dopamine system and suppress feeding. *Cell Metab,* 10**,** 89-98.
LEZNIK, E. & LLINAS, R. 2005. Role of gap junctions in synchronized neuronal oscillations in the inferior olive. *J Neurophysiol,* 94**,** 2447-56.
LIEBEN, C. K., BLOKLAND, A., SIK, A., SUNG, E., VAN NIEUWENHUIZEN, P. & SCHREIBER, R. 2005. The selective 5-HT6 receptor antagonist Ro4368554 restores memory performance in cholinergic and serotonergic models of memory deficiency in the rat. *Neuropsychopharmacology,* 30**,** 2169-79.
LLEWELLYN-SMITH, I. J., MINSON, J. B., WRIGHT, A. P. & HODGSON, A. J. 1990. Cholera toxin B-gold, a retrograde tracer that can be used in light and electron microscopic immunocytochemical studies. *J Comp Neurol,* 294**,** 179-91.
LLINAS, R. R., LEZNIK, E. & URBANO, F. J. 2002. Temporal binding via cortical coincidence detection of specific and nonspecific thalamocortical inputs: a voltage-dependent dye-imaging study in mouse brain slices. *Proc Natl Acad Sci U S A,* 99**,** 449-54.
LOGAN, S. D., PICKERING, A. E., GIBSON, I. C., NOLAN, M. F. & SPANSWICK, D. 1996. Electrotonic coupling between rat sympathetic preganglionic neurones in vitro. *J Physiol,* 495 (Pt 2)**,** 491-502.
LOH, K., FUKUSHIMA, A., ZHANG, X., GALIC, S., BRIGGS, D., ENRIORI, P. J., SIMONDS, S., WIEDE, F., REICHENBACH, A., HAUSER, C., SIMS, N. A., BENCE, K. K., ZHANG, S., ZHANG, Z. Y., KAHN, B. B., NEEL, B. G., ANDREWS, Z. B., COWLEY, M. A. & TIGANIS, T. 2011. Elevated hypothalamic TCPTP in obesity contributes to cellular leptin resistance. *Cell Metab,* 14**,** 684-99.
LONG, M. A., JUTRAS, M. J., CONNORS, B. W. & BURWELL, R. D. 2005. Electrical synapses coordinate activity in the suprachiasmatic nucleus. *Nat Neurosci,* 8**,** 61-6.
LOPEZ, M., LAGE, R., SAHA, A. K., PEREZ-TILVE, D., VAZQUEZ, M. J., VARELA, L., SANGIAO-ALVARELLOS, S., TOVAR, S., RAGHAY, K., RODRIGUEZ-CUENCA, S., DEOLIVEIRA, R. M., CASTANEDA, T., DATTA, R., DONG, J. Z., CULLER, M., SLEEMAN, M. W., ALVAREZ, C. V., GALLEGO, R., LELLIOTT, C. J., CARLING, D.,

TSCHOP, M. H., DIEGUEZ, C. & VIDAL-PUIG, A. 2008. Hypothalamic fatty acid metabolism mediates the orexigenic action of ghrelin. *Cell Metab,* 7**,** 389-99.
LOWRY, C. A., BURKE, K. A., RENNER, K. J., MOORE, F. L. & ORCHINIK, M. 2001. Rapid changes in monoamine levels following administration of corticotropin-releasing factor or corticosterone are localized in the dorsomedial hypothalamus. *Horm Behav,* 39**,** 195-205.
LUFT, F. C. 1998. Molecular genetics of human hypertension. *J Hypertens,* 16**,** 1871-8.
LUQUET, S., PEREZ, F. A., HNASKO, T. S. & PALMITER, R. D. 2005. NPY/AgRP neurons are essential for feeding in adult mice but can be ablated in neonates. *Science,* 310**,** 683-5.
LYNCH, C. O., JR., JOHNSON, M. D. & CROWLEY, W. R. 1984. Effects of the serotonin agonist, quipazine, on luteinizing hormone and prolactin release: evidence for serotonin-catecholamine interactions. *Life Sci,* 35**,** 1481-7.
MA, Y., HIOKI, H., KONNO, M., PAN, S., NAKAMURA, H., NAKAMURA, K. C., FURUTA, T., LI, J. L. & KANEKO, T. 2011. Expression of gap junction protein connexin36 in multiple subtypes of GABAergic neurons in adult rat somatosensory cortex. *Cereb Cortex,* 21**,** 2639-49.
MACCAFERRI, G. & MCBAIN, C. J. 1996. The hyperpolarization-activated current (Ih) and its contribution to pacemaker activity in rat CA1 hippocampal stratum oriens-alveus interneurones. *J Physiol,* 497 (Pt 1)**,** 119-30.
MAEDA, S., NAKAGAWA, S., SUGA, M., YAMASHITA, E., OSHIMA, A., FUJIYOSHI, Y. & TSUKIHARA, T. 2009. Structure of the connexin 26 gap junction channel at 3.5 A resolution. *Nature,* 458**,** 597-602.
MAFFEI, M., HALAAS, J., RAVUSSIN, E., PRATLEY, R. E., LEE, G. H., ZHANG, Y., FEI, H., KIM, S., LALLONE, R., RANGANATHAN, S. & ET AL. 1995. Leptin levels in human and rodent: measurement of plasma leptin and ob RNA in obese and weight-reduced subjects. *Nat Med,* 1**,** 1155-61.
MAGISTRETTI, P. J., PELLERIN, L., ROTHMAN, D. L. & SHULMAN, R. G. 1999. Energy on demand. *Science,* 283**,** 496-7.
MARKS, J. L., PORTE, D., JR., STAHL, W. L. & BASKIN, D. G. 1990. Localization of insulin receptor mRNA in rat brain by in situ hybridization. *Endocrinology,* 127**,** 3234-6.
MARTIN-RUIZ, R., PUIG, M. V., CELADA, P., SHAPIRO, D. A., ROTH, B. L., MENGOD, G. & ARTIGAS, F. 2001. Control of serotonergic function in medial prefrontal cortex by serotonin-2A receptors through a glutamate-dependent mechanism. *J Neurosci,* 21**,** 9856-66.
MATSUO, H., BABA, Y., NAIR, R. M., ARIMURA, A. & SCHALLY, A. V. 1971. Structure of the porcine LH- and FSH-releasing hormone. I. The proposed amino acid sequence. *Biochem Biophys Res Commun,* 43**,** 1334-9.
MATTHES, H., BOSCHERT, U., AMLAIKY, N., GRAILHE, R., PLASSAT, J. L., MUSCATELLI, F., MATTEI, M. G. & HEN, R. 1993. Mouse 5-hydroxytryptamine5A and 5-hydroxytryptamine5B receptors define a new family of serotonin receptors: cloning, functional expression, and chromosomal localization. *Mol Pharmacol,* 43**,** 313-9.
MCCONN, B., WANG, G., YI, J., GILBERT, E. R., OSUGI, T., UBUKA, T., TSUTSUI, K., CHOWDHURY, V. S., FURUSE, M. & CLINE, M. A. 2014. Gonadotropin-inhibitory hormone-stimulation of food intake is mediated by hypothalamic effects in chicks. *Neuropeptides,* 48**,** 327-34.

MCCORMICK, D. A. & PAPE, H. C. 1990. Properties of a hyperpolarization-activated cation current and its role in rhythmic oscillation in thalamic relay neurones. *J Physiol,* 431**,** 291-318.
MCCRIMMON, R. 2009. Glucose sensing during hypoglycemia: lessons from the lab. *Diabetes Care,* 32**,** 1357-63.
MCNAY, E. C. & GOLD, P. E. 1999. Extracellular glucose concentrations in the rat hippocampus measured by zero-net-flux: effects of microdialysis flow rate, strain, and age. *J Neurochem,* 72**,** 785-90.
MEECH, R. W. 1978. Calcium-dependent potassium activation in nervous tissues. *Annu Rev Biophys Bioeng,* 7**,** 1-18.
MEIER, C. & DERMIETZEL, R. 2006. Electrical synapses--gap junctions in the brain. *Results Probl Cell Differ,* 43**,** 99-128.
MELDRUM, B. S. & ROGAWSKI, M. A. 2007. Molecular targets for antiepileptic drug development. *Neurotherapeutics,* 4**,** 18-61.
MERGENTHALER, P., LINDAUER, U., DIENEL, G. A. & MEISEL, A. 2013. Sugar for the brain: the role of glucose in physiological and pathological brain function. *Trends Neurosci,* 36**,** 587-97.
MERMELSTEIN, P. G., SONG, W. J., TKATCH, T., YAN, Z. & SURMEIER, D. J. 1998. Inwardly rectifying potassium (IRK) currents are correlated with IRK subunit expression in rat nucleus accumbens medium spiny neurons. *J Neurosci,* 18**,** 6650-61.
MESAROS, A., KORALOV, S. B., ROTHER, E., WUNDERLICH, F. T., ERNST, M. B., BARSH, G. S., RAJEWSKY, K. & BRUNING, J. C. 2008. Activation of Stat3 signaling in AgRP neurons promotes locomotor activity. *Cell Metab,* 7**,** 236-48.
MESSAGER, S., CHATZIDAKI, E. E., MA, D., HENDRICK, A. G., ZAHN, D., DIXON, J., THRESHER, R. R., MALINGE, I., LOMET, D., CARLTON, M. B., COLLEDGE, W. H., CARATY, A. & APARICIO, S. A. 2005. Kisspeptin directly stimulates gonadotropin-releasing hormone release via G protein-coupled receptor 54. *Proc Natl Acad Sci U S A,* 102**,** 1761-6.
MIHAYLOVA, M. M. & SHAW, R. J. 2011. The AMPK signalling pathway coordinates cell growth, autophagy and metabolism. *Nat Cell Biol,* 13**,** 1016-23.
MIKI, T., LISS, B., MINAMI, K., SHIUCHI, T., SARAYA, A., KASHIMA, Y., HORIUCHI, M., ASHCROFT, F., MINOKOSHI, Y., ROEPER, J. & SEINO, S. 2001. ATP-sensitive K+ channels in the hypothalamus are essential for the maintenance of glucose homeostasis. *Nat Neurosci,* 4**,** 507-12.
MIKI, T., NAGASHIMA, K. & SEINO, S. 1999. The structure and function of the ATP-sensitive K+ channel in insulin-secreting pancreatic beta-cells. *J Mol Endocrinol,* 22**,** 113-23.
MILLINGTON, G. W. 2007. The role of proopiomelanocortin (POMC) neurones in feeding behaviour. *Nutr Metab (Lond),* 4**,** 18.
MINOKOSHI, Y., ALQUIER, T., FURUKAWA, N., KIM, Y. B., LEE, A., XUE, B., MU, J., FOUFELLE, F., FERRE, P., BIRNBAUM, M. J., STUCK, B. J. & KAHN, B. B. 2004. AMP-kinase regulates food intake by responding to hormonal and nutrient signals in the hypothalamus. *Nature,* 428**,** 569-74.
MINOKOSHI, Y., HAQUE, M. S. & SHIMAZU, T. 1999. Microinjection of leptin into the ventromedial hypothalamus increases glucose uptake in peripheral tissues in rats. *Diabetes,* 48**,** 287-91.

MORALES, M. & BLOOM, F. E. 1997. The 5-HT3 receptor is present in different subpopulations of GABAergic neurons in the rat telencephalon. *J Neurosci,* 17**,** 3157-67.
MURASE, S., GRENHOFF, J., CHOUVET, G., GONON, F. G. & SVENSSON, T. H. 1993. Prefrontal cortex regulates burst firing and transmitter release in rat mesolimbic dopamine neurons studied in vivo. *Neurosci Lett,* 157**,** 53-6.
MUROYA, S., YADA, T., SHIODA, S. & TAKIGAWA, M. 1999. Glucose-sensitive neurons in the rat arcuate nucleus contain neuropeptide Y. *Neurosci Lett,* 264**,** 113-6.
MUST, A., SPADANO, J., COAKLEY, E. H., FIELD, A. E., COLDITZ, G. & DIETZ, W. H. 1999. The disease burden associated with overweight and obesity. *JAMA,* 282**,** 1523-9.
MYNLIEFF, M. & BEAM, K. G. 1994. Adenosine acting at an A1 receptor decreases N-type calcium current in mouse motoneurons. *J Neurosci,* 14**,** 3628-34.
NAKASE, T. & NAUS, C. C. 2004. Gap junctions and neurological disorders of the central nervous system. *Biochim Biophys Acta,* 1662**,** 149-58.
NAKHATE, K. T., KOKARE, D. M., SINGRU, P. S. & SUBHEDAR, N. K. 2011. Central regulation of feeding behavior during social isolation of rat: evidence for the role of endogenous CART system. *Int J Obes (Lond),* 35**,** 773-84.
NASSIRI-ASL, M., ZAMANSOLTANI, F. & TORABINEJAD, B. 2009. Antiepileptic effects of quinine in the pentylenetetrazole model of seizure. *Seizure,* 18**,** 129-32.
NEDERGAARD, M., RANSOM, B. & GOLDMAN, S. A. 2003. New roles for astrocytes: redefining the functional architecture of the brain. *Trends Neurosci,* 26**,** 523-30.
NEWMAN, E. A. 2003. Glial cell inhibition of neurons by release of ATP. *J Neurosci,* 23**,** 1659-66.
NICE 2015. Type 2 Diabetes in Adults: Management. *NICE Guideline,* 28.
NIESLER, B., WEISS, B., FISCHER, C., NOTHEN, M. M., PROPPING, P., BONDY, B., RIETSCHEL, M., MAIER, W., ALBUS, M., FRANZEK, E. & RAPPOLD, G. A. 2001. Serotonin receptor gene HTR3A variants in schizophrenic and bipolar affective patients. *Pharmacogenetics,* 11**,** 21-7.
NISWENDER, K. D. & SCHWARTZ, M. W. 2003. Insulin and leptin revisited: adiposity signals with overlapping physiological and intracellular signaling capabilities. *Front Neuroendocrinol,* 24**,** 1-10.
NOLAN, M. F., LOGAN, S. D. & SPANSWICK, D. 1999. Electrophysiological properties of electrical synapses between rat sympathetic preganglionic neurones in vitro. *J Physiol,* 519 Pt 3**,** 753-64.
O'HEARN, E. & MOLLIVER, M. E. 1984. Organization of raphe-cortical projections in rat: a quantitative retrograde study. *Brain Res Bull,* 13**,** 709-26.
OLGIATI, V. R., NETTI, C., GUIDOBONO, F. & PECILE, A. 1980. The central GABAergic system and control of food intake under different experimental conditions. *Psychopharmacology (Berl),* 68**,** 163-7.
OOMURA, Y., OOYAMA, H., SUGIMORI, M., NAKAMURA, T. & YAMADA, Y. 1974. Glucose inhibition of the glucose-sensitive neurone in the rat lateral hypothalamus. *Nature,* 247**,** 284-6.
ORELLANA, J. A., MARTINEZ, A. D. & RETAMAL, M. A. 2013. Gap junction channels and hemichannels in the CNS: regulation by signaling molecules. *Neuropharmacology,* 75**,** 567-82.

ORELLANA, J. A., SAEZ, P. J., SHOJI, K. F., SCHALPER, K. A., PALACIOS-PRADO, N., VELARDE, V., GIAUME, C., BENNETT, M. V. & SAEZ, J. C. 2009. Modulation of brain hemichannels and gap junction channels by pro-inflammatory agents and their possible role in neurodegeneration. *Antioxid Redox Signal,* 11**,** 369-99.

PALMER, T. M., BENOVIC, J. L. & STILES, G. L. 1996. Molecular basis for subtype-specific desensitization of inhibitory adenosine receptors. Analysis of a chimeric A1-A3 adenosine receptor. *J Biol Chem,* 271**,** 15272-8.

PARSONS, A. A., BINGHAM, S., RAVAL, P., READ, S., THOMPSON, M. & UPTON, N. 2001. Tonabersat (SB-220453) a novel benzopyran with anticonvulsant properties attenuates trigeminal nerve-induced neurovascular reflexes. *Br J Pharmacol,* 132**,** 1549-57.

PARTON, L. E., YE, C. P., COPPARI, R., ENRIORI, P. J., CHOI, B., ZHANG, C. Y., XU, C., VIANNA, C. R., BALTHASAR, N., LEE, C. E., ELMQUIST, J. K., COWLEY, M. A. & LOWELL, B. B. 2007. Glucose sensing by POMC neurons regulates glucose homeostasis and is impaired in obesity. *Nature,* 449**,** 228-32.

PASQUALETTI, M., ORI, M., NARDI, I., CASTAGNA, M., CASSANO, G. B. & MARAZZITI, D. 1998. Distribution of the 5-HT5A serotonin receptor mRNA in the human brain. *Brain Res Mol Brain Res,* 56**,** 1-8.

PATTI, M. E. & KAHN, C. R. 1998. The insulin receptor--a critical link in glucose homeostasis and insulin action. *J Basic Clin Physiol Pharmacol,* 9**,** 89-109.

PAXINOS, F. A. 2008. The mouse brain; stereotaxic coordinates. *Elsevier*.

PENNARTZ, C. M., DE JEU, M. T., GEURTSEN, A. M., SLUITER, A. A. & HERMES, M. L. 1998. Electrophysiological and morphological heterogeneity of neurons in slices of rat suprachiasmatic nucleus. *J Physiol,* 506 (Pt 3)**,** 775-93.

PEREZ VELAZQUEZ, J. L. & CARLEN, P. L. 2000. Gap junctions, synchrony and seizures. *Trends Neurosci,* 23**,** 68-74.

PETRAGLIA, F., SUTTON, S., VALE, W. & PLOTSKY, P. 1987. Corticotropin-releasing factor decreases plasma luteinizing hormone levels in female rats by inhibiting gonadotropin-releasing hormone release into hypophysial-portal circulation. *Endocrinology,* 120**,** 1083-8.

PICARDI, P. K., CALEGARI, V. C., PRADA, P. O., MORAES, J. C., ARAUJO, E., MARCONDES, M. C., UENO, M., CARVALHEIRA, J. B., VELLOSO, L. A. & SAAD, M. J. 2008. Reduction of hypothalamic protein tyrosine phosphatase improves insulin and leptin resistance in diet-induced obese rats. *Endocrinology,* 149**,** 3870-80.

PIZARRO-DELGADO, J., FASCIANI, I., TEMPERAN, A., ROMERO, M., GONZALEZ-NIETO, D., ALONSO-MAGDALENA, P., NUALART-MARTI, A., ESTIL'LES, E., PAUL, D. L., MARTIN-DEL-RIO, R., MONTANYA, E., SOLSONA, C., NADAL, A., BARRIO, L. C. & TAMARIT-RODRIGUEZ, J. 2014. Inhibition of connexin 36 hemichannels by glucose contributes to the stimulation of insulin secretion. *Am J Physiol Endocrinol Metab,* 306**,** E1354-66.

PLUM, L., BELGARDT, B. F. & BRUNING, J. C. 2006a. Central insulin action in energy and glucose homeostasis. *J Clin Invest,* 116**,** 1761-6.

PLUM, L., MA, X., HAMPEL, B., BALTHASAR, N., COPPARI, R., MUNZBERG, H., SHANABROUGH, M., BURDAKOV, D., ROTHER, E., JANOSCHEK, R., ALBER, J., BELGARDT, B. F., KOCH, L., SEIBLER, J., SCHWENK, F., FEKETE, C., SUZUKI, A., MAK, T. W., KRONE, W., HORVATH, T. L., ASHCROFT, F. M. & BRUNING, J. C. 2006b. Enhanced PIP3 signaling in POMC neurons causes KATP channel activation and leads to diet-sensitive obesity. *J Clin Invest,* 116**,** 1886-901.

POCAI, A., LAM, T. K., GUTIERREZ-JUAREZ, R., OBICI, S., SCHWARTZ, G. J., BRYAN, J., AGUILAR-BRYAN, L. & ROSSETTI, L. 2005. Hypothalamic K(ATP) channels control hepatic glucose production. *Nature,* 434**,** 1026-31.
POMPEIANO, M., PALACIOS, J. M. & MENGOD, G. 1992. Distribution and cellular localization of mRNA coding for 5-HT1A receptor in the rat brain: correlation with receptor binding. *J Neurosci,* 12**,** 440-53.
POULAIN, D. A. & WAKERLEY, J. B. 1982. Electrophysiology of hypothalamic magnocellular neurones secreting oxytocin and vasopressin. *Neuroscience,* 7**,** 773-808.
PRASAD, P., OGAWA, S. & PARHAR, I. S. 2015. Serotonin reuptake inhibitor citalopram inhibits GnRH synthesis and spermatogenesis in the male zebrafish. *Biol Reprod,* 93**,** 102.
PRATT, G. D., BOWERY, N. G., KILPATRICK, G. J., LESLIE, R. A., BARNES, N. M., NAYLOR, R. J., JONES, B. J., NELSON, D. R., PALACIDS, J. M., SLATER, P. & ET AL. 1990. Consensus meeting agrees distribution of 5-HT3 receptors in mammalian hindbrain. *Trends Pharmacol Sci,* 11**,** 135-7.
PRICE, C. J., CAULI, B., KOVACS, E. R., KULIK, A., LAMBOLEZ, B., SHIGEMOTO, R. & CAPOGNA, M. 2005. Neurogliaform neurons form a novel inhibitory network in the hippocampal CA1 area. *J Neurosci,* 25**,** 6775-86.
PUIG, M. V., CELADA, P., DIAZ-MATAIX, L. & ARTIGAS, F. 2003. In vivo modulation of the activity of pyramidal neurons in the rat medial prefrontal cortex by 5-HT2A receptors: relationship to thalamocortical afferents. *Cereb Cortex,* 13**,** 870-82.
PUIG, M. V. & GULLEDGE, A. T. 2011. Serotonin and prefrontal cortex function: neurons, networks, and circuits. *Mol Neurobiol,* 44**,** 449-64.
PUIG, M. V., WATAKABE, A., USHIMARU, M., YAMAMORI, T. & KAWAGUCHI, Y. 2010. Serotonin modulates fast-spiking interneuron and synchronous activity in the rat prefrontal cortex through 5-HT1A and 5-HT2A receptors. *J Neurosci,* 30**,** 2211-22.
QIU, J., FANG, Y., RONNEKLEIV, O. K. & KELLY, M. J. 2010. Leptin excites proopiomelanocortin neurons via activation of TRPC channels. *J Neurosci,* 30**,** 1560-5.
QIU, J., ZHANG, C., BORGQUIST, A., NESTOR, C. C., SMITH, A. W., BOSCH, M. A., KU, S., WAGNER, E. J., RONNEKLEIV, O. K. & KELLY, M. J. 2014. Insulin excites anorexigenic proopiomelanocortin neurons via activation of canonical transient receptor potential channels. *Cell Metab,* 19**,** 682-93.
RAMIREZ, M. J. 2013. 5-HT6 receptors and Alzheimer's disease. *Alzheimers Res Ther,* 5**,** 15.
RAPPORT, M. M., GREEN, A. A. & PAGE, I. H. 1948. Crystalline Serotonin. *Science,* 108**,** 329-30.
RASH, J. E., STAINES, W. A., YASUMURA, T., PATEL, D., FURMAN, C. S., STELMACK, G. L. & NAGY, J. I. 2000. Immunogold evidence that neuronal gap junctions in adult rat brain and spinal cord contain connexin-36 but not connexin-32 or connexin-43. *Proc Natl Acad Sci U S A,* 97**,** 7573-8.
READ, S. J., SMITH, M. I., HUNTER, A. J., UPTON, N. & PARSONS, A. A. 2000. SB-220453, a potential novel antimigraine agent, inhibits nitric oxide release following induction of cortical spreading depression in the anaesthetized cat. *Cephalalgia,* 20**,** 92-9.
REZAI-ZADEH, K., YU, S., JIANG, Y., LAQUE, A., SCHWARTZENBURG, C., MORRISON, C. D., DERBENEV, A. V., ZSOMBOK, A. & MUNZBERG, H. 2014. Leptin

receptor neurons in the dorsomedial hypothalamus are key regulators of energy expenditure and body weight, but not food intake. *Mol Metab,* 3**,** 681-93.
RIVIER, C., RIVIER, J. & VALE, W. 1986. Stress-induced inhibition of reproductive functions: role of endogenous corticotropin-releasing factor. *Science,* 231**,** 607-9.
RORSMAN, P. & BRAUN, M. 2013. Regulation of insulin secretion in human pancreatic islets. *Annu Rev Physiol,* 75**,** 155-79.
ROSEN, E. D. & SPIEGELMAN, B. M. 2014. What we talk about when we talk about fat. *Cell,* 156**,** 20-44.
ROSSI, M., KIM, M. S., MORGAN, D. G., SMALL, C. J., EDWARDS, C. M., SUNTER, D., ABUSNANA, S., GOLDSTONE, A. P., RUSSELL, S. H., STANLEY, S. A., SMITH, D. M., YAGALOFF, K., GHATEI, M. A. & BLOOM, S. R. 1998. A C-terminal fragment of Agouti-related protein increases feeding and antagonizes the effect of alpha-melanocyte stimulating hormone in vivo. *Endocrinology,* 139**,** 4428-31.
ROUTH, V. H. 2010. Glucose sensing neurons in the ventromedial hypothalamus. *Sensors (Basel),* 10**,** 9002-25.
ROZENTAL, R., GIAUME, C. & SPRAY, D. C. 2000. Gap junctions in the nervous system. *Brain Res Brain Res Rev,* 32**,** 11-5.
SAADAT, N., IGLAYREGER, H. B., MYERS, M. G., JR., BODARY, P. & GUPTA, S. V. 2012. Differences in metabolomic profiles of male db/db and s/s, leptin receptor mutant mice. *Physiol Genomics,* 44**,** 374-81.
SAEZ, J. C., RETAMAL, M. A., BASILIO, D., BUKAUSKAS, F. F. & BENNETT, M. V. 2005. Connexin-based gap junction hemichannels: gating mechanisms. *Biochim Biophys Acta,* 1711**,** 215-24.
SAKAKURA, M., TAKEBE, K. & NAKAGAWA, S. 1975. Inhibition of luteinizing hormone secretion induced by synthetic LRH by long-term treatment with glucocorticoids in human subjects. *J Clin Endocrinol Metab,* 40**,** 774-9.
SAKATA, I., NAKAMURA, K., YAMAZAKI, M., MATSUBARA, M., HAYASHI, Y., KANGAWA, K. & SAKAI, T. 2002. Ghrelin-producing cells exist as two types of cells, closed- and opened-type cells, in the rat gastrointestinal tract. *Peptides,* 23**,** 531-6.
SAKURA, H., ASHCROFT, S. J., TERAUCHI, Y., KADOWAKI, T. & ASHCROFT, F. M. 1998. Glucose modulation of ATP-sensitive K-currents in wild-type, homozygous and heterozygous glucokinase knock-out mice. *Diabetologia,* 41**,** 654-9.
SANGER, F. 1988. Sequences, sequences, and sequences. *Annu Rev Biochem,* 57**,** 1-28.
SAWCHENKO, P. E. & SWANSON, L. W. 1981. Central noradrenergic pathways for the integration of hypothalamic neuroendocrine and autonomic responses. *Science,* 214**,** 685-7.
SCHALLY, A. V., ARIMURA, A., BABA, Y., NAIR, R. M., MATSUO, H., REDDING, T. W. & DEBELJUK, L. 1971. Isolation and properties of the FSH and LH-releasing hormone. *Biochem Biophys Res Commun,* 43**,** 393-9.
SCHALPER, K. A., RIQUELME, M. A., BRANES, M. C., MARTINEZ, A. D., VEGA, J. L., BERTHOUD, V. M., BENNETT, M. V. & SAEZ, J. C. 2012. Modulation of gap junction channels and hemichannels by growth factors. *Mol Biosyst,* 8**,** 685-98.

SCHNEIDER, H. P. & MCCANN, S. M. 1970. Luteinizing hormone-releasing factor discharged by dopamine in rats. *J Endocrinol,* 46**,** 401-2.
SCHNEIDER, J. E., WISE, J. D., BENTON, N. A., BROZEK, J. M. & KEEN-RHINEHART, E. 2013. When do we eat? Ingestive behavior, survival, and reproductive success. *Horm Behav,* 64**,** 702-28.
SCHUIT, F. C., HUYPENS, P., HEIMBERG, H. & PIPELEERS, D. G. 2001. Glucose sensing in pancreatic beta-cells: a model for the study of other glucose-regulated cells in gut, pancreas, and hypothalamus. *Diabetes,* 50**,** 1-11.
SCHWARTZ, M. W., WOODS, S. C., PORTE, D., JR., SEELEY, R. J. & BASKIN, D. G. 2000. Central nervous system control of food intake. *Nature,* 404**,** 661-71.
SCOTT, M. M., LACHEY, J. L., STERNSON, S. M., LEE, C. E., ELIAS, C. F., FRIEDMAN, J. M. & ELMQUIST, J. K. 2009. Leptin targets in the mouse brain. *J Comp Neurol,* 514**,** 518-32.
SEBASTIAO, A. M. & RIBEIRO, J. A. 2009. Adenosine receptors and the central nervous system. *Handb Exp Pharmacol***,** 471-534.
SEGRETAIN, D. & FALK, M. M. 2004. Regulation of connexin biosynthesis, assembly, gap junction formation, and removal. *Biochim Biophys Acta,* 1662**,** 3-21.
SEVER, P. S. & POULTER, N. R. 1989. A hypothesis for the pathogenesis of essential hypertension: the initiating factors. *J Hypertens Suppl,* 7**,** S9-12.
SHEKHAR, A., KATNER, J. S., SAJDYK, T. J. & KOHL, R. R. 2002. Role of norepinephrine in the dorsomedial hypothalamic panic response: an in vivo microdialysis study. *Pharmacol Biochem Behav,* 71**,** 493-500.
SHI, Y. C., LAU, J., LIN, Z., ZHANG, H., ZHAI, L., SPERK, G., HEILBRONN, R., MIETZSCH, M., WEGER, S., HUANG, X. F., ENRIQUEZ, R. F., BALDOCK, P. A., ZHANG, L., SAINSBURY, A., HERZOG, H. & LIN, S. 2013. Arcuate NPY controls sympathetic output and BAT function via a relay of tyrosine hydroxylase neurons in the PVN. *Cell Metab,* 17**,** 236-48.
SHIODA, S., NAKAI, Y., SATO, A., SUNAYAMA, S. & SHIMODA, Y. 1986. Electron-microscopic cytochemistry of the catecholaminergic innervation of TRH neurons in the rat hypothalamus. *Cell Tissue Res,* 245**,** 247-52.
SHYNG, S. L. & NICHOLS, C. G. 1998. Membrane phospholipid control of nucleotide sensitivity of KATP channels. *Science,* 282**,** 1138-41.
SILVER, I. A. & ERECINSKA, M. 1994. Extracellular glucose concentration in mammalian brain: continuous monitoring of changes during increased neuronal activity and upon limitation in oxygen supply in normo-, hypo-, and hyperglycemic animals. *J Neurosci,* 14**,** 5068-76.
SIMON, A., OLAH, S., MOLNAR, G., SZABADICS, J. & TAMAS, G. 2005. Gap-junctional coupling between neurogliaform cells and various interneuron types in the neocortex. *J Neurosci,* 25**,** 6278-85.
SIMONDS, S. E., PRYOR, J. T., RAVUSSIN, E., GREENWAY, F. L., DILEONE, R., ALLEN, A. M., BASSI, J., ELMQUIST, J. K., KEOGH, J. M., HENNING, E., MYERS, M. G., JR., LICINIO, J., BROWN, R. D., ENRIORI, P. J., O'RAHILLY, S., STERNSON, S. M., GROVE, K. L., SPANSWICK, D. C., FAROOQI, I. S. & COWLEY, M. A. 2014. Leptin mediates the increase in blood pressure associated with obesity. *Cell,* 159**,** 1404-16.
SIMPSON, I. A., CARRUTHERS, A. & VANNUCCI, S. J. 2007. Supply and demand in cerebral energy metabolism: the role of nutrient transporters. *J Cereb Blood Flow Metab,* 27**,** 1766-91.

SISK, C. L. & BRONSON, F. H. 1986. Effects of food restriction and restoration on gonadotropin and growth hormone secretion in immature male rats. *Biol Reprod,* 35**,** 554-61.
SMITH, J. T. 2009. Sex steroid control of hypothalamic Kiss1 expression in sheep and rodents: comparative aspects. *Peptides,* 30**,** 94-102.
SMITH, J. T., CLIFTON, D. K. & STEINER, R. A. 2006. Regulation of the neuroendocrine reproductive axis by kisspeptin-GPR54 signaling. *Reproduction,* 131**,** 623-30.
SMITH, J. T., RAO, A., PEREIRA, A., CARATY, A., MILLAR, R. P. & CLARKE, I. J. 2008. Kisspeptin is present in ovine hypophysial portal blood but does not increase during the preovulatory luteinizing hormone surge: evidence that gonadotropes are not direct targets of kisspeptin in vivo. *Endocrinology,* 149**,** 1951-9.
SMITH, P. M. & FERGUSON, A. V. 2008. Neurophysiology of hunger and satiety. *Dev Disabil Res Rev,* 14**,** 96-104.
SNYDER, P. J., BASHEY, H. M., KIM, S. U. & CHAPPEL, S. C. 1984. Secretion of uncombined subunits of luteinizing hormone by gonadotroph cell adenomas. *J Clin Endocrinol Metab,* 59**,** 1169-75.
SOGA, T., KITAHASHI, T., CLARKE, I. J. & PARHAR, I. S. 2014. Gonadotropin-inhibitory hormone promoter-driven enhanced green fluorescent protein expression decreases during aging in female rats. *Endocrinology,* 155**,** 1944-55.
SOGA, T., TEO, C. H., CHAM, K. L., IDRIS, M. M. & PARHAR, I. S. 2015. Early-Life Social Isolation Impairs the Gonadotropin-Inhibitory Hormone Neuronal Activity and Serotonergic System in Male Rats. *Front Endocrinol (Lausanne),* 6**,** 172.
SOGA, T., WONG, D. W., CLARKE, I. J. & PARHAR, I. S. 2010. Citalopram (antidepressant) administration causes sexual dysfunction in male mice through RF-amide related peptide in the dorsomedial hypothalamus. *Neuropharmacology,* 59**,** 77-85.
SOHL, G., MAXEINER, S. & WILLECKE, K. 2005. Expression and functions of neuronal gap junctions. *Nat Rev Neurosci,* 6**,** 191-200.
SOHL, G. & WILLECKE, K. 2004. Gap junctions and the connexin protein family. *Cardiovasc Res,* 62**,** 228-32.
SOHN, J. W. & WILLIAMS, K. W. 2012. Functional heterogeneity of arcuate nucleus pro-opiomelanocortin neurons: implications for diverging melanocortin pathways. *Mol Neurobiol,* 45**,** 225-33.
SPANSWICK, D., SMITH, M. A., GROPPI, V. E., LOGAN, S. D. & ASHFORD, M. L. 1997. Leptin inhibits hypothalamic neurons by activation of ATP-sensitive potassium channels. *Nature,* 390**,** 521-5.
SPANSWICK, D., SMITH, M. A., MIRSHAMSI, S., ROUTH, V. H. & ASHFORD, M. L. 2000. Insulin activates ATP-sensitive K+ channels in hypothalamic neurons of lean, but not obese rats. *Nat Neurosci,* 3**,** 757-8.
SPRAY, D. C., WHITE, R. L., MAZET, F. & BENNETT, M. V. 1985. Regulation of gap junctional conductance. *Am J Physiol,* 248**,** H753-64.
SRINIVAS, M., HOPPERSTAD, M. G. & SPRAY, D. C. 2001. Quinine blocks specific gap junction channel subtypes. *Proc Natl Acad Sci U S A,* 98**,** 10942-7.
SRINIVAS, M., ROZENTAL, R., KOJIMA, T., DERMIETZEL, R., MEHLER, M., CONDORELLI, D. F., KESSLER, J. A. & SPRAY, D. C. 1999. Functional

properties of channels formed by the neuronal gap junction protein connexin36. *J Neurosci,* 19**,** 9848-55.
STERN, J. E. 2001. Electrophysiological and morphological properties of pre-autonomic neurones in the rat hypothalamic paraventricular nucleus. *J Physiol,* 537**,** 161-77.
STERNSON, S. M., SHEPHERD, G. M. & FRIEDMAN, J. M. 2005. Topographic mapping of VMH --> arcuate nucleus microcircuits and their reorganization by fasting. *Nat Neurosci,* 8**,** 1356-63.
STOUT, C. E., COSTANTIN, J. L., NAUS, C. C. & CHARLES, A. C. 2002. Intercellular calcium signaling in astrocytes via ATP release through connexin hemichannels. *J Biol Chem,* 277**,** 10482-8.
SUADICANI, S. O., BROSNAN, C. F. & SCEMES, E. 2006. P2X7 receptors mediate ATP release and amplification of astrocytic intercellular Ca2+ signaling. *J Neurosci,* 26**,** 1378-85.
TACHIBANA, T., SATO, M., TAKAHASHI, H., UKENA, K., TSUTSUI, K. & FURUSE, M. 2005. Gonadotropin-inhibiting hormone stimulates feeding behavior in chicks. *Brain Res,* 1050**,** 94-100.
TAKAHASHI, K. A. & CONE, R. D. 2005. Fasting induces a large, leptin-dependent increase in the intrinsic action potential frequency of orexigenic arcuate nucleus neuropeptide Y/Agouti-related protein neurons. *Endocrinology,* 146**,** 1043-7.
TAMAS, G., BUHL, E. H., LORINCZ, A. & SOMOGYI, P. 2000. Proximally targeted GABAergic synapses and gap junctions synchronize cortical interneurons. *Nat Neurosci,* 3**,** 366-71.
TANG, L., PARKER, M., FEI, Q. & LOUTZENHISER, R. 1999. Afferent arteriolar adenosine A2a receptors are coupled to KATP in in vitro perfused hydronephrotic rat kidney. *Am J Physiol,* 277**,** F926-33.
TAO, R., GONG, J., LUO, X., ZANG, M., GUO, W., WEN, R. & LUO, Z. 2010. AMPK exerts dual regulatory effects on the PI3K pathway. *J Mol Signal,* 5**,** 1.
TAPIA-ARANCIBIA, L., ARANCIBIA, S. & ASTIER, H. 1985. Evidence for alpha 1-adrenergic stimulatory control of in vitro release of immunoreactive thyrotropin-releasing hormone from rat median eminence: in vivo corroboration. *Endocrinology,* 116**,** 2314-9.
TARTAGLIA, L. A., DEMBSKI, M., WENG, X., DENG, N., CULPEPPER, J., DEVOS, R., RICHARDS, G. J., CAMPFIELD, L. A., CLARK, F. T., DEEDS, J., MUIR, C., SANKER, S., MORIARTY, A., MOORE, K. J., SMUTKO, J. S., MAYS, G. G., WOOL, E. A., MONROE, C. A. & TEPPER, R. I. 1995. Identification and expression cloning of a leptin receptor, OB-R. *Cell,* 83**,** 1263-71.
TASKER, J. G. & DUDEK, F. E. 1991. Electrophysiological properties of neurones in the region of the paraventricular nucleus in slices of rat hypothalamus. *J Physiol,* 434**,** 271-93.
THOMPSON, A. J. & LUMMIS, S. C. 2007. The 5-HT3 receptor as a therapeutic target. *Expert Opin Ther Targets,* 11**,** 527-40.
THOMPSON, R. H. & SWANSON, L. W. 1998. Organization of inputs to the dorsomedial nucleus of the hypothalamus: a reexamination with Fluorogold and PHAL in the rat. *Brain Res Brain Res Rev,* 27**,** 89-118.
TIGANIS, T. 2013. PTP1B and TCPTP--nonredundant phosphatases in insulin signaling and glucose homeostasis. *FEBS J,* 280**,** 445-58.
TOBARI, Y., SON, Y. L., UBUKA, T., HASEGAWA, Y. & TSUTSUI, K. 2014. A new pathway mediating social effects on the endocrine system: female presence

acting via norepinephrine release stimulates gonadotropin-inhibitory hormone in the paraventricular nucleus and suppresses luteinizing hormone in quail. *J Neurosci,* 34**,** 9803-11.
TODA, C., KIM, J. D., IMPELLIZZERI, D., CUZZOCREA, S., LIU, Z. W. & DIANO, S. 2016. UCP2 Regulates Mitochondrial Fission and Ventromedial Nucleus Control of Glucose Responsiveness. *Cell,* 164**,** 872-83.
TONI, R., JACKSON, I. M. & LECHAN, R. M. 1990. Neuropeptide-Y-immunoreactive innervation of thyrotropin-releasing hormone-synthesizing neurons in the rat hypothalamic paraventricular nucleus. *Endocrinology,* 126**,** 2444-53.
TRAUB, R. D., PAIS, I., BIBBIG, A., LEBEAU, F. E., BUHL, E. H., HORMUZDI, S. G., MONYER, H. & WHITTINGTON, M. A. 2003. Contrasting roles of axonal (pyramidal cell) and dendritic (interneuron) electrical coupling in the generation of neuronal network oscillations. *Proc Natl Acad Sci U S A,* 100**,** 1370-4.
TSCHOP, M., SMILEY, D. L. & HEIMAN, M. L. 2000. Ghrelin induces adiposity in rodents. *Nature,* 407**,** 908-13.
TSCHOP, M., WAWARTA, R., RIEPL, R. L., FRIEDRICH, S., BIDLINGMAIER, M., LANDGRAF, R. & FOLWACZNY, C. 2001a. Post-prandial decrease of circulating human ghrelin levels. *J Endocrinol Invest,* 24**,** RC19-21.
TSCHOP, M., WEYER, C., TATARANNI, P. A., DEVANARAYAN, V., RAVUSSIN, E. & HEIMAN, M. L. 2001b. Circulating ghrelin levels are decreased in human obesity. *Diabetes,* 50**,** 707-9.
TSUCHIYA, Y., MORIOKA, K., SHIRAI, J., YOKOMIZO, Y. & YOSHIDA, K. 2003. Gene design of signal sequence for effective secretion of protein. *Nucleic Acids Res Suppl***,** 261-2.
TSUTSUI, K., BENTLEY, G. E., KRIEGSFELD, L. J., OSUGI, T., SEONG, J. Y. & VAUDRY, H. 2010. Discovery and evolutionary history of gonadotrophin-inhibitory hormone and kisspeptin: new key neuropeptides controlling reproduction. *J Neuroendocrinol,* 22**,** 716-27.
TSUTSUI, K., SAIGOH, E., UKENA, K., TERANISHI, H., FUJISAWA, Y., KIKUCHI, M., ISHII, S. & SHARP, P. J. 2000. A novel avian hypothalamic peptide inhibiting gonadotropin release. *Biochem Biophys Res Commun,* 275**,** 661-7.
TUNE, J. D. & CONSIDINE, R. V. 2007. Effects of leptin on cardiovascular physiology. *J Am Soc Hypertens,* 1**,** 231-41.
TUNG, Y. C., PIPER, S. J., YEUNG, D., O'RAHILLY, S. & COLL, A. P. 2006. A comparative study of the central effects of specific proopiomelancortin (POMC)-derived melanocortin peptides on food intake and body weight in pomc null mice. *Endocrinology,* 147**,** 5940-7.
UBUKA, T., INOUE, K., FUKUDA, Y., MIZUNO, T., UKENA, K., KRIEGSFELD, L. J. & TSUTSUI, K. 2012. Identification, expression, and physiological functions of Siberian hamster gonadotropin-inhibitory hormone. *Endocrinology,* 153**,** 373-85.
UBUKA, T., LAI, H., KITANI, M., SUZUUCHI, A., PHAM, V., CADIGAN, P. A., WANG, A., CHOWDHURY, V. S., TSUTSUI, K. & BENTLEY, G. E. 2009a. Gonadotropin-inhibitory hormone identification, cDNA cloning, and distribution in rhesus macaque brain. *J Comp Neurol,* 517**,** 841-55.
UBUKA, T., MORGAN, K., PAWSON, A. J., OSUGI, T., CHOWDHURY, V. S., MINAKATA, H., TSUTSUI, K., MILLAR, R. P. & BENTLEY, G. E. 2009b. Identification of human GnIH homologs, RFRP-1 and RFRP-3, and the cognate receptor, GPR147 in the human hypothalamic pituitary axis. *PLoS One,* 4**,** e8400.

UBUKA, T., SON, Y. L., BENTLEY, G. E., MILLAR, R. P. & TSUTSUI, K. 2013. Gonadotropin-inhibitory hormone (GnIH), GnIH receptor and cell signaling. *Gen Comp Endocrinol,* 190**,** 10-7.

UPTON, N., BLACKBURN, T. P., CAMPBELL, C. A., COOPER, D., EVANS, M. L., HERDON, H. J., KING, P. D., RAY, A. M., STEAN, T. O., CHAN, W. N., EVANS, J. M. & THOMPSON, M. 1997. Profile of SB-204269, a mechanistically novel anticonvulsant drug, in rat models of focal and generalized epileptic seizures. *Br J Pharmacol,* 121**,** 1679-86.

UPTON, N. & THOMPSON, M. 2000. Benzo[b]pyranols and related novel antiepileptic agents. *Prog Med Chem,* 37**,** 177-200.

VAN DEN TOP, M., LEE, K., WHYMENT, A. D., BLANKS, A. M. & SPANSWICK, D. 2004. Orexigen-sensitive NPY/AgRP pacemaker neurons in the hypothalamic arcuate nucleus. *Nat Neurosci,* 7**,** 493-4.

VAN DEN TOP, M., LYONS, D. J., LEE, K., CODERRE, E., RENAUD, L. P. & SPANSWICK, D. 2007. Pharmacological and molecular characterization of ATP-sensitive K(+) conductances in CART and NPY/AgRP expressing neurons of the hypothalamic arcuate nucleus. *Neuroscience,* 144**,** 815-24.

VANNUCCI, S. J., MAHER, F. & SIMPSON, I. A. 1997. Glucose transporter proteins in brain: delivery of glucose to neurons and glia. *Glia,* 21**,** 2-21.

VARNAS, K., HALLDIN, C., PIKE, V. W. & HALL, H. 2003. Distribution of 5-HT4 receptors in the postmortem human brain--an autoradiographic study using [125I]SB 207710. *Eur Neuropsychopharmacol,* 13**,** 228-34.

VERSELIS, V. K. & SRINIVAS, M. 2013. Connexin channel modulators and their mechanisms of action. *Neuropharmacology,* 75**,** 517-24.

VESSEY, J. P., LALONDE, M. R., MIZAN, H. A., WELCH, N. C., KELLY, M. E. & BARNES, S. 2004. Carbenoxolone inhibition of voltage-gated Ca channels and synaptic transmission in the retina. *J Neurophysiol,* 92**,** 1252-6.

VITALE, M. L., DE LAS NIEVES PARISI, M., CHIOCCHIO, S. R. & TRAMEZZANI, J. H. 1985. Serotonin stimulates gonadotrophin release by acting directly on the median eminence. *Acta Physiol Pharmacol Latinoam,* 35**,** 473-9.

VOGT, B. A. 1991. The role of layer I in cortical function. *Cerebral cortex***,** 49-79.

VOLTERRA, A. & MELDOLESI, J. 2005. Astrocytes, from brain glue to communication elements: the revolution continues. *Nat Rev Neurosci,* 6**,** 626-40.

VONG, L., YE, C., YANG, Z., CHOI, B., CHUA, S., JR. & LOWELL, B. B. 2011. Leptin action on GABAergic neurons prevents obesity and reduces inhibitory tone to POMC neurons. *Neuron,* 71**,** 142-54.

VOSS, L. J., GAUFFIN, E., RINGQVIST, A. & SLEIGH, J. W. 2014. Investigation into the role of gap junction modulation of intracortical connectivity in mouse neocortical brain slices. *Brain Res,* 1553**,** 24-30.

VOSS, L. J., JACOBSON, G., SLEIGH, J. W., STEYN-ROSS, A. & STEYN-ROSS, M. 2009. Excitatory effects of gap junction blockers on cerebral cortex seizure-like activity in rats and mice. *Epilepsia,* 50**,** 1971-8.

WANG, Y., BARAKAT, A. & ZHOU, H. 2010. Electrotonic coupling between pyramidal neurons in the neocortex. *PLoS One,* 5**,** e10253.

WATANABE, M., HAYASAKI, H., TAMAYAMA, T. & SHIMADA, M. 1998. Histologic distribution of insulin and glucagon receptors. *Braz J Med Biol Res,* 31**,** 243-56.

WATSON, J. D. & CRICK, F. H. 1953. The structure of DNA. *Cold Spring Harb Symp Quant Biol,* 18**,** 123-31.

WHO 2016. World Health Organization Global Report on Diabetes. 21.
WHYMENT, A. D., CODERRE, E., WILSON, J. M., RENAUD, L. P., O'HARE, E. & SPANSWICK, D. 2011. Electrophysiological, pharmacological and molecular profile of the transient outward rectifying conductance in rat sympathetic preganglionic neurons in vitro. *Neuroscience,* 178**,** 68-81.
WILLESEN, M. G., KRISTENSEN, P. & ROMER, J. 1999. Co-localization of growth hormone secretagogue receptor and NPY mRNA in the arcuate nucleus of the rat. *Neuroendocrinology,* 70**,** 306-16.
WILLIAMS, G., BING, C., CAI, X. J., HARROLD, J. A., KING, P. J. & LIU, X. H. 2001. The hypothalamus and the control of energy homeostasis: different circuits, different purposes. *Physiol Behav,* 74**,** 683-701.
WILLIAMS, K. W., MARGATHO, L. O., LEE, C. E., CHOI, M., LEE, S., SCOTT, M. M., ELIAS, C. F. & ELMQUIST, J. K. 2010. Segregation of acute leptin and insulin effects in distinct populations of arcuate proopiomelanocortin neurons. *J Neurosci,* 30**,** 2472-9.
WINTERMANTEL, T. M., CAMPBELL, R. E., PORTEOUS, R., BOCK, D., GRONE, H. J., TODMAN, M. G., KORACH, K. S., GREINER, E., PEREZ, C. A., SCHUTZ, G. & HERBISON, A. E. 2006. Definition of estrogen receptor pathway critical for estrogen positive feedback to gonadotropin-releasing hormone neurons and fertility. *Neuron,* 52**,** 271-80.
WITTMANN, G., HRABOVSZKY, E. & LECHAN, R. M. 2013. Distinct glutamatergic and GABAergic subsets of hypothalamic pro-opiomelanocortin neurons revealed by in situ hybridization in male rats and mice. *J Comp Neurol,* 521**,** 3287-302.
WOODS, S. C., LUTZ, T. A., GEARY, N. & LANGHANS, W. 2006. Pancreatic signals controlling food intake; insulin, glucagon and amylin. *Philos Trans R Soc Lond B Biol Sci,* 361**,** 1219-35.
WU, M., DUMALSKA, I., MOROZOVA, E., VAN DEN POL, A. N. & ALREJA, M. 2009. Gonadotropin inhibitory hormone inhibits basal forebrain vGluT2-gonadotropin-releasing hormone neurons via a direct postsynaptic mechanism. *J Physiol,* 587**,** 1401-11.
WU, W. W., CHAN, C. S. & DISTERHOFT, J. F. 2004. Slow afterhyperpolarization governs the development of NMDA receptor-dependent afterdepolarization in CA1 pyramidal neurons during synaptic stimulation. *J Neurophysiol,* 92**,** 2346-56.
XU, A. W., KAELIN, C. B., TAKEDA, K., AKIRA, S., SCHWARTZ, M. W. & BARSH, G. S. 2005. PI3K integrates the action of insulin and leptin on hypothalamic neurons. *J Clin Invest,* 115**,** 951-8.
XU, A. W., STE-MARIE, L., KAELIN, C. B. & BARSH, G. S. 2007. Inactivation of signal transducer and activator of transcription 3 in proopiomelanocortin (Pomc) neurons causes decreased pomc expression, mild obesity, and defects in compensatory refeeding. *Endocrinology,* 148**,** 72-80.
YAMADA, K., JI, J. J., YUAN, H., MIKI, T., SATO, S., HORIMOTO, N., SHIMIZU, T., SEINO, S. & INAGAKI, N. 2001. Protective role of ATP-sensitive potassium channels in hypoxia-induced generalized seizure. *Science,* 292**,** 1543-6.
YAMANAKA, A., MURAKI, Y., ICHIKI, K., TSUJINO, N., KILDUFF, T. S., GOTO, K. & SAKURAI, T. 2006. Orexin neurons are directly and indirectly regulated by catecholamines in a complex manner. *J Neurophysiol,* 96**,** 284-98.
YANG, L., QI, Y. & YANG, Y. 2015. Astrocytes control food intake by inhibiting AGRP neuron activity via adenosine A1 receptors. *Cell Rep,* 11**,** 798-807.

YANG, Y., ATASOY, D., SU, H. H. & STERNSON, S. M. 2011. Hunger states switch a flip-flop memory circuit via a synaptic AMPK-dependent positive feedback loop. *Cell,* 146**,** 992-1003.

ZHAN, C., ZHOU, J., FENG, Q., ZHANG, J. E., LIN, S., BAO, J., WU, P. & LUO, M. 2013. Acute and long-term suppression of feeding behavior by POMC neurons in the brainstem and hypothalamus, respectively. *J Neurosci,* 33**,** 3624-32.

ZHANG, S., CHEN, L., LUO, Y., GUNAWAN, A., LAWRENCE, D. S. & ZHANG, Z. Y. 2009. Acquisition of a potent and selective TC-PTP inhibitor via a stepwise fluorophore-tagged combinatorial synthesis and screening strategy. *J Am Chem Soc,* 131**,** 13072-9.

ZHANG, Y., KERMAN, I. A., LAQUE, A., NGUYEN, P., FAOUZI, M., LOUIS, G. W., JONES, J. C., RHODES, C. & MUNZBERG, H. 2011. Leptin-receptor-expressing neurons in the dorsomedial hypothalamus and median preoptic area regulate sympathetic brown adipose tissue circuits. *J Neurosci,* 31**,** 1873-84.

ZHANG, Y., PROENCA, R., MAFFEI, M., BARONE, M., LEOPOLD, L. & FRIEDMAN, J. M. 1994. Positional cloning of the mouse obese gene and its human homologue. *Nature,* 372**,** 425-32.

ZHANG, Z. Y., DODD, G. T. & TIGANIS, T. 2015. Protein Tyrosine Phosphatases in Hypothalamic Insulin and Leptin Signaling. *Trends Pharmacol Sci,* 36**,** 661-74.

ZHU, J. J., UHLRICH, D. J. & LYTTON, W. W. 1999. Properties of a hyperpolarization-activated cation current in interneurons in the rat lateral geniculate nucleus. *Neuroscience,* 92**,** 445-57.

ZIBURKUS, J., CRESSMAN, J. R., BARRETO, E. & SCHIFF, S. J. 2006. Interneuron and pyramidal cell interplay during in vitro seizure-like events. *J Neurophysiol,* 95**,** 3948-54.

ZIGMAN, J. M., JONES, J. E., LEE, C. E., SAPER, C. B. & ELMQUIST, J. K. 2006. Expression of ghrelin receptor mRNA in the rat and the mouse brain. *J Comp Neurol,* 494**,** 528-48.

ZSIROS, V., ARADI, I. & MACCAFERRI, G. 2007. Propagation of postsynaptic currents and potentials via gap junctions in GABAergic networks of the rat hippocampus. *J Physiol,* 578**,** 527-44.